“Fall seven times, stand up eight.”

Thanks to the 'Limburg Clinical Research Program (LCRP) UHasselt-ZOL-Jessa', supported by the foundation Limburg Sterk Merk, province of Limburg, Flemish government, Hasselt University, Ziekenhuis Oost-Limburg and Jessa Hospital.

Members of the jury

Prof. dr. Sven Hendrix, Hasselt University, Diepenbeek, Belgium, chairman

Prof. dr. Guy Massa, Jessa Hospital, Hasselt, Belgium, promoter
Prof. dr. Peter Adriaensens, Hasselt University, Diepenbeek, Belgium, co-promoter
Prof. dr. Jean-Paul Noben, Hasselt University, Diepenbeek, Belgium, co-promoter

Prof. dr. Luc Michiels, Hasselt University, Diepenbeek, Belgium
Prof. dr. Dominique Hansen, Hasselt University, Diepenbeek, Belgium
Prof. dr. Jean De Schepper, University Hospital Brussels, Brussels, Belgium
Prof. dr. Ilja Arts, Maastricht University, Maastricht, The Netherlands
Dr. Volker Behrends, Roehampton University, London, United Kingdom

List of Contents

List of Figures		II
List of Tables		VI
Abbreviations		VIII
CHAPTER 1	General introduction and aims	1
ANNEX	Fundamentals of ^{1}H-NMR spectroscopy	41
CHAPTER 2	Morbid obesity in childhood	76
CHAPTER 3	Shape of the plasma glucose curve	90
CHAPTER 4	Metabolically "healthy" obesity in childhood	111
CHAPTER 5	Optimization ^{1}H-NMR experimental analysis	129
CHAPTER 6	Preanalytical sampling conditions and SPREC	162
CHAPTER 7	^{1}H-NMR-based metabolic profiling of childhood obesity	184
CHAPTER 8	General discussion and main conclusions	221
Summary - Samenvatting		246
Curriculum Vitae		249
Academic Bibliography		250
Acknowledgements		257

List of Figures

Figure 1.1 Flemish reference centiles of BMI-for-age for (A) boys and (B) girls

Figure 1.2 Model of the MetS and its presumed precursors and consequences

Figure 1.3 Adipose tissue as an endocrine organ

Figure 1.4 Obesity-induced changes in adipokine secretion and the development of insulin resistance

Figure 1.5 Disease progression of T2DM

Figure 1.6 Complex interaction of each level of biological organization in systems biology

Figure 1.7 Bench-to-bedside model for biomarker discovery and validation for metabolomics research

Figure 1.8 Outside (left) and inside (right) of a 400 MHz NMR spectrometer

Figure 1.9 A typical sample workflow of NMR spectroscopy

Figure 1.10 ^{1}H-NMR CPMG spectra (3-4 ppm) of blood plasma acquired at 400 MHz (upper) and 900 MHz (lower)

Figure 1.11 Schematic diagram of the study

Figure S1 The electromagnetic spectrum

Figure S2 The magnetic dipole moment μ of a hydrogen nucleus

Figure S3 Two energy states (spin-up or spin-down) of the proton magnetic moment which precesses around an externally applied magnetic field B_0 oriented along the z-axis

Figure S4 Energy difference between two Zeeman energy states

Figure S5 Statistical distribution of μ-vectors over two cone halves which results in net or longitudinal magnetization, M_0, which is oriented in the same direction as vector B_0

Figure S6 Vector representation of transversal magnetization ($M_{y'}=M_0$) upon applying a 90° RF-pulse along the x'-axis by the B_1 field in the rotating frame which results in a flip over of M_0 towards the y'-axis (receiver)

Figure S7 Oscillating B_1-fields in the x'-y'-plane are achieved by applying a linear oscillating electromagnetic field with magnitude of $2B_1$ along the x'-axis

Figure S8 Net energy transfer from the B_1-field to the nuclei leading to a flip over of some nuclear spins from the low energy state to the high energy state

Figure S9 Orientation of nuclear spins after applying a 90° pulse

Figure S10 The free induction decay (FID) is the decay of the transversal magnetization which forms the observable NMR signals detected by the receiver in the x'y'-plane of the rotating frame

Figure S11 Longitudinal or T_1 relaxation

Figure S12 Transversal or T_2 relaxation

Figure S13 ^{1}H-NMR spectrum of diethyl ether ($C_4H_{10}O$)
Figure S14 ^{1}H-NMR chemical shifts (δ in ppm) for common functional chemical groups
Figure S15 J-coupling patterns of chloroethane, i.e. a triplet and quadruplet
Figure S16 Structure of data matrix X used for PCA analysis
Figure S17 Plotting the observations in K-dimensional space
Figure S18 Principal components for PCA
Figure S19 Two principal components define a model plane
Figure S20 PCA score and loading plot
Figure S21 Outlier detection
Figure S22 Structure of data matrix X and Y used for PLS analysis
Figure S23 In a regression model, the observations are two groups of points, one in the predictor (X) space and one in the response (Y) space
Figure S24 First principal component for PLS
Figure S25 Second principal component for PLS in the X-space is orthogonal to the first one
Figure S26 OPLS-DA score and loading plot
Figure S27 Classification models
Figure S28 Misclassification list
Figure S29 Variable influence on projection (VIP) plot
Figure S30 S-plots of an OPLS-DA model
Figure S31 PLS-DA permutation test
Figure 2.1 IOTF BMI percentile curves of boys (A) and girls (B)
Figure 2.2 The prevalence of MetS components among children and adolescents of different obesity classes defined according to the newly developed IOTF criteria
Figure 2.3 Prevalence of individual MetS components among the obese children and adolescents studied
Figure 3.1 Observed plasma glucose curve shape types
Figure 3.2 Glucose (A) and insulin (B) response curves of monophasic, biphasic and triphasic shape types
Figure 4.1 Prevalence rates of prediabetes (IFG and/or IGT) among MHO and MUO classified according to MR_{IDF}, $MR_{HOMA\text{-}IR}$ and $MR_{IDF/HOMA\text{-}IR}$
Figure 5.1 An example of spiking human blood plasma with L-glycine
Figure 5.2 CV (%) for the 110 variables of the reference plasma which are divided into three groups on the basis of their mean normalized integration values, i.e. those with a mean normalized integration value between 0.1-5 (80 variables), 5-10 (12 variables) and 10–200 (18 variables)

Figure 5.3 CV (%) for the 110 plasma variables of an obese subject which are divided into three groups on the basis of their mean normalized integration values, i.e. those with a mean normalized integration value between 0.1-5 (74 variables), 5-10 (17 variables) and 10–200 (19 variables)

Figure 5.4 Plasma OPLS-DA score plots of the models build with all 110 variables (A), with 91 variables (B), with 83 variables (C), with 69 variables (D) and with 43 variables (E)

Figure 5.5 CV (%) for the 134 variables of the reference urine which are divided into three groups on the basis of their mean normalized integration values, i.e. those with a mean normalized integration value between 0.01-5 (53 variables), 5-10 (34 variables) and 10–200 (47 variables)

Figure 5.6 CV (%) for the 134 urine variables of an obese subject which are divided into three groups on the basis of their mean normalized integration values, i.e. those with a mean normalized integration value between 0.01-5 (78 variables), 5-10 (33 variables) and 10–200 (23 variables)

Figure 5.7 Urine OPLS-DA score plots of the models build with all 134 variables (A), with 130 variables (B), with 127 variables (C), with 124 variables (D) and with 106 variables (E)

Figure 6.1 Overview of the study protocol for plasma

Figure 6.2 PCA score plots showing the influence of processing delay (time between blood collection and centrifugation) and made by using (A) all 110 integration values and (B) only the 83 'non-noisy' integration values of the plasma ^{1}H-NMR spectra

Figure 6.3 PCA score plots showing the influence of a double lithium-heparin (LiHe) concentration (A) and oxidative atmosphere (B), made by the 110 integration regions of the plasma ^{1}H-NMR spectra of study group 1 (n=6)

Figure 6.4 PCA score plots showing the influence of hemolysis (A) and processing delay (B), made by the 110 integration regions of the plasma ^{1}H-NMR spectra from study group 2 (n=6)

Figure 6.5 Relative concentrations of lactate, pyruvate and glucose in plasma originating from a cooled blood sample which is processed after 30 min (white), 3 h (grey) and 8 h (black)

Figure 6.6 PCA score plots showing the influence of centrifugation temperature (A) and initial plasma freezing on dry ice or in LN_2 (B), made by the 110 integration regions of the plasma ^{1}H-NMR spectra from study group 2 (n=6)

Figure 6.7 PCA score plots showing the influence of storage duration at -80°C, made by the 110 integration regions of the plasma ^{1}H-NMR spectra from study group 3 (n=10)

Figure 7.1 PCA score plots colored according to age (A), gender (B), ethnicity (C), and pubertal stage (D)

Figure 7.2 Supervised OPLS-DA score plot based on all 110 variables derived from plasma ^{1}H-NMR CPMG spectra of native (blue) and non-native (red) subjects

Figure 7.3 Unsupervised PCA score plot (A) and supervised OPLS-DA score plot (B) based on all 110 variables derived from plasma ^{1}H-NMR CPMG spectra of OB (●) and NW (○) subjects

Figure 7.4 Supervised OPLS-DA score plot (A), ROC-curve (B) and PLS-DA permutation test based on 83 variables derived from plasma ^{1}H-NMR CPMG spectra of 61 OB (●) and 36 NW (○) subjects

Figure 7.5 Supervised OPLS-DA S-plot based on 83 variables derived from plasma ^{1}H-NMR CPMG spectra of 61 OB and 36 NW subjects

Figure 7.6 PCA score plots of 35 OB subjects colored according to age (A), gender (B), ethnicity (C), pubertal stage (D) and BMI SDS (E)

Figure 7.7 PCA (A) and OPLS-DA (B) score plots based on 110 plasma ^{1}H-NMR variables of 18 MHO (○) and 17 MUO (●) subjects

Figure 7.8 Supervised OPLS-DA score plot based on 83 variables derived from plasma ^{1}H-NMR CPMG spectra of 18 MHO (○) and 17 MUO (●) subjects

Figure 7.9 Supervised OPLS-DA S-plot based on 83 variables derived from plasma ^{1}H-NMR CPMG spectra of 18 MHO and 17 MUO subjects

Figure 7.10 PCA score plot colored according to fasting plasma triglyceride concentration of the OB study group (A), and MHO and MUO subjects (B)

List of Tables

Table 1.1 Prevalence data of MetS in 7 to 19-year-old children from different geographical areas based on most commonly used criteria

Table 1.2 Classification of MetS in adults according to the WHO, NCEP/ATPIII, and IDF

Table 1.3 Classification of MetS in children and adolescents according to modified criteria developed by the WHO and NCEP/ATPIII

Table 1.4 IDF criteria for MetS in children and adolescents aged 6 to 18

Table 1.5 Advantages and limitations of NMR spectroscopy and MS as analytical tools for metabolomics research

Table 2.1 BMI cut-off points for obesity, severe obesity and morbid obesity by age and gender defined to pass through BMI of 30, 35 and 40 kg.m-2 at age 18 based on the newly derived LMS curves

Table 2.2 Comparison of anthropometric and biochemical parameters with corresponding age- and gender specific z-scores between class I, class II and class III obesity

Table 3.1 Baseline characteristics of the study population

Table 3.2 Parameters of glucose and insulin metabolism, and components of the metabolic syndrome in patients with a monophasic, biphasic or triphasic shape

Table 4.1 Descriptive characteristics of obese children and adolescents studied

Table 4.2 Clinical characteristics of MHO and MUO children and adolescents classified according to MR_{IDF}, $MR_{HOMA\text{-}IR}$ and $MR_{IDF/HOMA\text{-}IR}$

Table 5.1 ^{1}H-NMR chemical shifts (δ in ppm) of low molecular weight plasma and urine metabolites and their J-coupling constants (in Hz)

Table 5.2 Start and end values (in ppm) of the 110 fixed integration regions for plasma (plasma variables: VAR_{PL}) as well as their contributing metabolites, defined on the basis of metabolite spiking experiments

Table 5.3 Start and end values (in ppm) of the 134 fixed integration regions for urine (urine variables: VAR_{UR}) as well as their contributing metabolites, defined on the basis of metabolite spiking experiments

Table 5.4 Subject characteristics of the case-control training and validation cohorts used to evaluate the analysis procedure for plasma

Table 5.5 Subject characteristics of the case-control training and validation cohorts used to evaluate the analysis procedure for urine

Table 5.6 Overview of the number of noisy variables obtained for each defined CV for the reference and obese plasma sample

Table 5.7 The number of LV, the total explained variation in X and Y (R^2X(cum) and R^2Y(cum)), predictive ability (Q^2(cum)), and sensitivity and specificity for

OPLS-DA models constructed for the training and validation cohort of the plasma study with a decreasing number of variables

Table 5.8 Overview of the number of noisy variables obtained for each defined CV for the reference and obese urine sample

Table 5.9 The number of latent variables (LV), the total explained variation in X and Y ($R^2X(cum)$ and $R^2Y(cum)$), predictive ability ($Q^2(cum)$), and sensitivity and specificity for OPLS-DA models constructed for the training and validation cohort of the urine study with a decreasing number of variables

Table 6.1 SPREC annotation for preanalytical conditions tested in plasma samples by ^{1}H-NMR spectroscopy

Table 7.1 Descriptive characteristics of the study population

Table 7.2 Multivariate model characteristics (OPLS-DA and ROC analyses) of the plasma ^{1}H-NMR dataset consisting of 61 OB and 36 NW subjects presented according to a decreasing threshold limit for coefficient of variation

Table 7.3 Plasma variables that contributed most to the discrimination between OB and NW subjects with a VIP higher than 1, ranked from strongest to least strong discriminatory power

Table 7.4 Relative concentrations of VAR_{PL} differing between OB and NW children

Table 7.5 Descriptive characteristics of MHO and MUO children and adolescents

Table 7.6 Plasma variables that contributed most to the discrimination between MHO and MUO subjects with a VIP higher than 1, ranked from strongest to least strong discriminatory power

Table 7.7 Relative concentrations of VAR_{PL} differing between MHO and MUO children

Table 7.8 Clinical and biochemical characteristics of MHO and MUO children and adolescents

Table 7.9 Spearman correlations between triglyceride levels and VAR_{PL} discriminating most between MHO and MUO

List of Abbreviations

1D	one dimensional
2D	two dimensional
^{1}H-NMR	proton nuclear magnetic resonance
AGT	angiotensinogen
Ala	alanine
ALT	alanine transaminase
ANOVA	analysis of variance
ANCOVA	analysis of covariance
Arg	arginine
Asn	asparagine
Asp	aspartate
ASP	acylation stimulating protein
AST	aspartate transaminase
ATP	adenosine triphosphate
ATPIII	Adult Treatment Panel III
AUC	area under the curve
AUROC	receiver operating characteristic
BCAA	branched chain amino acids
BIA	bioelectrical impedance analysis
BMI	body mass index
BMI SDS	body mass index standard deviation score
BP	blood pressure
CDC	Centers for Disease Control and Prevention
cDI	clamp disposition index
CETP	cholesterol ester transfer protein
ChEBI	chemical entities of biological interest
CI	confidence interval
CPMG	Carr-Purcell-Meiboom-Gill
CV	coefficient of variation
CVD	cardiovascular disease
Cys	cysteine
d	doublet
D_2O	deuterium oxide
DBP	diastolic blood pressure
dd	double doublet
DEXA	dual-energy X-ray absorptiometry
DI	disposition index
DMA	dimethylamine
DModX	distance to model
DNA	deoxyribonucleic acid
dq	double quadriplet
EDTA	ethylenediaminetetraacetic acid
FDA	Food and Drug Administration
FFA	free fatty acids
FGIR	fasting glucose-to-insulin ratio
FID	free induction decay
FPG	fasting plasma glucose
FSIVGTT	frequently sampled intravenous glucose tolerance test
GC	gas chromatography
g-GT	gamma glutamyl transpeptidase
Gln	glutamine
GSD	geometric standard deviation
Glu	glutamate
Gly	glycine
HbA1c	hemoglobin A1c

HCl	hydrogen chloride
HDL-C	high-density lipoprotein cholesterol
His	histidine
HOMA-IR	homeostatic model assessment of insulin resistance
HPLC	high performance liquid chromatography
HSD	hydroxysteroid dehydrogenase
IDF	International Diabetes Federation
IFG	impaired fasting glucose
IGF	insulin-like growth factor
IGI	insulinogenic index
IGT	impaired glucose tolerance
IL	interleukin
Ile	isoleucine
IOTF	International Obesity Task Force
IR	insulin resistance
IRI	immuno-reactive insulin
IUB	International Union of Biochemistry
IUPAC	International Union of Pure and Applied Chemistry
LC	liquid chromatography
LDL-C	low-density lipoprotein cholesterol
LiHe	lithium heparin
LMS	lambda (skewness); mu (median); sigma (CV)
LPL	lipoprotein lipase
Leu	leucine
LN	liquid nitrogen
LV	latent variable
Lys	lysine
m	multiplet
MAS	magic angle spinning
MCP	monocyte chemoattractant protein
Met	methionine
MetS	metabolic syndrome
MHO	metabolically healthy obesity
MHz	megahertz
MI	myo-inositol
MR	metabolic risk
MS	mass spectrometry
MUO	metabolically unhealthy obesity
NA	not available
NAD	nicotinamide adenine dinucleotide
NAG	N-acetyl glycoproteins
NaOH	sodium hydroxide
NCEP	National Cholesterol Education Program
NEFA	non-esterified fatty acids
NGT	normal glucose tolerance
NI	non-identified
NW	normal-weight
OB	overweight and obese
oDI	oral disposition index
OGTT	oral glucose tolerance test
OPLS-DA	orthogonal PLS discriminant analysis
p	pentaplet
PAI	plasminogen activated inhibitor
PC	principal component
PC	phosphatidylcholine
PCA	principal component analysis
Phe	phenylalanine
PL	phospholipids

PLS	partial least squares projection to latent structures
ppm	parts per million
Pro	proline
q	quadriplet
QUICKI	quantitative insulin-sensitivity check index
RBP	retinol-binding protein
RF	radiofrequency
RNA	ribonucleic acid
ROCCET	receiver operating characteristic curve explorer and tester
RT	room temperature
s	singlet
S/N	signal-noise ratio
SBP	systolic blood pressure
SD	standard deviation
Ser	serine
SHBG	sex hormone-binding globulin
SM	sphingomyelin
SOP	standard operating procedure
SPREC	Standard PREanalytical Code
t	triplet
T2DM	type 2 diabetes mellitus
TCA	tricarboxylic acid
TG	triglycerides
Thr	threonine
TMAO	trimethylamine N-oxide
TNF	tumor necrosis factor
Trp	tryptophan
TSP	trimethylsilyl propanoic acid
Tyr	tyrosine
UA	uric acid
UBiLim	University Biobank of Limburg
UPLC-MS	ultra-performance liquid chromatography mass spectrometry
UV	unit variance
Val	valine
VAR	variable
VAR_{PL}	plasma variable
VAR_{UR}	urine variable
VIP	variable importance on projection
VLDL-C	very low density lipoprotein cholesterol
WBC	white blood cell
WBISI	whole body insulin sensitivity index
WC	waist circumference
WHO	World Health Organization

Chapter 1

General introduction and aims

1.1 Childhood obesity and the metabolic syndrome

In the past few decades, the number of overweight and obese children and adolescents has increased substantially [1, 2]. Although recent evidence suggest that the prevalence of childhood obesity is plateauing in some countries [3], prevalence rates are still high and are currently increasing in developing countries [4]. In addition, obese children are becoming more extremely obese [5]. Overweight and obese children are at increased risk to develop cardiometabolic morbidities in adult life such as type 2 diabetes (T2DM), hypertension, coronary heart disease and stroke [6]. A concept commonly used in describing the relationship between obesity and cardiometabolic complications is that of the metabolic syndrome (MetS). Theoretically, the MetS is a cluster of cardiometabolic risk factors including centrally distributed obesity, dyslipidemia, insulin resistance (IR), glucose intolerance (impaired fasting glycaemia, impaired glucose tolerance or T2DM) and elevated blood pressure thought to place an individual at increased risk for developing cardiovascular diseases (CVD) [7]. Childhood obesity may consequently lead to a reduced quality of life and reduced life expectancy of the current generation, and a substantial increase in healthcare and economic costs [8, 9].

1.1.1 Epidemiology

The worldwide prevalence of overweight and obesity in both adults and youth has increased substantially between 1980 and 2013 [2]. In developing countries, the number of children and adolescents being overweight or obese has also increased, i.e. 12.9% of boys and 13.4% of girls were overweight or obese in 2013, compared with 8.1% of boys and 8.4% of girls in 1980 [2]. The prevalence of childhood obesity is still rising in Latin America (Mexico, Brazil, Chile, Uruguay and Argentina), North Africa, the Middle East, India, and several Pacific Island and Caribbean nations [2, 4]. Although recent evidence has shown that the prevalence of childhood obesity is plateauing in some developed countries, prevalence rates remain high and obese children are becoming more severely obese [3, 5, 10]. In developed countries, 23.8% of boys and 22.6% of girls were overweight or obese in 2013, compared with 16.9% of boys and 16.2% of girls in 1980 [2]. Prevalence numbers of obesity are high in the United States of America (USA), i.e. around 12.5 million (16.9%) children aged 2 to 19

were obese in 2009-2010 [11]. In Europe, recent school-based survey among 10 to 12 year old children showed that 25.8% of boys and 21.8% of girls were overweight of which 5.4% boys and 4.1% girls were obese in 2010 [12]. In the Flemish part of Belgium, 13.2% boys and 11.2% girls aged 10 to 12 were overweight and 3.7% boys and 2.3% girls were obese [12]. In the province Limburg, it was estimated that 33% of children aged 12 to 13 was overweight and 19% was obese in 2002 [13].

In parallel with the increased prevalence of childhood obesity, the prevalence of MetS children and adolescents has also increased [14]. Important to note, however, the prevalence of MetS varies widely and depends strongly on the definition used, i.e. whether insulin resistance (IR) or central obesity are central to the MetS classification and whether and which child-specific cut-off values for MetS components are used [15, 16]. In general, MetS prevalence is higher in boys than in girls, higher in pubertal than in pre-pubertal children, higher in Hispanics than in whites or African-Americans, and higher in obese than in normal-weight children [17]. Table 1.1 gives an overview of prevalence numbers of MetS in 7 to 19-year-old children and adolescents from different geographical areas using three most commonly used MetS classifications, i.e. NCEP/ATPIII, WHO and IDF (see Table 1.2 and Table 1.3 for more information on the definitions used).

Table 1.1 Prevalence data of MetS in 7 to 19-year-old children from different geographical areas based on most commonly used criteria.

Region		NCEP/ATPIII	WHO	IDF
Europe	median prevalence in whole population, % (range)	2.1 (0.3-13.9)	6.0*	2.2 (0.3-5.0)
	median prevalence in OV and OB, % (range)	35.3 (16.9-45.5)	28.2 (23.3-39.0)	21.0 (8.9-50.0)
Middle East	median prevalence in whole population, % (range)	6.5 (0.4-10.1)	NA	6.8 (2.3-14.8)
	median prevalence in OV and OB, % (range)	25.5 (9.1-57.9)	27.2 (6.6-38.8)	35.6 (34.2-37.0)
Far East	median prevalence in whole population, % (range)	3.3 (0.2-7.3)	NA	3.1 (1.8-5.5)
	median prevalence in OV and OB, % (range)	21.8 (10.0-38.1)	42.3*	13.8 (3.2-24.3)
America	median prevalence in whole population, % (range)	4.8 (1.0-10.0)	1.2 (0.4-1.9)	2.6 (1.6-9.6)
	median prevalence in OV and OB, % (range)	25.8 (13.8-66.0)	38.7 (5.2-38.9)	15.3 (9.6-21.0)
Australia	median prevalence in whole population, %	14.0*	NA	NA
	median prevalence in OV and OB, %	NA	33.0*	NA

The presented data have been calculated from data obtained from several studies as described in a literature review by Friend et al. [18]. *Prevalence number obtained from only one study. IDF: International Diabetes Federation; NA: not available; NCEP/ATPIII: National Cholesterol Education Program's Adult Treatment Panel III; OB: obese; OV: overweight; WHO: World Health Organization.

1.1.2 Definition of childhood obesity

Obesity is defined as an excessive amount of body fat (adiposity) to such extent that health may be impaired [19]. The ideal definition of obesity would be one based on the measurement of absolute fat mass or percentage total body fat. Underwater weighing or dual energy X-ray absorptiometry (DEXA) are accurate and direct measures of body fat, however, they are impracticable and too expensive to apply in routine clinical practice [20]. The indirect bioelectrical impedance analysis (BIA) is less expensive, safe, portable and more comfortable for the patient than the other fatness measurements [21]. BIA measures the resistance to an electrical current that travels through water in the body. The more fat, the more resistance to the electrical current [22]. A number of child-specific equations has been proposed to calculate percent fat mass or fat-free mass from BIA output [23, 24]. The Schaefer equation is suggested to be the most valid predictor of percent fat mass, fat mass and fat-free mass in overweight and obese children aged 5 to 9 [23, 25]. However, up to now, there is still no single BIA equation that can be applied for both children and adolescents because of pubertal influences resulting in poor accuracy [26]. Another way to measure fatness in children are skinfolds, however, evidence about the accuracy of skinfold thicknesses to identify children with excess body fatness is contradictory [27, 28].

The use of another simpler proxy measurement of excessive fatness is often preferred. The most commonly used, widely accepted, inexpensive and non-invasive indicator to express the level of adiposity is the body mass index (BMI). The BMI is a simple, indirect measure obtained by dividing weight in kilogram by the square of height in meters (kg/m²). It was first described by the Belgian mathematician, astronomer and statistician Adolphe Quételet and has therefore also been referred to as the Quetelet's index [29]. Adults (≥ 18 years) with a BMI ≥ 25 kg/m² are classified as overweight and those with a BMI ≥ 30 kg/m² are classified as obese [30]. Although BMI is closely correlated with fat mass in adults and children [31, 32], assessing adiposity in children and adolescents is more complicated as a child's fat mass changes as a consequence of age, gender, maturation and ethnicity [33]. So instead of using fixed BMI values as for adults, the definition of childhood overweight and obesity is based on age- and sex-specific BMI cut-off values – presented in tables or pointed out as

centiles on a chart – which are generally derived from large national or international reference populations.

National BMI references

In Flanders, the northern part of Belgium, the Flemish growth charts provide centile curves for BMI for Belgian children aged 2 to 20 [34] (see Figure 1.1). They were obtained based on weight and height data of 16096 (7920 boys and 8176 girls) Flemish children and adolescents collected between 2001 and 2004. The growth curves were fitted using the LMS (L: skewness, M: median, and S: coefficient of variation) method [35]. The Flemish growth charts are recommended for population monitoring and clinical assessment of overweight (percentile crossing BMI 25 kg/m² at age 18) and obesity (percentile crossing BMI 30 kg/m² at age 18) in Flemish children and adolescents.

International BMI references

For international comparison of obesity prevalence or for presenting overweight and obesity data of children in international journals, the International Obesity Task Force (IOTF) reference values are preferred [36, 37]. The IOTF BMI thresholds are derived from six large nationally representative cross-sectional surveys from Great Britain, USA, the Netherlands, Brazil, Singapore and Hong Kong. Each national data set had BMI data from over 10000 children aged 2 to 18, and collected between 1963 and 1993. Subsequently, BMI values were averaged across countries by age to give sex-specific BMI curves passing through BMI 25 (overweight), 30 (obesity) and 35 (morbid obesity) at age 18 [36, 37]. Besides centiles, age- and gender-specific BMI z scores could also be calculated using a formula based on the LMS method [37]. The BMI z score represents the number of standard deviation (SD) units a child's measurement is located above or below the mean reference value derived from the survey. The pediatric IOTF BMI cut-offs correspond to adult BMI thresholds, and can consequently be used to predict adult disease risk [37].

Besides the IOTF BMI cut-off values, the WHO also provides BMI references for children aged 5 to 19 [38], and the Centers for Disease Control and Prevention (CDC) provides BMI references for children aged 2 to 20 [39].

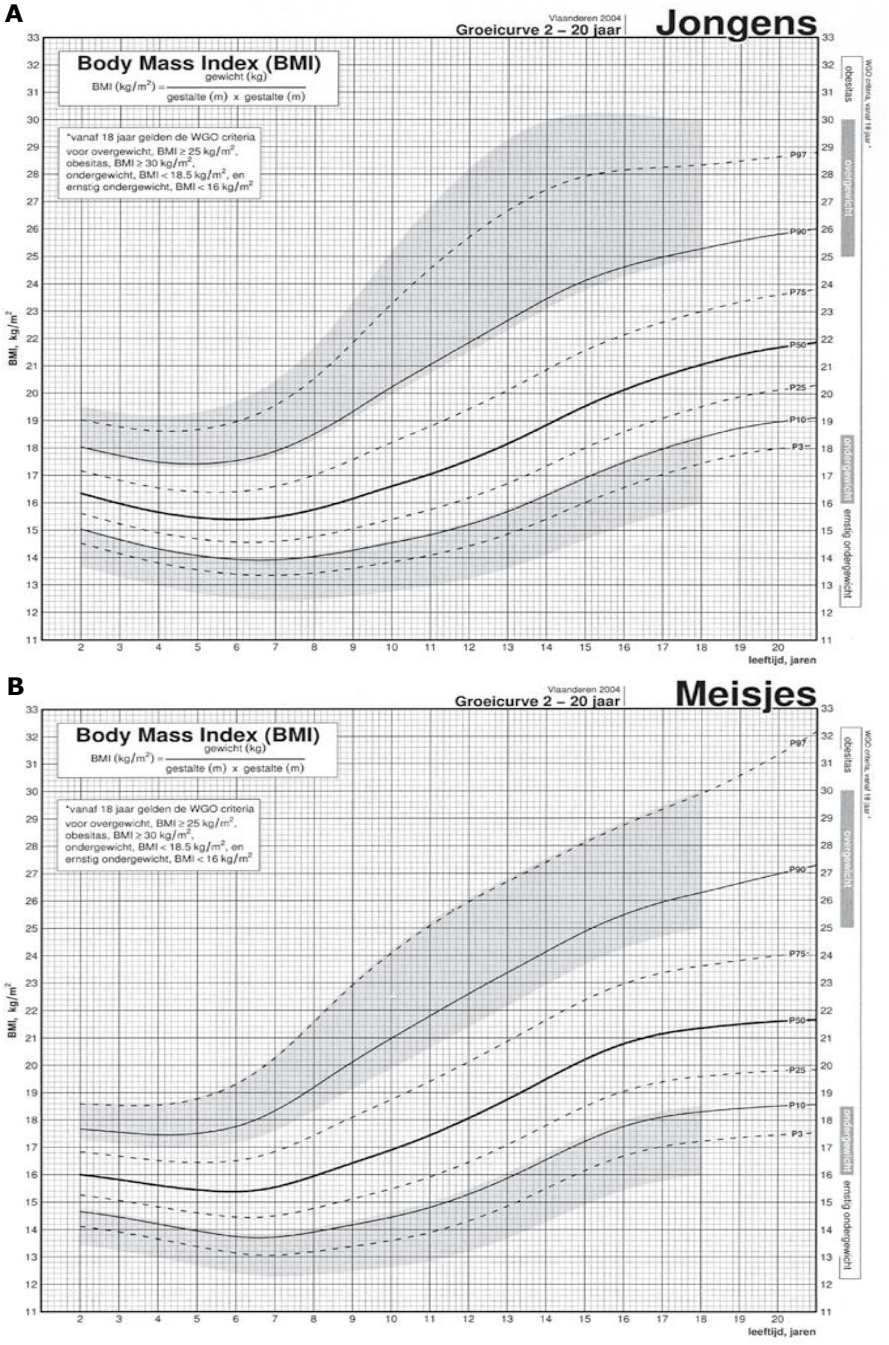

Figure 1.1 Flemish reference centiles of BMI-for-age for (A) boys and (B) girls. Percentiles that cross a BMI value of 25 and 30 kg/m² at age 18 are presented as age-specific reference values for overweight and obesity, respectively. Children with a BMI in the upper grey zone are classified as overweight. Children with a BMI above the upper grey zone are classified as obese. Reprinted with permission from Roelants et al. [34].

However, these reference values are derived from national data based on USA surveys from the early 1960s, before the present epidemic, and are therefore unsuitable for international and comparative purposes.

Current issues regarding the use of BMI in the obese pediatric population

Because of the wide variety of definitions for childhood obesity, there is still no widely accepted standard. The BMI is an easy indicator of weight status, however, many countries continue to use their own country-specific charts. In addition, the BMI is limited to distinguish between fat mass, fat-free tissue, muscles and bone and fails to account for fat distribution. It is known that centrally distributed or abdominal adiposity is a risk factor for IR and cardiometabolic disease in childhood, and therefore the measurement of waist circumference (WC) is often preferred instead of BMI [40-42]. However, there are still no universally validated WC cut off points available to identify children with centrally-distributed obesity and specific guidelines for clinical application are lacking [43].

1.1.3 Definition of the metabolic syndrome

The concept of MetS was initially established in 1988 by Reaven who called it 'Syndrome X', a constellation of factors including IR, impaired glucose tolerance, dyslipidemia which are associated with an increased risk for coronary artery disease [44]. In the meanwhile, both the terminology and definition of MetS have undergone a lot of changes in the medical literature. Nowadays, MetS is defined as the clustering of cardiometabolic risk factors including centrally distributed obesity, atherogenic dyslipidemia, elevated blood pressure, hyperglycemia, IR, pro-inflammatory and pro-thrombotic state which are associated with an increased risk of developing CVD and T2DM [7]. Although a general consensus regarding the MetS definition is still lacking, several international organizations and expert groups such as the WHO [45], NCEP/ATPIII [46], and IDF [47] attempted to introduce new definitions for adults (Table 1.2). These definitions include either 'centrally distributed obesity' or 'IR' as most important factor because they play a key role in the pathogenesis

of MetS [7]. The presence of MetS is not only limited to adulthood but has previously also been identified in children and adolescents [14, 48].

Definition of the metabolic syndrome in children and adolescents

Starting from 2003, over 40 unique pediatric definitions of MetS were published of which the most commonly used were that developed by NCEP/ATPIII, WHO and IDF based on modified criteria from adult definitions [49] (see Table 1.3 and Table 1.4). In an attempt to halt the explosion of different definitions, the IDF published the first consensus-based pediatric definition of MetS in 2007 [50] (Table 1.4). The pediatric IDF MetS definition divides subjects into three different age groups in order to adjust for the developmental stages.

All criteria – except for waist circumference – are expressed as fixed cut-off values instead of age- and sex-specific percentiles which makes this definition easy to use. However, for children younger than 10 years there are still no established values for the diagnosis of MetS. In addition, prevalence estimates of MetS in children using pediatric IDF criteria could be an underestimation as cut-off values used to define adult MetS are too high, although in adolescents it is more appropriate to have cut points that are based on adult health risk [16, 51, 52]. For overweight and obese children, the pediatric IDF definition appears to be more stringent than the adapted-NCEP definition [53]. Whether the pediatric IDF definition will lead to a uniformity remains to be seen. Regardless of an increased use of the IDF MetS definition, there is still no valid definition for the pediatric population. This is mainly due to several important methodological and physiological limitations which are discussed below.

Table 1.2 Classification of MetS in adults according to the WHO [4], NCEP/ATPIII [2], and IDF [3].

Definition	Number of criteria	Obesity (WC or BMI)	Dyslipidemia		Hypertension	Hyperglycemia	Other components
			TG	HDL-C			
WHO (1998)	IR as defined by T2DM, IFG or IGT plus 2 other components	Waist-to-Hip ratio: ♂ > 0.9 cm ♀ > 0.85 cm or BMI > 30 kg/m^2	≥ 150 mg/dl	♂ < 35 mg/dl ♀ < 39 mg/dl	≥ 140/90 mm Hg		Microalbuminuria (urinary albumin secretion rate ≥ 20 µg/min or albumin-to-creatinine ratio ≥ 30 mg/g)
NCEP/ATPIII (2001)	≥ 3	WC: ♂ > 102 cm ♀ > 88 cm	≥ 150 mg/dl	♂ < 40 mg/dl ♀ < 50 mg/dl	≥ 130/85 mm Hg	FPG ≥ 110 mg/dl	
IDF (2005)	Central obesity plus 2 other components	WC (but can be assumed if BMI > 30 kg/m^2) with ethnicity-specific values*	≥ 150 mg/dl	♂ < 40 mg/dl ♀ < 50 mg/dl	≥ 130/85 mm Hg	FPG ≥ 100 mg/dl	

BMI: body mass index; FPG: fasting plasma glucose; HDL-C: high-density lipoprotein cholesterol; IDF: International Diabetes Federation; IFG: impaired fasting glucose; IGT: impaired glucose tolerance; IR: insulin resistance; MetS: metabolic syndrome; NCEP/ATP III: National Cholesterol Education Program Adult Treatment Panel; T2DM: type 2 diabetes mellitus; TG: triglycerides; WC: waist circumference; WHO: World Health Organization. *To meet the criteria, WC must be: for Europeans, ♂ > 94 cm and ♀ > 80 cm; and for South Asians, Chinese, and Japanese, ♂ > 90 cm and ♀ > 80 cm. For ethnic South and Central Americans, South Asian data are used, and for sub-Saharan Africans and Eastern Mediterranean and Middle East (Arab) populations, European data are used.

Table 1.3 Classification of MetS in children and adolescents according to modified criteria developed by the WHO [4] and NCEP/ATPIII [2].

Definition	Number of criteria	Obesity (WC or BMI)	Dyslipidemia		Hypertension	Hyperglycemia
			TG	HDL-C		
WHO (1998)	IR as defined by T2DM, IFG or IGT plus 2 other components	> 95th or 97th centile for WC or BMI	> 95th centile	< 5th centile	> 95th centile	FPG ≥ 110 mg/dl
NCEP/ATPIII (2001)	≥ 3	Age-specific criteria (sometimes stated waist circumference 85–97th centile, BMI 75th–95th centile)	Age-specific criteria (sometimes stated > 90th or 95th centile)	Age-specific criteria (sometimes stated < 5th or 10th centile)	Age-specific criteria (sometimes stated > 90th or 95th centile)	Age-specific criteria

BMI: body mass index; FPG: fasting plasma glucose; HDL-C: high-density lipoprotein cholesterol; IFG: impaired fasting glucose; IGT: impaired glucose tolerance; IR: insulin resistance; MetS: metabolic syndrome; NCEP/ATP III: National Cholesterol Education Program Adult Treatment Panel; T2DM: type 2 diabetes mellitus; TG: triglycerides; WC: waist circumference; WHO: World Health Organization.

Table 1.4 IDF criteria for MetS in children and adolescents aged 6 to 18 [50].

Age group (years)	Obesity (WC)	Dyslipidemia		Hypertension	Hyperglycemia
		TG	HDL-C		
6 – <10[§]	≥ 90th percentile	No set value for diagnosis MetS	No set value for diagnosis MetS	No set value for diagnosis MetS	No set value for diagnosis MetS
10 – <16	≥ 90th percentile or adult cut-off if lower	≥ 150 mg/dl	< 40 mg/dl	SBP ≥ 130 or DBP ≥ 85 mm Hg	FPG ≥ 100 mg/dl[**] or known T2DM
16+ (adult criteria)	WC ≥ 94 cm for Europid males and ≥ 80 cm for Europid females, with ethnic-specific values for other groups[*]	≥ 150 mg/dl or specific treatment for high TG	♂ < 40 mg/dl ♀ < 50 mg/dl, or specific treatment for low HDL-C	SBP ≥ 130 or DBP ≥ 85 mm Hg or treatment of previously diagnosed hypertension	FPG ≥ 100 mg/dl[**] or known T2DM

Diagnosing the MetS requires the presence of central obesity plus any two of the other four factors. [**]For clinical purposes, but not for diagnosing the MetS, if FPG 100-125 mg/dl or known T2DM, an oral glucose tolerance test should be performed. BP: blood pressure; DBP: diastolic blood pressure; FPG: fasting plasma glucose; HDL-C: high-density lipoprotein cholesterol; IDF: International Diabetes Federation; MetS: metabolic syndrome; SBP: systolic blood pressure; T2DM: type 2 diabetes mellitus; TG: triglycerides; WC: waist circumference. [*]For those of South and South-East Asian, Japanese, and ethnic South and Central American origin, the cut-offs should be ≥ 90 cm for men, and ≥ 80 cm for women. The IDF Consensus group recognize that there are ethnic, gender and age differences but research is still needed on outcomes to establish risk. [§]MetS cannot be diagnosed, but further measurements should be made if there is a family history of metabolic syndrome, T2DM, dyslipidemia, cardiovascular disease, hypertension and/or obesity.

Current issues regarding the definition of pediatric metabolic syndrome

In contrast to the adult MetS definition, individual components of the pediatric MetS definition are only moderate quantitatively. Unlike adults, children undergo different stages of growth and pubertal development and therefore, age-, sex-, puberty and/or height specific normal values (or percentiles) are generally used in the definition of MetS. However, these values are mostly population-specific resulting in inconsistent MetS definitions across countries that could complicate the comparison of study findings. In addition, reference values for some MetS components are not always available for a specific study population and using MetS definitions based on percentiles is more cumbersome than using fixed cut-off values.

IR has been suggested to play a major role in the development of MetS, CVD and T2DM [54]. However, IR is rarely included in pediatric MetS definitions which may result in the underdiagnosis of obese children and adolescents at increased metabolic risk [55]. The term IR in itself is problematic as there is no definitive test for its measurement. The two most commonly used techniques to accurately measure insulin sensitivity are the euglycemic hyperinsulinemic clamp technique (gold standard) [56] and the frequently sampled intravenous glucose tolerance test (FSIVGTT) [57]. However, these tests are complex, burdensome, expensive and used for research purposes only. Alternatively, an OGTT can be performed which is less invasive, less expensive and can be easily applied in clinic [58]. OGTT-derived indices can be calculated based on glucose and insulin values obtained after the glucose load. The measurement of fasting glucose or insulin is more convenient for the patient and is less costly than performing a clamp or OGTT. Fasting glucose and fasting insulin can be used to evaluate children and adolescents for impaired fasting glucose and fasting hyperinsulinemia, respectively. Fasting insulin shows a good correlation with the euglycemic hyperinsulinemic clamp in obese children [59, 60]. Indices based on fasting glucose and insulin values such as the homeostatic model assessment for insulin resistance (HOMA-IR), quantitative insulin-sensitivity check index (QUICKI) or fasting glucose-to-insulin ratio (FGIR) have proven to be reliable to use as estimates of insulin sensitivity in obese children and adolescents [61, 62]. HOMA-IR has been widely used in clinical and epidemiological research to

assess the level of insulin resistance [63, 64]. However, reports about the validity of HOMA-IR in obese children and adolescents are contradictory [61, 62, 65-67]. Obese children generally have higher fasting insulin levels and insulin resistance (as calculated by HOMA-IR) compared with their lean counterparts [68]. The whole body insulin sensitivity index (WBISI) based on glucose and insulin response values has also been proven to be a valid estimate of insulin sensitivity in obese youth [65]. Obese children and adolescents with impaired glucose tolerance have lower WBISI values compared to normal glucose tolerant individuals [69]. The disposition index (DI) can also be calculated from glucose and insulin response values obtained during an OGTT and reflects the β-cell function relative to insulin sensitivity [70]. The DI obtained during a euglycemic hyperinsulinemic clamp correlated well with that obtained during an OGTT in obese adolescents who were categorized by varying degrees of glucose tolerance [70]. In addition, obese adolescents with normal glucose tolerance but with 2-hour glucose levels in the higher range show reduced DI levels indicating an increased risk for future impaired glucose tolerance (IGT) [71]. Nonetheless, the use of different insulin assays between different laboratories [72], and the lack of normal ranges for insulin concentration through childhood [73] complicates the inclusion of IR in the pediatric MetS definitions. Although efforts were recently made to establish pediatric reference values for insulin [74, 75], longitudinal follow-up studies to relate definitions of IR to long-term outcomes are still lacking. Especially in obese children and adolescents, it is still unclear how to adequately define IR [76]. At present, there exist no specific laboratory screening tests for insulin resistance in children. Laboratory results for children are often extrapolated from adult diagnostic values, i.e. fasting insulin greater than 15 μU/ml or insulin peak levels of more than 150 μU/ml during OGTT, and/or more than 75 μU/ml at 120 min of OGTT infer IR [77]. For obese children and adolescents, the most commonly used parameters to define IR are the sum of insulin levels during an OGTT exceeding 300 μU/ml [78], a HOMA-IR greater than 3.16, a ratio fasting glucose/insulin lower than 7 or a QUICKI lower than 0.34 [61]. Nonetheless, reference and cut-off values of plasma insulin measured with any of the described methods still need to be satisfactorily established for children, including obese individuals.

The physiological increase in IR during puberty further complicates the establishment of MetS criteria in pediatrics. It has previously been shown that children with MetS show pronounced changes in MetS components before the onset of puberty and these changes worsen during puberty [79]. Indeed, pubertal transition is a crucial period in which rapid and dynamic changes in an individual's metabolism occur and therefore it is an additional risk factor for the development of IR, IGT and potentially future T2DM [80]. The most utilized staging system to define pubertal maturation is that published by Marshall and Tanner, and is commonly referred to as "Tanner stages" [81, 82]. In a normal physiological response, insulin sensitivity is recovered in post-pubertal Tanner V stage [83]. However, obese adolescents in a later maturation stage (Tanner III-V) show a blunted beta-cell compensation and are failing to recover from pubertal IR [84]. Therefore, pubertal IR in obese adolescents can act as a 'trigger' of the progression to T2DM.

Ethnicity-specific MetS definitions may also be needed, because MetS manifests differently among different ethnicities. Several studies have shown that Caucasian children are more insulin sensitive and have a better insulin secretory pattern compared with African-American children, which is mainly ascribed to genetic differences [85, 86]. Weiss et al. even demonstrated that an African-American background is one of the key predictors of developing T2DM [69]. Although African-American children have higher rates of IR, which is known to be associated with dyslipidemia [87], they have lower triglycerides (TG) and higher high-density lipoprotein cholesterol (HDL-C) levels compared with Caucasians [88]. Important to note is that this lipid profile does not lower their risk for T2DM or CVD [89]. Nonetheless, African-American adolescents are possibly underdiagnosed with MetS using current criteria [90]. Therefore, Fitzpatrick et al. recently developed a plausible model of the MetS specific to African American adolescents [90].

1.1.4 Causes and consequences

The etiology of obesity is multifactorial, exceedingly complex and, to date, not fully understood. It is generally accepted that the major cause of childhood obesity is an imbalance between energy intake from diet and energy expenditure from metabolism, growth and physical activity [91]. The overconsumption of fat-, sugar- and salt-rich food and sweetened beverages is a

substantial feature in the development of childhood obesity [92]. In addition, larger portion sizes, increased snacking, less regular eating patterns and shorter meals are speculated to contribute to its development [93]. Newborns who are formula-fed are more susceptible to develop obesity later in life compared to infants who are breastfed [94]. Also the increase in car transport and electronic devices, and the fact that children are less playing outside has a substantial impact on increasing obesity rates [95]. Obesity caused by monogenetic mutations is rare, however, it is postulated that polygenetic mutations (i.e. common genetic variants) contribute for 40 to 70% to the heritability of common obesity [96]. Besides that, biological (e.g. endocrine disorders such as hypothyroidism), iatrogenic (e.g. use of antipsychotics), psychosocial (e.g. low self-esteem, learning problems and social status) and "non-traditional" environmental factors (e.g. poor sleep quality, gut microbiota and environmental chemicals) have also been suggested to contribute to the development of childhood obesity [33].

The presence of MetS appears to be explained ~10% by genetic susceptibility and ~90% to changes in the environment and/or to epigenetic interactions with potential for hereditary imprinting [97]. Especially dietary substances such as trans-unsaturated fatty acids, branched-chain amino acids, ethanol and fructose seem to play a major role in the development of MetS [97, 98]. However, the exact mechanisms remain undiscovered.

In general, obese children are at increased risk for developing MetS, T2DM, premature coronary artery disease, some types of cancer, orthopedic problems, depression, anxiety disorders, underachievement in school, lower self-esteem, sleep-disordered breathing, early puberty, skin infections, respiratory problems and adult obesity [99]. Children with MetS, who can also be lean, are at increased risk to develop chronic low-grade inflammation, oxidative stress, hyperuricemia, hyperandrogenism, polycystic ovary syndrome, non-alcohol fatty liver disease, impaired glucose tolerance, obstructive sleep apnea, hypogonadism, vascular dementia, and certain forms of cancer, T2DM and CVD [98].

1.1.5 Pathophysiology

Despite the progress in research of pathophysiological mechanisms of the MetS, it has been poorly investigated in the pediatric population. The two key

metabolic indicators of MetS are obesity and IR. Obesity is closely related with the manifestation of visceral fat and IR and therefore plays a central role in the pathophysiology of and predisposition to endocrine disorders such as the MetS, CVD and/or T2DM [100] (see Figure 1.2).

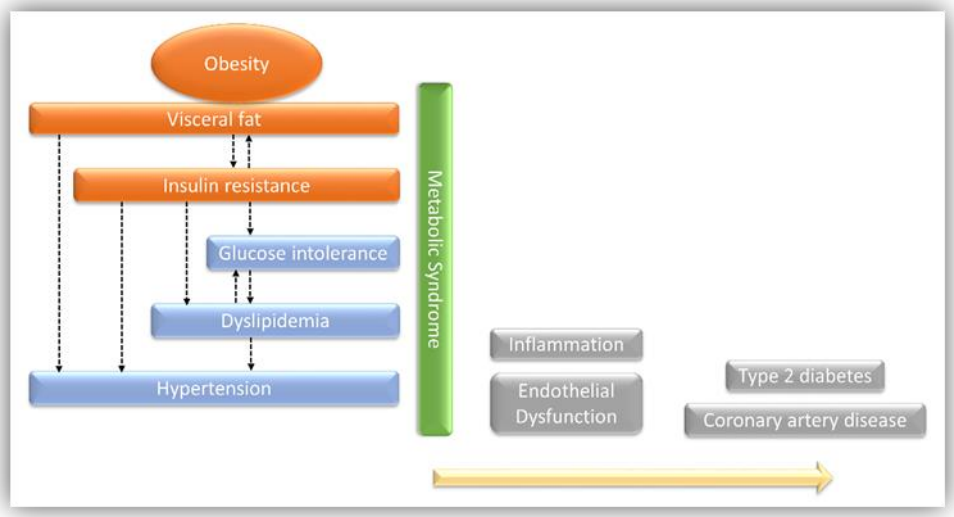

Figure 1.2 Model of the MetS and its presumed precursors and consequences. Visceral fat and insulin resistance (IR) are key factors of the MetS, and together with the presence of impaired glucose tolerance, dyslipidemia and hypertension they constitute the full spectrum of MetS. Individuals with MetS are at increased risk for inflammation and endothelial dysfunction eventually developing in T2DM and/or coronary artery disease [89].

Fat as an endocrine organ

Adipose tissue – consisting of white (most prevalent and site of energy storage) and brown (mainly in neonates and role in thermogenesis) adipose tissue – is made up of adipocytes, pre-adipocytes, endothelial cells, fibroblasts, leukocytes and macrophages [101]. The primary function of adipose tissue is energy storage, i.e. it stores excess nutrients as TG and releases free fatty acids (FFA) during fasting [102]. In addition, adipose tissue is characterized as an endocrine organ secreting many hormones and adipocytokines – both locally (autocrine or paracrine) and systemically (endocrine) – that have various functions (see Figure 1.3) [103, 104].

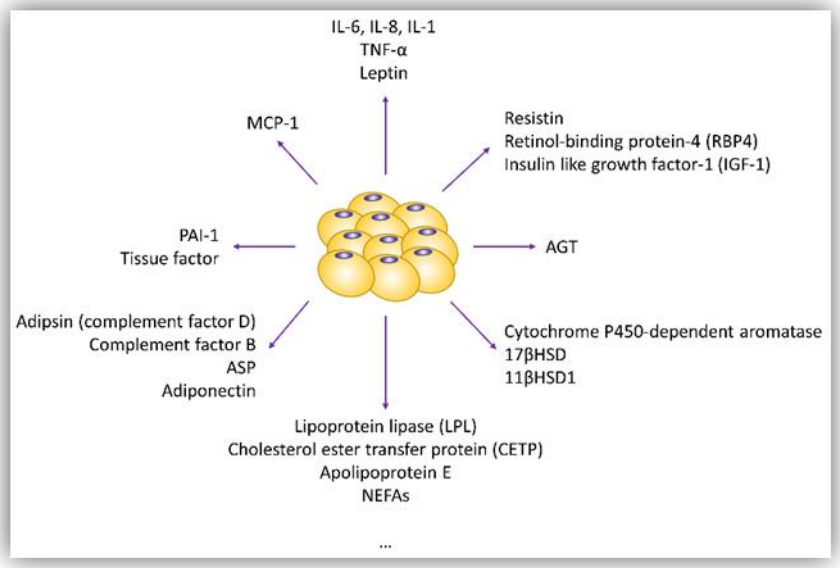

Figure 1.3 Adipose tissue as an endocrine organ. Adipose tissue secretes a number of hormones and adipocytokines with various endocrine functions. AGT: angiotensinogen; ASP: acylation stimulating protein; CETP: cholesterol ester transfer protein; HSD: hydroxysteroid dehydrogenase; IGF: insulin-like growth factor; IL: interleukin; LPL: lipoprotein lipase; MCP: monocyte chemoattractant protein; NEFA: non-esterified fatty acids; PAI: plasminogen activated inhibitor; RBP: retinol-binding protein; TNF: tumor necrosis factor [103, 104].

Obesity or adiposity is characterized by a high adipocyte size (hypertrophy), high adipocyte number (hyperplasia), and the release of pro-inflammatory cytokines (e.g. TNF-α and IL-6) and chemokines secreted by adipose tissue that induce the recruitment of 'classically activated' adipose tissue macrophages (that are not observed in lean adipose tissue) from the blood circulation [105]. This results in an increased release of FFA and dysregulated secretion of leptin, adiponectin, resistin and RBP4 which further exacerbate adipose tissue inflammation [104] (Figure 1.4). Consequently, this leads to an increased food intake, reduced energy expenditure, and increased hepatic glucose production through actions in the hypothalamus. In addition, inflammation, ectopic fat accumulation and IR will develop in muscle and liver tissues resulting in systemic IR [104].

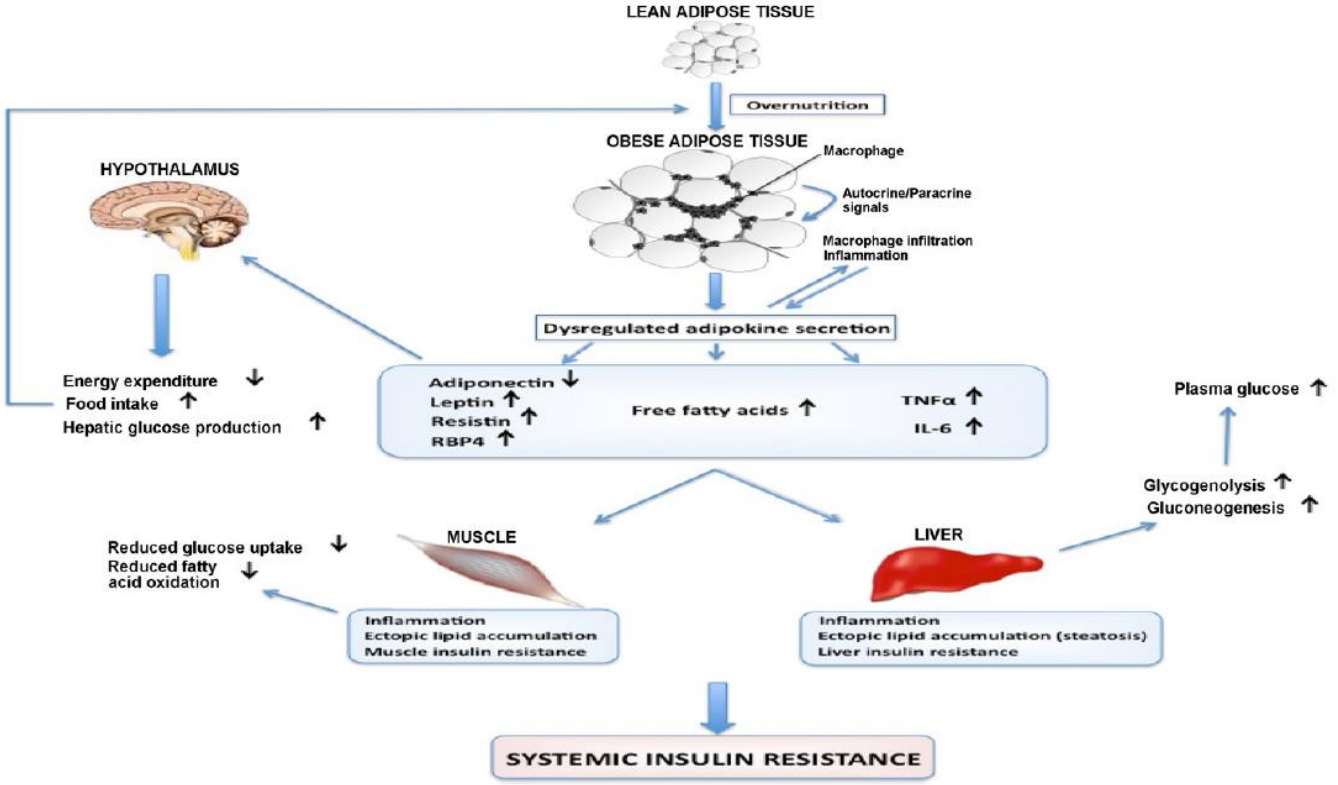

Figure 1.4 Obesity-induced changes in adipokine secretion and the development of insulin resistance. Expansion of adipose tissue in obesity leads to increased macrophage infiltration and inflammation with enhanced production of pro-inflammatory cytokines such as TNF-α and IL-6. This is accompanied by an increased release of free fatty acids and dysregulated secretion of leptin, adiponectin, resistin and retinol binding protein-4 (RBP4). Together, these adipocyte- and macrophage-derived substances can act in a paracrine or autocrine fashion to further exacerbate adipose tissue inflammation. On the systemic level, altered adipokine secretion can lead to increased food intake and reduced energy expenditure through actions in the hypothalamus and to decreased muscle and liver insulin sensitivity through enhanced ectopic lipid deposition and inflammation. Reprinted from Galic et al. [104].

Insulin resistance

IR is generally characterized by a reduced sensitivity of peripheral tissues (e.g. liver, muscle, adipose tissue) to insulin-mediated biological activity (i.e. inhibition of hepatic gluconeogenesis and glycogenolysis and promotion of glucose uptake, utilization and storage by liver and peripheral tissues) [97]. A physiological compensatory response to IR is hyperinsulinemia (i.e. greater pancreatic β-cell insulin secretory response or reduced insulin clearance) aiming to maintain normal blood glucose levels. The magnitude to which pancreatic β-cells can compensate for the IR is reflective of an individual's glucose homeostasis, i.e. if the β-cell is not able to sustain the degree of hyperinsulinemia needed to compensate for IR, hyperglycemia develops. IR and impaired β-cell function are key factors in the pathogenesis of T2DM [106] (see Figure 1.5).

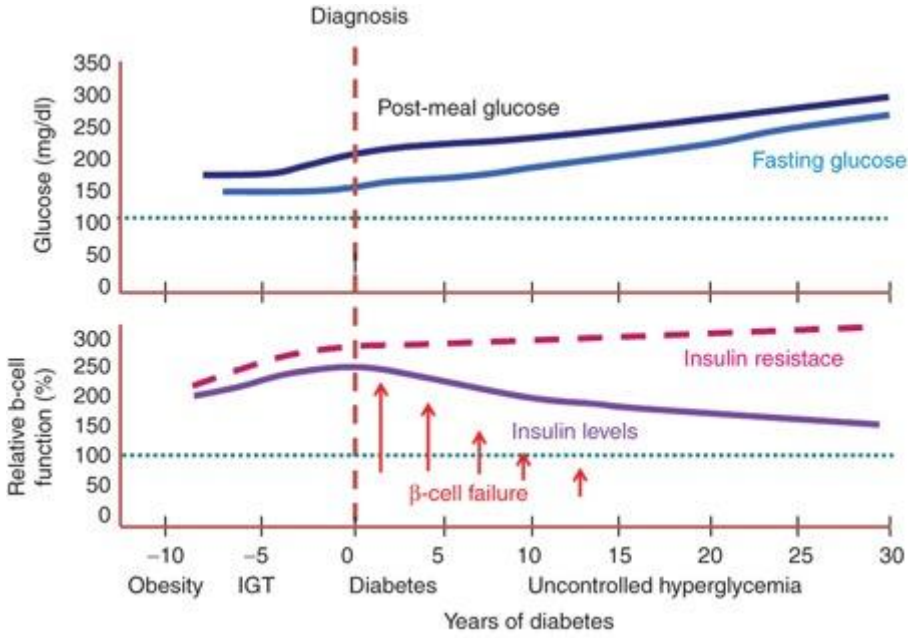

Figure 1.5 Disease progression of T2DM. Time course of glucose and insulin under different states in T2DM. IR is apparent well before the onset of T2DM and is characterized by a poor glycemic control. The increase of the β-cell function acts as a compensatory effect to stabilize glucose levels in the blood. However, as one progresses toward the development of T2DM, the persistent IR causes the exhaustion of the pancreas and prevents secretion of more new insulin. IGT: impaired glucose tolerance. Modified from Ramlo-Halsted et al. [107].

It is suggested that different tissues show different degrees of IR and within the same tissue different signal transduction pathways could be affected by IR [108].

Hepatic IR is primary in the pathogenesis of MetS [97]. The liver is the central site of glucose metabolism and is therefore the main target of insulin action. Following a glucose load, the pancreatic β-cell secretes insulin, which travels via the portal vein to the liver. Next, binding of insulin to the insulin receptor in the liver stimulates the phosphorylation of forkhead box protein 01 that prevents it from entering the nucleus and consequently diminishes gene expression required for gluconeogenesis [109]. Binding of insulin to its receptor also activates the sterol regulatory element-binding protein transcription factor which enhances the gene transcription of genes required for fatty acid and TG synthesis [110]. TGs are synthesized by de novo lipogenesis and packaged with apolipoprotein B into very low-density lipoproteins (VLDL) [111]. VLDLs are subsequently transported to the periphery for storage or utilization by activation of lipoprotein lipase (LPL) on endothelial cell surfaces in adipose or muscle tissues [112]. In subjects with IR, hepatic de novo lipogenesis is increased resulting in an increased hepatic FFA influx which impairs hepatic insulin action, resulting in an increased hepatic glucose output, synthesis of proinflammatory cytokines such as IL-6 and TNF-α, and an altered lipoprotein metabolism [113]. Excess of VLDL secretion by the liver is considered the primary cause of dyslipidemia (i.e. increased TG, decreased HDL-C and increased number of LDL particles) associated with MetS [114]. In addition, the increase in hepatic FFA flux leads to the production of toxic lipid-derived metabolites (e.g. diacylglycerol and fatty acyl CoA) that trigger the activation of protein kinase C-ε and serine/threonine phosphorylation of insulin receptor substrate-1, that diminishes hepatic insulin signal transduction [115].

Adipose tissue IR is characterized by an accelerated adipose tissue lipolysis leading to increased FFA released into the circulation. Visceral adipocytes and macrophage foam cells further increase the FFA flux. In addition, the circulating cytokines that are release from adipose tissue not only affect insulin action in other tissues, such as liver and muscle, but may also have local paracrine effects in fat [97].

Downstream of an IR liver, increased plasma FFA levels lead to disruption of the glucose-fatty acid or "Randle" cycle and impairment of insulin signaling in skeletal muscle [97]. Consequently, insulin-stimulated glucose uptake in skeletal muscle and glycogen synthesis are reduced, facilitating the progression to hyperglycemia [116]. In addition, the accumulation of intramyocellular lipids in skeletal muscle has also been associated with decreased insulin sensitivity, and might play a role in the development of IR and MetS in obese youth via lipid metabolite-induced activation of protein kinase C-ε with subsequent impairment of insulin signaling [117].

1.1.6 Treatment

Treatment of childhood obesity is generally designed to control weight gain and to alleviate associated co-morbidities [118]. Effective treatment of childhood obesity and MetS has important implications for both the individual (better quality of life and longevity) and society (reduce in healthcare and economic costs). At the moment, treatment of childhood obesity can only be successful in a multidisciplinary, familial-based setting including a pediatrician, dietician, physical therapist and psychologist, however, this approach is expensive [119].

The first-line treatment to reduce relative body weight in children is the reduction of dietary energy intake in combination with increasing physical activity. Obese children following a short-term, first-line treatment program show decreased levels of adiposity (BMI z-score and waist circumference), a decreased systolic blood pressure and better lipid profile [120-122]. Results from an intervention study suggest that weight-loss in obese European children before the onset of puberty is promising for long-term weight maintenance in these children [123]. Roberts et al. recently demonstrated that a short-term, intensive lifestyle modification program – i.e. high-fiber, low-fat diet and about 2 h of daily exercise – was effective in reducing levels of insulin, IL-6 and TNF-α in both normal-weight and obese children [124]. In addition, it was suggested that obesity per se was not responsible for the improvement in metabolic health, but that changes in diet and physical activity may be the underlying causes [124]. Recent data from longitudinal cohort studies indicated that recovering an individual's metabolic at-risk status between youth and adulthood largely restores an individual's risk to nearly the same level of those who were not at-risk in youth or adulthood [125].

Pharmacotherapy can assist in the management of extreme obesity in children older than 12 years who continue to gain weight despite a one-year dietary and lifestyle treatment [126]. The US Food and Drug Administration (FDA) approved the use of orlistat (a gastric and pancreatic lipase inhibitor) for treatment of obesity in adolescence aged 12 years and older, however, its effect on weight loss is small [127, 128]. Although the prescription of metformin (also known as Glucophage®) as an anti-obesity drug increased between 2000 and 2010, particularly amongst girls aged 16 to 18, it is not licensed for treatment of childhood obesity but only for T2DM treatment in children older than 10 years [129, 130]. Metformin inhibits intestinal glucose absorption, reduces hepatic glucose production and increases insulin sensitivity in peripheral insulin-targeted tissues [131]. From a systematic review it became evident that metformin only modestly facilitates weight loss in obese children and adolescents with and without T2DM [132]. To treat T2DM in youth, metformin alone is inadequate possibly because T2DM is an aggressive disease that rapidly progresses in youth [133]. Treatment of T2DM in youth therefore necessitates a multidisciplinary approach that includes family-based lifestyle intervention together with pharmacotherapy (metformin or insulin in exceptional cases) [134]. While waiting for ethically approved pharmacological agents to treat obese children and adolescents, longitudinal clinical trials based on larger sample sizes are needed to be established [126]. On the horizon, incretin-based therapies such as glucagon-like peptide 1 agonists may prove beneficial for obese children and adolescents with or without T2DM [126, 134].

The ultimate treatment option for extreme adolescent obesity is bariatric surgery [135]. However, this treatment can only be offered in specialized multidisciplinary centers including experienced pediatric surgeons, dieticians, and psychological management [136]. In some countries, bariatric surgery in adolescents is already considered [136-138]. It was previously demonstrated that values of fasting insulin, glucose and triglycerides declined in obese adolescents following surgical weight-loss [139].

It can be concluded that, once established, childhood obesity is very difficult to treat, underlining the usefulness of comprehensive screening, prevention and early intervention.

1.1.7 Prevention

To combat the current childhood obesity epidemic, it is crucial to intervene early in the life cycle of children from pregnancy and infancy onward [140]. As such, prevention programs can focus on weight gain, smoking and breast-feeding during pregnancy, and the promotion of healthy eating behaviors as foods are introduced to infants and toddlers [141]. Prevention of obesity in later childhood is mainly focused on a healthy diet and ample physical activity. In a recent longitudinal follow-up study, it was demonstrated that greater adherence to a Mediterranean dietary pattern (consisting mainly of vegetables, fruits, whole grains, nuts, legumes and fish) beginning in adolescence, was mainly associated with lower blood pressure, but also lower total cholesterol levels, and lower BMI during adolescence and into young adulthood [142]. Another recent study suggested that achieving approximately 90 minutes per day of moderate to vigorous physical activity could prevent the development of MetS in adolescents [143]. Unfortunately, maintaining a healthy lifestyle is not evident for a child whose parents frequently work, and whose access to fresh fruits, vegetables and outdoor playing is limited. Parents play an important role and they should be educated on how to prevent their children from becoming overweight or obese, but also on the adverse effects of obesity and MetS. On the other hand, schools are making progress in offering healthy lunches and physical activity programs, however, more efforts are needed [144]. The government can also aid by banning advertisements of unhealthy foods targeting children, just as it was for cigarettes. In conclusion, it is important to join forces in order to combat childhood obesity and associated co-morbidities.

1.2 Metabolomics

The term metabolomics is often used interchangeably with metabonomics, and in broad terms, they describe the study of the metabolome which is defined as the complete set of metabolites in a biological system [145]. However, their exact definitions are slightly different. Metabonomics is defined as the study of time-related metabolic responses of multicellular organisms to a pathophysiological intervention or genetic modification [146], whereas metabolomics focuses on the detection and quantification of low molecular weight metabolites (<1 kDa) in an organism or specified biological sample resulting from genetic or environmental perturbations [147, 148]. In this thesis, the focus is on metabolomics. Next to genomics, transcriptomics and proteomics, metabolomics is a relatively new discipline within the field of systems biology [145] (Figure 1.6).

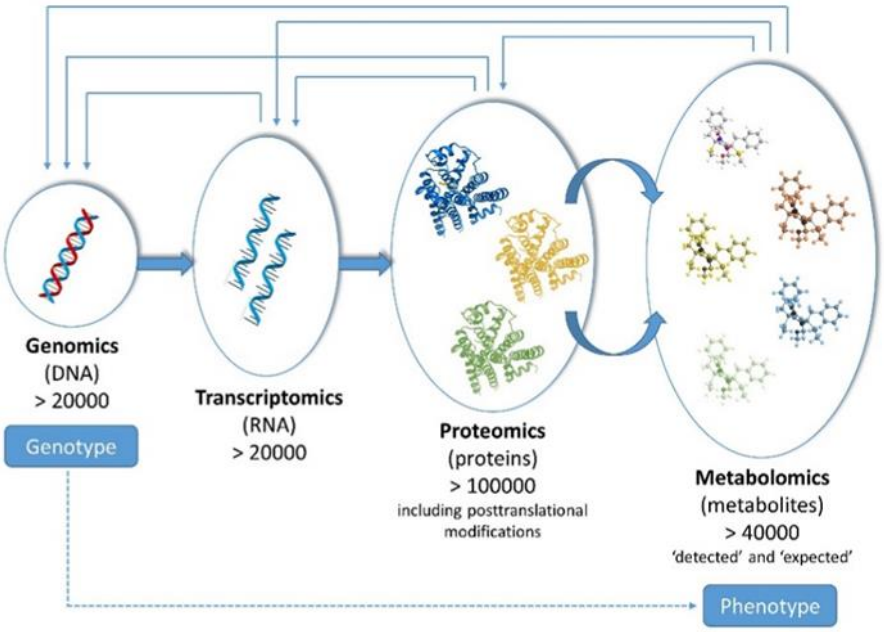

Figure 1.6 Complex interaction of each level of biological organization in systems biology. The building blocks of biological systems (organelles, cells, tissues, organs and organisms) can be divided into four main biochemical components: genes (DNA), transcripts (RNA), proteins (including posttranslational modifications) and metabolites which are intimately connected within a dynamic network consisting of many feedback loops. The metabolome is highly dynamic and constitutes a large network of metabolic reactions by the interaction with other metabolites and biochemical species in metabolic pathways. The dynamics of primary metabolism functions in a timescale of seconds allowing the metabolome to be an instantaneous and 'real-time' snapshot of the organisms' phenotype. DNA: deoxyribonucleic acid; RNA: ribonucleic acid [149-151].

Human-based metabolomics has developed into a routine application for the measurement and quantification of endogenous (produced by the host organism, e.g. amino acids or lipids) and exogenous (originating from external sources, e.g. nutrients, microbiota or drugs) metabolites [150]. The Human Metabolome Project recently estimated that the human metabolome consists of more than 40000 detected and expected metabolites, a considerably higher number compared to the 6500 detected metabolites in 2007 [151, 152]. The enormous increase in the number of metabolites is mainly due to the inclusion of 'expected' metabolites (those for which biochemical pathways are known or human exposure/intake is frequent but the compound has yet to be detected in the body) into the database [151]. However, this huge number of metabolites is probably still under-estimating the actual number of expected metabolites to be defined in the future due to an underestimation of lipids, microbiome-derived metabolites and xenobiotics [150]. Moreover, it is technically challenging to detect the entire range of metabolites within a biological matrix because of either a lack of sensitivity or a bias toward particular metabolites [153]. In order to gain the best metabolite coverage possible in a reasonable time, several analytical methods can be combined [154, 155].

Other 'omics' technologies (e.g. genomics, proteomics or transcriptomics) also provide valuable information about biological molecules [156]. Omics strategies lend themselves to biomarker discovery as they investigate multiple molecules simultaneously. The combined information obtained by different 'omics' technologies can aid in the greater understanding of both normal and disease physiological processes and the etiology of diseases [156]. In the future, this may enable us to develop new approaches that will be predictive, preventive and personalized.

The major strength of metabolomics is that it reflects changes in the metabolome as a result of the complex interplay between host genes, lifestyle, diet, environment, drugs and microbiota [157]. The metabolome is the final end-product of gene expression and protein synthesis and is thus most closely related to the metabolic phenotype (i.e. metabotype) than most other 'omics' technologies [150, 157]. Therefore, the metabolome of a single biological sample (biofluids, cell or tissue extracts) reflects a direct functional read-out of the clinical, biochemical or pathophysiological state of an organism at the time

of sampling, giving it an advantage as disease diagnostic tool [146]. In addition, the measurement of metabolites is inexpensive on a per-sample cost basis compared to the measurement of DNA, RNA or proteins [158]. Consequently, metabolomics can be employed as a powerful high-throughput tool for the discovery of biomarkers (need for large-scale studies), understanding and prognosis/diagnosis of the disease, design of new treatment approaches and prognosis of treatment outcomes [150, 159]. To eventually enable the discovery and development of valid biomarkers, it is necessary to follow an extensive study path of both untargeted and targeted analyses (Figure 1.7) [159]. Untargeted metabolomics studies the metabolome in a holistic approach without knowing in advance which metabolites are of specific biological interest. It is characterized by highly specialized small-scale studies in which a number of metabolites are identified and quantified in a single sample (i.e. metabolic profiling) [150]. Mostly, relative instead of absolute changes in metabolite responses or concentrations are reported. It is important to note that in human-based metabolomic studies it is highly important to correct for known potential confounding factors (such as age, gender and BMI) to minimize misinterpretation of biological conclusions [160]. Untargeted metabolomics is a hypothesis-generating approach to discover new disease processes or putative biomarkers.

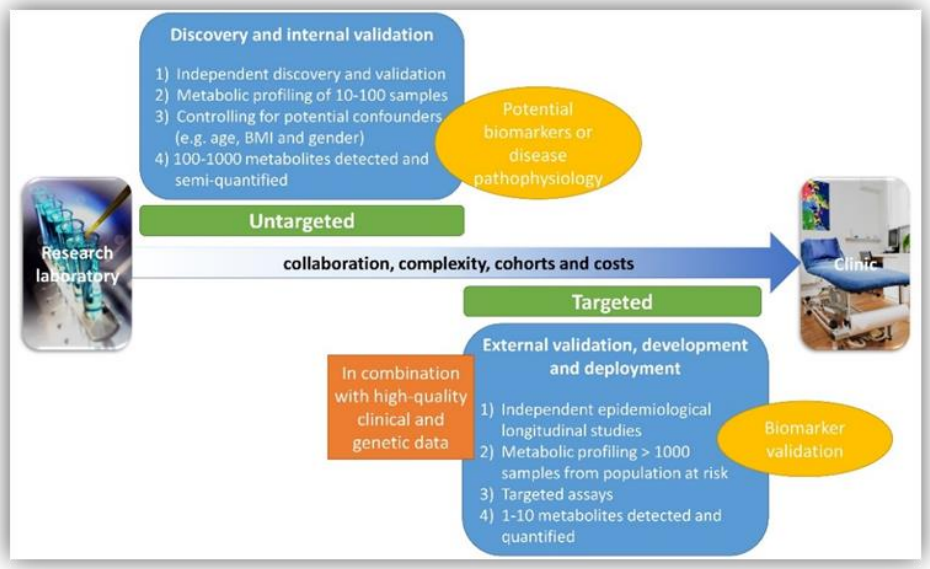

Figure 1.7 Bench-to-bedside model for biomarker discovery and validation for metabolomics research. The process involves untargeted small-scale discovery studies for the detection of potential metabolic biomarkers followed by targeted large-scale validation studies of a limited number of metabolites [150, 159]. During the successive phase of the development of a biomarker, researchers face increasing costs and complex regulatory requirements, and they have to cooperate with competing groups to gain large and independent validation cohorts [161].

From the knowledge of multiple independent discovery studies combined with internal validation, large-scale targeted studies can be established. The latter are hypothesis-driven where a limited number of metabolites are known in advance to be biologically relevant. Here, absolute quantification of metabolites is mostly performed [159]. Human-focused targeted validation studies require thousands of samples to define biological variation in human populations adequately, because biological variability introduced by genes, the environment, lifestyle, etc. can greatly differ between human [160]. The combination with high-quality clinical and genetic data is a prerequisite to develop valid biomarkers [159]. A biomarker is defined as 'a biological characteristic that is objectively measured and evaluated as an indicator of normal biological processes, pathological processes or pharmacologic responses to a therapeutic intervention' [162]. A biomarker can serve as a tool for early detection of subclinical disease; diagnosis of acute or chronic disease; risk stratification for a clinical syndrome; selecting an appropriate therapeutic intervention; and monitoring the response to therapy [150, 159]. Since metabolite concentrations

can change upon pathological and physiological changes in a disease process, measuring metabolite profiles in human biofluids or tissues has been suggested as an effective way to monitor an individual's health status [163]. Moreover, small changes in protein levels can introduce greater changes in metabolite concentrations, further enhancing the role of metabolomics in diagnostics [164].

Both mass spectrometry (MS) and NMR spectroscopy have become well-established high-throughput analytical platforms for the identification and quantification of a selective number of metabolites [165]. In Table 1.5, the relative strengths and weaknesses of both techniques for untargeted and targeted analysis are presented. Although MS is much more sensitive than NMR spectroscopy, it requires sample separation for different classes of substances which lengthens the sample preparation time [166]. On the other hand, NMR spectroscopy requires little sample preparation, is thus non-destructive, non-invasive and has a higher reproducibility [167]. In addition, it is possible to quantify a high number of metabolites in a single run using NMR spectroscopy which is more complex for MS due to variations in ionization properties of instruments and molecules [166, 167]. However, the inclusion of quantitative labeled and unlabeled internal standards can overcome this problem for targeted MS analysis [160]. Fundamentally, MS and NMR provide distinct spectral analysis of the same sample but can be complementary as has already been demonstrated by other studies using both techniques [154, 155].

Table 1.5 Advantages and limitations of NMR spectroscopy and MS as analytical tools for metabolomics research.

Strategy/platform	Advantages	Disadvantages
Untargeted		
NMR spectroscopy	• Very high analytical reproducibility and robust • Comprehensive single non-destructive analysis • Minimal sample preparation • Fully automated with high-throughput capacity • Mathematical and statistical tool box is well established • Metabolite structure and dynamic information • Molecular identification from databases and by self-consistent analysis of 1D and 2D spectra • Study of various nuclei (^{1}H, ^{13}C, ^{19}F, ^{31}P) and tissue samples with MAS NMR • Cost-effective	• Low sensitivity: detection in the micromole range (can be increased using cryoprobes, microprobes, higher magnetic field strength and dynamic nuclear polarization) • Complexity for biofluids (e.g., serum) in terms of overlapping spectral signals requires the collection of extra data by a range of sophisticated spectral editing pulse sequences • Validity is dependent on quality of sample collection, handling, and the available metadata • Requires typically 200-400 µl specimen volumes, but much less for microcoil probes (5-10 µl) • Requires very skilled operators
Mass spectrometry (hyphenated with chromatographic separation)	• Highly sensitivity: detection in the picomole range and above • Requires small specimen volumes (several µl) • Individual identification and quantification of metabolite • Relatively easily automated and suitable for use in high-throughput mode	• Software and algorithms for routine data analysis are relatively more complex • Time consuming relative to untargeted NMR (except for UPLC-MS) • Poor representation of highly polar metabolites when using standard chromatography protocols • Relatively lower analytical reproducibility • Expensive consumables
Targeted		
NMR spectroscopy	• Technique is non-destructive, hence able to subprofile molecular classes using spectral editing parameters • In combination with spectral editing and appropriate standards, metabolites can be individually detected and quantified	• Software and algorithms for reliable automated quantitation are needed
Mass spectrometry (hyphenated with chromatographic separation)	• Separation by chromatography enables metabolites to be individually identified and quantified	• Optimization of separation methods for each class of metabolites is necessary • Reduced universality of metabolite detection • Quantification is dependent on a labeled or unlabeled internal standard, subject to availability

NMR: nuclear magnetic resonance; MAS: magic angle spinning; UPLC-MS: ultra-performance liquid chromatography mass spectrometry. Based on Lindon and Nicholson [165], Bictash et al. [160] and Emwas et al. [163].

1.2.1 ^{1}H-NMR spectroscopy

Proton (^{1}H)-NMR spectroscopy was firstly introduced in the field of metabolomics in 1980s by Prof. Dr. Jeremy Nicholson (Imperial College London) who showed that this technique could be useful in the diagnose of diabetes mellitus [168]. From then on, ^{1}H-NMR spectroscopy was sensitive enough to identify metabolites in biological samples [148]. ^{1}H-NMR spectroscopic identification is based on the simultaneous detection of all hydrogen nuclei of structurally diverse molecules in a single run using a strong and homogeneous magnetic field [169] (Figure 1.8). The hydrogen nucleus is the most commonly used nucleus for NMR spectroscopic studies on biofluids, since it is the most prevalent in organic molecules and gives the highest relative sensitivity of all naturally occurring spin-active nuclei [153]. For a more throughout technical explanation of ^{1}H-NMR spectroscopy, see annex at the end of this chapter.

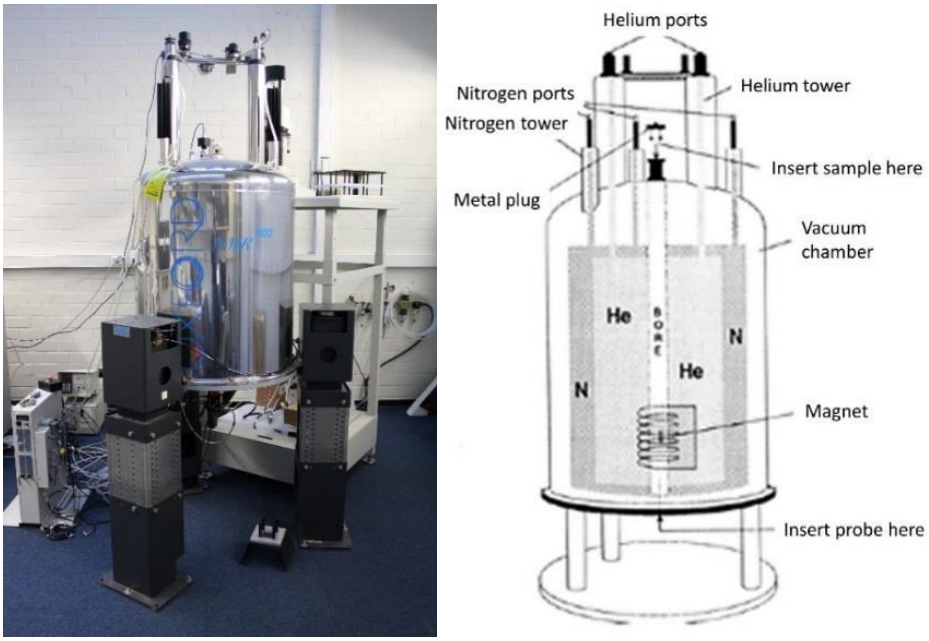

Figure 1.8 Outside (left) and inside (right) of a 400 MHz NMR spectrometer. A probe is used to insert test samples into the center of a superconducting magnet. Under control of a host computer and NMR software, the NMR console generates radiofrequency pulses (not illustrated in this figure).

^{1}H-NMR spectroscopy is capable to provide a metabolic "snapshot" of the biofluid of interest at a particular time point [153]. It has proven to be a very powerful, robust and reproducible technology for metabolic profiling with an inter- and

intra-laboratory coefficient of variation around 5% in contrast to MS which is much more prone to experimental variation (>8%) [160, 170, 171]. Nonetheless, a key goal within metabolomics is to develop standard operating procedures (SOPs) in order to minimize artifacts and bias due to biological and experimental variability which can lead to false conclusions [172].

Workflow of ^{1}H-NMR spectroscopy

^{1}H-NMR-based metabolomics is typically performed according to a workflow starting from a biological question and experiment, proceeding through sample collection and preparation, analytical experiments to acquire data, data processing and data analysis followed by biological interpretation [150, 173] (Figure 1.9).

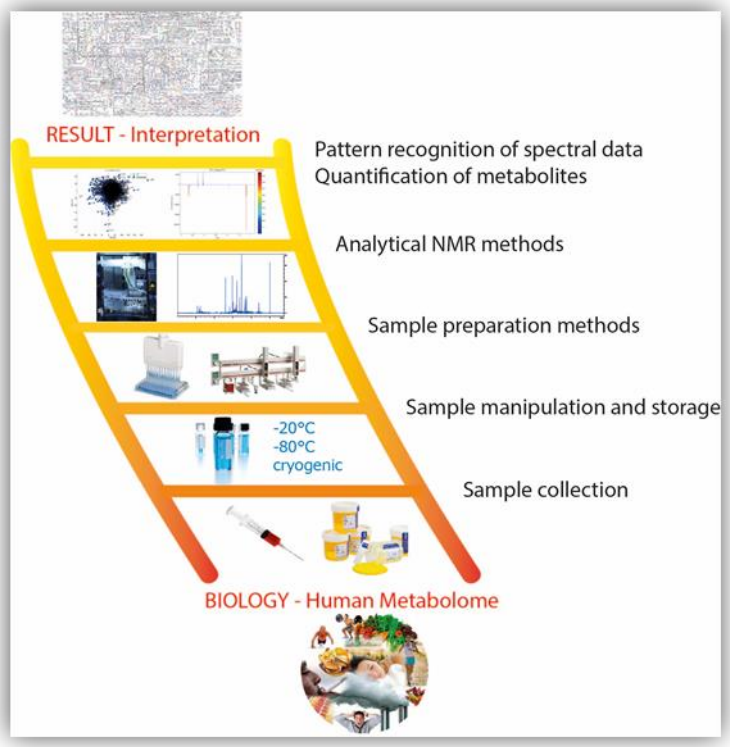

Figure 1.9 A typical sample workflow of NMR spectroscopy. Reprinted with permission from Dona et al. [173].

Sample collection and preparation

The largest body of work by ^{1}H-NMR spectroscopy has been performed on biofluids, such as plasma (or serum) and urine of rodent and human origin [153]. Collection of blood and urine is essentially noninvasive and therefore these biospecimens are easily obtainable, making them very suitable for metabolomics research [174]. Plasma (or serum) reflects the metabolic state of an organism at the time of sampling, and they contain a combination of both macromolecules (proteins, lipoproteins and glycoproteins), lipids and low molecular weight metabolites (e.g. amino acids, glucose and lactate) [150]. Urine reflects an organism's waste products produced by filtration in the kidneys and stored in the bladder (e.g. water, urea, salts and amino acids) [150]. Human-based metabolomics studies have to be conducted under well-controlled conditions since a wide variety of external stimuli (such as diet, physical activity, etc.) but also inappropriate sample handling and storage can influence the metabolome [163].

For blood and urine, it is recommended to collect samples at a specified time in the morning after 8 to 12 h of fasting to reduce diurnal variation and consequently produce a baseline sample [174]. Urine samples are more prone to the influence of diurnal variation or exercise and hence can be pooled to average variability [175]. The collection of blood samples for ^{1}H-NMR spectroscopy in lithium-heparin (LiHe) tubes is mostly preferred, since ethylenediaminetetraacetic acid (EDTA) and sodium citrate can interfere with metabolite signals [176]. For urine, sterility is a prerequisite and therefore the collection into sterile containers or the addition of preservatives to minimize microbial contamination is highly advisable [177]. High-speed pre-centrifugation of blood to obtain plasma and of urine to eliminate cell debris is a prerequisite [172]. During sample preparation, a deuterated solvent (D_2O) is added to control magnetic field drift and a chemical shift reference compound such as trimethylsilylpropionic acid (TSP) is added as calibration standard for water-based solutions [178, 179]. For urine, it is important to fix the pH (mostly at 7.4) of all samples prior to NMR measurement [179]. Therefore, manual pH adjustment using hydrogen chloride (HCl) or sodium hydroxide (NaOH) can be performed in small-scale studies, however, for large-scale studies it is more suitable to use a buffer solution with a concentration ranging 0.3 to 1 M [177].

For the actual ^{1}H-NMR analysis, a 5 mm NMR tube is filled with a fixed volume of 200 to 600 µl plasma or urine (in addition to D_2O, contingent buffer and TSP) in order to determine the optimal compromise between sensitivity and resolution [150].

^{1}H-NMR spectroscopic analysis

Most ^{1}H-NMR-based metabolomics studies rely on one-dimensional (1D) proton NMR spectra (Figure 1.8) [180]. The narrow chemical shift range of 1D ^{1}H-NMR spectra increases the likelihood of overlap of proton resonance signals of specific metabolites, leading to uncertainty in NMR signal assignments [153]. Broad resonances originating from macromolecules and lipids overlay reasonably sharp resonances of smaller metabolites [181]. This problem is mostly encountered on 'low-medium' field spectrometers with resonance frequencies ranging 200 to 400 MHz (Figure 1.10). Broader signals of macromolecules are generally attenuated using appropriate sample preparation (i.e. centrifugation) and dedicated NMR pulse sequences such as Carr-Purcell-Meiboom-Gill (CPMG) [182]. Higher field instruments with resonance frequencies ranging 600 to 950 MHz provide a greater signal dispersion and enhanced sensitivity contributing to a reduced spectral-complexity [183].

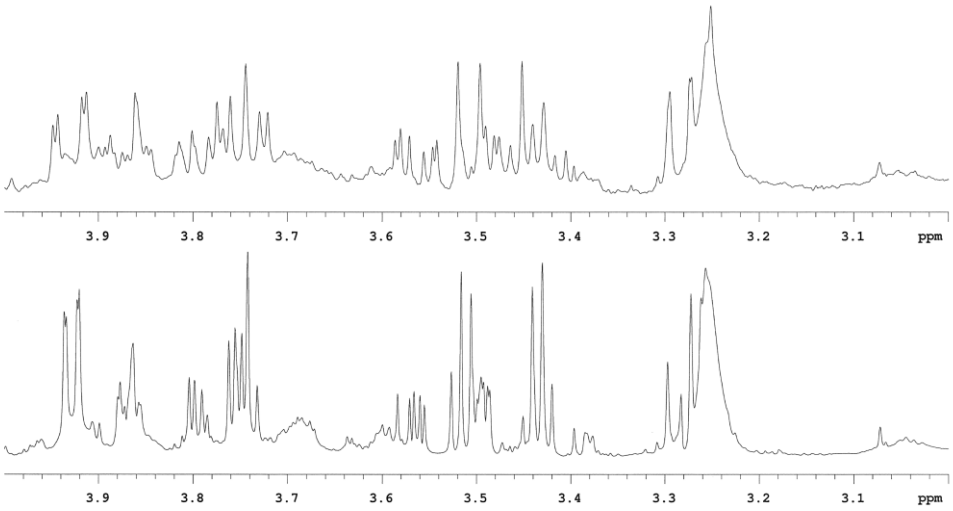

Figure 1.10 ^{1}H-NMR CPMG spectra (3-4 ppm) of blood plasma acquired at 400 MHz (upper) and 900 MHz (lower). A greater signal dispersion is observed for the 900 MHz NMR spectrum which represents sharper peaks as a result of a higher resolution compared to the 400 MHz spectrum.

The ^{1}H-NMR spectral assignment of low-molecular weight metabolites in biofluids is a time-consuming and complex procedure [184]. It is generally based on the determination of chemical shifts, relative intensities and J coupling constants of the proton resonance signals to provide structure-specific information for individual metabolites [153]. By adding a known compound to the biofluid of interest (i.e. spiking), the presence and location of a suspected metabolite in the ^{1}H-NMR spectrum can be confirmed as an increased signal intensity of the corresponding resonances can be observed [153]. Next to spiking experiments, two-dimensional (2D) ^{1}H-NMR spectroscopy can aid in the assignment of metabolite signals by increasing signal dispersion and elucidating connectivities between signals [185, 186]. Additionally, since ^{1}H-NMR spectroscopy is a non-destructive technique, the sample can still be subjected to complementary analytical techniques such as high-performance liquid chromatography (HPLC)-NMR-MS in order to identify specific molecules [187, 188].

Data processing

To achieve optimal characterization of metabolites in the sample, NMR data sets require several steps of data pre-processing prior to multivariate analysis. First, all measured ^{1}H-NMR spectra are subjected to phasing, baseline correction and chemical referencing using NMR software. Next, ^{1}H-NMR spectral data can be divided into spectral regions using several methods to derive quantitative metabolite information, i.e. continuous spectral data are converted to segmented data for matrix analysis (data reduction) [189]. The most commonly used method to process ^{1}H-NMR spectral data is called 'bucketing' which is a simple automated manner to integrate spectra into fixed (e.g. 0.01 or 0.04 ppm) or variable-sized (e.g. intelligent) buckets [189, 190]. By applying variable-sized bucketing, the impact of small pH-dependent chemical shift changes is reduced [191]. A major drawback of fixed bucketing is that peaks can possibly become divided between adjacent buckets resulting in loss of information and more complicated data interpretation. Alternatively, variable-sized bucketing defines relevant variable-sized spectral regions in which peak splitting is avoided. However, problems with overlapping signals still remain and the identification of single metabolites remains a challenging task [184]. Moreover, instrumental noise can arise in spectral regions where weakly concentrated metabolites are present. However, this noise can be filtered out by

exclusion of noisy regions according to a predefined cut-off [192]. Next to bucketing, peak fitting or automatic peak picking are other techniques that can be applied [193, 194]. Following to spectral editing, data normalization is a crucial step in data pre-processing to allow for objective comparisons of samples within one dataset [195, 196]. The most common method of data normalization is dividing each single integral value by the total sum of integral values (i.e. integral normalization) [195]. However, this method could influence subsequent multivariate data analysis especially in samples that contain large amounts of a single substance (such as urea or creatinine in urine samples) or particularly high concentrations of drug metabolites [195]. Hence, scaling of the most abundant metabolites overwhelms scaling of other metabolites in a way that low-intensity metabolites that might be biologically relevant are disregarded. To overcome this limitation, dominating resonances can be excluded from data normalization of NMR spectra [163]. Moreover, data can also be log-transformed in order to keep the variance between data within a narrow range [197]. Other so-called scaling methods are including Pareto scaling, unit variance (UV) scaling or vast scaling [195, 197, 198].

Statistical data analysis

In order to extract biologically meaningful information from complex multivariate data derived from ^{1}H-NMR spectroscopy, multivariate projection methods are necessary to perform [199, 200]. Multivariate analysis by projections has several advantages, i.e. it deals with the dimensionality problem, it can handle many variables and few observations, it copes with multicollinearity and missing data, it is robust to noise in both X and Y, and provides diagnostic and graphical tools. It is very useful as it can provide a clear overview of the data (e.g. principal component analysis: PCA), it can be used for classification purposes (e.g. orthogonal partial least squares projection to latent structures discriminant analysis: OPLS-DA) and for regression analysis (e.g. partial least squares projection to latent structures: PLS-DA) [201]. For more information on multivariate projection methods, see annex at the end of this chapter.

1.2.2 Metabolomics and its application in obesity

It is known that obesity is a complex and multifactorial condition that requires a long-term management to combat weight gain [202]. In order to provide

appropriate tools to monitor the disease, a better understanding of the pathophysiology of obesity and metabolic consequences is required. Metabolomics provides a systems approach to study the molecular events that control body weight and the metabolic state [203]. Biomarkers for obesity and metabolic consequences can subsequently be developed to identify high-risk individuals who would benefit most from targeted preventive therapy [204]. In recent years, metabolomics has been increasingly used to study the pathophysiological mechanisms of obesity. Up to now, rodent models have been widely used and significantly contributed to the investigation of the onset and progression of obesity [205]. That is because animal studies allow strict control of factors such as diet, environmental exposure and/or genetic background. In obese Zucker rats lacking the leptin receptor, it was found that disturbances in the metabolism of glucose, tricarboxylic acid (TCA) cycle, lipid, choline, amino acid and creatine contributed to the obese phenotype [206]. In mice fed a high-fat diet, lipid and energy metabolism became disturbed resulting in fat accumulation via a decreased β-oxidation [207]. It was previously also been demonstrated that gut microbiota metabolism differed between mice fed a high-fat or high-carbohydrate diet [208]. In contrast to studies in rodents, humans are under direct influence of lifestyle, diet, physical activity or drugs, which complicates the interpretation of study findings.

Targeted MS-based metabolomics studies have previously shown higher blood concentrations of lactate, pyruvate, branched chain amino acids (BCAA: valine, isoleucine and leucine), alanine, phenylalanine, tyrosine, glutamate, glutamine, glycine, aspartate, asparagine, arginine and certain phosphotidylcholines in obese versus lean adults [209-211]. Indeed, alterations in amino acid profiles are associated with obesity [212]. In addition, BCAAs that are essential for human, could contribute to the development of obesity-associated IR in adults [209]. Together with tyrosine and phenylalanine, BCAAs might even predict the risk of future diabetes [213]. Elevations in blood pyruvate and alanine might contribute to the development of IGT in obese adults, possibly related to an overload of the BCAA metabolism in obesity [209]. Increased levels of lactate and pyruvate might indicate a perturbed hepatic glucose production, lipid synthesis and energy metabolism [206]. Another study using MS, demonstrated that α-hydroxybutyrate is an early marker for both IR

and impaired glucose regulation in non-diabetic subjects [214]. It was stated that the underlying biochemical mechanisms might include increased lipid oxidation and oxidative stress [214]. A study based on ^{1}H-NMR spectroscopy, found lower concentrations of hippurate in urine samples of morbidly obese compared to lean patients [215]. Hippurate is a gut microbial mammalian co-metabolite of benzoic acid which is produced by intestinal bacteria [216]. It is formed by the conjugation of benzoic acid with glycine in the liver mitochondria, and subsequently excreted into urine [217]. The same ^{1}H-NMR-based study also showed that also trigonelline, 2-hydroxyisobutyrate and xanthine contributed to the discrimination between the obese and lean metabolic profile [215]. Gut microbiota metabolism seems therefore to be strongly linked to the human obesity phenotype.

Studies investigating the obese metabolic phenotype in children are limited. It is known that obese children are at increased risk to develop IR, dyslipidemia and hypertension and eventually become obese as an adult with high risk to develop associated chronic pathologies such as T2DM and CVD [218, 219]. In addition, the underlying cause of childhood obesity is still not fully understood [33]. Therefore, metabolomics could provide insight into early molecular mechanisms associated with obesity and support the refinement of strategies for intervention in early life to prevent childhood obesity. Up to now, however, only MS-based metabolomic studies were performed to study the pathophysiology of childhood obesity. It is suggested that metabolites altered in fasting blood of obese children play a role in pathways of oxidative stress, energy metabolism, hepatic gluconeogenesis, amino acid metabolism, lipid metabolism and β-oxidation [220-222]. The effect of weight loss during lifestyle intervention in obese children was also evaluated using MS-based metabolomics. As a result, the metabolism of phosphatidylcholine seems to be important in the search for weight loss predictors [223, 224].

1.3 Aims of the study

Obesity is one of the most serious health issues facing the current generation of children and adolescents, and evidence is rising that the next generation of children is likely to be fatter and less fit than the current generation. In **Chapter 2**, we hypothesized that the prevalence of morbid childhood obesity is high in a clinical population of obese children and adolescents referred to the multidisciplinary pediatric obesity clinic of the Jessa Hospital Hasselt (Belgium). However, up to now, internationally applicable criteria to define morbid childhood obesity are lacking, thereby complicating the comparison of prevalence rates of this extreme form of obesity between different pediatric populations. Therefore, our first aim was to develop internationally accepted criteria to define morbid childhood obesity. In 2000, Cole and Lobstein published the International Obesity Task Force (IOTF) BMI criteria to define overweight and obesity in children and adolescents aged between 2 and 18. The IOTF BMI criteria are based on a heterogeneous mix of surveys from different countries, with widely differing prevalence rates for obesity, which makes it highly suitable for use in international clinical research. In 2012, these criteria were reformulated, which makes it now possible to construct your own cut-offs for any required BMI at age 18. However, the current IOTF BMI values are not including the definition of class III obesity. We therefore calculated the IOTF cut-offs for BMI 40 at age 18 for both boys and girls aged between 2 and 18, and suggested to refer to it as the BMI reference of 'morbid' obesity in line with the terminology of the adult WHO 1995 definition. Next, we calculated the prevalence of morbid obesity in a referred population of obese children and adolescents aged between 2 and 18.

It is generally known that obese children are at high risk to develop metabolic complications such as insulin resistance, dyslipidemia or impaired glucose tolerance that eventually may progress into type 2 diabetes (T2DM) and cardiovascular disease (CVD). However, these metabolic conditions often remain undetected and the development of T2DM and premature CVD is accelerated in children compared to adults. Therefore, early identification of obesity-associated metabolic complications in children and adolescents is very important. Additionally to **Chapter 2**, we hypothesized that morbidly obese children and adolescents show more and more serious metabolic complications compared to

less severely obese children. Hereto, we investigated and compared components of the metabolic syndrome and its prevalence in a clinical cohort of obese children and adolescents subdivided according to the degree of obesity, i.e. class I or obese, class II or severe and class III or morbid.

The results of **Chapter 2** revealed that although class III or morbidly obese children had a larger waist circumference, higher systolic blood pressure and higher fasting insulin levels compared to class I obese children, levels of cholesterol and triglyceride, and the prevalence of the metabolic syndrome were not significantly elevated in morbidly obese children. Hence, our next aim was to search for other clinically useful screening measures besides BMI for the detection of metabolic complications in the obese pediatric population.

In **Chapter 3**, we evaluated the ability of different shape types of the plasma glucose curve obtained during an oral glucose tolerance test (OGTT) to identify the metabolic health risk of end-pubertal obese girls. In this study, only end-pubertal obese girls were selected to eliminate for the confounding effect of puberty that is characterized by transient insulin resistance. The OGTT was chosen because it is simpler, more practical and child-friendly compared to the hyperinsulinemic euglycemic clamp (gold standard). In addition, the OGTT is part of the routine clinical check-up for the diagnosis of (pre)diabetes and the estimation of insulin resistance and secretion in obese adolescents.

Nonetheless, screening measures that are based on fasting metabolic parameters might be even more practical and widely applicable to detect metabolic complications in obese children and adolescents. Recently, the concept of metabolically "healthy" obesity (MHO) was introduced into the field of pediatric obesity to describe obese children without any metabolic complications. However, as studies concerning MHO in the pediatric population are scarce and insulin resistance is often disregarded from the definition, additional research is needed to further define and identify the MHO phenotype in the pediatric population. In **Chapter 4**, we defined MHO children and adolescents according to three definitions: (i) the absence of the metabolic syndrome as defined by the pediatric International Diabetes Federation (IDF) criteria, (ii) the absence of insulin resistance as defined by HOMA-IR and (iii) the combination of the previous two definitions. The prevalence of MHO children and adolescents was calculated according to all three definitions. In addition, metabolic parameters

and prevalence rates of prediabetes were investigated and compared between MHO and metabolically unhealthy obese (MUO) children and adolescents.

Besides clinical research, additional research may be needed to identify metabolic risk factors and biomarkers of metabolic complications in the obese pediatric population. Metabolomics is a relatively new technology in the discovery of biomarkers and distinguishes itself from the other 'omics' tools by reflecting the metabolome, the final end-product of the complex interaction between genetic and environmental factors, which is most closely related to the metabolic phenotype. NMR-based metabolomics could serve as a robust, accurate and comprehensive tool to further investigate the metabolic profile of obese children and adolescents. Because studies in obese children and adolescents using ^{1}H-NMR spectroscopy as an analytical characterization tool are scarce, and because little is known about the altered biochemical pathways in childhood obesity and associated metabolic complications, we evaluated NMR-based metabolomics as an accurate and clinically useful tool for the search for biomarkers.

At first, it deemed necessary to scientifically improve ^{1}H-NMR spectroscopy on the level of ^{1}H-NMR experimental analysis (**Chapter 5**). Hereto, metabolites that are important in obesity-associated metabolic complications were identified in the plasma and urine ^{1}H-NMR spectrum by spiking experiments. Subsequently, the plasma and urine ^{1}H-NMR spectrum could be rationally divided into well-defined integration regions, being the variables for multivariate statistical analyses. To further optimize ^{1}H-NMR experimental analyses, the impact of noisy integration regions (or noisy variables) on the multivariate group classification of obese and normal-weight children and adolescents was examined. To note, further research was performed only on plasma of the study participants, because the number of urine samples subsequently collected was too low.

Next to the optimization of ^{1}H-NMR experimental analysis, a robust and practical protocol had to be developed for sample collection and preparation in a clinical setting (**Chapter 6**). Hereto, the impact of preanalytical conditions that commonly occur in clinical practice at the level of collection, processing and freezing, on the plasma ^{1}H-NMR metabolic profile was examined. In addition, we evaluated the usefulness and validity of the Standard PREanalytical Code

(SPREC) within the field of clinical NMR-based metabolomics. SPREC allows for an appropriate sample encoding and exclusion of samples that were subjected to unwanted, interfering preanalytical conditions, and has recently been developed by the biobanking community. The implementation of SPREC within clinical metabolomics may contribute to its validation in clinical, biobank and multicenter research.

Finally, we performed NMR-based metabolic profiling on plasma of obese and normal-weight children in the search for biomarkers of obesity-related metabolic alterations in children and adolescents (**Chapter 7**). A statistical classifier was built in order to differentiate between obese and normal-weight children, and metabolic pathways important in the pathophysiology of childhood obesity were explored. In addition, we introduced the concept of MHO (see Chapter 4) in NMR-based metabolomics and relevant associations between conventionally measured biochemical parameters (e.g. fasting glucose, insulin, triglycerides, etc.) and plasma metabolites differentiating between MHO and MUO were investigated.

ANNEX

Fundamentals of ^{1}H-NMR spectroscopy and multivariate projection methods

This technical note describes the fundamentals of ^{1}H-NMR spectroscopy which rely on quantum mechanical laws, and are therefore quite complex and need to be explained in order to gain a better understanding of this technique. In addition, multivariate projection methods used for statistical processing of multidimensional ^{1}H-NMR datasets are explained.

Fundamentals of ^{1}H-NMR spectroscopy

^{1}H-NMR spectroscopy is a technique that measures the resonance frequencies of hydrogen nuclei that are subjected to a low-frequency radiation and a strong magnetic field. The resonation of nuclei at a specific frequency occurs in the radiofrequency range of the electromagnetic spectrum (Figure S1).

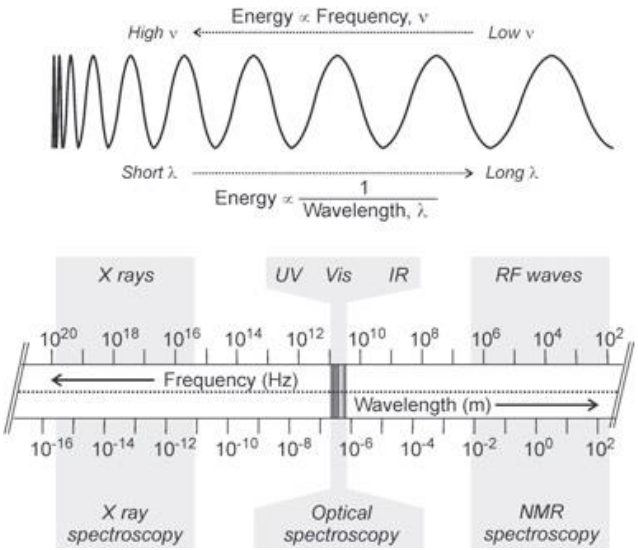

Figure S1 The electromagnetic spectrum. Adapted from Bothwell et al. [225].

Nuclear spin in a static magnetic field

NMR spectroscopy relies on the spin (or angular momentum) of protons and neutrons. Protons and neutrons are 'spin ½ particles', i.e. they have a spin with a spin quantum number s=1/2. The nuclear spin of an atom is expressed as the vector sum of unpaired proton and neutron spins and its nuclear spin quantum number I = n/2 with n the sum of unpaired protons and neutrons. Nuclei with an even number of *both* protons and neutrons have a spin quantum number I=0, for example, ^{12}C. These kinds of nuclei do not have a net nuclear spin and will

not give rise to an NMR signal, and are therefore called NMR inactive nuclei. Nuclei with an odd number of protons *as well as* neutrons have a spin quantum number I=1, for example, ^{2}H. However, if the number of protons *or* neutrons is odd, then I=half-integer. For example, the hydrogen nucleus consists of only one proton (^{1}H) and therefore has a nuclear spin quantum number I=1/2, making it NMR-active. The positively charged hydrogen nucleus creates a small magnetic field around the hydrogen atom which is called the magnetic dipole moment (μ-vector) (Figure S2).

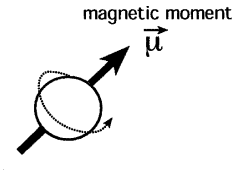

Figure S2 The magnetic dipole moment μ of a hydrogen nucleus. The orientations of the magnetic moment are defined by magnetic quantum number (m) values. The magnetic moment is directly proportional to the angular momentum ($\mu = \gamma \times P$, where μ: magnetic moment of the nucleus; γ: gyromagnetic constant; P: spin angular momentum).

If the ^{1}H atom is placed in a homogenous, strong and static external magnetic field (B_0), the μ-vector can appear in two states: parallel (spin-up or m=+1/2; α-state or low energy state) or anti-parallel (spin-down or m=-1/2; β-state or higher energy state) with respect to B_0 (Figure S3). Due to the interaction between the magnetic moment and the magnetic field, the magnetic moment will precess around the magnetic field B_0.

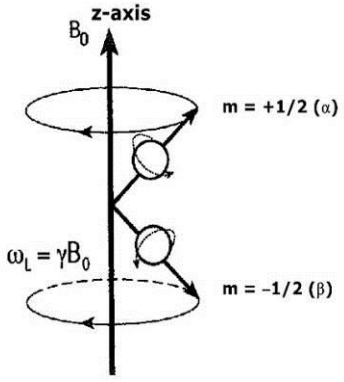

Figure S3 Two energy states (spin-up or spin-down) of the proton magnetic moment which precesses around an externally applied magnetic field B_0 oriented along the z-axis.

Energy states and population

For each spin state, there is energy associated with it, which is characterized by the frequency of the precession of nuclei in the presence of a magnetic field. The frequency with which the μ-vector spins around B_0 is called the Larmor frequency (ω_0) which depends on the strength of B_0 and the proton gyromagnetic constant (γ):

$$\omega = \gamma B_0 \qquad \text{or} \qquad \nu = \frac{\gamma B_0}{2\pi}$$

where γ is the nuclear gyromagnetic constant which is a characteristic constant for a specific nucleus; B_0 is the magnetic field strength in the units of Tesla (T); ω is expressed in rad/s and ν in Hz. Therefore, the energy difference of the allowed transition is given by:

$$\Delta E = \gamma \hbar B_0 = \hbar \omega$$

where $\hbar$ is the Planck constant h divided by 2π (Figure S4).

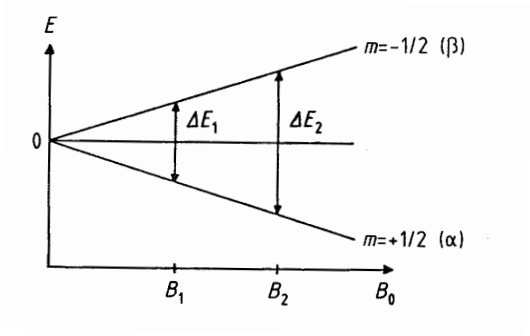

Figure S4 Energy difference between two Zeeman energy states. The intensity of the NMR signal relates to the population difference between two Zeeman energy states of the transition.

Consequently, spin transitions can be induced between the two different energy states by irradiation with electromagnetic radiation of the appropriate frequency. To this end, the following resonance conditions must be met:

$$E = h\nu = h\nu_L = h\frac{\gamma B_0}{2\pi} = \Delta E$$

The Boltzmann equation quantitatively describes the ratio of the spin populations in the two energy states. Both the energy difference between the transition states and the population difference between the states increases with the magnetic field strength. At room temperature, the amount of spins (μ-

vectors) in the low energy state is slightly higher than in the high energy state. Thus, the sum of all these μ-vectors along the z-axis results in a net z-magnetization along the z-axis, and is presented as the magnetization vector M_0 (Figure S5). This indicates that only a small fraction of the spins will contribute to the NMR signal intensity due to the small energy difference between the two states and hence NMR spectroscopy intrinsically is a spectroscopic technique with rather low sensitivity. Therefore, stronger magnetic fields lead to improvement in sensitivity, in addition to a higher resolution.

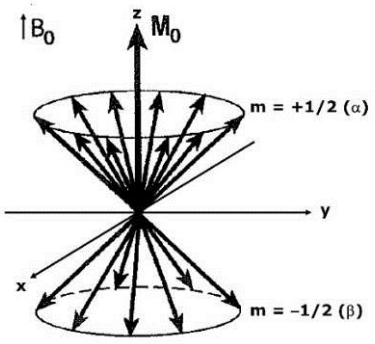

Figure S5 Statistical distribution of μ-vectors over two cone halves which results in net or longitudinal magnetization, M_0, which is oriented in the same direction as vector B_0. The vector sum of the components of the nuclear magnetic moments in the x-y plane is zero. At equilibrium, M_0 is generated by the small population difference between α and β states, and is parallel to the direction of the static magnetic field B_0.

Rotating frame

In order to create a NMR signal, the proton spins have to be flipped over from a low energy level to a high energy level. This is achieved by imposing a short but strong radio frequency pulse (RF-pulse) or B_1-pulse into right angles on the B_0 field. This causes a simultaneous excitation of all protons by energy transfer from the B_1-pulse to the protons, called resonance. Because the Larmor frequency is not observed in an NMR experiment, a new coordinate frame is introduced to remove the effect of the Larmor frequency, called the rotating frame (rotating with frequency ν). If a 90° pulse is applied on the spins, the M_0 vector will end up in the transversal x'-y' plane (Figure S6). Nuclear moments are no longer spinning along the z-axis but are stationary in this rotating frame. It should be noted that M_0 shifts away from the z-axis in a clockwise angle α, depending on the duration and strength of the B_1 field.

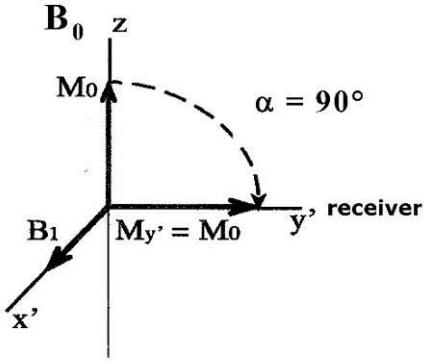

Figure S6 Vector representation of transversal magnetization ($M_{y'}=M_0$) upon applying a 90° RF-pulse along the x'-axis by the B_1 field in the rotating frame which results in a flip over of M_0 towards the y'-axis (receiver).

In practice, the B_1-pulse consists of a linear oscillating B_1 field along the x'-axis with carrier frequency ν (same as the frequency of the rotating frame and in the order of the Larmor frequency) and magnitude $2B_1$ and which is easily produced by applying an electric current through the probe coil (Figure S7). The linear oscillating B_1 field can be decomposed in two circular oscillating magnetic fields with Larmor frequency and magnitude B_1. Resonance can now be achieved by interaction of the μ-vectors with the circular magnetic B_1-field that is oscillating in the same direction and with frequency ν. This situation is called resonance condition.

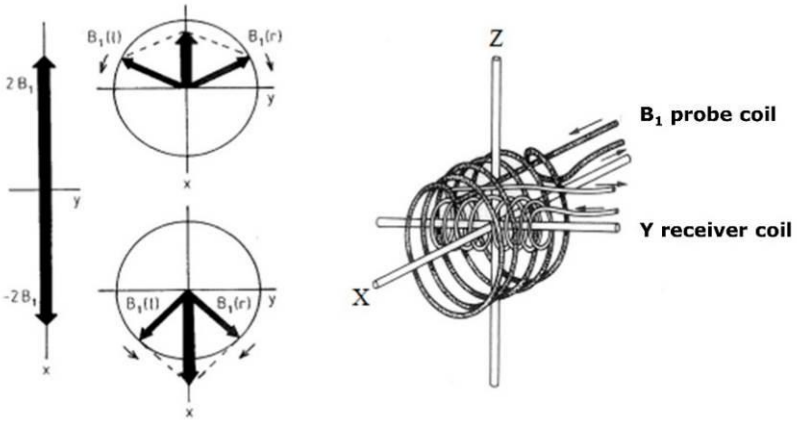

Figure S7 Oscillating B_1-fields in the x'-y'-plane are achieved by applying a linear oscillating electromagnetic field with magnitude of $2B_1$ along the x'-axis. The B_1 probe coil is oriented along the x-axis and the receiver coil along the y-axis.

A 90° pulse arises when the B_1 field is turned on and then turned off while M_0 moves from the z-axis to the x'-y' plane. The time during which B_1 is applied is called the 90° pulse width (pw; in the order of μs). During a 90° pulse, the

maximal NMR signal is obtained by the occurrence of two phenomena: (1) phase coherence, i.e. clustering of a part of the μ-vectors at the surface of the precession coin resulting in a shift of the equilibrium magnetization M_0 from the z-axis (longitudinal axis) towards the y'-axis of the transversal x'-y' plane ($M_{y'}$); (2) a net energy transfer from the B_1-field (transmitter) to the nuclear spins, leading to a flip over of some of the spins of the low energy state to the high energy state (Figure S8).

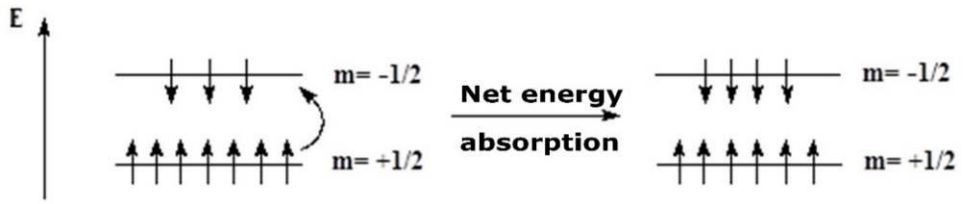

Figure S8 Net energy transfer from the B_1-field to the nuclei leading to a flip over of some nuclear spins from the low energy state to the high energy state.

After a 90° pulse, the magnetization along the z-axis becomes zero resulting in an equal distribution of nuclear spins over the two energy states, i.e. an equal amount of spins (μ-vectors) that are oriented parallel or anti-parallel to B_0 (Figure S9). The population difference between the two energy states than also becomes zero. In addition, the y-component achieves a maximal M_0 value ($M_{y'}$) and a magnetization vector is created in the transversal plane ($M_{y'}=M_0$), i.e. transversal (detectable) magnetization.

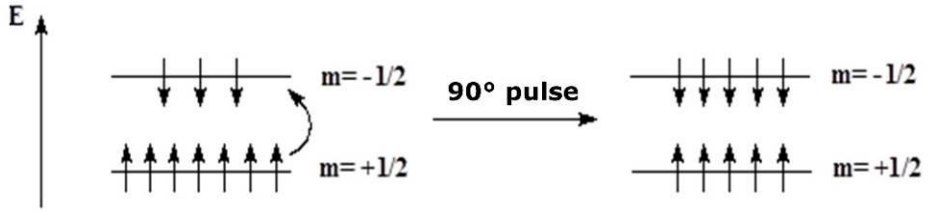

Figure S9 Orientation of nuclear spins after applying a 90° pulse.

Free induction decay

After the B_1-pulse is switched off, the NMR signal is detected while the nuclei return back to their equilibrium (relaxation, see next paragraph). The detection of the NMR signal is achieved when μ-vectors – with their unique frequency ν_i (or in the rotating frame $\Delta\nu_i = \nu_i - \nu$) – will spin back around the z-axis under the

influence of B_0. This induces a fluctuating electric current in the detection coil (receiver) along the y'-axis. In the rotating frame, spins with $\nu_i = \nu$ ($\Delta\nu_i = 0$) will not spin around the z-axis, and as a function of time they induce a constant current in the receiver coil. Nuclei with $\nu_i > \nu$ will oscillate with respect to the y'-axis and as a function of time they induce a fluctuating current with frequency $\Delta\nu_i$, allowing to retrieve $\nu_i = \Delta\nu_i + \nu$. Nuclei with $\nu_i >> \nu$ will oscillate faster with respect to the y'-axis and as a function of time they induce a fluctuating current with a higher frequency (Figure S10). Hence, a free induction decay (FID; Free of the influence in the B_1 field; Induced in the receiver coil; Decaying back to the equilibrium) is induced in the detector. This is a complex and time dependent signal which is induced in the detector as a result of the different resonance frequencies of protons having a different electron (chemical) environment. By means of a Fourier transformation, the complex time signal can be unraveled in its constituent frequencies and amplitudes, establishing the NMR spectrum.

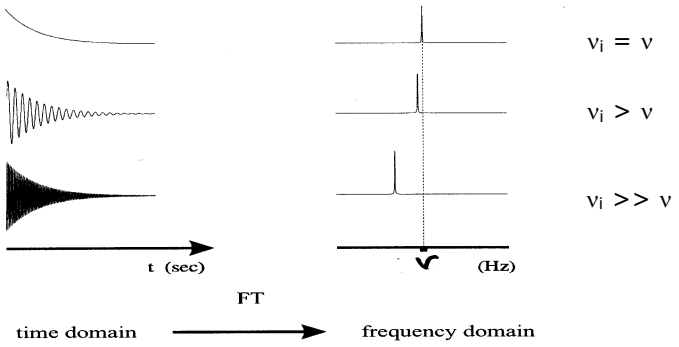

Figure S10 The free induction decay (FID) is the decay of the transversal magnetization which forms the observable NMR signals detected by the receiver in the x'y'-plane of the rotating frame. The FID is the sum of many time domain signals and is transformed via Fourier Transformation into the frequency domain signals or NMR spectrum.

Relaxation

After the B_1 pulse, the μ-vectors will also be subjected to relaxation. Two relaxation processes, i.e. T_1 and T_2 relaxation, can be described by an exponential function with a characteristic relaxation decay time constant. The inverse of the relaxation decay time constant is a measure of the speed of relaxation: the shorter the relaxation time is, the more efficient the relaxation will be.

The longitudinal relaxation or T_1 relaxation is the decay time by which the z-magnetization (M_z) aims to reach its original value M_0 by energy exchange between the nuclei and the environment (back to the Boltzmann equilibrium: excess of spins in the low energy state). Longitudinal relaxation corresponds with a change in energy because the energy absorbed by the spins under influence of B_1-pulse has to be returned to the environment. Hence, the original equilibrium distribution of the two spin states will be restored (Figure S11).

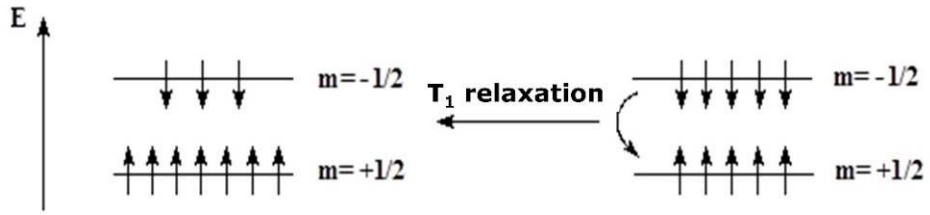

Figure S11 Longitudinal or T_1 relaxation.

Transversal relaxation or T_2 relaxation is the decay time by which the x'-y' magnetization disappears. The individual μ-vectors of the hydrogen protons will lose their phase coherence by shared spin-spin interactions (Figure S12). Consequently, the transversal magnetization $M_{x'y'}$ completely disappears by strong spin-spin interactions, while the equilibrium magnetization might still not reached ($M_z \ll M_0$). Generally, T_2 is equal to or shorter than T_1.

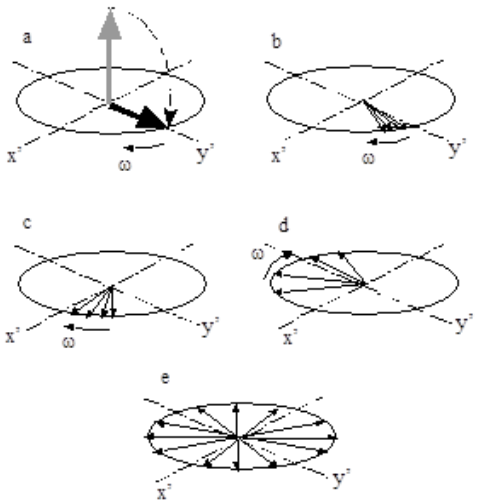

Figure S12 Transversal or T_2 relaxation.

Carr-Purcell-Meiboom-Gill (CPMG) pulse sequence

For this thesis, slightly T_2-weighted spectra were acquired using the Carr-Purcell-Meiboom-Gill (CPMG)-presat pulse sequence which is named after its inventors [226, 227]. The CPMG pulse sequence uses the faster T_2 relaxation of protons in macromolecules (such as proteins and polysaccharides), i.e. protons with shorter T_2 relaxation times – to suppress these particular signals and generate spectra in which only the signals of small molecule metabolites are observed. In addition, water suppression (CPMG-'presat', i.e. presaturation) was performed in order to allow optimal detection and quantification of the signals close to the water resonance. The CPMG-presat pulse sequence has the form $[RD\text{-}90°\text{-}(\tau\text{-}180°\text{-}\tau)_m\text{-}ACQ]_n$ where RD is the relaxation delay, 90° is the 90° RF-pulse, 180° is the 180° RF-pulse, mx2τ is the spin-echo delay, m represent the number of loops, and ACQ is the acquisition time. During RD (0.5 s), the water signal is irradiated. Another advantage of this spin-echo pulse-sequence is the elimination of the influence of inhomogeneities in B_0 over the sample volume (by dephasing-rephasing). By this, the detected echo signal is only attenuated by real T_2 relaxation. An increase in the number of 'spin-echo' cycles (m) corresponds with an extension of the total spin-echo delay.

In this thesis, all ^{1}H-NMR spectra were acquired with 96 scans (total acquisition time of 7'44'') at 21.2 °C on a 400 MHz Varian Inova NMR spectrometer (Agilent Technologies Inc., Santa Clara, CA, USA) having a magnetic field strength of 9.4 Tesla. In addition, ^{1}H-NMR spectra were acquired with 13 K complex data points, 6000 Hz spectral width, a presaturation of 3 s, an acquisition time of 1.1 s and a relaxation delay of 0.5 s. Each free induction decay (FID) was zero-filled to 65 K points and multiplied by a 0.7 Hz exponential line-broadening function prior to Fourier transformation.

The ^{1}H-NMR spectrum

The ^{1}H-NMR spectrum is determined by three parameters that can be related to the structure of the molecule under study: (1) chemical shift or the location of ^{1}H signals in the spectrum; (2) integration of signal area or signal intensity; (3) J-coupling patterns or shape of signals in the spectrum (Figure S13).

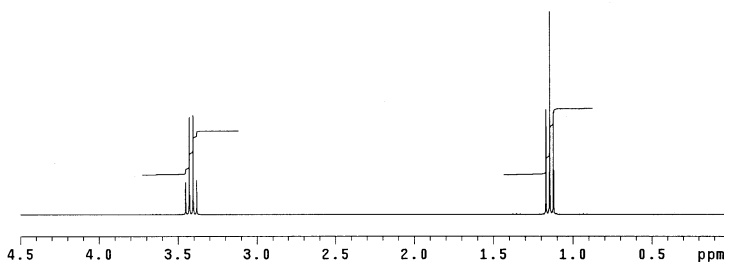

Figure S13 ^{1}H-NMR spectrum of diethyl ether ($C_4H_{10}O$). The place in the spectrum is determined by the chemical shift, the lines above the signals are indicating the integration values and regions, and the quadruplet and triplet pattern is determined by the J-coupling.

Chemical shift

When an atom is placed in a magnetic field, it will not sense the true value of the external B_0 field since local and neighboring electrons will shield the nucleus from the B_0 field. Hence, the effective field (B_{0i}) that a hydrogen nucleus feels depends on its chemical environment determining the neighboring electron density. The higher the electron density around the hydrogen nucleus, the more it is shielded. For a nucleus i with a dimensionless magnetic shielding constant σi the following applies:

$$B_{0i} = B_0 - \sigma_i B_0 = (1-\sigma_i)B_0$$

so that $\omega_i = \gamma(1-\sigma_i)B_0 = \gamma B_{0i}$ or $\nu_i = \frac{\gamma}{2\pi}(1-\sigma_i)B_0 = \frac{\gamma}{2\pi}B_{0i}$

Hence, B_{0i} will be different from B_0 explaining why the resonance frequency ω_i (or ν_i in Hz) is different for different chemical environments. Absolute frequencies are rarely used. The location of the resonance signal in the NMR spectrum is represented by the chemical shift (δ):

$$\delta = \frac{\nu_i - \nu_{TMS}}{\nu_{TMS}} \cdot 10^6$$

in which ν_i is the resonance frequency of the proton considered and νTMS is the resonance frequency of the generally accepted reference compound tetramethylsilane. In most cases $\nu_i > \nu$TMS.

For example, for protons of a –O-CH_3 group on a 200 MHz (4.7 Tesla) NMR spectrometer applies:

νi = 200.000.646 Hz if νTMS = 200.000.000 Hz

$$\delta_{OCH_3} = \frac{200.000.646 - 200.000.000}{200\ x\ 10^6}\ x\ 10^6 = 3{,}23 ppm$$

On a 400 MHz (9.4 Tesla) NMR device the following applies:

νi = 400.001.292 Hz if νTMS = 400.000.000 Hz

$$\delta_{OCH_3} = \frac{400.001.292 - 400.000.000}{400\ x\ 10^6}\ x\ 10^6 = 3{,}23 ppm$$

Hence, on a 200 MHz NMR spectrometer, 200 Hz equals 1 ppm and on a 400 MHz NMR spectrometer – as used in this thesis – 400 Hz equals also 1 ppm. This is explained by the fact that the chemical shift is independent of B_0. Hence, the resolution of a 400 MHz NMR spectrometer is greater than that of a 200 MHz NMR spectrometer.

The chemical shift is dimensionless and expressed in parts per million (ppm). Most of the proton resonance signals are located between 0 and 12 ppm (Figure S14). The reference used in this thesis is trimethylsilyl-2,2,3,3-tetradeuteropropionic acid (TSP) which is composed of three equivalent CH_3 methyl groups single bonded to a silicon atom. All CH_3 group protons have the same electronic environment, and therefore result in only a single ^{1}H-NMR signal at 0.015 ppm.

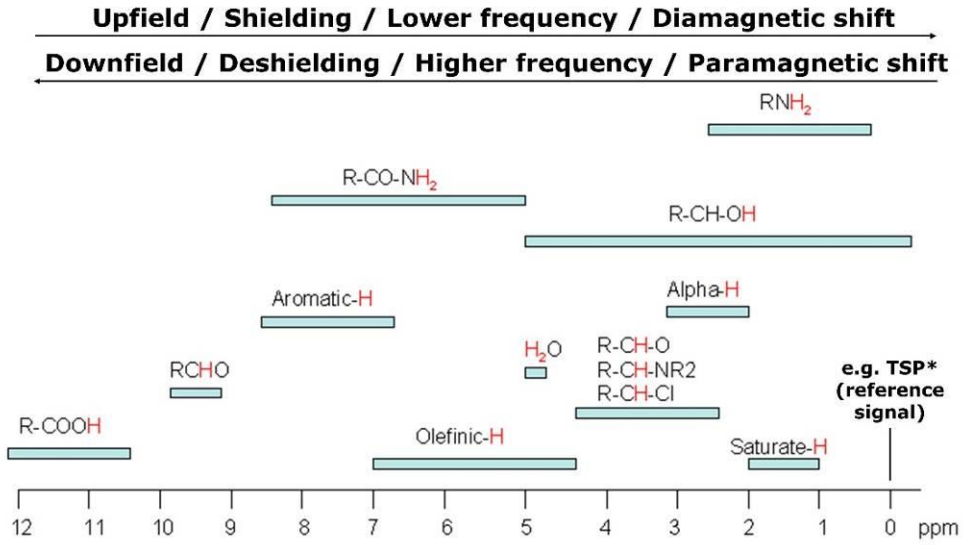

Figure S14 ^{1}H-NMR chemical shifts (δ in ppm) for common functional chemical groups [228]. *^{1}H-NMR spectra of this thesis were referenced to the methyl resonance of trimethylsilyl-2,2,3,3-tetradeuteropropionic acid (TSP) at 0.015 ppm.

Integration region

The integration value of an integration (or spectral) region is a measure for the number of contributing protons. Integration values are obtained by putting integration lines over well-defined integration regions (Figure S13). For this thesis, the ^{1}H-NMR spectra of plasma, in the range between 8 and 0.8 ppm, were segmented into 110 variable-sized spectral regions, excluding the water region between 5.2 and 4.7 ppm and the TSP signal between 0.3 and -0.3 ppm. The 110 spectral regions, subsequently named variables (VAR_{PL}), were defined by means of spiking experiments with known metabolites (see Chapter 5) . The resulting spectral regions were integrated and normalized relative to the total integrated area of all spectral regions. For urine, the ^{1}H-NMR spectra in the range between 9.5 and 0.7 ppm were segmented into 134 variable-sized spectral regions, excluding the water region between 5.1 and 4.6 ppm and the TSP signal between 0.3 and -0.3 ppm. The 134 spectral regions, subsequently named variables (VAR_{UR}), were defined by means of spiking experiments with known metabolites (see Chapter 5). The resulting spectral regions were integrated and normalized relative to the total integrated area of all spectral regions, except those of high-intensity resonances of the following integration

regions or variables (VAR_{UR}): 35, 43, 54, 56, 59, 60, 88, 116, 134 (see Chapter 5 for information on metabolite assignments).

J-coupling

Two nuclei with a different chemical environment (non-equivalent nuclei with different chemical shift values) can induce the phenomena of spin-spin coupling or J-coupling via binding electrons. The J-coupling pattern is determined by the rule of multiplicity: $(2n_1*I_1 +1) * (2n_2*I_2 +1)$, where n is the number of nuclei equivalent to each other but not equivalent to the nucleus under investigation, and I is the spin quantum number.

For example, chloroethane (CH_3CH_2Cl) consists of CH_3 and CH_2 protons. In this case, the CH_3 signal splits into a triplet: 2*2*1/2 +1 = 3, and the CH_2 signal into a quadruplet: 2*3*1/2 +1 = 4. Or in other words, the CH_3 protons sense the orientation of the CH_2 proton spins, resulting in a triplet with a 1-2-1 intensity ratio: (A) ↑↑; (B) ↑↓ or ↓↑; (C) ↓↓. And the other way around for the CH_2 protons sensing the CH_3 proton spins and producing a quadruplet with a 1-3-3-1 intensity ratio: (A) ↑↑↑; (B) ↑↑↓ or ↑↓↑ or ↓↑↑; (C) ↓↓↑ or ↓↑↓ or ↑↓↓; (D) ↓↓↓ (Figure S15).

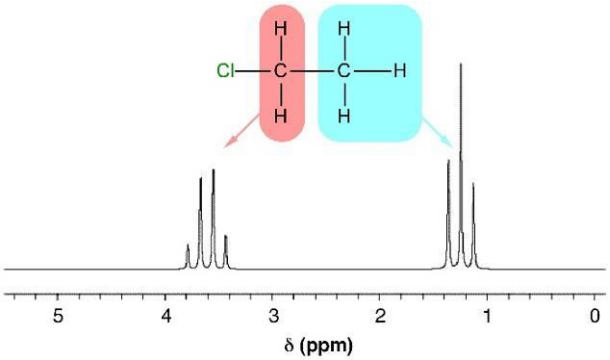

Figure S15 J-coupling patterns of chloroethane, i.e. a triplet and quadruplet [229].

In general, J-couplings can result in singlets, doublets, triplets, etc. in the ^{1}H-NMR spectrum. It should be noted that the J-coupling between chemically equivalent protons is not observed in the ^{1}H-NMR spectrum.

Multivariate projection methods

Unsupervised PCA analysis

Principal component analysis (PCA) forms the basis for multivariate data analysis and it is performed on a data matrix X with *N rows* (observations) and *K columns* (variables) (Figure S16). Data matrix X is then converted to a variable space with as many dimensions as there are variables. Each variable represents one co-ordinate axis.

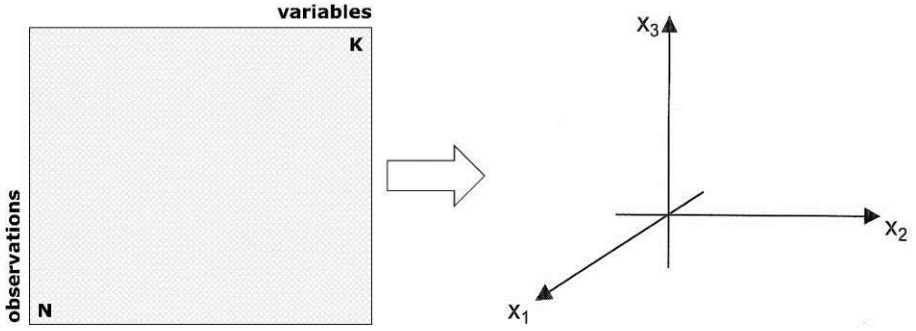

Figure S16 Structure of data matrix X used for PCA analysis. The N observations (rows) can be biological individuals, analytical samples, etc. The K variables (columns) can be NMR variables derived from spectral data.

Next, each observation of the X-matrix is placed in the K-dimensional variable space (Figure S17A). After mean-centering and scaling of the data, the coordinate system is re-positioned such that the average point now is the origin.

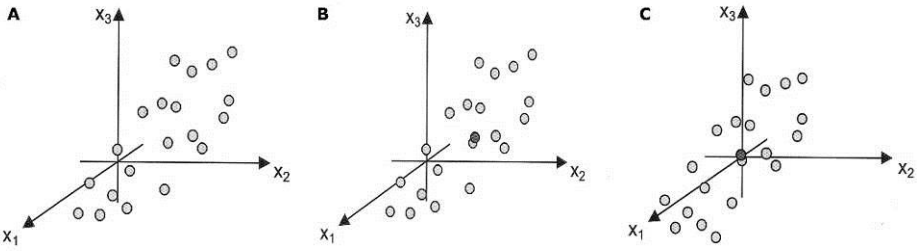

Figure S17 Plotting the observations in K-dimensional space. (A) Observations (N, rows) in data matrix X are a group of points in the variable space K; (B) The vector of variable averages is computed and is a point (black dot) situated in the middle of the group of points; (C) After mean-centering and scaling, the origin of the co-ordinate system is moved to coincide with the average point (black dot).

Data matrix X can then be converted to principal components (PC). PC1 (first principal component) is the line in the K-dimensional space that best approximates the shape of the group of points (observations), i.e. it represents the maximum variance direction in the data (Figure S18A). Each observation is projected onto this line in order to get a value which is known as a score. However, one component is insufficient to model the systemic variation of a multidimensional dataset. Thus, PC2 (second principal component) which is orthogonal to PC1 and improves the approximation of the X-data to a feasible extent, is also calculated (Figure S18B).

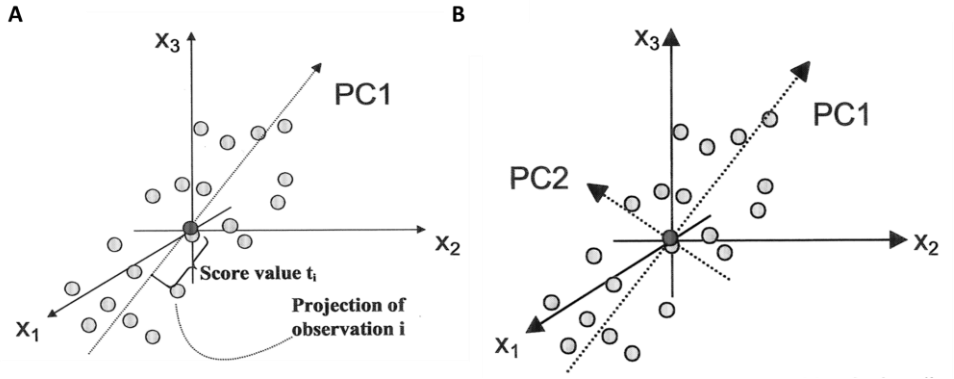

Figure S18 Principal components for PCA. (A) The first principal component, PC1; (B) The second principal component, PC2.

This results in a plane into the K-dimensional variable space (Figure S19).

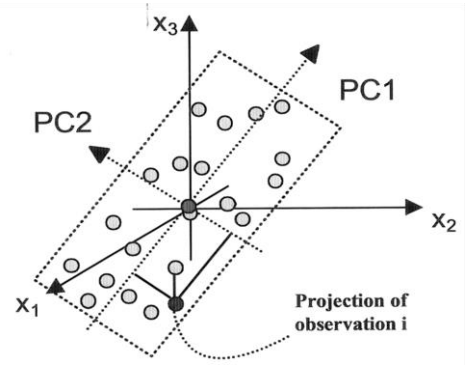

Figure S19 Two principal components define a model plane.

The co-ordinate values of the observations on this plane are called *scores*, and hence the plotting of such a projected configuration is known as a *score plot*. A score plot is always accompanied by a *loading plot* that reveals which variables are responsible for the patterns seen among the observations [201] (Figure S20).

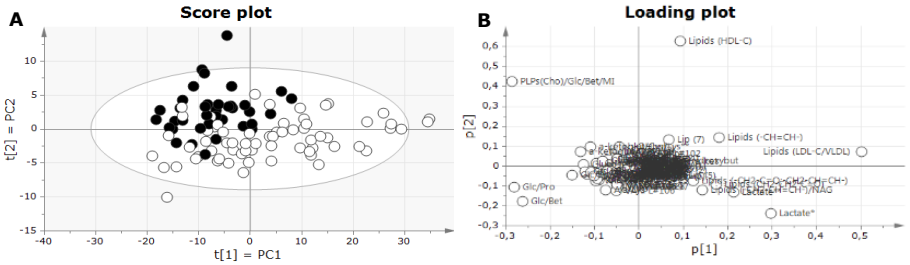

Figure S20 PCA score and loading plot. (A) PCA score plot of the two first PCs: PC1 and PC2 of the PCA score plot explain the largest and second largest variation within the data, respectively. Each point in the score plot represents an observation. Observations that lie outside the white circle (95% CI) can be assumed as being outliers. (B) PCA loading plot of the two first PCs (p_2 vs p_1). Each point in the loading plot represents the variables that are responsible for the pattern seen among the observations. The plots are based on data extracted from this thesis.

Consequently, PCA score and loading plots can be used to identify clustering patterns and dominant variation in the dataset which may not be associated with the real biological effect but could also be due to a secondary effect such as diet, age, gender and instrumental error (e.g. batch effect). In addition, PCA score plots allows the observation of outliers, i.e. observations that lie outside the 95% CI (see Figure S20). However, additional confirmatory methods such as Distance to Model (DModX) or Hotelling's T^2 range plot to determine outliers in the orthogonal plane are recommended to perform (Figure S21).

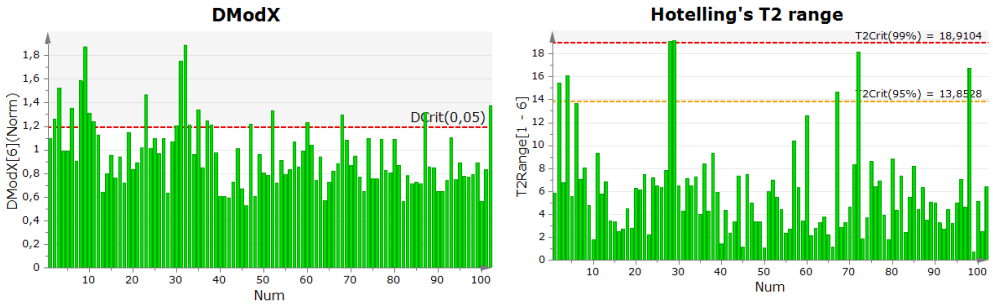

Figure S21 Outlier detection. (A) DModX is the distance of an observation in the dataset to the X model plane. DModX is displayed as the absolute DModX divided by the pooled residual standard deviation of the model. The critical value of DModX (Dcrit) is computed from the F-distribution. Observations with a DModX twice as large as Dcrit are moderate outliers. (B) Hotelling's T^2 range plot displays the distance from the origin in the model plane (score space) for each selected observation. This plot shows the T^2 calculated as the sum over the selected range of components of the scores, i.e. 1 to 6 in this case, in square divided by their standard deviations in square. Values larger than 95% CI are suspect, and values larger than 99% CI can be considered as serious. The plots are based on data extracted from this thesis.

Supervised PLS and OPLS-DA analysis

Unsupervised methods are commonly used together with supervised methods such as partial least squares (PLS) and discriminant function analysis (e.g. OPLS-DA) [230].

PLS is a method for relating two data matrices, X and Y, to each other by a linear multivariate model, i.e. it models the association between X and Y by regression. Data matrix X with *N observations* and *K factors/predictors* (independent variables) is related to data matrix Y with N observations and *M responses* (dependent variables) (Figure S22).

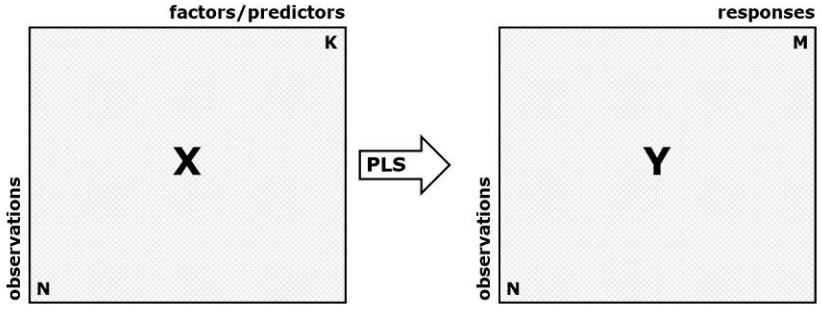

Figure S22 Structure of data matrix X and Y used for PLS analysis. The N observations (rows) can be biological individuals, analytical samples, etc. The X-variables (K, factors/predictors) can be NMR variables derived from spectral data. The Y-variables (M, responses) are often gathered to reflect properties of samples, clinical variables, etc.

In contrast to PCA, each row (observation) now represents two points instead of one, one in the X-space and one in the Y-space (see Figure S23). Also here, data have to be mean-centered and scaled.

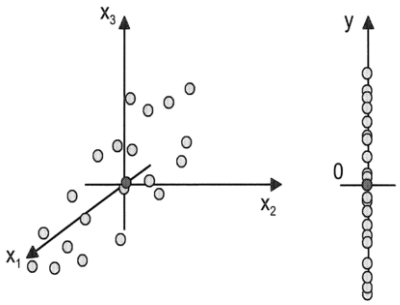

Figure S23 In a regression model, the observations are two groups of points, one in the predictor (X) space and one in the response (Y) space. Note that in this figure, a single Y-variable instead of a matrix Y of responses is considered.

In PLS, the first PLS component is a line in the X-space that well approximates the groups of points and provides a good correlation with the Y-vector (Figure S24). The co-ordinate of an observation along this line is obtained by projecting the sample onto the line. This co-ordinate is termed the score, t_{i1}, of observation i. The scores of all the observations constitute the first X-score vector t_1 (a latent variable). Score vector t_1 can then be used to acquire an estimate of y, $\hat{y}_1$, after PC1 of PLS, which is t_1 multiplied by the weight of the y-vector, c_1. The differences between the measured and estimated response data are called residuals. The y-residuals represent the variation that is left unexplained by the first PLS component. The residual vector f_1 is calculated as $y - \hat{y}_1$.

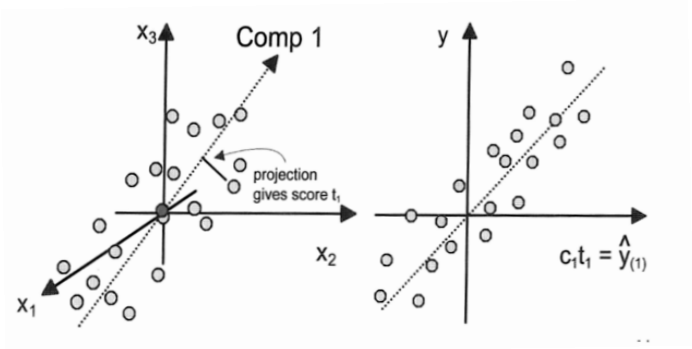

Figure S24 First principal component for PLS. With one single Y-variable, the Y-space reduces to a one dimensional vector. PC1 will orient itself so that it well describes the group of points in the X-space while at the same time giving a good correlation with the Y-vector. Score vector t_1 summarizes the information in the original X-variables.

Here too, one PLS component is insufficient to adequately model the variation in the Y-data. Therefore, a second component is calculated which is also a line in the X-space, which passes through the origin and is orthogonal to the first component (Figure S25). This component finds the direction in X-space that improves the description of the X-data as much as possible, while providing a good correlation with the y-residuals, f_1, remaining after the first component. The second set of score values of the observations arises from the co-ordinates along the second projection direction in the X-space, i.e. second score vector t_2. In general, the tighter the scatter around the diagonal, the stronger the correlation between X and Y [201].

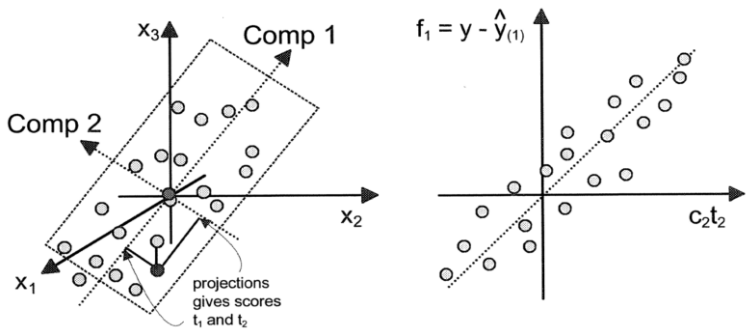

Figure S25 Second principal component for PLS in the X-space is orthogonal to the first one. By projecting the observations onto this line, one obtains the score vector t_2. The second score vector times the second weight of the y-data, c_2, correlates with the y-residual, f_1, after the first dimension. The two components together define a plane in the X-space.

In addition, the combined power of t_1 and t_2 in modeling and predicting y can also be examined with PLS. An estimate of y after two model components, $\hat{y}_2$, is obtained through computing $c_1t_1 + c_2t_2$. The y-variable is better modeled by two components than by one because the agreement between observed and estimated Y-data improves.

Supervised methods such as discriminant analysis (DA) can also be used for sample classification (e.g. disease vs. healthy). Orthogonal PLS (OPLS) separates the systemic variation in X into two parts, one part that is correlated (predictive) to Y and one part that is uncorrelated (orthogonal) to Y. In other words, it models the variation orthogonal to the Y response, resulting in models that are equally predictive but easier to interpret than conventional PLS [231] (Figure S26). In OPLS-DA, knowledge about the class membership (e.g. disease vs. healthy) is used to help discriminate groups of metabolites that are significant in combination (e.g. biomarker signature/classifier).

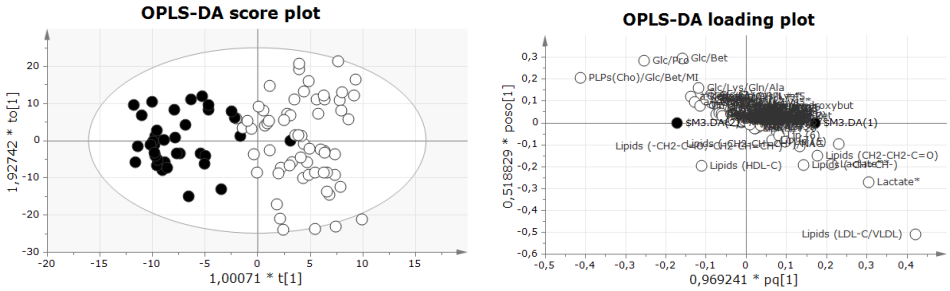

Figure S26 OPLS-DA score and loading plot. (A) OPLS-DA score plot: The first predictive component (t[1]) explains the variation between both study groups and the first orthogonal component (to[1]) explains the variation within both study groups. (B) OPLS-DA loading plot: The horizontal axis displays the X-loadings p and the Y-loadings q of the predictive component. The vertical axis displays the X-loadings p(o) and the Y-loadings s(o) for the Y-orthogonal component. The plots are based on data extracted from this thesis.

The model performance can be explored by evaluating the total amount of predictive and orthogonal variation in X ($R^2X(cum)$) and total amount of variation in Y ($R^2Y(cum)$), and the predictive ability of the model ($Q^2(cum)$). The higher these values, the higher the association between X and Y variables, the better the model (Figure S26).

In OPLS-DA it is important to define both a training set (original data) and an independent validation set (a class of separate samples that can be predicted

based on a series of mathematical models derived from the training set) in order to validate study results [201] (Figure S27).

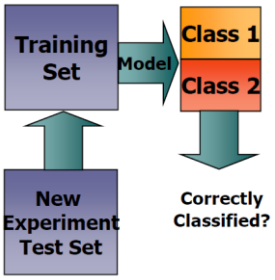

Figure S27. Classification models. First, the model must be trained on representative data (training set). Next, the model must be tested using new data (validation set).

Diagnostic tools

OPLS-DA provides many diagnostics which help in the model interpretation, and in the assessment of model performance and relevance.

The *misclassification list* summarizes how well the OPLS-DA models classify the observations into known classes (Figure S28). Sensitivity is explained as the percentage of patients that are actually classified as patients, and specificity is explained as the percentage of controls that are actually classified as controls.

	Members	Correct	0	1	No class (YPred < 0)
0 = Spec.	36	91,67%	33	3	0
1 = Sens.	61	95,08%	3	58	0
No class	5		2	3	0
Total	102	93,81%	38	64	0

Figure S28 Misclassification list. 33 out of 36 (94.67%) controls are correctly classified and 58 out of 61 (95.08%) patients are correctly classified. The overall classification rate is 93.81%. The list is based on data extracted from this thesis.

The *variable influence on projection (VIP)* parameter gives the importance of the X-variables, both for X- and Y-models (see Figure S29). The VIP is a weighted sum of squares of the OPLS-DA weights, taking into account the amount of explained Y-variance in each dimension. Hence, one VIP-vector summarizes all components and Y-variables. Predictors with a large VIP, larger than 1, are most influential for the model. The VIP-value and/or visual thresholds on the VIP plot may be used for a variable selection. Note, however, that variable selection

should be carried out with caution as there are strong correlations among the X-variables.

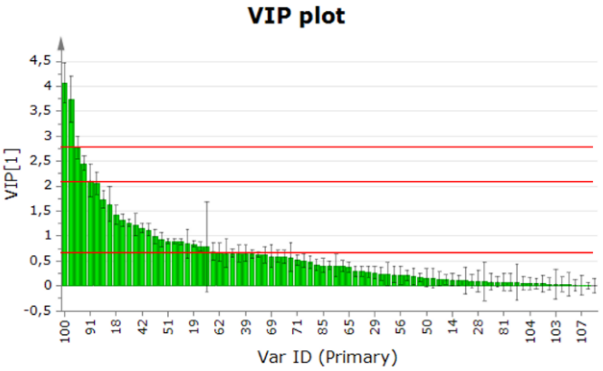

Figure S29 Variable influence on projection (VIP) plot. The red lines are indicating different thresholds which might be used and tested for variable selection. The plot is based on data extracted from this thesis.

Especially for NMR data, an *S-plot* of the variables that are responsible for the pattern seen among the observations, is very useful and can be illustrated as a points or a line (Figure S30). The S-plot is a practical and reliable way to identify important discriminating variables.

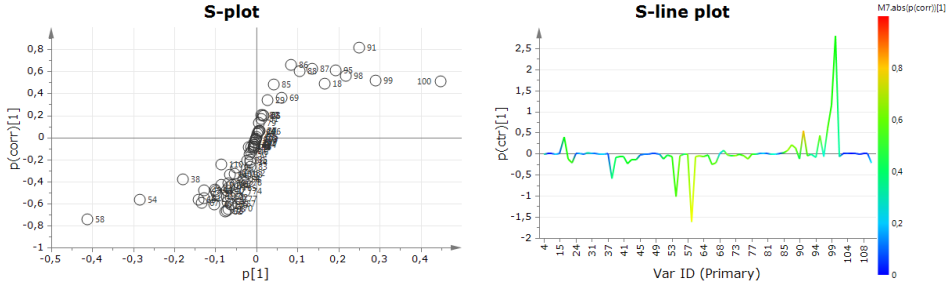

Figure S30 S-plots of an OPLS-DA model. (A) S-plot with variables in the bottom left or upper right as being those with a strong contribution to the model and high statistical reliability. (B) S-line plot has the advantage of taking the spectral order of NMR data into account. The relevance of the model is indicated by the signal amplitude and the significance by color. Strongly discriminating variables combine a high numerical loading value and red to orange color. The plots are based on data extracted from this thesis.

A *permutation plot* for PLS-DA can be developed to assess the risk that the current OPLS-DA model is spurious, i.e. if the model fits the training set well but does not predict Y well for new observations (Figure S31).

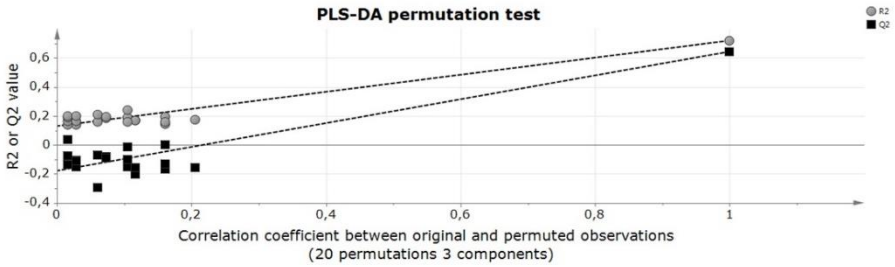

Figure S31. PLS-DA permutation test. The PLS-DA permutation test illustrates the validity of the model. For a model to be valid, R^2 (grey dots) and Q^2 (black boxes) values for each permuted observation have to be lower than 0.3 and 0.05, respectively

The *permutation plot* compares the goodness of fit (R^2 and Q^2) of the original model with the goodness of fit of several models based on data where the order of the Y-observations has been randomly permuted, while the X-matrix has been kept intact. The plot shows, for a selected Y-variable, on the vertical axis the values of R^2 and Q^2 for the original model (on the right side) and of the Y-permuted models (on the left side). The horizontal axis shows the correlation between the permuted Y-vectors and the original Y-vector for the selected Y. Criteria for a valid OPLS-DA model are: (i) all Q^2 values on the left are lower than the original point on the right; (ii) the regression line of the Q^2 points intersects the vertical axis (on the left) at, or below zero; (iii) all R^2 values to the left are lower than the original point to the right.

References

1. De Onis M, Blössner M, Borghi E. Global prevalence and trends of overweight and obesity among preschool children. Am J Clin Nutr. 2010;92(5):1257-64.
2. Ng M, Fleming T, Robinson M, Thomson B, Graetz N, Margono C, et al. Global, regional, and national prevalence of overweight and obesity in children and adults during 1980-2013: a systematic analysis for the Global Burden of Disease Study 2013. Lancet. 2014;384(9945):766-81.
3. Olds T, Maher C, Zumin S, Péneau S, Lioret S, Castetbon K, et al. Evidence that the prevalence of childhood overweight is plateauing: data from nine countries. Int J Pediatr Obes. 2011;6(5-6):342-60.
4. Gupta N, Goel K, Shah P, Misra A. Childhood obesity in developing countries: epidemiology, determinants, and prevention. Endocr Rev. 2012;33(1):48-70.
5. Skinner AC, Skelton JA. Prevalence and trends in obesity and severe obesity among children in the United States, 1999-2012. JAMA Pediatr. 2014;168(6):561-6.
6. Reilly JJ, Kelly J. Long-term impact of overweight and obesity in childhood and adolescence on morbidity and premature mortality in adulthood: systematic review. Int J Obes. 2011;35(7):891-8.
7. Eckel RH, Grundy SM, Zimmet PZ. The metabolic syndrome. Lancet. 2005;365(9468):1415-28.
8. Wang G, Dietz WH. Economic burden of obesity in youths aged 6 to 17 years: 1979–1999. Pediatrics. 2002;109(5):e81.
9. Olshansky SJ, Passaro DJ, Hershow RC, Layden J, Carnes BA, Brody J, et al. A potential decline in life expectancy in the United States in the 21st century. N Engl J Med. 2005;352(11):1138-45.
10. Farrant B, Utter J, Ameratunga S, Clark T, Fleming T, Denny S. Prevalence of severe obesity among New Zealand adolescents and associations with health risk behaviors and emotional well-being. J Pediatr. 2013;163(1):143-9.
11. Ogden CL, Carroll MD, Kit BK, Flegal KM. Prevalence of obesity and trends in body mass index among US children and adolescents, 1999-2010. JAMA. 2012;307(5):483-90.
12. Brug J, van Stralen MM, te Velde SJ, Chinapaw MJ, De Bourdeaudhuij I, Lien N, et al. Differences in weight status and energy-balance related behaviors among schoolchildren across Europe: the ENERGY-project. PLoS One. 2012;7(4):e34742.
13. Massa G. Body mass index measurements and prevalence of overweight and obesity in school-children living in the province of Belgian Limburg. Eur J Pediatr. 2002;161(6):343-6.
14. Weiss R, Dziura J, Burgert TS, Tamborlane WV, Taksali SE, Yeckel CW, et al. Obesity and the metabolic syndrome in children and adolescents. N Engl J Med. 2004;350(23):2362-74.
15. Goodman E, Daniels SR, Morrison JA, Huang B, Dolan LM. Contrasting prevalence of and demographic disparities in the World Health Organization and National Cholesterol Education Program Adult Treatment Panel III definitions of metabolic syndrome among adolescents. J Pediatr. 2004;145(4):445-51.
16. Golley RK, Magarey AM, Steinbeck KS, Baur LA, Daniels LA. Comparison of metabolic syndrome prevalence using six different definitions in overweight pre-pubertal children enrolled in a weight management study. Int J Obes (Lond). 2006;30(5):853-60.
17. Owens S, Galloway R. Childhood obesity and the metabolic syndrome. Curr Atheroscler Rep. 2014;16(9):436.
18. Friend A, Craig L, Turner S. The prevalence of metabolic syndrome in children: a systematic review of the literature. Metab Syndr Relat Disord. 2013;11(2):71-80.
19. World Health Organisation. Obesity: preventing and managing the global epidemic. Report of a WHO Expert Committee, WHO Technical Report Series, N°894. Geneva: WHO, 2000.

20. Reilly JJ. Assessment of body composition in infants and children. Nutrition. 1998;14(10):821-5.
21. Kyle UG, Bosaeus I, De Lorenzo AD, Deurenberg P, Elia M, Manuel Gomez J, et al. Bioelectrical impedance analysis-part II: utilization in clinical practice. Clin Nutr. 2004;23(6):1430-53.
22. Kyle UG, Bosaeus I, De Lorenzo AD, Deurenberg P, Elia M, Gomez JM, et al. Bioelectrical impedance analysis-part I: review of principles and methods. Clin Nutr. 2004;23(5):1226-43.
23. Cleary J, Daniells S, Okely AD, Batterham M, Nicholls J. Predictive validity of four bioelectrical impedance equations in determining percent fat mass in overweight and obese children. J Am Diet Assoc. 2008;108(1):136-9.
24. Clasey JL, Bradley KD, Bradley JW, Long DE, Griffith JR. A new BIA equation estimating the body composition of young children. Obesity (Silver Spring). 2011;19(9):1813-7.
25. Schaefer F, Georgi M, Zieger A, Scharer K. Usefulness of bioelectric impedance and skinfold measurements in predicting fat-free mass derived from total body potassium in children. Pediatr Res. 1994;35(5):617-24.
26. Montagnese C, Williams JE, Haroun D, Siervo M, Fewtrell MS, Wells JC. Is a single bioelectrical impedance equation valid for children of wide ranges of age, pubertal status and nutritional status? Evidence from the 4-component model. Eur J Clin Nutr. 2013;67(S1):S34-9.
27. Watts K, Naylor LH, Davis EA, Jones TW, Beeson B, Bettenay F, et al. Do skinfolds accurately assess changes in body fat in obese children and adolescents? Med Sci Sports Exerc. 2006;38(3):439-44.
28. Freedman DS, Ogden CL, Blanck HM, Borrud LG, Dietz WH. The abilities of body mass index and skinfold thicknesses to identify children with low or elevated levels of dual-energy X-ray absorptiometry-determined body fatness. J Pediatr. 2013;163(1):160-6.
29. Eknoyan G. Adolphe Quetelet (1796-1874)-the average man and indices of obesity. Nephrol Dial Transplant. 2008;23(1):47-51.
30. World Health Organisation. Physical status: the use and interpretation of anthropometry. Report of a WHO Expert Committee, WHO Technical Report Series N°854. Geneva: WHO, 1995.
31. Dietz WH, Bellizzi MC. Introduction: the use of body mass index to assess obesity in children. Am J Clin Nutr. 1999;70(1):S123-5.
32. Bouchard C. BMI, fat mass, abdominal adiposity and visceral fat: where is the 'beef'? Int J Obes. 2007;31(10):1552-3.
33. Han JC, Lawlor DA, Kimm SY. Childhood obesity. Lancet. 2010;375(9727):1737-48.
34. Roelants M, Hauspie R, Hoppenbrouwers K. References for growth and pubertal development from birth to 21 years in Flanders, Belgium. Ann Hum Biol. 2009;36(6):680-94.
35. Cole TJ, Green PJ. Smoothing reference centile curves: the LMS method and penalized likelihood. Stat Med. 1992;11(10):1305-19.
36. Cole TJ, Bellizzi MC, Flegal KM, Dietz WH. Establishing a standard definition for child overweight and obesity worldwide: international survey. BMJ. 2000;320(7244):1-6.
37. Cole T, Lobstein T. Extended international (IOTF) body mass index cut-offs for thinness, overweight and obesity. Pediatr Obes. 2012;7(4):284-94.
38. de Onis M, Onyango AW, Borghi E, Siyam A, Nishida C, Siekmann J. Development of a WHO growth reference for school-aged children and adolescents. Bull World Health Organ. 2007;85(9):660-7.
39. Kuczmarski RJ, Ogden CL, Grummer-Strawn LM, Flegal KM, Guo SS, Wei R, et al. CDC growth charts: United States. Adv Data. 2000;314:1-27.
40. Reilly JJ, Dorosty AR, Emmett PM, Avon Longitudinal Study of Pregnancy, Childhood Study Team. Identification of the obese child: adequacy of the body mass index for clinical practice and epidemiology. Int J Obes Relat Metab Disord. 2000;24(12):1623-7.
41. Savva SC, Tornaritis M, Savva ME, Kourides Y, Panagi A, Silikiotou N, et al. Waist circumference and waist-to-height ratio are better predictors of cardiovascular

disease risk factors in children than body mass index. Int J Obes Relat Metab Disord. 2000;24(11):1453-8.
42. Janssen I, Katzmarzyk PT, Srinivasan SR, Chen W, Malina RM, Bouchard C, et al. Combined influence of body mass index and waist circumference on coronary artery disease risk factors among children and adolescents. Pediatrics. 2005;115(6):1623-30.
43. Krebs NF, Himes JH, Jacobson D, Nicklas TA, Guilday P, Styne D. Assessment of child and adolescent overweight and obesity. Pediatrics. 2007;120 (Suppl 4):S193-228.
44. Reaven GM. Role of insulin resistance in human disease. Diabetes. 1988;37(12):1595-607.
45. Alberti KGMM, Zimmet Pf. Definition, diagnosis and classification of diabetes mellitus and its complications. Part 1: diagnosis and classification of diabetes mellitus. Provisional report of a WHO consultation. Diabetic Med. 1998;15(7):539-53.
46. Expert Panel on Detection Evaluation Treatment of High Blood Cholesterol in Adults. Executive summary of the third report of the National Cholesterol Education Program (NCEP) expert panel on detection, evaluation, and treatment of high blood cholesterol in adults (Adult Treatment Panel III). JAMA. 2001;285(19):2486-97.
47. Alberti KG, Zimmet P, Shaw J, IDF Epidemiology Task Force Consensus Group. The metabolic syndrome - a new worldwide definition. Lancet. 2005;366(9491):1059-62.
48. Cook S, Weitzman M, Auinger P, Nguyen M, Dietz WH. Prevalence of a metabolic syndrome phenotype in adolescents: findings from the third National Health and Nutrition Examination Survey, 1988-1994. Arch Pediatr Adolesc Med. 2003;157(8):821-7.
49. Ford ES, Li C. Defining the metabolic syndrome in children and adolescents: will the real definition please stand up? J Pediatr. 2008;152(2):160-4.
50. Zimmet P, Alberti K, George MM, Kaufman F, Tajima N, Silink M, et al. The metabolic sydrome in children and adolescents - an IDF consensus report. Pediatr Diabetes. 2007;8:299-306.
51. Jolliffe CJ, Janssen I. Development of age-specific adolescent metabolic syndrome criteria that are linked to the Adult Treatment Panel III and International Diabetes Federation criteria. J Am Coll Cardiol. 2007;49(8):891-8.
52. Mancini MC. Metabolic syndrome in children and adolescents - criteria for diagnosis. Diabetol Metab Syndr. 2009;1(1):20.
53. Druet C, Ong K, Levy Marchal C. Metabolic syndrome in children: comparison of the International Diabetes Federation 2007 consensus with an adapted National Cholesterol Education Program definition in 300 overweight and obese French children. Horm Res Paediatr. 2010;73(3):181-6.
54. Sinaiko AR, Caprio S. Insulin resistance. J Pediatr. 2012;161(1):11-5.
55. Kurtoglu S, Akin L, Kendirci M, Hatipoglu N, Elmali F, Mazicioglu M. The absence of insulin resistance in metabolic syndrome definition leads to underdiagnosing of metabolic risk in obese patients. Eur J Pediatr. 2012;171(9):1331-7.
56. DeFronzo RA, Tobin JD, Andres R. Glucose clamp technique: a method for quantifying insulin secretion and resistance. Am J Physiol Endocrinol Metab. 1979;237(3):214-23.
57. Coates PA, Luzio SD, Brunel P, Owens DR. Comparison of estimates of insulin sensitivity from minimal model analysis of the insulin-modified frequently sampled intravenous glucose tolerance test and the isoglycemic hyperinsulinemic clamp in subjects with NIDDM. Diabetes. 1995;44(6):631-5.
58. Stumvoll M, Mitrakou A, Pimenta W, Jenssen T, Yki-Järvinen H, Van Haeften T, et al. Use of the oral glucose tolerance test to assess insulin release and insulin sensitivity. Diabetes Care. 2000;23(3):295-301.
59. Gungor N, Saad R, Janosky J, Arslanian S. Validation of surrogate estimates of insulin sensitivity and insulin secretion in children and adolescents. J Pediatr. 2004;144(1):47-55.
60. George L, Bacha F, Lee S, Tfayli H, Andreatta E, Arslanian S. Surrogate estimates of insulin sensitivity in obese youth along the spectrum of glucose tolerance from normal to prediabetes to diabetes. J Clin Endocrinol Metab. 2011;96(7):2136-45.

61. Keskin M, Kurtoglu S, Kendirci M, Atabek ME, Yazici C. Homeostasis model assessment is more reliable than the fasting glucose/insulin ratio and quantitative insulin sensitivity check index for assessing insulin resistance among obese children and adolescents. Pediatrics. 2005;115:500-3.
62. Atabek ME, Pirgon O. Assessment of insulin sensitivity from measurements in fasting state and during an oral glucose tolerance test in obese children. J Pediatr Endocrinol Metab. 2007;20(2):187-95.
63. Hanson RL, Pratley RE, Bogardus C, Narayan KM, Roumain JM, Imperatore G, et al. Evaluation of simple indices of insulin sensitivity and insulin secretion for use in epidemiologic studies. Am J Epidemiol. 2000;151(2):190-8.
64. Wallace TM, Levy JC, Matthews DR. Use and abuse of HOMA modeling. Diabetes Care. 2004;27(6):1487-95.
65. Yeckel CW, Weiss R, Dziura J, Taksali SE, Dufour S, Burgert TS, et al. Validation of insulin sensitivity indices from oral glucose tolerance test parameters in obese children and adolescents. J Clin Endocrinol Metab. 2004;89(3):1096-101.
66. Conwell LS, Trost SG, Brown WJ, Batch JA. Indexes of insulin resistance and secretion in obese children and adolescents a validation study. Diabetes Care. 2004;27(2):314-9.
67. Schwartz B, Jacobs DR, Jr., Moran A, Steinberger J, Hong CP, Sinaiko AR. Measurement of insulin sensitivity in children: comparison between the euglycemic-hyperinsulinemic clamp and surrogate measures. Diabetes Care. 2008;31(4):783-8.
68. Bennett B, Larson-Meyer DE, Ravussin E, Volaufova J, Soros A, Cefalu WT, et al. Impaired insulin sensitivity and elevated ectopic fat in healthy obese vs. nonobese prepubertal children. Obesity (Silver Spring). 2012;20(2):371-5.
69. Weiss R, Taksali SE, Tamborlane WV, Burgert TS, Savoye M, Caprio S. Predictors of changes in glucose tolerance status in obese youth. Diabetes Care. 2005;28(4):902-9.
70. Sjaarda LG, Bacha F, Lee S, Tfayli H, Andreatta E, Arslanian S. Oral disposition index in obese youth from normal to prediabetes to diabetes: relationship to clamp disposition index. J Pediatr. 2012;161:51-7.
71. Giannini C, Weiss R, Cali A, Bonadonna R, Santoro N, Pierpont B, et al. Evidence for early defects in insulin sensitivity and secretion before the onset of glucose dysregulation in obese youths: a longitudinal study. Diabetes. 2012;61(3):606-14.
72. Staten MA, Stern MP, Miller WG, Steffes MW, Campbell SE, Insulin Standardization W. Insulin assay standardization: leading to measures of insulin sensitivity and secretion for practical clinical care. Diabetes Care. 2010;33(1):205-6.
73. Mansoub S, Chan MK, Adeli K. Gap analysis of pediatric reference intervals for risk biomarkers of cardiovascular disease and the metabolic syndrome. Clin Biochem. 2006;39(6):569-87.
74. Mellerio H, Alberti C, Druet C, Capelier F, Mercat I, Josserand E, et al. Novel modeling of reference values of cardiovascular risk factors in children aged 7 to 20 years. Pediatrics. 2012;129(4):e1020-9.
75. Peplies J, Jimenez-Pavon D, Savva SC, Buck C, Gunther K, Fraterman A, et al. Percentiles of fasting serum insulin, glucose, HbA1c and HOMA-IR in pre-pubertal normal weight European children from the IDEFICS cohort. Int J Obes (Lond). 2014;38 (Suppl 2):S39-47.
76. Levy-Marchal C, Arslanian S, Cutfield W, Sinaiko A, Druet C, Marcovecchio ML, et al. Insulin resistance in children: consensus, perspective, and future directions. J Clin Endocrinol Metab. 2010;95(12):5189-98.
77. Ten S, Maclaren N. Insulin resistance syndrome in children. J Clin Endocrinol Metab. 2004;89(6):2526-39.
78. Zannolli R, Rebeggiani A, Chiarelli F, Morgese G. Hyperinsulinism as a marker in obese children. Am J Dis Child. 1993;147(8):837-41.
79. Tobisch B, Blatniczky L, Barkai L. Cardiometabolic risk factors and insulin resistance in obese children and adolescents: relation to puberty. Pediatr Obes. 2015;10(1):37-44.

80. Xekouki P, Nikolakopoulou NM, Papageorgiou A, Livadas S, Voutetakis A, Magiakou MA, et al. Glucose dysregulation in obese children: predictive, risk, and potential protective factors. Obesity (Silver Spring). 2007;15(4):860-9.
81. Marshall WA, Tanner JM. Variations in pattern of pubertal changes in girls. Arch Dis Child. 1969;44(235):291-303.
82. Marshall WA, Tanner JM. Variations in the pattern of pubertal changes in boys. Arch Dis Child. 1970;45(239):13-23.
83. Goran MI. Metabolic precursors and effects of obesity in children: a decade of progress, 1990-1999. Am J Clin Nutr. 2001;73(2):158-71.
84. Pilia S, Casini MR, Foschini ML, Minerba L, Musiu MC, Marras V, et al. The effect of puberty on insulin resistance in obese children. J Endocrinol Invest. 2009;32(5):401-5.
85. Arslanian SA. Metabolic differences between Caucasian and African-American children and the relationship to type 2 diabetes mellitus. J Pediatr Endocrinol Metab. 2002;15 (Suppl 1):509-17.
86. Goran MI, Bergman RN, Avila Q, Watkins M, Ball GD, Shaibi GQ, et al. Impaired glucose tolerance and reduced beta-cell function in overweight Latino children with a positive family history for type 2 diabetes. J Clin Endocrinol Metab. 2004;89(1):207-12.
87. Cook S, Kavey RE. Dyslipidemia and pediatric obesity. Pediatr Clin North Am. 2011;58(6):1363-73.
88. Sumner AE. Ethnic differences in triglyceride levels and high-density lipoprotein lead to underdiagnosis of the metabolic syndrome in black children and adults. J Pediatr. 2009;155(3: S7):e7-11.
89. Steinberger J, Daniels SR, Eckel RH, Hayman L, Lustig RH, McCrindle B, et al. Progress and challenges in metabolic syndrome in children and adolescents: a scientific statement from the American Heart Association Atherosclerosis, Hypertension, and Obesity in the Young Committee of the Council on Cardiovascular Disease in the Young; Council on Cardiovascular Nursing; and Council on Nutrition, Physical Activity, and Metabolism. Circulation. 2009;119(4):628-47.
90. Fitzpatrick SL, Lai BS, Brancati FL, Golden SH, Hill-Briggs F. Metabolic syndrome risk profiles among African American adolescents: national health and nutrition examination survey, 2003-2010. Diabetes Care. 2013;36(2):436-42.
91. Wyllie R. Obesity in childhood: an overview. Curr Opin Pediatr. 2005;17(5):632-5.
92. Astrup A, Dyerberg J, Selleck M, Stender S. Nutrition transition and its relationship to the development of obesity and related chronic diseases. Obes Rev. 2008;9 (Suppl 1):48-52.
93. Agostoni C, Braegger C, Decsi T, Kolacek S, Koletzko B, Mihatsch W, et al. Role of dietary factors and food habits in the development of childhood obesity: a commentary by the ESPGHAN Committee on Nutrition. J Pediatr Gastroenterol Nutr. 2011;52(6):662-9.
94. Owen CG, Martin RM, Whincup PH, Smith GD, Cook DG. Effect of infant feeding on the risk of obesity across the life course: a quantitative review of published evidence. Pediatrics. 2005;115(5):1367-77.
95. Swinburn BA, Sacks G, Hall KD, McPherson K, Finegood DT, Moodie ML, et al. The global obesity pandemic: shaped by global drivers and local environments. Lancet. 2011;378(9793):804-14.
96. El-Sayed Moustafa JS, Froguel P. From obesity genetics to the future of personalized obesity therapy. Nat Rev Endocrinol. 2013;9(7):402-13.
97. Bremer AA. Insulin resistance in pediatric disease. Pediatr Ann. 2012;41(2):e1-7.
98. Weiss R, Bremer AA, Lustig RH. What is metabolic syndrome, and why are children getting it? Ann N Y Acad Sci. 2013;1281:123-40.
99. Lakshman R, Elks CE, Ong KK. Childhood obesity. Circulation. 2012;126(14):1770-9.
100. Steinberger J, Kelly AS. Obesity, metabolic syndrome and type 2 diabetes. In: da Cruz EM, Ivy D, Jaggers J, editors. Pediatric and congenital cardiology, cardiac surgery and intensive care. Denver: Springer London; 2014. p. 499-507.
101. Tilg H, Moschen AR. Adipocytokines: mediators linking adipose tissue, inflammation and immunity. Nat Rev Immunol. 2006;6(10):772-83.

102. Makki K, Froguel P, Wolowczuk I. Adipose tissue in obesity-related inflammation and insulin resistance: cells, cytokines, and chemokines. ISRN Inflamm. 2013;2013:139239.
103. Gustafson B, Hammarstedt A, Andersson CX, Smith U. Inflamed adipose tissue: a culprit underlying the metabolic syndrome and atherosclerosis. Arterioscler Thromb Vasc Biol. 2007;27(11):2276-83.
104. Galic S, Oakhill JS, Steinberg GR. Adipose tissue as an endocrine organ. Mol Cell Endocrinol. 2010;316(2):129-39.
105. Yao L, Herlea-Pana O, Heuser-Baker J, Chen Y, Barlic-Dicen J. Roles of the chemokine system in development of obesity, insulin resistance, and cardiovascular disease. J Immunol Res. 2014;2014:181450.
106. Cali AMG, Dalla Man C, Cobelli C, Dziura J, Seyal A, Shaw M, et al. Primary defects in beta-cell function further exacerbated by worsening of insulin resistance mark the development of impaired glucose tolerance in obese adolescents. Diabetes Care. 2009;32(3):456-61.
107. Ramlo-Halsted BA, Edelman SV. The natural history of type 2 diabetes: implications for clinical practice. Prim Care. 1999;26(4):771-90.
108. Rask-Madsen C, Kahn CR. Tissue-specific insulin signaling, metabolic syndrome, and cardiovascular disease. Arterioscler Thromb Vasc Biol. 2012;32(9):2052-9.
109. Matsumoto M, Han S, Kitamura T, Accili D. Dual role of transcription factor FoxO1 in controlling hepatic insulin sensitivity and lipid metabolism. J Clin Invest. 2006;116(9):2464-72.
110. Horton JD, Goldstein JL, Brown MS. SREBPs: activators of the complete program of cholesterol and fatty acid synthesis in the liver. J Clin Invest. 2002;109(9):1125-31.
111. Goldberg IJ. Lipoprotein lipase and lipolysis: central roles in lipoprotein metabolism and atherogenesis. J Lipid Res. 1996;37(4):693-707.
112. Lewis GF, Uffelman KD, Szeto LW, Steiner G. Effects of acute hyperinsulinemia on VLDL triglyceride and VLDL apoB production in normal weight and obese individuals. Diabetes. 1993;42(6):833-42.
113. Brown MS, Goldstein JL. Selective versus total insulin resistance: a pathogenic paradox. Cell Metab. 2008;7(2):95-6.
114. Ginsberg HN, Zhang YL, Hernandez-Ono A. Regulation of plasma triglycerides in insulin resistance and diabetes. Arch Med Res. 2005;36(3):232-40.
115. Samuel VT, Petersen KF, Shulman GI. Lipid-induced insulin resistance: unravelling the mechanism. Lancet. 2010;375(9733):2267-77.
116. Randle PJ. Regulatory interactions between lipids and carbohydrates: the glucose fatty acid cycle after 35 years. Diabetes Metab Rev. 1998;14(4):263-83.
117. Weiss R, Dufour S, Taksali SE, Tamborlane WV, Petersen KF, Bonadonna RC, et al. Prediabetes in obese youth: a syndrome of impaired glucose tolerance, severe insulin resistance, and altered myocellular and abdominal fat partitioning. Lancet. 2003;362(9388):951-7.
118. Barlow SE, Expert C. Expert committee recommendations regarding the prevention, assessment, and treatment of child and adolescent overweight and obesity: summary report. Pediatrics. 2007;120 (Suppl 4):S164-92.
119. Lobstein T, Baur L, Uauy R, IASO International Obesity Task Force. Obesity in children and young people: a crisis in public health. Obes Rev. 2004;5 (Suppl 1):4-104.
120. Mirza NM, Palmer MG, Sinclair KB, McCarter R, He J, Ebbeling CB, et al. Effects of a low glycemic load or a low-fat dietary intervention on body weight in obese Hispanic American children and adolescents: a randomized controlled trial. Am J Clin Nutr. 2013;97(2):276-85.
121. Davis AM, Daldalian MC, Mayfield CA, Dean K, Black WR, Sampilo ML, et al. Outcomes from an urban pediatric obesity program targeting minority youth: the Healthy Hawks program. Child Obes. 2013;9(6):492-500.
122. Pedrosa C, Oliveira BM, Albuquerque I, Simoes-Pereira C, Vaz-de-Almeida MD, Correia F. Markers of metabolic syndrome in obese children before and after 1-year lifestyle intervention program. Eur J Nutr. 2011;50(6):391-400.

123. Wiegand S, Keller K, Lob-Corzilius T, Pott W, Reinehr T, Robl M, et al. Predicting weight loss and maintenance in overweight/obese pediatric patients. Horm Res Paediatr. 2014:380-7.
124. Roberts CK, Izadpanah A, Angadi SS, Barnard RJ. Effects of an intensive short-term diet and exercise intervention: comparison between normal-weight and obese children. Am J Physiol Regul Integr Comp Physiol. 2013;305(5):R552-7.
125. Magnussen CG, Smith KJ, Juonala M. What the long term cohort studies that began in childhood have taught us about the origins of coronary heart disease. Curr Cardiovasc Risk Rep. 2014;8:373.
126. Sherafat-Kazemzadeh R, Yanovski SZ, Yanovski JA. Pharmacotherapy for childhood obesity: present and future prospects. Int J Obes (Lond). 2013;37(1):1-15.
127. US Food and Drug Administration. Xenical approval letter; 2014. Available from: www.accessdata.fda.gov/drugsatfda_docs/appletter/2003/20766se5-018ltr.pdf.
128. Peirson L, Fitzpatrick-Lewis D, Morrison K, Warren R, Usman Ali M, Raina P. Treatment of overweight and obesity in children and youth: a systematic review and meta-analysis. CMAJ Open. 2015;3(1):E35-46.
129. Kostev K, Richter H. Unlicensed use of metformin in children and adolescents in Germany and France. Br J Clin Pharmacol. 2012;73(2):307-8.
130. Hsia Y, Dawoud D, Sutcliffe AG, Viner RM, Kinra S, Wong IC. Unlicensed use of metformin in children and adolescents in the UK. Br J Clin Pharmacol. 2012;73(1):135-9.
131. Bailey CJ, Turner RC. Metformin. N Engl J Med. 1996;334(9):574.
132. Brufani C, Crino A, Fintini D, Patera PI, Cappa M, Manco M. Systematic review of metformin use in obese nondiabetic children and adolescents. Horm Res Paediatr. 2013;80(2):78-85.
133. Group TS, Zeitler P, Hirst K, Pyle L, Linder B, Copeland K, et al. A clinical trial to maintain glycemic control in youth with type 2 diabetes. N Engl J Med. 2012;366(24):2247-56.
134. Flint A, Arslanian S. Treatment of type 2 diabetes in youth. Diabetes Care. 2011;34 (Suppl 2):S177-83.
135. Katzmarzyk PT, Barlow S, Bouchard C, Catalano PM, Hsia DS, Inge TH, et al. An evolving scientific basis for the prevention and treatment of pediatric obesity. Int J Obes (Lond). 2014;38(7):887-905.
136. Fried M, Yumuk V, Oppert JM, Scopinaro N, Torres AJ, Weiner R, et al. Interdisciplinary European Guidelines on metabolic and bariatric surgery. Obes Facts. 2013;6(5):449-68.
137. Baur LA, Fitzgerald DA. Recommendations for bariatric surgery in adolescents in Australia and New Zealand. J Paediatr Child Health. 2010;46(12):704-7.
138. Kelly AS, Barlow SE, Rao G, Inge TH, Hayman LL, Steinberger J, et al. Severe obesity in children and adolescents: identification, associated health risks, and treatment approaches a scientific statement from the American Heart Association. Circulation. 2013;128(15):1689-712.
139. Lawson ML, Kirk S, Mitchell T, Chen MK, Loux TJ, Daniels SR, et al. One-year outcomes of Roux-en-Y gastric bypass for morbidly obese adolescents: a multicenter study from the Pediatric Bariatric Study Group. J Pediatr Surg. 2006;41(1):137-43.
140. Nader PR, Huang TT, Gahagan S, Kumanyika S, Hammond RA, Christoffel KK. Next steps in obesity prevention: altering early life systems to support healthy parents, infants, and toddlers. Child Obes. 2012;8(3):195-204.
141. Wojcicki JM, Heyman MB. Let's Move-childhood obesity prevention from pregnancy and infancy onward. N Engl J Med. 2010;362(16):1457-9.
142. van de Laar RJ, Stehouwer CD, van Bussel BC, Prins MH, Twisk JW, Ferreira I. Adherence to a Mediterranean dietary pattern in early life is associated with lower arterial stiffness in adulthood: the Amsterdam Growth and Health Longitudinal Study. J Intern Med. 2013;273(1):79-93.
143. Stabelini Neto A, de Campos W, Dos Santos GC, Mazzardo Junior O. Metabolic syndrome risk score and time expended in moderate to vigorous physical activity in adolescents. BMC Pediatr. 2014;14:42.

144. Story M, Nanney MS, Schwartz MB. Schools and obesity prevention: creating school environments and policies to promote healthy eating and physical activity. Milbank Q. 2009;87(1):71-100.
145. Oliver SG, Winson MK, Kell DB, Baganz F. Systematic functional analysis of the yeast genome. Trends Biotechnol. 1998;16(9):373-8.
146. Nicholson JK, Lindon JC, Holmes E. 'Metabonomics': understanding the metabolic responses of living systems to pathophysiological stimuli via multivariate statistical analysis of biological NMR spectroscopic data. Xenobiotica. 1999;29(11):1181-9.
147. Nicholson JK. Global systems biology, personalized medicine and molecular epidemiology. Mol Syst Biol. 2006;2:52.
148. Nicholson JK, Lindon JC. Systems biology: Metabonomics. Nature. 2008;455(7216):1054-6.
149. Goodacre R. Metabolomics of a superorganism. J Nutr. 2007;137:S259-66.
150. Dunn WB, Broadhurst DI, Atherton HJ, Goodacre R, Griffin JL. Systems level studies of mammalian metabolomes: the roles of mass spectrometry and nuclear magnetic resonance spectroscopy. Chem Soc Rev. 2011;40(1):387-426.
151. Wishart DS, Jewison T, Guo AC, Wilson M, Knox C, Liu Y, et al. HMDB 3.0-The Human Metabolome Database in 2013. Nucleic Acids Res. 2012;41:D801-7.
152. Wishart DS, Tzur D, Knox C, Eisner R, Guo AC, Young N, et al. HMDB: the Human Metabolome Database. Nucleic Acids Res. 2007;35:D521-6.
153. Lenz EM, Wilson ID. Analytical strategies in metabonomics. J Proteome Res. 2007;6(2):443-58.
154. Lanza IR, Zhang S, Ward LE, Karakelides H, Raftery D, Nair KS. Quantitative metabolomics by H-NMR and LC-MS/MS confirms altered metabolic pathways in diabetes. PLoS One. 2010;5(5):e10538.
155. Zheng S, Zhang S, Yu M, Tang J, Lu X, Wang F, et al. An 1H NMR and UPLC–MS-based plasma metabonomic study to investigate the biochemical changes in chronic unpredictable mild stress model of depression. Metabolomics. 2011;7(3):413-23.
156. Joyce AR, Palsson BO. The model organism as a system: integrating 'omics' data sets. Nat Rev Mol Cell Biol. 2006;7(3):198-210.
157. Holmes E, Wilson ID, Nicholson JK. Metabolic phenotyping in health and disease. Cell. 2008;134(5):714-7.
158. Fiehn O. Metabolomics–the link between genotypes and phenotypes. Plant Mol Biol. 2002;48(1-2):155-71.
159. Mamas M, Dunn WB, Neyses L, Goodacre R. The role of metabolites and metabolomics in clinically applicable biomarkers of disease. Arch Toxicol. 2011;85(1):5-17.
160. Bictash M, Ebbels TM, Chan Q, Loo RL, Yap IK, Brown IJ, et al. Opening up the "Black Box": metabolic phenotyping and metabolome-wide association studies in epidemiology. J Clin Epidemiol. 2010;63(9):970-9.
161. Leichtle AB, Dufour JF, Fiedler GM. Potentials and pitfalls of clinical peptidomics and metabolomics. Swiss Med Wkly. 2013;143:w13801.
162. Buyse M, Sargent DJ, Grothey A, Matheson A, De Gramont A. Biomarkers and surrogate end points—the challenge of statistical validation. Nat Rev Clin Oncol. 2010;7(6):309-17.
163. Emwas AH, Salek RM, Griffin JL, Merzaban J. NMR-based metabolomics in human disease diagnosis: applications, limitations, and recommendations. Metabolomics. 2013;9:1048-72.
164. Kell DB. Systems biology, metabolic modelling and metabolomics in drug discovery and development. Drug Discov Today. 2006;11(23-24):1085-92.
165. Lindon JC, Nicholson JK. Spectroscopic and statistical techniques for information recovery in metabonomics and metabolomics. Annu Rev Anal Chem. 2008;1:45-69.
166. Drexler DM, Reily MD, Shipkova PA. Advances in mass spectrometry applied to pharmaceutical metabolomics. Anal Bioanal Chem. 2011;399(8):2645-53.
167. Powers R. NMR metabolomics and drug discovery. Magn Reson Chem. 2009;47 (Suppl 1):S2-11.

168. Nicholson JK, O'Flynn MP, Sadler PJ, Macleod AF, Juul SM, Sonksen PH. Proton-nuclear-magnetic-resonance studies of serum, plasma and urine from fasting normal and diabetic subjects. Biochem J. 1984;217(2):365-75.
169. Nicholson JK, Wilson ID. Opinion: understanding 'global' systems biology: metabonomics and the continuum of metabolism. Nat Rev Drug Discov. 2003;2(8):668-76.
170. Fiehn O, Kopka J, Dormann P, Altmann T, Trethewey RN, Willmitzer L. Metabolite profiling for plant functional genomics. Nat Biotechnol. 2000;18(11):1157-61.
171. Dumas ME, Maibaum EC, Teague C, Ueshima H, Zhou B, Lindon JC, et al. Assessment of analytical reproducibility of 1H NMR spectroscopy based metabonomics for large-scale epidemiological research: the INTERMAP Study. Anal Chem. 2006;78(7):2199-208.
172. Bernini P, Bertini I, Luchinat C, Nincheri P, Staderini S, Turano P. Standard operating procedures for pre-analytical handling of blood and urine for metabolomic studies and biobanks. J Biomol NMR. 2011;49(3-4):231-43.
173. Dona AC, Jimenez B, Schafer H, Humpfer E, Spraul M, Lewis MR, et al. Precision high-throughput proton NMR spectroscopy of human urine, serum, and plasma for large-scale metabolic phenotyping. Anal Chem. 2014;86(19):9887-94.
174. Teahan O, Gamble S, Holmes E, Waxman J, Nicholson JK, Bevan C, et al. Impact of analytical bias in metabonomic studies of human blood serum and plasma. Anal Chem. 2006;78(13):4307-18.
175. Slupsky CM, Rankin KN, Wagner J, Fu H, Chang D, Weljie AM, et al. Investigations of the effects of gender, diurnal variation, and age in human urinary metabolomic profiles. Anal Chem. 2007;79(18):6995-7004.
176. Issaq HJ, Van QN, Waybright TJ, Muschik GM, Veenstra TD. Analytical and statistical approaches to metabolomics research. J Sep Sci. 2009;32(13):2183-99.
177. Lauridsen M, Hansen SH, Jaroszewski JW, Cornett C. Human urine as test material in 1H NMR-based metabonomics: recommendations for sample preparation and storage. Anal Chem. 2007;79(3):1181-6.
178. Wishart DS, Bigam CG, Yao J, Abildgaard F, Dyson HJ, Oldfield E, et al. 1H, 13C and 15N chemical shift referencing in biomolecular NMR. J Biomol NMR. 1995;6(2):135-40.
179. Beckonert O, Keun HC, Ebbels TM, Bundy J, Holmes E, Lindon JC, et al. Metabolic profiling, metabolomic and metabonomic procedures for NMR spectroscopy of urine, plasma, serum and tissue extracts. Nat Protoc. 2007;2(11):2692-703.
180. Bales JR, Higham DP, Howe I, Nicholson JK, Sadler PJ. Use of high-resolution proton nuclear magnetic resonance spectroscopy for rapid multi-component analysis of urine. Clin Chem. 1984;30(3):426-32.
181. Nicholson JK, Foxall PJ, Spraul M, Farrant RD, Lindon JC. 750 MHz 1H and 1H-13C NMR spectroscopy of human blood plasma. Anal Chem. 1995;67(5):793-811.
182. de Graaf RA, Behar KL. Quantitative 1H NMR spectroscopy of blood plasma metabolites. Anal Chem. 2003;75(9):2100-4.
183. Bertram HC, Malmendal A, Petersen BO, Madsen JC, Pedersen H, Nielsen NC, et al. Effect of magnetic field strength on NMR-based metabonomic human urine data. Comparative study of 250, 400, 500, and 800 MHz. Anal Chem. 2007;79(18):7110-5.
184. Creek DJ, Dunn WB, Fiehn O, Griffin JL, Hall RD, Lei Z, et al. Metabolite identification: are you sure? And how do your peers gauge your confidence? Metabolomics. 2014;10:350-3.
185. Lewis IA, Schommer SC, Hodis B, Robb KA, Tonelli M, Westler WM, et al. Method for determining molar concentrations of metabolites in complex solutions from two-dimensional 1H-13C NMR spectra. Anal Chem. 2007;79(24):9385-90.
186. Jeannerat D, Furrer J. NMR experiments for the analysis of mixtures: beyond 1D 1H spectra. Comb Chem High Throughput Screen. 2012;15(1):15-35.
187. Lindon JC. HPLC-NMR-MS: past, present and future. Drug Discov Today. 2003;8(22):1021-2.
188. Duarte IF, Legido-Quigley C, Parker DA, Swann JR, Spraul M, Braumann U, et al. Identification of metabolites in human hepatic bile using 800 MHz 1H NMR spectroscopy, HPLC-NMR/MS and UPLC-MS. Mol Biosyst. 2009;5(2):180-90.

189. Holmes E, Nicholson JK, Nicholls AW, Lindon JC, Connor SC, Polley S, et al. The identification of novel biomarkers of renal toxicity using automatic data reduction techniques and PCA of proton NMR spectra of urine. Chemom Intell Lab Syst. 1998;44(1):245-55.
190. De Meyer T, Sinnaeve D, Van Gasse B, Tsiporkova E, Rietzschel ER, De Buyzere ML, et al. NMR-based characterization of metabolic alterations in hypertension using an adaptive, intelligent binning algorithm. Anal Chem. 2008;80(10):3783-90.
191. Beckwith-Hall BM, Nicholson JK, Nicholls AW, Foxall PJ, Lindon JC, Connor SC, et al. Nuclear magnetic resonance spectroscopic and principal components analysis investigations into biochemical effects of three model hepatotoxins. Chem Res Toxicol. 1998;11(4):260-72.
192. Halouska S, Powers R. Negative impact of noise on the principal component analysis of NMR data. J Magn Reson. 2006;178(1):88-95.
193. Weljie AM, Newton J, Mercier P, Carlson E, Slupsky CM. Targeted profiling: quantitative analysis of 1H NMR metabolomics data. Anal Chem. 2006;78(13):4430-42.
194. Rubtsov DV, Griffin JL. Time-domain Bayesian detection and estimation of noisy damped sinusoidal signals applied to NMR spectroscopy. J Magn Reson. 2007;188(2):367-79.
195. Craig A, Cloarec O, Holmes E, Nicholson JK, Lindon JC. Scaling and normalization effects in NMR spectroscopic metabonomic data sets. Anal Chem. 2006;78(7):2262-7.
196. Kohl SM, Klein MS, Hochrein J, Oefner PJ, Spang R, Gronwald W. State-of-the art data normalization methods improve NMR-based metabolomic analysis. Metabolomics. 2012;8(1):146-60.
197. van den Berg RA, Hoefsloot HC, Westerhuis JA, Smilde AK, van der Werf MJ. Centering, scaling, and transformations: improving the biological information content of metabolomics data. BMC Genomics. 2006;7(1):142.
198. Keun HC, Ebbels T, Antti H, Bollard ME, Beckonert O, Holmes E, et al. Improved analysis of multivariate data by variable stability scaling: application to NMR-based metabolic profiling. Anal Chim Acta. 2003;490(1):265-76.
199. Liland KH. Multivariate methods in metabolomics–from pre-processing to dimension reduction and statistical analysis. Trends Analyt Chem. 2011;30(6):827-41.
200. Smolinska A, Blanchet L, Buydens LM, Wijmenga SS. NMR and pattern recognition methods in metabolomics: from data acquisition to biomarker discovery: a review. Anal Chim Acta. 2012;750:82-97.
201. Eriksson L, Byrne T, Johansson E, Trygg J, Vikstrom C. Multi-and megavariate data analysis. Sweden: MKS Umetrics AB; 2006.
202. Friedman JM. Obesity: Causes and control of excess body fat. Nature. 2009;459(7245):340-2.
203. Zhang A, Sun H, Wang X. Power of metabolomics in biomarker discovery and mining mechanisms of obesity. Obes Rev. 2013;14(4):344-9.
204. Blüher M. The distinction of metabolically 'healthy' from 'unhealthy' obese individuals. Curr Opin Lipidol. 2010;21(1):38-43.
205. Speakman J, Hambly C, Mitchell S, Krol E. The contribution of animal models to the study of obesity. Lab Anim. 2008;42(4):413-32.
206. Xie B, Waters MJ, Schirra HJ. Investigating potential mechanisms of obesity by metabolomics. J Biomed Biotechnol. 2012;2012:805683.
207. Kim HJ, Kim JH, Noh S, Hur HJ, Sung MJ, Hwang JT, et al. Metabolomic analysis of livers and serum from high-fat diet induced obese mice. J Proteome Res. 2011;10(2):722-31.
208. Jung JY, Kim IY, Kim YN, Kim JS, Shin JH, Jang ZH, et al. 1H NMR-based metabolite profiling of diet-induced obesity in a mouse mode. BMB Rep. 2012;45(7):419-24.
209. Newgard CB, An J, Bain JR, Muehlbauer MJ, Stevens RD, Lien LF, et al. A branched-chain amino acid-related metabolic signature that differentiates obese and lean humans and contributes to insulin resistance. Cell Metab. 2009;9(4):311-26.
210. Kim JY, Park JY, Kim OY, Ham BM, Kim HJ, Kwon DY, et al. Metabolic profiling of plasma in overweight/obese and lean men using ultra performance liquid

chromatography and Q-TOF mass spectrometry (UPLC-Q-TOF MS). J Proteome Res. 2010;9(9):4368-75.
211. Oberbach A, Bluher M, Wirth H, Till H, Kovacs P, Kullnick Y, et al. Combined proteomic and metabolomic profiling of serum reveals association of the complement system with obesity and identifies novel markers of body fat mass changes. J Proteome Res. 2011;10(10):4769-88.
212. Morris C, O'Grada C, Ryan M, Roche HM, Gibney MJ, Gibney ER, et al. The relationship between BMI and metabolomic profiles: a focus on amino acids. Proc Nutr Soc. 2012;71(4):634-8.
213. Wang TJ, Larson MG, Vasan RS, Cheng S, Rhee EP, McCabe E, et al. Metabolite profiles and the risk of developing diabetes. Nat Med. 2011;17(4):448-53.
214. Gall WE, Beebe K, Lawton KA, Adam KP, Mitchell MW, Nakhle PJ, et al. Alpha-hydroxybutyrate is an early biomarker of insulin resistance and glucose intolerance in a nondiabetic population. PLoS One. 2010;5(5):e10883.
215. Calvani R, Miccheli A, Capuani G, Tomassini Miccheli A, Puccetti C, Delfini M, et al. Gut microbiome-derived metabolites characterize a peculiar obese urinary metabotype. Int J Obes (Lond). 2010;34(6):1095-8.
216. Harris K, Kassis A, Major G, Chou CJ. Is the gut microbiota a new factor contributing to obesity and its metabolic disorders? J Obes. 2012;2012:879151.
217. Nicholson JK, Holmes E, Wilson ID. Gut microorganisms, mammalian metabolism and personalized health care. Nat Rev Microbiol. 2005;3(5):431-8.
218. Dietz WH. Health consequences of obesity in youth: childhood predictors of adult disease. Pediatrics. 1998;101(3):518-25.
219. Biro FM, Wien M. Childhood obesity and adult morbidities. Am J Clin Nutr. 2010;91(5):S1499-505.
220. Zeng M, Liang Y, Li H, Wang M, Wang B, Chen X, et al. Plasma metabolic fingerprinting of childhood obesity by GC/MS in conjunction with multivariate statistical analysis. J Pharm Biomed Anal. 2010;52(2):265-72.
221. Wahl S, Yu Z, Kleber M, Singmann P, Holzapfel C, He Y, et al. Childhood obesity is associated with changes in the serum metabolite profile. Obes Facts. 2012;5(5):660-70.
222. Mihalik SJ, Michaliszyn SF, de las Heras J, Bacha F, Lee S, Chace DH, et al. Metabolomic profiling of fatty acid and amino acid metabolism in youth with obesity and type 2 diabetes: evidence for enhanced mitochondrial oxidation. Diabetes Care. 2012;35(3):605-11.
223. Wahl S, Holzapfel C, Yu Z, Breier M, Kondofersky I, Fuchs C, et al. Metabolomics reveals determinants of weight loss during lifestyle intervention in obese children. Metabolomics. 2013;9(6):1157-67.
224. Reinehr T, Wolters B, Knop C, Lass N, Hellmuth C, Harder U, et al. Changes in the serum metabolite profile in obese children with weight loss. Eur J Nutr. 2015;54(2):173-81.
225. Bothwell JH, Griffin JL. An introduction to biological nuclear magnetic resonance spectroscopy. Biol Rev Camb Philos Soc. 2011;86(2):493-510.
226. Carr HY, Purcell EM. Effects of diffusion on free precession in nuclear magnetic resonance experiments. Physical Review. 1954;94(3):630.
227. Meiboom S, Gill D. Modified spin-echo method for measuring nuclear relaxation times. Rev Sci Instrum. 1958;29(8):688-91.
228. Principles of NMR; 1998-2008 [17/09/2014]. Available from: http://www.process-nmr.com/nmr1.htm.
229. NMR Spin Coupling; 2014 [16/09/2014]. Available from: http://cnx.org/contents/ba27839d-5042-4a40-afcf-c0e6e39fb454@20.16:58.
230. Wold S, Sjöström M, Eriksson L. PLS-regression: a basic tool of chemometrics. Chemom Intell Lab Syst. 2001;58(2):109-30.
231. Trygg J, Wold S. Orthogonal projections to latent structures (O-PLS). J Chemom. 2002;16(3):119-28.

Chapter 2

Morbid obesity in childhood and cardiometabolic health consequences

Based on:

Liene Bervoets[1] and Guy Massa[1,2] (2014) **Defining morbid obesity in children based on BMI 40 at age 18 using the extended international (IOTF) cut-offs.** *Pediatric Obesity* 2014; 9(5):e94-98.

[1]Faculty of Medicine and Life Sciences, Hasselt University, Hasselt, Belgium; [2]Department of Pediatrics, Jessa Hospital, Hasselt, Belgium

This study was presented as orally by Liene Bervoets at the Belgian Association for the Study of Obesity Free Communications Meeting, 15th February 2014, Brussels, Belgium

Abstract

Although there is growing evidence that the number of children with obesity is stabilizing, obese children are becoming more severely obese with all its consequences. In order to classify obese children internationally according to age and gender-specific criteria, Cole and Lobstein (2012) developed the International Obesity Task Force (IOTF) body mass index (BMI) cut-off values corresponding to BMI 30 and 35 at age 18. However, the most extreme IOTF BMI cut-offs corresponding to BMI 40 at age 18 are still lacking. Therefore, we calculated the BMI cut-off values corresponding to BMI 40 at age 18 using the LMS (L: skewness, M: median, and S: coefficient of variation) method proposed by Cole and Lobstein. In order to standardize the terminology use of obesity in children, we defined BMI 30, 35 and 40 at age 18 as 'class I', 'class II' or severe, and 'class III' or morbid obesity. To demonstrate the proof of concept, we classified 217 obese children and adolescents according to the newly defined IOTF BMI classification. Fifty-six (25.8%) children had class III obesity, 73 (33.6%) class II obesity and 88 (40.6%) class I obesity. Class III obese children had a larger waist circumference, higher systolic blood pressure and higher fasting insulin compared to less obese children. In conclusion, we here present the IOTF BMI 40 cut-off values to classify morbidly obese children between 2 and 18 years. Morbidly obese children are at higher risk for cardiometabolic complications than children with less severe obesity. Our findings underscore the clinical importance of identifying morbidly obese children. Current treatments for morbidly obese children should focus on personalized and more aggressive therapy.

2.1 Introduction

Cole and Lobstein have recently reformulated the IOTF BMI cut-off criteria for thinness, overweight and obesity in children in terms of underlying LMS curves [1], which makes it now possible to express BMI as a centile or standard deviation (SD) score, and to construct your own cut-offs for any required BMI at age 18. Additionally, they developed a new BMI cut-off of 35 $kg.m^{-2}$ for what they called 'morbid obesity', corresponding to the 99.83^{th} percentile at age 18. In an accompanying editorial, Rolland-Cachera [2] proposed to simplify the terminology of obesity, according to the adult WHO 1995 definition [3], and suggested to use in children 'grade 1' and 'grade 2' overweight instead of overweight and obesity, respectively. However, as for adults [4], the typical definition of obesity, a BMI ≥ 30 $kg.m^{-2}$ or its corresponding IOTF cut-off value, obscures the heterogeneity of this group. In 2000, the WHO [5] already subdivided adult obesity into 3 classes: class I obesity (BMI 30.00 – 34.99), class II obesity (BMI 35.00 – 39.99), and class III obesity (BMI ≥ 40.00), with moderate, severe and very severe risk of comorbidities, respectively.

There is emerging evidence that the prevalence of obesity in children is stabilizing in a number of countries [6]. However, it appears that children who are obese are becoming more severely obese [7-9]. It has been shown that severely obese children have a higher risk of developing cardio-metabolic and -respiratory complications compared to moderately obese children [10-12], and have a higher risk to become severely obese as an adult [13]. Hence early identification of severely obese children is of utmost importance, and therefore an accurate definition of this obesity class is required. To date, however, it is unclear which anthropometric cut-off point should be used to define morbid obesity in children and adolescents.

In this study, we aimed to implement the LMS curves for children between 2 and 18 years to calculate the IOTF BMI cut-offs which reaches 40 at age 18. To demonstrate the proof of concept, we classified 217 obese children and adolescents according to the newly defined IOTF BMI classification and evaluated components of the metabolic syndrome (MetS) between children of different obesity classes.

2.2 Material and methods

2.2.1 Calculation of BMI 40 cut off values

The original method for constructing the IOTF BMI cut off values has previously been described by Cole et al. [14]. This method was based on data from six large nationally representative growth studies that had taken place in the following countries: Great Britain, USA, the Netherlands, Brazil, Singapore and Hong Kong. Data on BMI from over 10000 children and adolescents with ages ranging from 2 to 18 years (6 to 18 years for Singapore) were collected between 1963 and 1993. For each survey, age-specific BMI centiles were constructed by gender using the LMS method [15]. Subsequently, survey data were averaged in terms of three smooth age- and gender-specific curves called L (λ), M (μ) and S (σ), representing the skewness (L), median (M) and coefficient of variation (S), respectively. Cole and Lobstein [1] recently published these L, M and S curves by gender for ages between 2 and 18 and used them to derive new BMI cut-off values. They provided the following formula to express BMI cut-off values as BMI centiles:

$$C_{100\alpha} = M(1 + L\ x\ S\ x\ z_{\alpha})^{1/L}$$

where L, M and S correspond to the values of the fitted curves by age and gender given by Cole and Lobstein [1]. The value of z_{α} (z score) can be calculated using the formula:

$$\mathrm{z} = \frac{(BMI/M)^{L} - 1}{L\ x\ S}$$

Hence, the z score or SD corresponding to a given BMI value at age 18 is firstly obtained using formula (2), and subsequently this is substituted as z_{α} into formula (1). In this way, Cole and Lobstein [1] calculated the BMI centile curves which were then averaged by gender and age across all six countries to present a single cut-off corresponding to the chosen BMI value.

Based on the LMS method as described above, we calculated the BMI cut-off values of 40 $kg.m^{-2}$ – corresponding to the 99.95^{th} percentile at age 18 – by gender for each 6 months of age from 2 to 18 years.

2.2.2 IOTF BMI classification

To consolidate the terminology of obesity in childhood, we defined different obesity classes in line with the WHO classification [5] for adults. We classified obese children based on age- and gender-specific centile curves passing through BMI 30 at age 18 as 'class I obesity' or 'obesity', through BMI 35 as 'class II obesity' or 'severe obesity', and through BMI 40 as 'class III obesity' or 'morbid obesity'.

2.2.3 Study population

Two hundred seventeen children referred to our Childhood Obesity Centre (Jessa Ziekenhuis, Hasselt, Belgium) between January 2011 and December 2012 were included in this study. Inclusion criteria were: 1) aged between 2 and 18; 2) BMI above IOTF cut-off of obesity. Of a subsample of 90 obese children aged between 7 and 18, who underwent a fasting venous blood sampling, metabolic risk factors were examined. The study was approved by the medical Ethics Committee of the Jessa Hospital and Hasselt University.

2.2.4 Anthropometric measurements

Patients were weighed wearing underwear only. Standing height was measured to the nearest 0.1 cm using a Harpenden wall stadiometer, and weight was measured to the nearest 0.1 kg using an electronic balance scale. BMI was calculated by dividing weight in kilograms by height in meters squared (BMI = kg/m^2). Waist circumference (WC) was measured at the approximate midpoint between the lower margin of the last palpable rib and the top of the iliac crest [16], in duplicate to the nearest of 0.1 cm using a soft non-stretchable tape and with the subject in a standing position. Seated blood pressure was measured with an electronic sphygmomanometer (Omron®, Omron Healthcare, IL, USA).

2.2.5 Biochemical analysis

After an overnight fast, venous blood samples were taken from the patients for the measurement of glucose, insulin, HDL-C and TG. Plasma glucose was measured by the glucose oxidase method using a Synchron LX20 analyzer (Beckman Coulter, Brea, CA, USA). Serum insulin was determined by immuno-reactive insulin (IRI) assay (ADVIA Centaur Insulin IRI; Siemens Medical Solutions Diagnostics, Tarrytown, NY, USA). Total cholesterol, HDL-C and TG were

measured on a Beckman Coulter AU 2700 automatic analyser (Brea, CA, USA). LDL-C was calculated according to the Friedewald equation [17].

2.2.6 Calculations metabolic health determinants

We retrospectively analyzed metabolic risk factors (i.e. WC, systolic blood pressure (SBP) and diastolic blood pressure (DBP), glucose, insulin, total cholesterol, HDL-C, TG and LDL-C) of a subsample of 90 obese children aged between 7 and 18, who underwent a fasting venous blood sampling. For each factor, age- and gender-specific z-scores were calculated according to Mellerio et al. [18] (see supplementary information of Mellerio et al. [18] for more details on the statistical methods for estimating age- and gender-specific reference intervals). The prevalence of the components of MetS was assessed according to the International Diabetes Federation (IDF) criteria for children and adolescents [19]. Subjects were classified as having MetS when they had obesity as classified according to IOTF criteria and two or more of the following abnormalities: (1) HDL-C < 40 mg/dl (females 16 years or older: HDL-C < 50 mg/dl) (2) TG ≥ 150 mg/dl; (3) SBP ≥ 130 mm Hg or DBP ≥ 85 mm Hg; (4) fasting plasma glucose (FPG) ≥ 100 mg/dl.

2.2.7 Statistical analyses

Statistical analyses were performed with IBM SPSS version 20.0 (SPSS Inc., Chicago, IL, USA). Results of continuous variables are presented as mean ± SD and nominal or ordinal scale variables are presented as a number with percentage (%). Distribution of the data was tested by the Kolmogorov-Smirnov test. Non-normally distributed variables were log-transformed. One-way analysis of variance (ANOVA) with post-hoc Bonferroni test for interval scale variables and Chi square test (n>10) or Fisher's exact probability test (n≤10) for nominal scale variables were implemented to calculate differences between the study groups. Statistical significance was assessed at the 5% level. To reduce the chances of obtaining false-positive results (type I errors), Bonferroni corrected p-values were applied.

2.3 Results

2.3.1 Age- and gender-specific BMI 40 cut off values

The newly calculated BMI cut-off values corresponding to BMI 40 kg.m^{-2} at age 18 are presented in Table 2.1 together with the IOTF cut-offs corresponding to BMI 30 and 35 kg.m^{-2} adapted from Cole and Lobstein [1].

Table 2.1 BMI cut-off points for obesity, severe obesity and morbid obesity by age and gender defined to pass through BMI of 30, 35 and 40 kg.m^{-2} at age 18 based on the newly derived LMS curves [1].

Age (years)	Boys			Girls		
	BMI 30*	BMI 35*	BMI 40	BMI 30*	BMI 35*	BMI 40
2	19.99	21.20	22.12	19.81	21.13	22.15
2.5	19.73	20.95	21.89	19.57	20.90	21.95
3	19.50	20.75	21.72	19.38	20.74	21.83
3.5	19.33	20.61	21.62	19.25	20.65	21.77
4	19.23	20.56	21.61	19.16	20.62	21.80
4.5	19.20	20.60	21.73	19.14	20.67	21.94
5	19.27	20.79	22.03	19.20	20.85	22.22
5.5	19.46	21.15	22.57	19.36	21.16	22.69
6	19.76	21.69	23.35	19.62	21.61	23.35
6.5	20.15	22.35	24.32	19.96	22.19	24.19
7	20.59	23.08	25.37	20.39	22.88	25.17
7.5	21.06	23.83	26.44	20.89	23.65	26.26
8	21.56	24.61	27.55	21.44	24.50	27.47
8.5	22.11	25.45	28.76	22.04	25.42	28.77
9	22.71	26.40	30.14	22.66	26.39	30.18
9.5	23.34	27.39	31.60	23.31	27.38	31.62
10	23.96	28.35	33.03	23.97	28.36	33.01
10.5	24.54	29.22	34.29	24.62	29.28	34.26
11	25.07	29.97	35.31	25.25	30.14	35.37
11.5	25.56	30.63	36.16	25.87	30.93	36.34
12	26.02	31.21	36.86	26.47	31.66	37.19
12.5	26.45	31.73	37.46	27.04	32.33	37.95
13	26.87	32.19	37.95	27.57	32.91	38.57
13.5	27.26	32.61	38.34	28.03	33.39	39.03
14	27.64	32.98	38.65	28.42	33.78	39.38
14.5	28.00	33.29	38.88	28.74	34.07	39.60
15	28.32	33.56	39.02	29.01	34.28	39.73
15.5	28.61	33.78	39.12	29.22	34.43	39.78
16	28.88	33.98	39.20	29.40	34.55	39.80
16.5	29.15	34.19	39.30	29.55	34.64	39.81
17	29.43	34.43	39.48	29.70	34.75	39.85
17.5	29.71	34.71	39.71	29.85	34.87	39.91
18	30.00	35.00	40.00	30.00	35.00	40.00

*IOTF references from Cole and Lobstein, 2012 [1]

In our study population, 88 (40.6%) children were classified as class I obese, 73 (33.6%) as class II obese and 56 (25.8%) as class III obese (Figure 2.1)

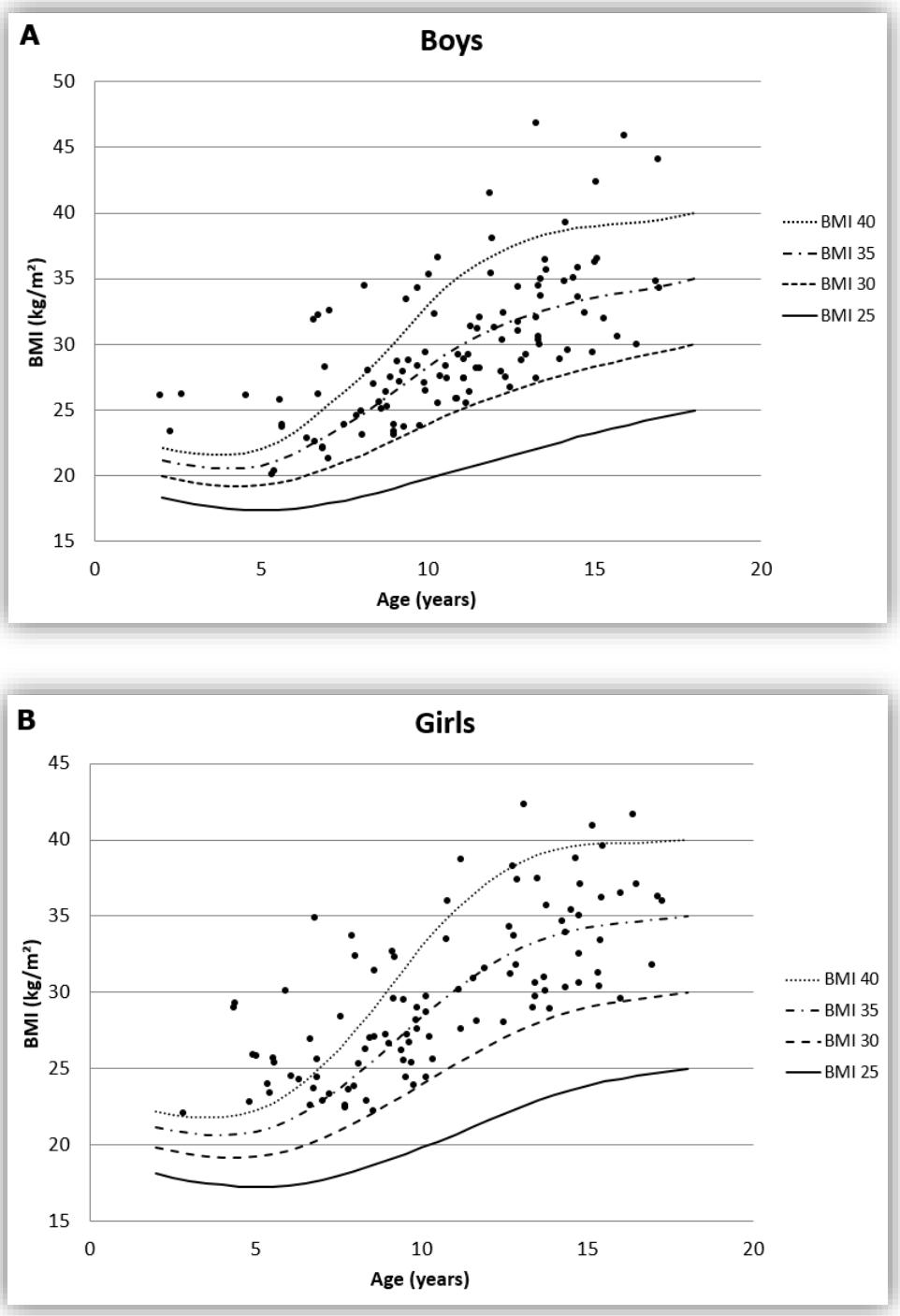

Figure 2.1 IOTF BMI percentile curves of boys (A) and girls (B). Study subjects are presented as a dot.

2.3.2 Cardiometabolic risk factors in morbidly obese children

Components of the MetS with corresponding age- and gender-specific z-scores of the subsample of 90 obese children and adolescents for class I, II and III obesity are shown in Table 2.2.

Table 2.2 Comparison of anthropometric and biochemical parameters with corresponding age- and gender specific z-scores between class I, class II and class III obesity.

	Class I obesity	Class II obesity	Class III obesity	*p-value*
Number, n (%)	36 (40.0)	35 (38.9)	19 (21.1)	
Age, years	12.6 ± 2.2	13.0 ± 2.5	13.1 ± 2.6	0.580
Gender, n (%)				0.752
Male	19 (52.8)	17 (48.6)	8 (42.1)	
Female	17 (47.2)	18 (51.4)	11 (57.9)	
WC, cm	99.9 ± 8.8	108.9 ± 10.1	119.1 ± 14.7	<0.001
WC z-score	3.3 ± 0.4	3.6 ± 0.4	4.0 ± 0.5	<0.001
SBP, mmHg	124 ± 11	126 ± 12	137 ± 14	0.001
SBP z-score	1.0 ± 1.0	1.3 ± 1.0	2.1 ± 0.9	0.001
DBP, mmHg	75 ± 9	78 ± 10	82 ± 9	0.052
DBP z-score	1.4 ± 1.1	1.7 ± 1.1	2.1 ± 0.8	0.058
Fasting glucose, mg/dl	93 ± 8	92 ± 7	95 ± 7	0.357
Fasting glucose z-score	1.2 ± 1.2	1.0 ± 1.1	1.5 ± 0.9	0.364
Fasting insulin, mU/l	18.4 ± 7.5	26.5 ± 11.7	27.9 ± 9.7	0.001
Fasting insulin z-score	1.8 ± 0.9	2.7 ± 1.0	2.8 ± 1.0	<0.001
Total cholesterol, mg/dl	173 ± 29	152 ± 24	164 ± 36	0.011
Total cholesterol z-score	0.1 ± 1.0	-0.6 ± 1.0	-0.2 ± 1.2	0.013
HDL-C, mg/dl	46 ± 13	41 ± 7	44 ± 8	0.121
HDL z-score	-1.1 ± 1.3	-1.6 ± 1.0	-1.3 ± 1.1	0.163
TG, mg/dl	127 ± 76	117 ± 71	106 ± 60	0.577
TG z-score	1.4 ± 1.2	1.1 ± 1.3	0.9 ± 1.4	0.325
LDL-C, mg/dl	103 ± 22	87 ± 19	99 ± 27	0.009
LDL-C z-score	-0.2 ± 0.9	-0.8 ± 0.8	-0.4 ± 1.1	0.007
$MetS_{IDF}$, n (%)	13 (36.1)	12 (34.3)	9 (47.4)	0.616

Values are presented as mean ± SD, unless otherwise indicated. Data in the final column are p values resulting from one-way ANOVA. An adjusted p-value < 0.003 was considered significant. DBP: diastolic blood pressure; HDL-C: high-density lipoprotein cholesterol; IDF: International Diabetes Federation; LDL-C: low-density lipoprotein cholesterol; MetS: metabolic syndrome; SBP: systolic blood pressure; TG: triglycerides; WC: waist circumference.

Children with class III obesity had a larger waist circumference, higher systolic blood pressure and higher levels of fasting insulin compared to class I obese children ($p<0.001$; $p<0.001$ and $p=0.002$ respectively). Levels of total cholesterol, HDL-C, TG and LDL-C did not differ between children with class III obesity and those with less severe obesity.

Although almost 50% of children with class III obesity suffered from MetS compared to about 35% of the children with less severe obesity, the prevalence of MetS between the groups was not significantly different. Moreover, class III

obese children had not significantly more components of MetS than less obese children (see Figure 2.2).

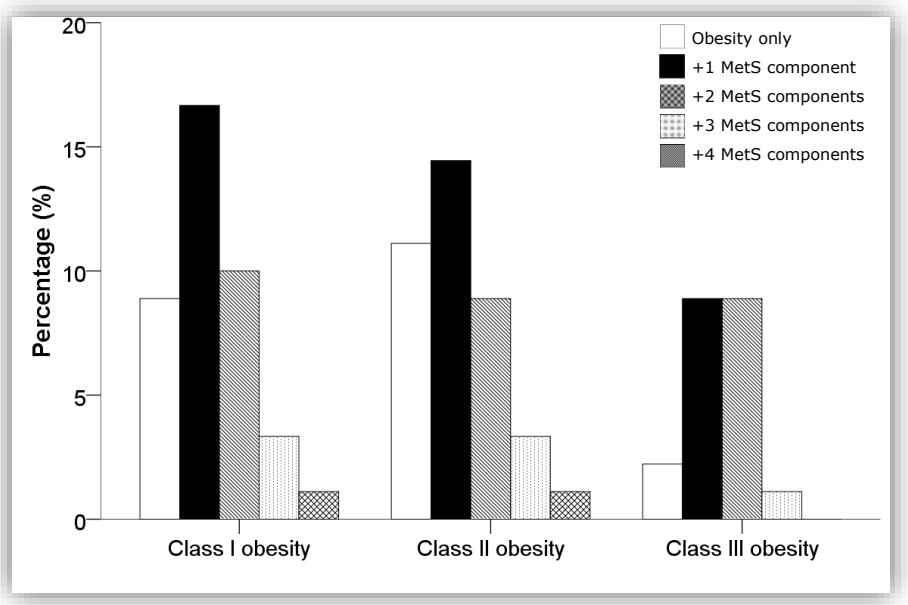

Figure 2.2 The prevalence of MetS components among children and adolescents of different obesity classes defined according to the newly developed IOTF criteria. Data were analyzed by Fisher's exact probability test. p=0.846.

In general, hypertension was the most observed and IFG was the less observed MetS component in the obese children and adolescents studied Figure 2.3.

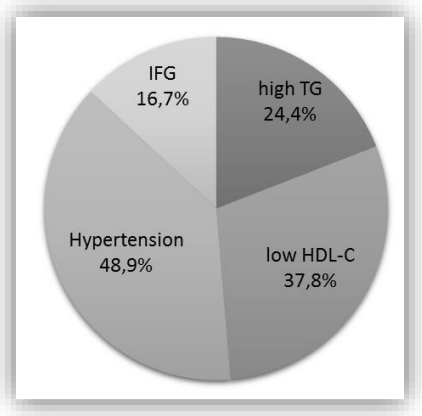

Figure 2.3 Prevalence of individual MetS components among the obese children and adolescents studied. HDL-C: high-density lipoprotein cholesterol; IFG: impaired fasting glucose; TG: triglycerides.

2.4 Discussion

Since numbers of extremely obese children are rising [7-9], it is important to have international BMI cut-off values to define these extreme obesity classes. These cut-offs allow the comparison of prevalence rates of extreme obesity between different countries and with adult prevalence of extreme obesity. In adults, the WHO [5] subdivides adult obesity into 3 classes: class I obesity (BMI 30.00 – 34.99), class II obesity (BMI 35.00 – 39.99), and class III obesity (BMI ≥ 40.00). Here, we present the BMI cut-off of 40 $kg.m^{-2}$, corresponding to the 99.95^{th} percentile at age 18, for children aged 2 to 18. This BMI percentile is an addition to the previously developed IOTF BMI percentiles corresponding to BMI 16, 17, 18.5, 25, 30 and 35 at age 18 [1]. By introducing these additional BMI cut-offs, it is now possible to identify and classify extremely obese children. However, this should always be considered with caution since extreme BMI percentiles are approximates based on fairly arbitrary samples and should not be over-interpreted as though they truly measure any underlying physiological state.

It is striking that 34% and 26% of the obese children referred to our obesity clinic were classified as class II and class III obese, respectively. Due to the fact that our study group was selected from patients referred to our clinic, we are not able to calculate regional prevalence data of severe or morbid obesity. Until now, only two studies have reported prevalence numbers of severe obesity based on the IOTF criteria [1] in children. In the US, 4% of children between 2 and 18 years [1] were classified as severely obese, and in New Zealand 2.5% of the adolescents between 13 and 17 years were reported to be severely obese [20]. However, prevalence numbers of morbid obesity in children based on the IOTF criteria are still lacking. We recommend to reanalyze obesity prevalence studies, especially in countries with a high prevalence of childhood obesity, in order to define the prevalence of severe and morbid childhood obesity.

To explore the clinical importance of this additional IOTF BMI cut-off of 40 $kg.m^{-2}$, we compared anthropometric and biochemical parameters between the different classes of childhood obesity. Children with class III obesity had a larger waist circumference, higher systolic blood pressure and higher fasting insulin levels compared to class I obese children. These observations are in line with the data from Rank et al. [12] who showed that severely obese children had a larger waist circumference, higher blood pressure and higher fasting insulin levels

compared to children with moderate obesity. Consequently, extremely obese children are at a higher risk for cardiometabolic abnormalities. Contrary to general expectations, levels of total cholesterol, HDL-C, triglycerides and LDL-C were not significantly different in class III compared to class I obese children and adolescents. This finding requires further investigation in studies with larger sample sizes. A possible explanation for this contradictory finding is that although cholesterol and triglyceride abnormalities are independent of the degree of childhood obesity, it may result from the duration of exposure to obesity and the presence of metabolic adaptive mechanisms among children and adolescents. Longitudinal follow-up studies are needed to further examine this hypothesis.

In this study, we expected that the MetS was more prevalent in morbidly obese children, but this was not the case. This finding is in line with the study of Sen et al. [11] in which only a weak correlation between the prevalence of MetS and BMI z-score was found. Nevertheless, several studies have shown that children with a higher degree of obesity are at higher risk to develop metabolic complications than less severe obese children [10, 12]. In general, we found that hypertension was the most observed MetS component and IFG was the less observed MetS component in obese children and adolescents. Indeed, hypertension is commonly observed in obese children [21] and IFG is rare in childhood [22].

The rapid increase in the prevalence of more extreme childhood obesity will undoubtedly have a significant impact on our health care system. At the moment, it remains a great challenge to offer an appropriate treatment for morbidly obese children. Since conventional approaches are often ineffective, the treatment of morbidly obese children needs to be more aggressive [23]. Hence, early detection of children at risk for or with extreme obesity is of utmost importance. Nonetheless, larger studies are needed to confirm that the proposed IOTF classification of class I, II and III obesity is clinically useful.

References

1. Cole T, Lobstein T. Extended international (IOTF) body mass index cut-offs for thinness, overweight and obesity. Pediatr Obes. 2012;7(4):284-94.
2. Rolland-Cachera MF. Towards a simplified definition of childhood obesity? A focus on the extended IOTF references. Pediatr Obes. 2012;7(4):259-60.
3. World Health Organisation. Physical status: the use and interpretation of anthropometry. Report of a WHO Expert Committee, WHO Technical Report Series N°854. Geneva: WHO, 1995.
4. Sturm R. Increases in morbid obesity in the USA: 2000–2005. Public Health. 2007;121(7):492-6.
5. World Health Organisation. Obesity: preventing and managing the global epidemic. Report of a WHO Expert Committee, WHO Technical Report Series, N°894. Geneva: WHO, 2000.
6. Olds T, Maher C, Zumin S, Péneau S, Lioret S, Castetbon K, et al. Evidence that the prevalence of childhood overweight is plateauing: data from nine countries. Int J Pediatr Obes. 2011;6(5-6):342-60.
7. Skelton JA, Cook SR, Auinger P, Klein JD, Barlow SE. Prevalence and trends of severe obesity among US children and adolescents. Acad Pediatr. 2009;9(5):322-9.
8. Wang YC, Gortmaker SL, Taveras EM. Trends and racial/ethnic disparities in severe obesity among US children and adolescents, 1976–2006. Int J Pediatr Obes. 2011;6(1):12-20.
9. Pan L, Blanck HM, Sherry B, Dalenius K, Grummer-Strawn LM. Trends in the prevalence of extreme obesity among US preschool-aged children living in low-income families, 1998-2010. JAMA. 2012;308(24):2563-5.
10. Gidding SS, Nehgme R, Heise C, Muscar C, Linton A, Hassink S. Severe obesity associated with cardiovascular deconditioning, high prevalence of cardiovascular risk factors, diabetes mellitus/hyperinsulinemia, and respiratory compromise. J Pediatr. 2004;144(6):766-9.
11. Sen Y, Kandemir N, Alikasifoglu A, Gonc N, Ozon A. Prevalence and risk factors of metabolic syndrome in obese children and adolescents: the role of the severity of obesity. Eur J Pediatr. 2008;167(10):1183-9.
12. Rank M, Siegrist M, Wilks DC, Langhof H, Wolfarth B, Haller B, et al. The cardio-metabolic risk of moderate and severe obesity in children and adolescents. J Pediatr. 2013;163(1):137-42.
13. Singh AS, Mulder C, Twisk JW, Van Mechelen W, Chinapaw MJ. Tracking of childhood overweight into adulthood: a systematic review of the literature. Obes Rev. 2008;9(5):474-88.
14. Cole TJ, Bellizzi MC, Flegal KM, Dietz WH. Establishing a standard definition for child overweight and obesity worldwide: international survey. BMJ. 2000;320(7244):1-6.
15. Cole TJ, Green PJ. Smoothing reference centile curves: the LMS method and penalized likelihood. Stat Med. 1992;11(10):1305-19.
16. World Health Organisation. WHO Expert Consultation on waist circumference and waist-hip ratio. Geneva, Switzerland: 2008 8-11 December 2008. Report No.
17. Friedewald WT, Levy RI, Fredrickson DS. Estimation of the concentration of low-density lipoprotein cholesterol in plasma, without use of the preparative ultracentrifuge. Clin Chem. 1972;18(6):499-502.
18. Mellerio H, Alberti C, Druet C, Capelier F, Mercat I, Josserand E, et al. Novel modeling of reference values of cardiovascular risk factors in children aged 7 to 20 years. Pediatrics. 2012;129(4):e1020-9.
19. Zimmet P, Alberti K, George MM, Kaufman F, Tajima N, Silink M, et al. The metabolic sydrome in children and adolescents - an IDF consensus report. Pediatr Diabetes. 2007;8:299-306.
20. Farrant B, Utter J, Ameratunga S, Clark T, Fleming T, Denny S. Prevalence of severe obesity among New Zealand adolescents and associations with health risk behaviors and emotional well-being. J Pediatr. 2013;163(1):143-9.

21. Flynn J. The changing face of pediatric hypertension in the era of the childhood obesity epidemic. Pediatr Nephrol. 2013;28(7):1059-66.
22. Weiss R, Dziura J, Burgert TS, Tamborlane WV, Taksali SE, Yeckel CW, et al. Obesity and the metabolic syndrome in children and adolescents. N Engl J Med. 2004;350(23):2362-74.
23. Lenders C, Gorman K, Lim-Miller A, Puklin S, Pratt J. Practical approaches to the treatment of severe pediatric obesity. Pediatr Clin North Am. 2011;58(6):1425-38.

Chapter 3

Shape of the plasma glucose curve in end-pubertal obese girls

This study is published as:

Liene Bervoets[1], Alex Mewis[2], Guy Massa[1,3] (2015) **The shape of the plasma glucose curve during an oral glucose tolerance test as an indicator of beta-cell function and insulin sensitivity in end-pubertal obese girls.**
Hormone and Metabolic Research DOI: 10.1055/s-0034-1395551

[1] Faculty of Medicine and Life Sciences, Hasselt University, Hasselt, Belgium; [2] Clinical Laboratory, Jessa Hospital, Hasselt, Belgium,; [3] Department of Pediatrics, Jessa Hospital, Hasselt, Belgium

This study was presented by Liene Bervoets at:

- Belgian Association for the Study of Obesity Free Communications Meeting, 4th February 2012, Leuven, Belgium (oral presentation)
- 22nd Workshop of European Childhood Obesity Group. 17th – 19th October 2012, Palma de Mallorca, Spain (poster)
- 51th Annual Meeting of the European Society for Pediatric Endocrinology, 20th – 23rd September 2012, Leipzig, Germany (poster)

Abstract

It is hypothesized that the shape of the glucose curve during an oral glucose tolerance test is an early indicator of the risk for developing T2DM. In this study, we aimed to examine the shape of plasma glucose response curves and study their relationship with insulin sensitivity, insulin secretion and components of MetS in end-pubertal obese girls. Eighty one end-pubertal obese girls (median (range) age: 14.4 (11.2 – 18.0) years; BMI: 34.6 (25.4–50.8) kg/m²) who underwent a 2-hour OGTT were classified according to the shape of the glucose curve. Four shape types of the plasma glucose response curve were observed: 28 (34.6%) monophasic, 30 (37.0%) biphasic, 14 (17.3%) triphasic, and 9 (11.1%) unclassified. Patients with a monophasic shape had a higher area under the curve for glucose (p=0.008), a lower early-phase insulin secretion (p=0.005), and a poorer beta-cell function relative to insulin sensitivity – as reflected by the oral disposition index (p=0.022) – as compared to the bi- and triphasic shape types. In addition, the TG level and TG/HDL-C ratio was higher in patients with a monophasic shape compared to those with a biphasic shape (p = 0.040 and p = 0.048, respectively). In conclusion, end-pubertal obese girls with a monophasic plasma glucose curve showed a reduced insulin secretion relative to IR and dyslipidemia which can contribute to the development of T2DM and CVD.

3.1 Introduction

Obese children and adolescents are at increased risk of developing insulin resistance, impaired glucose tolerance, dyslipidemia and hypertension which eventually may lead to the development of T2DM and premature cardiovascular disease [1-4]. These complications contribute to a higher likelihood of adult morbidity and mortality [5, 6]. Within the obese paediatric population, especially girls at the end of their puberty are at high-risk of insulin resistance-induced complications [7-9]. Hence, there is a need for a method to early detect reduced insulin secretion and sensitivity in obese youth [10, 11]. The gold standard method for assessing insulin secretion and sensitivity is the hyperinsulinemic-euglycemic clamp [12]. However, it is an invasive, time-consuming, and expensive method, which makes it difficult to use in routine clinical practice or in large-population based epidemiological studies, particularly in children. Therefore, the OGTT is often preferred as a simpler and practical method, from which surrogate indices for insulin resistance and secretion, and glucose tolerance status can be derived [13-15].

It has been previously shown that the shape of the glucose curve obtained during an OGTT may be useful as a metabolic screening parameter [16] and could give insight into the future risk of T2DM [17]. In general, it is suggested that a monophasic shape of the OGTT curve is indicative of a lower insulin sensitivity and impaired beta-cell function compared to a biphasic shape [18]. Additionally, more complex OGTT shapes are associated with a better glucose tolerance [19]. So far, only one study has examined the relationship between the shape of the OGTT curve and insulin action and secretion in normal glucose-tolerant obese adolescents [20]. The authors found that different curves of the OGTT – i.e. monophasic, biphasic, triphasic and monotonous – presented different metabolic phenotypes of insulin action and secretion. More specifically, the monophasic shape was associated with a higher BMI compared to the biphasic shape, and with a lower oral disposition index and higher area under the curve (AUC) for glucose compared to triphasic shape types.

The aim of the current study was to identify different shape types of the glucose curves obtained during an OGTT in a group of end-pubertal obese girls. We opted for this specific study group to eliminate for the influence of transient insulin resistance occurring during puberty [21]. In addition, we examined the

relationship of the different glucose shape types with insulin sensitivity, insulin secretion and components of MetS.

3.2 Materials and methods

3.2.1 Patients

We retrospectively analysed data of 93 end-pubertal – Tanner [22] breast stage M4 or M5 – girls who attended the outpatient paediatric obesity clinic from the Jessa Hospital Hasselt (Belgium) between May 2004 and December 2012. Patients taking any medication, including oral contraceptives, or having any serious medical illness were excluded from the analysis (n = 12). Patients of non-native origin, e.g. Turkish or Moroccan, were classified as non-native. The parental occurrence of T2DM was enquired. The study was conducted in accordance with the ethical rules of the Helsinki Declaration. The study protocol was approved by the Ethics Committee of the Jessa Hospital. Informed consent was obtained from all patients and their parents or legal guardian.

3.2.2 Anthropometric measurements

Patients were weighed wearing underwear only and results were rounded to the nearest 0.1 kg. Standing height was measured to the nearest 0.1 cm. BMI was calculated by dividing weight in kilograms by height in meters squared (BMI = kg/m^2). The BMI SDS was calculated on the basis of the LMS values using the formula: BMI SDS = $[(BMI/M)^{L}-1]/[L \times S]$ as presented by Cole and Lobstein [23]. Patients were classified according to the IOTF criteria, i.e. by age- and gender-specific centile curves passing through BMI 25 at age 18 as 'overweight', through BMI 30 as 'class I obesity', through BMI 35 as 'class II obesity', and through BMI 40 as 'class III obesity' [23, 24]. The pubertal developmental stage (Tanner 4 and 5) was evaluated on the basis of breast development [22]. The majority (96.3%) of the patients were postmenarcheal (age menarche: 12.0 ± 1.5 years). Seated blood pressure was measured with an electronic sphygmomanometer (Omron®, Omron Healthcare, IL, USA).

3.2.3 Blood sampling and OGTT

After an overnight fast, venous blood samples were taken for measurement of plasma glucose, serum insulin, HDL-C and TG. Thereafter, a standard OGTT was performed with the ingestion of 75 g glucose. Venous blood samples were obtained at 30, 60, 90 and 120 minutes. Plasma glucose was measured by the

glucose oxidase method using a Synchron LX20 analyzer (Beckman Coulter, Brea, CA, USA). Serum insulin was assessed by immunoassay (ADVIA Centaur Insulin IRI; Siemens Medical Solutions Diagnostics, Tarrytown, NY). Intra- and interassay variations were less than 5%. Hemolytic test results were excluded prior to further analysis. HDL-C and TG were measured on a Beckman Coulter AU 2700 automatic analyzer (Brea, CA, USA).

3.2.4 Classification of glucose tolerance status

Normal glucose tolerance (NGT) was defined as FPG < 100 mg/dl and 2-h plasma glucose < 140 mg/dl. Prediabetes was defined as having IFG (fasting plasma glucose: 100-125 mg/dl) and/or IGT (2-h plasma glucose: 140-199 mg/dl), according to the Expert Committee on the Diagnosis and Classification of Diabetes Mellitus criteria [25]. None of the patients suffered from T2DM (fasting plasma glucose ≥ 126 mg/dl and/or 2-h plasma glucose ≥ 200 mg/dl).

3.2.5 Definition of the metabolic syndrome

The MetS was defined according to the IDF consensus for children older than 10 years [26]. Patients with the MetS were classified as having obesity (age- and gender-specific centile curves passing through BMI 30 at age 18) according to IOTF criteria [23] and at least two of the following components: TG ≥ 150 mg/dl; HDL-C < 40 mg/dl; SBP ≥ 130 mm Hg and/or DBP ≥ 85 mg Hg; FPG ≥ 100 mg/dl.

3.2.6 Classification of glucose curve shapes

Figure 3.1 gives an overview of the plasma glucose curve shapes obtained during an OGTT in the studied end-pubertal obese girls. The shapes were classified in line with previous studies [16-18, 27]. This was done with a plasma glucose threshold of 2 mg/dl to minimize fluctuations in glucose concentrations, which may be caused by the method of glucose analysis rather than physiological reasons [28].

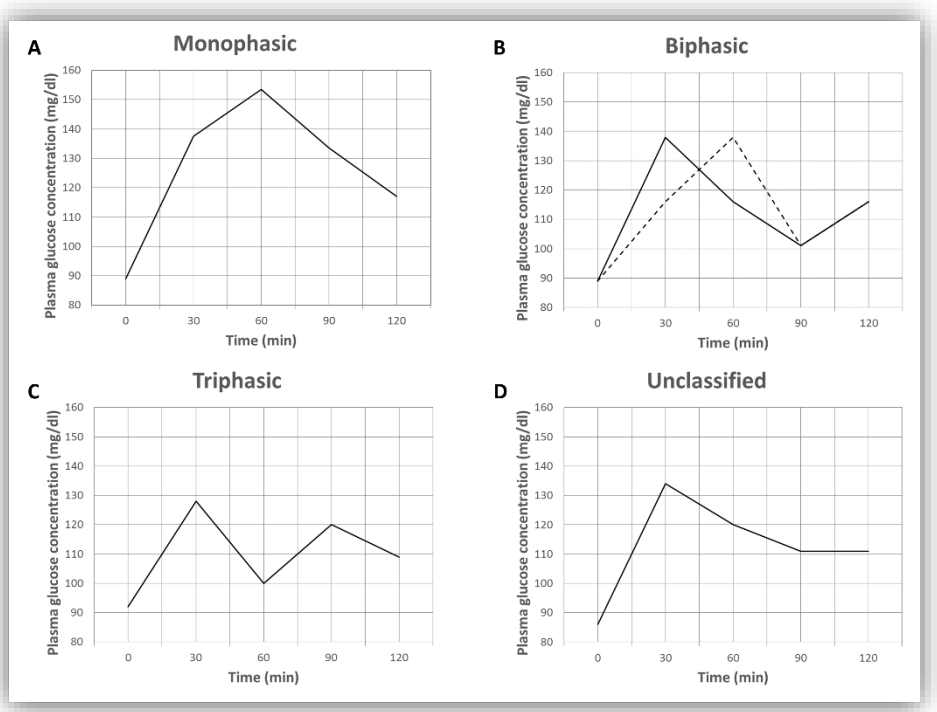

Figure 3.1 Observed plasma glucose curve shape types. A: monophasic; B: biphasic; C: triphasic; D: unclassified.

A "monophasic" shape is characterized by a rise in plasma glucose concentrations until a maximum value between 30 min and 90 min is reached, followed by a subsequent decrease until 120 min. A "biphasic" shape is characterized by a rise in plasma glucose concentrations until a maximum value at 30 min or 60 min is reached, followed by a fall, with a second rise of glucose prior to 120 min. A "triphasic" shape is characterized by two complete peaks of the plasma glucose curve. Shapes which could not be classified according to previous criteria were considered "unclassified".

3.2.7 Calculations of metabolic health determinants

We assessed fasting glucose and insulin, and 2-h glucose and insulin concentrations. The total glucose response and insulin secretion were evaluated from the AUC estimated by the trapezoidal rule [29].

$$\mathrm{AUCglucose} = \left(30\mathrm{x}\left(\frac{\mathrm{G0}+\mathrm{G30}}{2}\right)\right) + \left(30\mathrm{x}\left(\frac{\mathrm{G30}+\mathrm{G60}}{2}\right)\right) + \left(30\mathrm{x}\left(\frac{\mathrm{G60}+\mathrm{G90}}{2}\right)\right) + \left(30\mathrm{x}\left(\frac{\mathrm{G90}+\mathrm{G120}}{2}\right)\right)$$

$$\text{AUCinsulin} = \left(30\text{x}\left(\frac{\text{I0} + \text{I30}}{2}\right)\right) + \left(30\text{x}\left(\frac{\text{I30} + \text{I60}}{2}\right)\right) + \left(30\text{x}\left(\frac{\text{I60} + \text{I90}}{2}\right)\right) + \left(30\text{x}\left(\frac{\text{I90} + \text{I120}}{2}\right)\right)$$

where G stands for glucose (mg/dl) and I for insulin (µU/ml) at zero/baseline and after 30, 60, 90 and 120 minutes. Estimates for insulin sensitivity and secretion were calculated from parameters obtained during the OGTT. Insulin sensitivity was determined by two indices, i.e. whole body insulin sensitivity index (WBISI) as described by Matsuda et al. [14]:

$$\text{WBISI} = \frac{10000}{\sqrt{\left(\text{fasting glucose } \left(\frac{\text{mg}}{\text{dl}}\right) \text{x fasting insulin } \left(\frac{\mu\text{U}}{\text{ml}}\right) \text{ x mean glucose } \left(\frac{\text{mg}}{\text{dl}}\right) \text{x mean insulin } \left(\frac{\mu\text{U}}{\text{ml}}\right)\right)}}$$

and the homeostasis model assessment of insulin resistance (HOMA-IR) [13]:

$$\text{HOMA-IR} = \frac{\text{fasting glucose } \left(\frac{\text{mg}}{\text{dl}}\right) \text{x fasting insulin } \left(\frac{\mu\text{U}}{\text{ml}}\right)}{405}$$

To assess beta-cell function, we used the insulinogenic index (IGI) calculated as [30]:

$$\text{IGI (insulinogenic index)} = \frac{\text{insulin 30 min } \left(\frac{\mu\text{U}}{\text{ml}}\right) \text{- fasting insulin } \left(\frac{\mu\text{U}}{\text{ml}}\right)}{\text{glucose 30 min } \left(\frac{\text{mg}}{\text{dl}}\right) \text{-fasting glucose } \left(\frac{\text{mg}}{\text{dl}}\right)}$$

In addition, in order to assess beta-cell function relative to insulin sensitivity, the oral disposition index (oDI) was calculated as [31]:

$$\text{oDI} = \text{IGI x} \frac{1}{\text{fasting insulin } \left(\frac{\mu\text{U}}{\text{ml}}\right)}$$

The triglyceride-to-HDL cholesterol (TG/HDL-C) ratio was also calculated as an early indicator of insulin resistance [32].

3.2.8 Statistical analysis

Statistical analyses were implemented in IBM SPSS version 20.0 (SPSS Inc., Chicago, IL, USA). Results are presented as median (range) or geometric mean ± geometric standard deviation (GSD), as indicated. To compare interval-scaled characteristics between all glucose response curves, Kruskal Wallis test was used

to compare more than 2 groups, followed by post-hoc Mann Whitney U test to compare two groups. Fisher exact probability test – with the Freeman-Halton extension in case of 3 x 2 contingency table – was applied to test nominal scale variables between groups, and data are presented as numbers (percentages). P values smaller than 0.05 are considered significant.

3.3 Results

3.3.1 Prevalence of the glucose curve shapes

Figure 3.1 illustrates the observed shapes of the plasma glucose curve of end-pubertal obese girls (see above). Of all 72 classifiable plasma glucose curve shapes, 28 (34.6%) patients showed a monophasic, 30 (37.0%) showed a biphasic and 14 (17.3%) showed a triphasic shape during the OGTT. The remaining 9 (11.1%) patients had a glucose curve shape that could not be classified, i.e. unclassified, which was mainly due to a change in glucose concentration of less than 2 mg/dl between 90 and 120 minutes.

3.3.2 Baseline characteristics according to glucose curve shapes

Table 3.1 compares the baseline characteristics between the patients grouped according to the shape of the glucose curve. The unclassified shape group (n = 9) showed no differences compared to the other shape groups, and was subsequently excluded in further analysis. Median age of total study population was 14.4 (11.2 – 18.0) years and BMI was 34.6 (25.4–50.8) kg/m². In total, thirteen (16.0%) of all patients suffered from prediabetes and the majority of the girls (56.8%) had a family history of T2DM. No statistically significant differences were detected for age, BMI, BMI SDS, ethnic origin, glycemic status and family history of diabetes between the glucose shape types.

Table 3.1 Baseline characteristics of the study population.

	Monophasic (n = 28)	Biphasic (n = 30)	Triphasic (n = 14)	*p value*	Unclassified (n = 9)	Total (n = 81)
Age, years	14.6 (12.0 – 18.0)	14.3 (11.2 – 17.9)	14.4 (12.4 – 17.4)	0.786	14.3 (11.9 – 16.9)	14.4 (11.2 – 18.0)
BMI (kg/m²)	36.0 (25.4 – 50.8)	34.1 (25.7 – 44.9)	34.7 (30.2 – 39.9)	0.438	31.6 (27.0 – 37.9)	34.6 (25.4 – 50.8)
BMI SDS	3.0 (1.5 – 3.8)	2.7 (1.5 – 3.6)	2.8 (2.3 – 3.3)	0.380	2.7 (2.0 – 3.1)	2.8 (1.5 – 3.8)
BMI categories, n (%)				0.687		
Overweight	3 (10.7)	2 (6.7)	0 (0.0)		2 (22.2)	7 (8.6)
Obese Class I	8 (28.6)	12 (40.0)	8 (57.1)		5 (55.6)	33 (40.7)
Obese Class II	9 (32.1)	10 (33.3)	4 (28.6)		2 (22.2)	25 (30.9)
Obese Class III	8 (28.6)	6 (20.0)	2 (14.3)		0 (0.0)	16 (19.8)
Ethnicity, n (%)				0.349		
Native	16 (57.1)	22 (73.3)	8 (57.1)		5 (55.6)	51 (63.0)
Non-native	12 (42.9)	8 (26.7)	6 (42.9)		4 (44.4)	30 (37.0)
Glycemic status, n (%)				0.221		
NGT	20 (71.4)	26 (86.7)	13 (92.9)		9 (100.0)	68 (84.0)
Prediabetic (IFG and/or IGT)	8 (28.6)	4 (13.3)	1 (7.1)		0 (0.0)	13 (16.0)
Parental diabetes, n (%)				0.432		
No	12 (42.9)	15 (50.0)	4 (28.6)		4 (44.4)	35 (43.2)
Yes	16 (57.1)	15 (50.0)	10 (71.4)		5 (55.6)	46 (56.8)

Values are presented as median (range), unless otherwise indicated. The p values shown are the result of the Kruskal-Wallis and Fisher exact probability test between monophasic, biphasic and triphasic group. BMI: body mass index; IFG: impaired fasting glucose; IGT: impaired glucose tolerance; NGT: normal glucose tolerance; SDS: standard deviation score.

3.3.3 Comparison of glucose and insulin levels between the glucose curve shapes

Figure 3.2 shows glucose (Figure 3.2A) and insulin (Figure 3.2B) concentrations at different time points of the OGTT according to each classified glucose response shape.

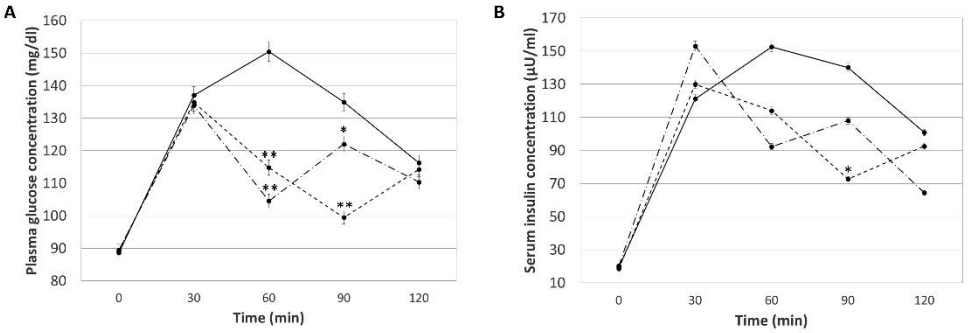

Figure 3.2 Glucose (A) and insulin (B) response curves of monophasic, biphasic and triphasic shape types. Values are presented as geometric means ± GSD. **p < 0.001 *p < 0.02.

Significant differences of the plasma glucose concentration were present at 60 and 90 minutes between the monophasic and biphasic shape ($p < 0.001$ for both time points) and at 60 minutes between monophasic and triphasic shape ($p < 0.001$). The glucose concentration at 90 minutes also significantly differed between the biphasic and triphasic shape ($p = 0.018$). Significant differences of the insulin concentration were found at 90 minutes between the monophasic and biphasic shape ($p = 0.005$).

3.3.4 Glucose shape types in relation to OGTT derived-indices and components of the metabolic syndrome

Table 3.2 compares OGTT-derived indices and components of MetS among the different glucose shape types.

Table 3.2 Parameters of glucose and insulin metabolism, and components of the metabolic syndrome in patients with a monophasic, biphasic or triphasic shape.

	Monophasic (n=28)	**Biphasic (n=30)**	**Triphasic (n=14)**	***p value***
Fasting plasma glucose, mg/dl	89 (74 – 109)	88 (68 – 109)	90 (74 – 98)	0.394
2–h glucose, mg/dl	121 (81 – 160)	115 (69 – 167)	113 (73 – 170)	0.344
AUC glucose, mg.dl^{-1}.min [a, b]	**15981 (11250 – 20910)**	**13933 (9855 – 19020)**	**14239 (10665 – 18870)**	**0.008**
Fasting serum insulin, µU/ml	22.4 (4.3 – 48.9)	22.2 (6.2 – 55.1)	24.7 (9.0 – 49.4)	0.956
2–h insulin, µU/ml	131.8 (30.2 – 383.7)	120.5 (17.2 – 306.9)	110.2 (9.9 – 362.4)	0.550
AUC insulin, µU.ml^{-1}.min	16834.9 (2481.0 – 38190.0)	14767.1 (3802.5 – 30996.0)	15995.9 (5037.0 – 36994.5)	0.739
WBISI	2.4 (0.5 – 7.5)	2.7 (0.8 – 7.3)	2.6 (0.8 – 5.7)	0.775
HOMA–IR	5.6 (1.0 – 21.1)	4.8 (1.3 – 12.1)	5.6 (2.0 – 11.2)	0.947
IGI [a, b]	**2.4 (0.6 – 8.3)**	**3.1 (1.2 – 7.3)**	**3.9 (1.9 – 7.6)**	**0.005**
oDI [b]	**0.110 (0.021 – 0.730)**	**0.169 (0.050 – 0.433)**	**0.208 (0.045 – 0.307)**	**0.022**
TG, mg/dl [a]	107 (52 – 245)	88 (30 – 229)	110 (44 – 361)	0.115
HDL-C, mg/dl	45 (32 – 68)	47 (33 – 63)	48 (36 – 70)	0.732
TG/HDL-C ratio, mg/dl [a]	2.5 (0.8 – 5.7)	2.0 (0.6 – 5.2)	2.6 (0.8 – 10.0)	0.130
SBP, mm Hg	137 (116 – 160)	136 (119 – 158)	130 (100 – 150)	0.279
DBP, mm Hg	83 (70 – 100)	83 (64 – 100)	80 (68 – 110)	0.330
Prevalence of MetS, n (%)	8 (28.6)	9 (30.0)	5 (35.7)	0.893

Values are presented as median (range) or number (percentage). The p values shown are the result of the Kruskal-Wallis test with additional Mann-Whitney *U* test (for interval scale variables) or Fisher exact probability test (for nominal scale variables) between the monophasic, biphasic and triphasic shape group. AUC: area under the curve; WBISI: whole body insulin sensitivity index; HOMA-IR: homeostasis model assessment of insulin resistance; IGI: insulinogenic index; oDI: oral disposition index; TG: triglycerides; HDL-C: high-density lipoprotein cholesterol; SBP: systolic blood pressure; DBP: diastolic blood pressure; MetS: metabolic syndrome

[a] Significantly different between monophasic and biphasic: AUC glucose: p = 0.004; IGI: p = 0.021; TG: p = 0.040; TG/HDL ratio: p = 0.048

[b] Significantly different between monophasic and triphasic: AUC glucose: p = 0.033; IGI: p = 0.004; oDI: p = 0.008

End-pubertal obese girls with a monophasic shaped curve displayed significantly higher levels of AUC glucose and lower levels of IGI and oDI compared to the biphasic and triphasic shape groups. Out of all patients with a classified shape, 30.6% had the MetS. No difference was detected in the prevalence of MetS between the three shape types. However, patients with a monophasic shape showed higher levels of triglycerides and TG/HDL-C ratio compared to patients with a biphasic pattern. There were no significant differences between the biphasic and triphasic shapes for OGTT-derived indices and components of MetS.

3.4 Discussion

In end-pubertal obese girls, we observed four different shape types of the plasma glucose response curve during an OGTT, i.e. monophasic, biphasic, triphasic and unclassified. Patients with a monophasic shape showed higher AUC glucose, lower early-phase insulin secretion and poorer beta-cell insulin secretory capacity relative to insulin sensitivity – as reflected by the oDI – compared to patients with a biphasic or triphasic shape. Moreover, patients with a monophasic curve showed higher levels of triglycerides and TG/HDL-C ratio compared to patients with a biphasic shape pattern.

Studies in adults have demonstrated that different patterns of the plasma glucose curve during an OGTT exist and can be discriminated on the basis of the severity of glucose intolerance, insulin resistance and secretion [16-19, 33, 34]. Generally, subjects with a biphasic shape pattern have a lower BMI, better glucose tolerance, better insulin sensitivity and beta-cell function compared to subjects with a monophasic shape [16, 18, 19]. In addition, it seemed that a more complex glucose shape pattern – i.e. shape with more phases – is associated with a better glucose tolerance [19]. It appears that insulin secretion by the beta-cell is not sufficient to fully compensate for higher glucose concentrations in less complex shape patterns (monophasic and biphasic), and furthermore, insulin sensitivity is found to be lower [19]. Findings from these cross-sectional studies were confirmed by a 7-8 year follow-up study in non-diabetic normal-weight Caucasian adults [17], in which those with a monophasic glucose response curve exhibited a 3.5-fold greater risk of future T2DM compared to those with a biphasic curve.

In a study on 522 Caucasian normal glucose-tolerant obese children and adolescents aged 4 to 18 Nolfe et al. observed that the monophasic shape type was associated with a higher BMI compared to the biphasic shape type, and a higher AUC glucose and lower oDI (i.e. DI_{ISI} calculated as the product of IGI and WBISI) compared to the triphasic pattern [20]. This is in line with our findings. It should be noted, however, that we calculated the oDI as a product of IGI and 1/fasting insulin which is in contrast with their methodology. We opted to use the oDI since it shows the strongest correlation with the disposition index calculated on the basis of the hyperinsulinemic euglycemic clamp (cDI) in obese youth. In addition, Nolfe et al. [20] identified a monotonous curve of plasma glucose during an OGTT which was not present in our study population. The monotonous shape

pattern was described as a gradual increase in the concentration of glucose which reaches its maximum after 2 hours. A possible reason for the fact we could not detect this shape type in our study might be due to its low prevalence as it was only 4% in the study of Nolfe et al., and the difference in age between the study populations [20]. Moreover, differences in genetic background, geographical location and/or differences in environmental factors such as diet or physical activity might also determine whether or not a certain shape exists in the study population. For example, Kim et al. [28] did not detect the triphasic shape pattern in 156 Latino adolescents, whereas in our study and that of Nolfe et al. [20], this shape pattern is clearly present.

In our study population, obese girls with a monophasic glucose curve showed higher AUC glucose, a lower IGI and lower oDI compared to those with a biphasic or triphasic shape. The IGI describes early insulin secretion in response to glucose increment during the first 30 minutes of an OGTT [30]. It can be speculated that the earlier the insulin peak occurs (i.e. in the bi- and triphasic shape patterns), the more efficient the glucose load can be cleared and the faster glucose values decline to their nadir. It has indeed been shown that obese youth with an early insulin response to glucose loading are less likely to have insulin resistance and have a lower risk to develop T2DM compared to those with a late response [35-37]. In addition, it has previously been shown that the oDI – calculated as the product of IGI and WBISI – of obese adolescents is a good predictor of the development of IGT after two years [38]. In nondiabetic adults, it has been shown that the oDI is a strong predictor of future type 2 diabetes [39, 40]. Hence, our findings point towards an important role of beta-cell insulin secretory capacity in the establishment of different glucose curve shapes in end-pubertal obese girls and reinforce the hypothesis that the shape of the plasma glucose curve may serve as a predictor for the T2DM risk [17].

In the present study, we also found that patients with a monophasic shape pattern displayed higher levels of triglycerides and a higher TG/HDL-C ratio compared to patients with a biphasic pattern. Nolfe et al. [20] found no differences in lipid concentrations, including triglycerides and HDL-C, between different plasma glucose curve shapes in obese children and adolescents. This might be explained by the fact that in our study population patients with NGT as well as IGT were included, whereas Nolfe et al. [20] included only NGT patients for the

analysis of the glucose curves. It has previously been shown that obese children and adolescents with IGT present significantly higher triglyceride levels compared to NGT individuals [41]. It is important to note that the TG/HDL-C ratio has, to our knowledge, never been investigated in relationship with the shape of the OGTT. The TG/HDL-C ratio is suggested to be an indicator of insulin resistance and early dysglycemia in obese youth [32], and a predictor of atherosclerosis and CVD [42-44]. Hence, the finding of an elevated TG/HDL-C ratio in the monophasic shape group further point towards a role of the OGTT shape as an early indicator of insulin resistance and a predictor of T2DM and CVD. On the other hand, blood pressure, fasting and 2-hour glucose concentrations, and the prevalence of MetS did not significantly differ between the shape types. Perhaps, the shape of the glucose curve may differentiate in the risk for T2DM and CVD even before the dysregulation of blood pressure, fasting and 2-hour glucose, and the development of MetS becomes evident. However, further research to investigate the predictive properties of the plasma glucose shape is recommended.

We opted to focus our research on a rather homogeneous group of end-pubertal obese girls who are at increased risk of having insulin resistance [7-9]. Consequently, the effect of changing insulin levels during puberty could not confound our study results. End-pubertal obese girls with a monophasic glucose response curve present the most unfavourable glucose and insulin metabolism, which could indicate that they are at higher risk of prediabetes development and consequent T2DM. Family history of T2DM, which is known to be a major risk factor of impaired glucose metabolism and T2DM in obese youth [45], was also examined in this study. We expected that patients with a monophasic shape had a higher prevalence of parental T2DM, however, we were unable to prove this, which might be due to the small sample size. Nonetheless, previous studies of OGTT shapes in obese adolescents did not consider pubertal stage nor the presence of family history of T2DM [20, 28].

A limitation of the current study is that we did not investigate the reproducibility of the OGTT curves because patients included in this study followed a therapeutic weight loss program which started after their first OGTT and a second OGTT would not represent a valid replicate of the first one. A recent study by Kramer et al. [46] demonstrated a poor reproducibility of the monophasic and biphasic glucose shapes in a population of 30 normal glucose-tolerant healthy

adults who underwent three replicate OGTTs. Of course, this has to be interpret with respect to the physiological context of the OGTT, i.e. plasma glucose concentration is influenced by physiological factors including enteric hormones and neural responses to nutrient ingestion, as well as gastrointestinal motility and gastric emptying [47, 48]. Moreover, it has previously been shown that an OGTT in obese youth is poorly reproducible for fasting plasma glucose and especially for 2-hour plasma glucose [49]. Therefore, when undertaking future research to study the shape of the OGTT in obese children and adolescents, we suggest to perform a duplicate or confirmatory OGTT. Additionally, it has been previously shown that a 3-hour OGTT displays a more complex pattern of glucose and insulin responses (i.e. higher number of phases), and a greater complexity is associated with a better glucose tolerance, a better beta-cell function and higher insulin sensitivity [19]. Although our current findings are based on data from routinely performed 2-hour OGTTs and the studied sample size is small, in future it would be interesting to study the shapes of a 3-hour OGTT more thoroughly in order to gain more information on glucose and insulin metabolism.

In summary, we observed four different shape types of the plasma glucose curve in end-pubertal obese girls. Girls with a monophasic glucose curve shape during an OGTT are more frequently characterized by a lower early-phase insulin secretion, a poorer beta-cell function relative to insulin sensitivity and elevated triglyceride levels and TG/HDL-C ratio. We recommend to focus future research on longitudinal studies in obese children and adolescents in order to confirm, validate and complement our findings. In this way, the predictive properties of the shape of the glucose OGTT curve could be further examined with regard to the development of T2DM and CVD in obese children and adolescents.

References

1. Wiegand S, Maikowski U, Blankenstein O, Biebermann H, Tarnow P, Gruters A. Type 2 diabetes and impaired glucose tolerance in European children and adolescents with obesity - a problem that is no longer restricted to minority groups. Eur J Endocrinol. 2004;151(2):199-206.
2. Sen Y, Kandemir N, Alikasifoglu A, Gonc N, Ozon A. Prevalence and risk factors of metabolic syndrome in obese children and adolescents: the role of the severity of obesity. Eur J Pediatr. 2008;167(10):1183-9.
3. Franks PW, Hanson RL, Knowler WC, Sievers ML, Bennett PH, Looker HC. Childhood obesity, other cardiovascular risk factors, and premature death. N Engl J Med. 2010;362(6):485-93.
4. Makkes S, Renders CM, Bosmans JE, van der Baan-Slootweg OH, Seidell JC. Cardiometabolic risk factors and quality of life in severely obese children and adolescents in the Netherlands. BMC Pediatr. 2013;13(62):1-9.
5. Dietz WH. Childhood weight affects adult morbidity and mortality. J Nutr. 1998;128(2):S411-4.
6. Reilly JJ, Kelly J. Long-term impact of overweight and obesity in childhood and adolescence on morbidity and premature mortality in adulthood: systematic review. Int J Obes. 2011;35(7):891-8.
7. Roemmich JN, Clark PA, Lusk M, Friel A, Weltman A, Epstein LH, et al. Pubertal alterations in growth and body composition. VI. Pubertal insulin resistance: relation to adiposity, body fat distribution and hormone release. Int J Obes. 2002;26:701-9.
8. Brufani C, Tozzi A, Fintini D, Ciampalini P, Grossi A, Fiori R, et al. Sexual dimorphism of body composition and insulin sensitivity across pubertal development in obese Caucasian subjects. Eur J Endocrinol. 2009;160(5):769-75.
9. Pilia S, Casini MR, Foschini ML, Minerba L, Musiu MC, Marras V, et al. The effect of puberty on insulin resistance in obese children. J Endocrinol Invest. 2009;32(5):401-5.
10. Chiarelli F, Marcovecchio ML. Insulin resistance and obesity in childhood. Eur J Endocrinol. 2008;159(Suppl 1):S67-74.
11. Weiss R, Kaufman FR. Metabolic complications of childhood obesity: identifying and mitigating the risk. Diabetes Care. 2008;31 (Suppl 2):S310-6.
12. DeFronzo RA, Tobin JD, Andres R. Glucose clamp technique: a method for quantifying insulin secretion and resistance. Am J Physiol Endocrinol Metab. 1979;237(3):214-23.
13. Matthews DR, Hosker JP, Rudenski AS, Naylor BA, Treacher DF, Turner RF. Homeostasis model assessment: insulin resistance and β-cell function from fasting plasma glucose and insulin concentrations in man. Diabetologia. 1985;28(7):412-9.
14. Matsuda M, DeFronzo RA. Insulin sensitivity indices obtained from oral glucose tolerance testing: comparison with the euglycemic insulin clamp. Diabetes Care. 1999;22(9):1462-70.
15. Stumvoll M, Mitrakou A, Pimenta W, Jenssen T, Yki-Järvinen H, Van Haeften T, et al. Use of the oral glucose tolerance test to assess insulin release and insulin sensitivity. Diabetes Care. 2000;23(3):295-301.
16. Tschritter O, Fritsche A, Shirkavand F, Machicao F, Häring H, Stumvoll M. Assessing the shape of the glucose curve during an oral glucose tolerance test. Diabetes Care. 2003;26(4):1026-33.
17. Abdul-Ghani MA, Lyssenko V, Tuomi T, Defronzo RA, Groop L. The shape of plasma glucose concentration curve during OGTT predicts future risk of type 2 diabetes. Diabetes Metab Res Rev. 2010;26(4):280-6.
18. Kanauchi M, Kimura K, Kanauchi K, Saito Y. Beta-cell function and insulin sensitivity contribute to the shape of plasma glucose curve during an oral glucose tolerance test in non-diabetic individuals. Int J Clin Pract. 2005;59:427-32.
19. Tura A, Morbiducci U, Sbrignadello S, Winhofer Y, Pacini G, Kautzy-Willer A. Shape of glucose, insulin, C-peptide curves during a 3-h oral glucose tolerance test: any

relationship with the degree of glucose tolerance? Am J Physiol Regul Integr Comp Physiol. 2011;300:941-8.
20. Nolfe G, Spreghini MR, Sforza RW, Morino G, Manco M. Beyond the morphology of the glucose curve following an oral glucose tolerance test in obese youth. Eur J Endocrinol. 2012;166:107-14.
21. Sorensen K, Aksglaede L, Petersen JH, Andersson AM, Juul A. Serum IGF1 and insulin levels in girls with normal and precocious puberty. Eur J Endocrinol. 2012;166(5):903-10.
22. Marshall WA, Tanner JM. Variations in pattern of pubertal changes in girls. Arch Dis Child. 1969;44(235):291-303.
23. Cole T, Lobstein T. Extended international (IOTF) body mass index cut-offs for thinness, overweight and obesity. Pediatr Obes. 2012;7(4):284-94.
24. Bervoets L, Massa G. Defining morbid obesity in children based on BMI 40 at age 18 using the extended international (IOTF) cut-offs. Pediatr Obes. 2014;9(5):e94-8.
25. American Diabetes Association. Diagnosis and classification of diabetes mellitus. Diabetes Care. 2014;37:S81-90.
26. Zimmet P, Alberti K, George MM, Kaufman F, Tajima N, Silink M, et al. The metabolic sydrome in children and adolescents - an IDF consensus report. Pediatr Diabetes. 2007;8:299-306.
27. Trujillo-Arriaga HM, Roman-Ramos R. Fitting and evaluating the glucose curve during a quasi continuous sampled oral glucose tolerance test. Comput Biol Med. 2008;38(2):185-95.
28. Kim JY, Coletta DK, Mandarino LJ, Shaibi GQ. Glucose response curve and type 2 diabetes risk in Latino adolescents. Diabetes Care. 2012;35(9):1925-30.
29. Matthews JN, Altman DG, Campbell MJ, Royston P. Analysis of serial measurements in medical research. BMJ. 1990;300:230-5.
30. Yeckel CW, Weiss R, Dziura J, Taksali SE, Dufour S, Burgert TS, et al. Validation of insulin sensitivity indices from oral glucose tolerance test parameters in obese children and adolescents. J Clin Endocrinol Metab. 2004;89(3):1096-101.
31. Sjaarda LG, Bacha F, Lee S, Tfayli H, Andreatta E, Arslanian S. Oral disposition index in obese youth from normal to prediabetes to diabetes: relationship to clamp disposition index. J Pediatr. 2012;161:51-7.
32. Giannini C, Santoro N, Caprio S, Kim G, Lartaud D, Shaw M, et al. The triglyceride-to-HDL cholesterol ratio: association with insulin resistance in obese youths of different ethnic backgrounds. Diabetes Care. 2011;34(8):1869-74.
33. Fuchigami M, Nakano H, Oba K, Metori S. [Oral glucose tolerance test using a continuous blood sampling technique for analysis of the blood glucose curve]. Nihon Ronen Igakkai Zasshi. 1994;31(7):518-24.
34. Zhou W, Gu Y, Li H, Luo M. Assessing 1-h plasma glucose and shape of the glucose curve during oral glucose tolerance test. Eur J Endocrinol. 2006;155(1):191-7.
35. Weiss R, Taksali SE, Tamborlane WV, Burgert TS, Savoye M, Caprio S. Predictors of changes in glucose tolerance status in obese youth. Diabetes Care. 2005;28(4):902-9.
36. Tfayli H, Lee SJ, Bacha F, Arslanian S. One-hour plasma glucose concentration during the OGTT: what does it tell about beta-cell function relative to insulin sensitivity in overweight/obese children? Pediatr Diabetes. 2011;12(6):572-9.
37. Manco M, Del Giudice EM, Spreghini MR, Cappa M, Perrone L, Brufani C, et al. 1-Hour plasma glucose in obese youth. Acta Diabetol. 2012;49(6):435-43.
38. Giannini C, Weiss R, Cali A, Bonadonna R, Santoro N, Pierpont B, et al. Evidence for early defects in insulin sensitivity and secretion before the onset of glucose dysregulation in obese youths: a longitudinal study. Diabetes. 2012;61(3):606-14.
39. Lyssenko V, Almgren P, Anevski D, Perfekt R, Lahti K, Nissen M, et al. Predictors of and longitudinal changes in insulin sensitivity and secretion preceding onset of type 2 diabetes. Diabetes. 2005;54(1):166-74.
40. Abdul-Ghani MA, Williams K, DeFronzo RA, Stern M. What is the best predictor of future type 2 diabetes? Diabetes Care. 2007;30(6):1544-8.

41. Wabitsch M, Hauner H, Hertrampf M, Muche R, Hay B, Mayer H, et al. Type II diabetes mellitus and impaired glucose regulation in Caucasian children and adolescents with obesity living in Germany. Int J Obes. 2004;28(2):307-13.
42. Quijada Z, Paoli M, Zerpa Y, Camacho N, Cichetti R, Villarroel V, et al. The triglyceride/HDL-cholesterol ratio as a marker of cardiovascular risk in obese children; association with traditional and emergent risk factors. Pediatr Diabetes. 2008;9(5):464-71.
43. Weiss R, Otvos JD, Sinnreich R, Miserez AR, Kark JD. The triglyceride to high-density lipoprotein–cholesterol ratio in adolescence and subsequent weight gain predict nuclear magnetic resonance–measured lipoprotein subclasses in adulthood. J Pediatr. 2011;158(1):44-50.
44. Urbina EM, Khoury PR, McCoy CE, Dolan LM, Daniels SR, Kimball TR. Triglyceride to HDL-C ratio and increased arterial stiffness in children, adolescents, and young adults. Pediatrics. 2013;131(4):e1082-90.
45. Reinehr T, Wabitsch M, Kleber M, De Sousa G, Denzer C, Toschke AM. Parental diabetes, pubertal stage, and extreme obesity are the main risk factors for prediabetes in children and adolescents: a simple risk score to identify children at risk for prediabetes. Pediatr Diabetes. 2009;10(6):395-400.
46. Kramer CK, Vuksan V, Choi H, Zinman B, Retnakaran R. Emerging parameters of the insulin and glucose response on the oral glucose tolerance test: reproducibility and implications for glucose homeostasis in individuals with and without diabetes. Diabetes Res Clin Pract. 2014;105(1):88-95.
47. Dedik L, Durisova M, Penesova A, Miklovicova D, Tvrdonova M. Estimation of influence of gastric emptying on shape of glucose concentration-time profile measured in oral glucose tolerance test. Diabetes Res Clin Pract. 2007;77(3):377-84.
48. Salehi M, Aulinger B, D'Alessio DA. Effect of glycemia on plasma incretins and the incretin effect during oral glucose tolerance test. Diabetes. 2012;61(11):2728-33.
49. Libman I, Barinas-Mitchell E, Bartucci A, Robertson R, Arslanian S. Reproducibility of the oral glucose tolerance test in overweight children. J Clin Endocrinol Metab. 2008;93(11):4231-7.

Chapter 4

Classification and clinical characterization of metabolically "healthy" obese children and adolescents.

In preparation for submission:

Liene Bervoets[1] and Guy Massa[1,2] (2015) **Classification and clinical characterization of metabolically "healthy" obese children and adolescents.**

[1] Faculty of Medicine and Life Sciences, Hasselt University, Hasselt, Belgium; [2] Department of Pediatrics, Jessa Hospital, Hasselt, Belgium

This study was presented orally by Liene Bervoets at the Belgian Association for the Study of Obesity Free Communications Meeting, 23rd February 2013, Brussels, Belgium

Abstract

Childhood obesity is often associated with metabolic complications such as prediabetes, insulin resistance (IR), dyslipidemia and hypertension, which may eventually lead to the development of type 2 diabetes mellitus and premature cardiovascular disease. However, it appears that some obese children do not show any of these cardiometabolic complications, and they are so-called metabolically "healthy" obese (MHO). The aim of the current study was to classify 156 obese children and adolescents as MHO or metabolically unhealthy obese (MUO) using three different definitions based on: (1) the metabolic syndrome as defined according to the pediatric IDF criteria; (2) IR as defined by HOMA-IR [=fasting glucose (mg/dl) x fasting insulin (μU/ml)/405]; (3) the combination of the previous two definitions. Subsequently, cardiometabolic features were compared between MHO and MUO children and adolescents classified according to the three proposed different definitions. Accordingly, 6 to 19% obese children and adolescents were classified as MHO. The MHO phenotype was generally characterized by a better insulin sensitivity, lower triglyceride (TG) levels, and a lower TG/HDL-C ratio compared to their MUO peers. In addition, MHO subjects showed a significantly lower prevalence of prediabetes. In conclusion, the implementation of the proposed classifications in clinical research may provide new insights into the MHO phenotype in children and adolescents. However, further research in large-scale longitudinal follow-up studies is highly recommended. Eventually, this might lead to the implementation of the concept of MHO in clinical practice that might offer new perspectives for targeted prevention and individual treatment strategies of childhood obesity and associated cardiometabolic complications.

4.1 Introduction

Although it is assumed that the prevalence of childhood obesity is stabilizing [1], the number of children being overweight and obese is still considerably high [2, 3]. Childhood obesity is often associated with metabolic complications such as prediabetes, IR, dyslipidemia and hypertension [4], which may eventually lead to the development of T2DM and premature CVD [5, 6]. Nevertheless, it appears that some obese children do not show any of these cardiometabolic complications, and they are so-called metabolically "healthy" or protected obese (MHO) [7, 8]. The classification of obese children according to their risk for cardiometabolic complications – i.e. the concept of MHO – could therefore shed new light on current prevention and treatment strategies.

MHO is mostly defined as the absence of MetS, a clustering of cardiometabolic risk factors including atherogenic dyslipidemia, hypertension, and hyperglycemia in obese individuals [9]. Although there is still no universally accepted definition for MetS in children and adolescents, it is suggested to use the consensus-based pediatric IDF criteria in an attempt to achieve uniformity [10]. However, the subdivision of obese children and adolescents in MHO and MUO according to the pediatric IDF definition may lead to an underestimation of the number of obese children and adolescents at increased risk for cardiometabolic complications because IR – a central factor leading to the abnormalities observed in MetS – is not part of the definition [11, 12]. It is known that hyperinsulinemia (i.e. greater pancreatic β-cell insulin secretory response and/or reduced insulin clearance) occurs before glucose metabolism becomes dysregulated (i.e. IGT and T2DM) [13]. In addition, fasting glucose alone often fails to detect obese individuals with prediabetes or T2DM [14]. Therefore, it can be hypothesized that the addition of IR to the pediatric MetS definition could identify more obese children and adolescents at risk for cardiometabolic complications.

One recent study in overweight and obese children and adolescents already used a combination of the MetS with IR in the definition of the MHO phenotype [8]. It was found that dietary fat intake and moderate-to-vigorous physical activity are strong predictors of insulin sensitivity and MHO phenotypes, respectively. However, they did not use the pediatric consensus-based IDF

criteria to define MHO but a self-assembled definition based on various pediatric references [8].

The aim of the current study was to classify obese children and adolescents as MHO using three different definitions based on: (1) the absence of MetS defined according to the pediatric IDF criteria; (2) the absence of IR as defined by HOMA-IR; (3) the combination of the previous two definitions. Subsequently, cardiometabolic features were compared between MHO and MUO children and adolescents classified according to the three different definitions.

4.2 Material and methods

4.2.1 Subjects

Obese children and adolescents who attended the outpatient pediatric obesity clinic from the Jessa Hospital Hasselt (Belgium) between January 2006 and December 2013 were included in this study. Patients were included when they were: (1) between 10 and 18 years of age; (2) classified as obese according to the IOTF criteria [15]; (3) not taking any medication or having any serious medical illness. The presence of parental obesity/T2DM and ethnic background were queried. Subjects of non-Flemish origin were classified as non-native. Data were collected during their first visit to the clinic and during an OGTT, and were retrieved retrospectively from the medical records. The study was conducted in accordance with the ethical rules of the Helsinki Declaration. The study protocol was approved by the Ethics Committee of the Jessa Hospital. Informed consent was obtained from all patients and their parents or legal guardian.

4.2.2 Anthropometric measurements

Subjects were measured wearing underwear only. The pubertal developmental stage was evaluated by a pediatric endocrinologist according to Tanner on the basis of breast development and genital size [16], and subjects were categorized into three groups: pre-pubertal (Tanner stage M1 or G1), pubertal (Tanner stage M2-M4 or G2-G4) and post-pubertal (Tanner stage M5 or G5). Body weight was measured with an electronic scale and rounded to the nearest 0.1 kg. Standing height was measured with a Harpenden stadiometer to the nearest 0.1 cm. BMI was calculated by dividing weight in kilograms by height in meters squared (BMI = kg/m²). BMI SDS was calculated on the basis of the LMS values using the formula: BMI SDS = $[(BMI/M)^{L}-1]/[L\times S]$ as presented by Cole and Lobstein [15]. BMI classes were defined according to age- and gender-specific IOTF centile curves passing through BMI 30 as 'class I obesity', through BMI 35 as 'class II obesity', and through BMI 40 as 'class III obesity' [15, 17]. Seated blood pressure was measured once with an electronic sphygmomanometer (Omron®, Omron Healthcare, IL, USA).

4.2.3 Biochemical analyses

After an overnight fast, venous blood samples were taken from the patients for the measurement of biochemical parameters (see below). Following the fasting blood sampling, a standard OGTT was performed using 1.75 g/kg (maximum 75 g) glucose and venous blood samples were obtained at 30, 60, 90 and 120 minutes for the determination of plasma glucose and serum insulin levels. Plasma glucose was measured by the glucose oxidase method using a Synchron LX20 analyzer (Beckman Coulter, Brea, CA, USA). Serum insulin was determined by IRI assay (ADVIA Centaur Insulin IRI; Siemens Medical Solutions Diagnostics, Tarrytown, NY, USA). Hemoglobin A1C (HbA1C) was measured using ion exchange chromatography (Menarini HA-8160 HbA1C auto-analyzer, Menarini Diagnostics, Belgium). Serum total cholesterol, HDL-C and TG were measured on a Beckman Coulter AU 2700 automatic analyzer (Brea, CA, USA). Two lipid ratios were calculated: total cholesterol divided by HDL-C, and TG divided by HDL-C. LDL-C was calculated according to the Friedewald equation [18]. Aspartate transaminase (AST), alanine transaminase (ALT), gamma glutamyl transpeptidase (g-GT) and uric acid (UA) were measured on a Beckman Coulter AU 2700 automatic analyzer (Brea, CA, USA). White blood cell (WBC) count was automatically assessed using Siemens Advia 2120 (Siemens Healthcare Diagnostics, Deerfield, IL, USA). Sex hormone-binding globulin (SHBG) concentrations were measured by immunoassay on an Architect i2000SR (Abbott Diagnostics, Ill., USA). For all blood measurements, the coefficient of variation was <5% for both inter- and intra-assay quality control.

4.2.4 Definition of glucose tolerance status

Subjects were classified as having prediabetes when they had IFG (FPG between 100 – 125 mg/dl) and/or IGT (2h plasma glucose between 140 – 199 mg/dl). T2DM was defined as having FPG ≥ 126 mg/dl and/or 2h plasma glucose ≥ 200 mg/dl, according to the Expert Committee on the Diagnosis and Classification of Diabetes Mellitus criteria [19].

4.2.5 Definition of the metabolic syndrome

MetS was defined according to the criteria of the IDF consensus for children older than 10 years [10]. Subjects were classified as having MetS when they had obesity as defined according to IOTF BMI criteria and two or more of the

following abnormalities: (1) HDL-C < 40 mg/dl (females 16 years or older: HDL-C < 50 mg/dl) (2) TG ≥ 150 mg/dl; (3) SBP ≥ 130 mm Hg or DBP ≥ 85 mm Hg; (4) FPG ≥ 100 mg/dl. BMI was used to define obesity because waist circumference was not always measured [4].

4.2.6 Definition of metabolically "healthy" obesity

We applied three classification strategies to determine the metabolic risk (MR) status, i.e. MHO and MUO. The first strategy (MR_{IDF}) is based on the definition of MetS according to the pediatric IDF criteria [10] (see above). MHO were classified as being obese but not having other components of MetS and MUO children were classified as having two or more additional MetS components. The second strategy ($MR_{HOMA\text{-}IR}$) is based on presence or absence of IR as defined by HOMA-IR [20]:

$$\text{HOMA} - \text{IR} = \frac{\text{fasting glucose } \left(\frac{\text{mg}}{\text{dl}}\right) \text{x fasting insulin } \left(\frac{\mu\text{U}}{\text{ml}}\right)}{405}$$

Subjects with HOMA-IR < 3.16 were categorized as MHO, and those with HOMA-IR ≥ 3.16 were classified as MUO. The cut-off value of 3.16 was chosen in line with previous studies in obese children and adolescents [8, 11, 21]. The final strategy was based on a combination of both classifications ($MR_{IDF/HOMA\text{-}IR}$). MHO were classified as having none of the additional MetS components and HOMA-IR < 3.16. MUO were classified as having two or more of MetS components and HOMA-IR ≥ 3.16. For the MR_{IDF} and $MR_{IDF/HOMA\text{-}IR}$ classification, there was a group that fell in-between the classification of MHO and MUO and was termed metabolically "at-risk" obese, however, this group was not included for statistical analyses.

4.2.7 Statistical analysis

Statistical analyses were implemented in IBM SPSS version 20.0 (SPSS Inc., Chicago, IL, USA). Results of continuous variables are presented as mean ± SD and nominal or ordinal scale variables are presented as a number with percentage (%). Distribution of the data was tested by the Shapiro-Wilk test. Non-normally distributed variables were log-transformed. The independent samples *t* test was used to assess differences in continuous variables between

MHO and MUO groups. Following, an analysis of covariance (ANCOVA) was performed to correct for the effect of BMI SDS, age and gender. Chi square test of association ($n \geq 10$) or Fisher exact probability test ($n < 10$) was applied to test nominal or ordinal variables between two or more groups. For 3 x 2 contingency tables with $n < 10$, the Freeman-Halton extension of the Fisher exact probability test was used. All p-values smaller than 0.05 are considered significant. To reduce the chances of obtaining false-positive results (type I errors), Bonferroni corrected p-values were applied.

4.3 Results

4.3.1 General characteristics

Data of 156 obese children and adolescents (77 boys) aged 10 to 18 (mean age: 13.6 ± 1.7 years) with a BMI ranging between 26.0 and 47.3 kg/m² were examined. The descriptive characteristics of the study population are presented in Table 4.1 along with the percentage of children having abnormal values for each individual MetS component, those having MetS, and those having IR.

Table 4.1 Descriptive characteristics of obese children and adolescents studied.

	Boys	Girls	All
Number, n (%)	77 (49.4)	79 (50.6)	156 (100.0)
Age, years	13.4 ± 1.7	13.8 ± 1.7	13.6 ± 1.7
Ethnicity, n (%)			
Native	47 (61.0)	50 (63.3)	97 (62.2)
Non-native	30 (39.0)	29 (36.7)	59 (37.8)
Anthropometric characteristics			
Pubertal stage§,*, n (%)			
Tanner stage I	20 (26.0)	0 (0.0)	20 (12.8)
Tanner stage II to IV	39 (50.6)	18 (22.8)	57 (36.5)
Tanner stage V	11 (14.3)	58 (73.4)	69 (44.2)
BMI, kg/m²	33.8 ± 4.7	34.1 ± 3.9	33.9 ± 4.3
IOTF classification, n (%)			
Class I obesity	32 (41.6)	37 (46.8)	69 (44.2)
Class II obesity	30 (38.9)	30 (37.9)	60 (38.5)
Class III obesity	15 (19.5)	12 (15.3)	27 (17.3)
BMI SDS	3.0 ± 0.4	2.9 ± 0.3	2.9 ± 0.4
Metabolic characteristics			
HDL-C, mg/dl	43 ± 8	45 ± 8	44 ± 8
Abnormal, n (%)	29 (37.7)	23 (29.1)	52 (33.3)
TG, mg/dl	116 ± 63	105 ± 65	111 ± 64
Abnormal, n (%)	19 (24.7)	9 (11.4)	28 (17.9)
SBP, mm Hg	131 ± 13	131 ± 14	131 ± 14
Abnormal, n (%)	42 (54.5)	44 (55.7)	86 (55.1)
DBP, mm Hg	77 ± 11	81 ± 9	79 ± 10
Abnormal, n (%)	14 (18.2)	27 (34.2)	41 (26.3)
Fasting glucose, mg/dl	93 ± 7	89 ± 7	91 ± 7
Abnormal, n (%)	12 (15.6)	5 (6.3)	17 (10.9)
MetS, n (%)	34 (44.2)	23 (29.1)	57 (36.5)
IGT, n (%)	12 (15.6)	14 (17.7)	26 (16.7)
Prediabetes, n (%)	22 (28.6)	18 (22.8)	40 (25.6)
Fasting insulin, µU/ml	23.1 ± 11.1	23.5 ± 11.3	23.3 ± 11.2
HOMA-IR	5.4 ± 2.7	5.2 ± 2.7	5.3 ± 2.7
Abnormal, n (%)	63 (81.8)	62 (78.5)	125 (80.1)

Results of continuous variables are presented as mean ± standard deviation (SD) and nominal or ordinal scale variables are presented as a number with percentage (%). *Significantly different between boys and girls with adjusted p-value < 0.003. §Missing data of patients (n = 10) who refused clinical examination for the determination of Tanner stage. BMI: body mass index; DBP: diastolic blood pressure; HDL-C: high density lipoprotein; HOMA-IR: homeostasis model assessment of IR; IGT: impaired glucose tolerance; IOTF: international obesity task force; MetS: metabolic syndrome; SBP: systolic blood pressure; SDS: standard deviation score; TG: triglycerides.

Of all children and adolescents, 37.8% were of non-native origin. Only pubertal status was significantly different between boys and girls (adjusted p-value < 0.003). The majority (44.2%) were postpubertal with more girls than boys (73.4% vs 14.3%) being post-pubertal. Overall, 36.5% had the MetS (obesity plus any two of the other risk factors) defined according to the pediatric IDF criteria. Most of the subjects (55.1%) were diagnosed with high SBP, followed by those with abnormal HDL-C levels (33.3%), DBP (26.3%), TG (17.9%) and fasting glucose (10.9%). Of all subjects, 25.6% suffered from prediabetes. None of the subjects was diagnosed with T2DM. Of all subjects, 125 (80.1%) had IR defined by HOMA-IR.

4.3.2 Prevalence of metabolically healthy obesity

According to the MR_{IDF} classification, 29 (18.6%) children and adolescents were classified as MHO. According to the $MR_{HOMA\text{-}IR}$ classification, 30 (19.2%) were MHO. According to the combined $MR_{IDF/HOMA\text{-}IR}$ classification, only 10 (6.4%) children and adolescents were classified as MHO.

4.3.3 Cardiometabolic profile of metabolically healthy obesity

For all three MR classifications, no differences were detected for gender, ethnicity, parental obesity or T2DM, pubertal stage, degree of obesity according to IOTF classification. As can be derived from Table 4.2, BMI SDS is higher in MUO compared to MHO subjects for all three classifications. To exclude for the additional effect of BMI SDS on the clinical variables, we performed an ANCOVA analysis with correction for BMI SDS, age and gender.

According to the MR_{IDF} definition, MHO subjects had significantly lower fasting insulin levels as well as lower HOMA-IR, lower total cholesterol/HDL-C ratio and lower TG/HDL-C ratio. UA was significantly lower in MHO subjects compared to MUO, however, when corrected for BMI SDS, the statistical significance disappeared.

According to the $MR_{HOMA\text{-}IR}$ definition, MHO subjects had significantly lower fasting and 2-h insulin levels, lower TG, lower TG/HDL-C, and higher SHBG. HDL-C and total cholesterol/HDL-C ratio were not significantly different between MHO and MUO subjects.

According to the $MR_{IDF/HOMA-IR}$ definition, MHO subjects had significantly lower fasting and 2-h insulin as well as lower total cholesterol/HDL-C ratio and lower TG/HDL-C.

According to all three MR definitions, MHO subjects had lower fasting insulin including lower HOMA-IR, lower TG and lower TG/HDL-C ratio. No significant differences were found for fasting and 2-h glucose, HbA1C, total cholesterol, LDL-C, AST, ALT, g-GT and WBC.

Table 4.2 Clinical characteristics of MHO and MUO children and adolescents classified according to MR_{IDF}, $MR_{HOMA-IR}$ and $MR_{IDF/HOMA-IR}$.

	MR_{IDF}		$MR_{HOMA-IR}$		$MR_{IDF/HOMA-IR}$	
	MHO	*MUO*	*MHO*	*MUO*	*MHO*	*MUO*
Number, n (%)	29 (18.6)	57 (36.5)	30 (19.9)	126 (80.1)	10 (6.4)	51 (32.7)
Age, years	13.4 ± 1.6	13.7 ± 1.8	13.6 ± 1.6	13.6 ± 1.7	13.9 ± 1.6	13.6 ± 1.8
Gender, n (%)						
Male	12 (41.4)	34 (59.6)	14 (46.7)	63 (50.0)	4 (40.0)	29 (56.9)
Female	17 (58.6)	23 (40.4)	16 (53.3)	63 (50.0)	6 (60.0)	22 (43.1)
BMI, kg/m²	32.4 ± 3.1	35.0 ± 5.1	32.8 ± 3.8	34.2 ± 4.4	32.1 ± 3.4	35.2 ± 5.3
BMI SDS	2.8 ± 0.3	3.0 ± 0.4	2.8 ± 0.4	3.0 ± 0.4	2.7 ± 0.4	3.1 ± 0.4
SBP, mm Hg	118 ± 7*†	135 ± 14	128 ± 12	132 ± 14	118 ± 8*	135 ± 15
DBP, mm Hg	72 ± 8*†	81 ± 11	74 ± 10*	80 ± 10	71 ± 10	82 ± 10
FPG, mg/dl	90 ± 5	93 ± 9	88 ± 6	92 ± 7	90 ± 4	94 ± 9
2-hour glucose, mg/dl	110 ± 23	119 ± 24	110 ± 25	120 ± 24	110 ± 30	122 ± 24
HbA1C, %	5.4 ± 0.2	5.5 ± 0.3	5.3 ± 0.3	5.4 ± 0.2	5.3 ± 0.3	5.5 ± 0.2
Fasting insulin, µU/ml	**16.7 ± 9.3*†**	**27.1 ± 11.0**	**10.6 ± 2.8*†**	**26.5 ± 10.2**	**9.8 ± 2.5*†**	**29.1 ± 9.9**
2-hour insulin, µU/ml	88.2 ± 72.3	133.5 ± 118.0	55.2 ± 31.6*†	137.3 ± 115.7	49.7 ± 23.8*†	143.3 ± 120.6
HOMA-IR	**3.7 ± 2.3*†**	**6.3 ± 2.7**	**2.3 ± 0.6*†**	**6.0 ± 2.5**	**2.2 ± 0.6*†**	**6.8 ± 2.5**
Total cholesterol, mg/dl	152 ± 32	161 ± 33	155 ± 35	161 ± 31	158 ± 32	166 ± 31
HDL-C, mg/dl	49 ± 8*†	39 ± 6	47 ± 10	43 ± 8	50 ± 9*†	39 ± 6
Total cholesterol/HDL-C ratio, mg/dl	3.1 ± 0.6*†	4.2 ± 0.9	3.4 ± 0.6	3.8 ± 0.9	3.2 ± 0.6*†	4.3 ± 0.9
LDL-C, mg/dl	91 ± 32	100 ± 25	97 ± 30	100 ± 27	99 ± 34	102 ± 25
TG, mg/dl	**75 ± 30*†**	**143 ± 85**	**77 ± 37*†**	**119 ± 67**	**63 ± 18*†**	**152 ± 84**
TG/HDL-C ratio, mg/dl	**1.6 ± 0.7*†**	**3.8 ± 2.4**	**1.7 ± 1.2*†**	**2.9 ± 1.9**	**1.3 ± 0.5*†**	**4.0 ± 2.4**
AST, U/l	26 ± 14	29 ± 13	25 ± 9	27 ± 12	22 ± 5	29 ± 13
ALT, U/l	27 ± 31	35 ± 29	24 ± 12	31 ± 26	19 ± 6	36 ± 31
g-GT, U/l	19 ± 13	25 ± 16	16 ± 8	23 ± 14	16 ± 4	26 ± 17
UA, mg/dl	5.6 ± 1.2*	6.7 ± 1.5	5.5 ± 1.0	6.2 ± 1.4	5.5 ± 0.7	6.7 ± 1.5
WBC count, 10^9/l	7.2 ± 1.6	7.2 ± 1.9	6.5 ± 2.0	7.2 ± 2.0	7.0 ± 1.5	7.4 ± 2.0
SHBG, nmol/l	30 ± 13	22 ± 10	37 ± 18*†	25 ± 13	35 ± 13	22 ± 10

Results of continuous variables are presented as mean ± SD and nominal or ordinal scale variables are presented as a number with percentage (%). *Significantly different between MHO and MUO according to the independent samples t test (adjusted p-value < 0.002). †Significantly different between MHO and MUO according to analysis of covariance (ANCOVA) with correction for BMI SDS, age and gender (adjusted p-value < 0.002). ** Significantly different between MHO and MUO according to the Chi² test (adjusted p-value < 0.002). ALT: alanine transaminase; AST: aspartate transaminase; BMI: body mass index; DBP: diastolic blood pressure; FPG: fasting plasma glucose; g-GT: gamma glutamyl transpeptidase; HbA1C: hemoglobin A1C; HDL-C: high density lipoprotein; HOMA-IR: homeostasis model assessment of IR; IGT: impaired glucose tolerance; LDL-C: low-density lipoprotein cholesterol; MetS: metabolic syndrome; SBP: systolic blood pressure; SDS: standard deviation score; SHBG: sex-hormone binding globulin; TG: triglycerides; UA: uric acid; WBC: white blood cell.

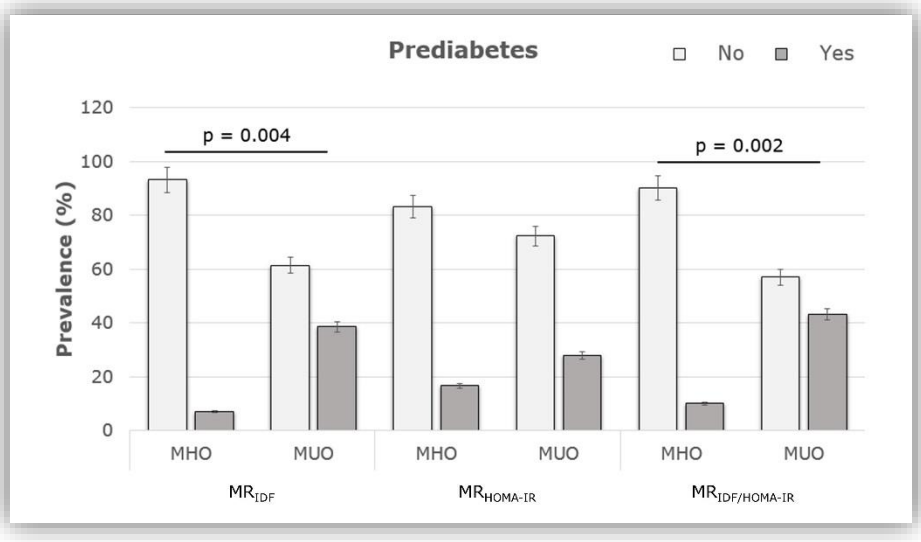

Figure 4.1 Prevalence rates of prediabetes (IFG and/or IGT) among MHO and MUO classified according to MR_{IDF}, $MR_{HOMA-IR}$ and $MR_{IDF/HOMA-IR}$.

The number of MHO subjects classified according to MR_{IDF} and $MR_{IDF/HOMA-IR}$ without prediabetes (93.1% and 90.0%, respectively) was significantly higher than those with prediabetes (6.9% and 10.0%, respectively) (Figure 4.1).

Of all MHO subjects classified according to $MR_{HOMA-IR}$, 6 (20.0%) had MetS and 10 (33.3%) had no MetS (p = 0.033).

4.4 Discussion

To the best of our knowledge, we here demonstrate for the first time a comprehensive clinical and metabolic analysis of MHO and MUO children and adolescents classified according to criteria of MetS as defined by pediatric IDF criteria and/or IR as defined by HOMA-IR. In this study, 6 to 19% obese children and adolescents were classified as MHO. The MHO phenotype was characterized by a better insulin sensitivity, lower TG, and lower TG/HDL-C ratio compared to their MUO peers. Moreover, MHO subjects showed a significantly lower prevalence of prediabetes.

The prevalence rates of MHO in children and adolescents greatly vary due to the application of different classification systems. In previous reports, the prevalence of MHO children and adolescents was estimated to be between 4 to 36% [7, 8, 22-24]. The use of different classification strategies makes it difficult to compare prevalence rates but also clinical findings between studies. In an attempt to harmonize the classification criteria to identify MHO children and adolescents, we here present a classification strategy on the basis of MetS as defined by the pediatric consensus-based IDF criteria, and IR as defined by HOMA-IR [10, 21]. The major advantages of using these specific definitions is that they are widely used in obese youth, they are based on fasting values, and have proven to be reliable and valid to apply in a population of obese children and adolescents [10, 21].

MUO children and adolescents had higher BMI SDS values compared to MHO, which is a frequently observed characteristic [7, 8]. However, it has previously been shown that the MUO phenotype also occurs in normal-weight individuals and that a higher degree of obesity in children and adolescents is not always associated with a higher prevalence of prediabetes and/or the metabolic syndrome [17, 25]. In this study, we therefore corrected for the influence of BMI SDS on the clinical and metabolic parameters.

Although the IDF definition includes fasting glucose greater than or equal to 100 mg/dl as a component of MetS, it appears that this parameter contributes least to the diagnosis of MetS and IR in obese youth [26]. Interestingly, although the MR_{IDF} and $MR_{IDF/HOMA\text{-}IR}$ definition were unable to discriminate between MHO and MUO on the basis of fasting and 2-h glucose, the prevalence of prediabetes was significantly lower in MHO according to both definitions. This

finding was not observed for the $MR_{HOMA-IR}$ definition. Overall, fasting insulin levels were significantly lower in the MHO compared to MUO subjects according to all definitions. This might indicate that fasting insulin is more important than fasting glucose in the detection of obese children and adolescents at increased risk for cardiometabolic disorders.

In line with previous research [8], we found significantly lower levels of TGs and TG/HDL-C ratio in the MHO compared to MUO group. In addition, HDL-C levels were significantly higher in the MHO group, but only for the MR_{IDF} and $MR_{IDF/HOMA-IR}$ definitions. The TG/HDL-C ratio is suggested to be an indicator of IR and early dysglycemia in obese youth [27], and a predictor of atherosclerosis and CVD [28-30]. Hence, the finding of a lower TG/HDL-C ratio in the MHO group may point towards the significance of the MR classification as an early indicator of IR and a predictor of T2DM and CVD.

According to the $MR_{HOMA-IR}$ classification, SHBG levels were significantly higher in MHO compared to MUO children and adolescents. SHBG is a specific steroid-binding plasma glycoprotein, and is mainly produced in the liver [31]. Its main function is to transport sex steroids, but it has potential insulin sensitizing effects independent of its transport function [32]. In children and adolescents, it has already been reported that reduced levels of SHBG are related to IR and alterations in the components of MetS [33, 34]. In this study, however, SHBG was not significantly different between MHO and MUO classified according to MR_{IDF} and $MR_{IDF/HOMA-IR}$. Hence, high SHBG levels might only be a reflection of low fasting insulin levels. Indeed, after correction for fasting insulin, SHBG levels were not significantly different anymore between MHO and MUO classified according to the $MR_{HOMA-IR}$ classification.

One major limitation of the current study is its retrospective cross-sectional design whereby potentially important data (e.g. waist circumference, physical fitness, diet, psychosocial factors, adipokine profile, gut microbiome, metabolome, etc.) were lacking and findings were obtained at one specific point in time. To overcome this gap, we recommend to perform longitudinal prospective studies including these important parameters in future. In this way, a more comprehensive overview of the MHO phenotype can be obtained and the risk for future T2DM and CVD may be predicted. A second important aspect to mention is that, although not included for statistical analysis, a metabolically

'intermediate'/'at risk' phenotype that fell in-between the MHO and MUO phenotypes defined according to MR_{IDF} and $MR_{IDF/HOMA-IR}$ definition was present. It still remains uncertain whether and how fast a MHO child can develop into 'at risk' and consequently MUO, or vice versa. It was previously shown that individuals who maintain MHO show a significantly lower risk to develop T2DM and CVD [35]. So if the metabolic risk status in obese children is reversal, a focused and intensive intervention could be useful in managing obese children with MUO.

In conclusion, the implementation of the proposed classifications in clinical research may provide new insights into the MHO phenotype in children and adolescents. It remains to be determined which classification has the highest ability to predict future T2DM and CVD. It is suggested to perform large-scale longitudinal follow-up studies to provide a more comprehensive overview of the MHO phenotype and to monitor the development of the MHO state. In future, the implementation of the concept of MHO in clinical practice might offer new perspectives for targeted prevention and individual treatment strategies of childhood obesity and associated cardiometabolic complications.

References

1. Olds T, Maher C, Zumin S, Péneau S, Lioret S, Castetbon K, et al. Evidence that the prevalence of childhood overweight is plateauing: data from nine countries. Int J Pediatr Obes. 2011;6(5-6):342-60.
2. Pigeot I, Barba G, Chadjigeorgiou C, De Henauw S, Kourides Y, Lissner L, et al. Prevalence and determinants of childhood overweight and obesity in European countries: pooled analysis of the existing surveys within the IDEFICS Consortium. Int J Obes. 2009;33(10):1103-10.
3. Skinner AC, Skelton JA. Prevalence and trends in obesity and severe obesity among children in the United States, 1999-2012. JAMA Pediatr. 2014;168(6):561-6.
4. Weiss R, Kaufman FR. Metabolic complications of childhood obesity: identifying and mitigating the risk. Diabetes Care. 2008;31 (Suppl 2):S310-6.
5. Wiegand S, Maikowski U, Blankenstein O, Biebermann H, Tarnow P, Gruters A. Type 2 diabetes and impaired glucose tolerance in European children and adolescents with obesity - a problem that is no longer restricted to minority groups. Eur J Endocrinol. 2004;151(2):199-206.
6. Franks PW, Hanson RL, Knowler WC, Sievers ML, Bennett PH, Looker HC. Childhood obesity, other cardiovascular risk factors, and premature death. N Engl J Med. 2010;362(6):485-93.
7. Mangge H, Zelzer S, Puerstner P, Schnedl WJ, Reeves G, Postolache TT, et al. Uric acid best predicts metabolically unhealthy obesity with increased cardiovascular risk in youth and adults. Obesity. 2013;21(1):E71-7.
8. Prince RL, Kuk JL, Ambler KA, Dhaliwal J, Ball GD. Predictors of metabolically healthy obesity in children. Diabetes Care. 2014;37(5):1462-8.
9. Blüher M. Are metabolically healthy obese individuals really healthy? Eur J Endocrinol. 2014;171(6):R209-19.
10. Zimmet P, Alberti K, George MM, Kaufman F, Tajima N, Silink M, et al. The metabolic sydrome in children and adolescents - an IDF consensus report. Pediatr Diabetes. 2007;8:299-306.
11. Kurtoglu S, Akin L, Kendirci M, Hatipoglu N, Elmali F, Mazicioglu M. The absence of insulin resistance in metabolic syndrome definition leads to underdiagnosing of metabolic risk in obese patients. Eur J Pediatr. 2012;171(9):1331-7.
12. Steinberger J, Kelly AS. Obesity, metabolic syndrome and type 2 diabetes. In: da Cruz EM, Ivy D, Jaggers J, editors. Pediatric and congenital cardiology, cardiac surgery and intensive care. Denver: Springer London; 2014. p. 499-507.
13. Cali AMG, Dalla Man C, Cobelli C, Dziura J, Seyal A, Shaw M, et al. Primary defects in beta-cell function further exacerbated by worsening of insulin resistance mark the development of impaired glucose tolerance in obese adolescents. Diabetes Care. 2009;32(3):456-61.
14. Eriksson J, Jousilahti P, Lindström J, Qiao Q, Tuomilehto J, Group DS. Is fasting glucose sufficient to define diabetes? Epidemiological data from 20 European studies. Diabetologia. 1999;42:647-54.
15. Cole T, Lobstein T. Extended international (IOTF) body mass index cut-offs for thinness, overweight and obesity. Pediatr Obes. 2012;7(4):284-94.
16. Tanner J. Normal growth and techniques of growth assessment. Clin Endocrinol Metab. 1986;15(3):411-51.
17. Bervoets L, Massa G. Defining morbid obesity in children based on BMI 40 at age 18 using the extended international (IOTF) cut-offs. Pediatr Obes. 2014;9(5):e94-8.
18. Friedewald WT, Levy RI, Fredrickson DS. Estimation of the concentration of low-density lipoprotein cholesterol in plasma, without use of the preparative ultracentrifuge. Clin Chem. 1972;18(6):499-502.
19. American Diabetes Association. Diagnosis and classification of diabetes mellitus. Diabetes Care. 2014;37:S81-90.

20. Matthews DR, Hosker JP, Rudenski AS, Naylor BA, Treacher DF, Turner RF. Homeostasis model assessment: insulin resistance and β-cell function from fasting plasma glucose and insulin concentrations in man. Diabetologia. 1985;28(7):412-9.
21. Keskin M, Kurtoglu S, Kendirci M, Atabek ME, Yazici C. Homeostasis model assessment is more reliable than the fasting glucose/insulin ratio and quantitative insulin sensitivity check index for assessing insulin resistance among obese children and adolescents. Pediatrics. 2005;115:500-3.
22. Li S, Chen W, Srinivasan SR, Xu J, Berenson GS. Relation of childhood obesity/cardiometabolic phenotypes to adult cardiometabolic profile the Bogalusa Heart study. Am J Epidemiol. 2012;176(Suppl 7):S142-9.
23. Vukovic R, Mitrovic K, Milenkovic T, Todorovic S, Soldatovic I, Sipetic-Grujicic S, et al. Insulin-sensitive obese children display a favorable metabolic profile. Eur J Pediatr. 2013;172(2):201-6.
24. Weghuber D, Zelzer S, Stelzer I, Paulmichl K, Kammerhofer D, Schnedl W, et al. High risk vs. "metabolically healthy" phenotype in juvenile obesity-neck subcutaneous adipose tissue and serum uric acid are clinically relevant. Exp Clin Endocrinol Diabetes. 2013;121(7):384-90.
25. Dvorak RV, DeNino WF, Ades PA, Poehlman ET. Phenotypic characteristics associated with insulin resistance in metabolically obese but normal-weight young women. Diabetes. 1999;48(11):2210-4.
26. Weiss R, Dziura J, Burgert TS, Tamborlane WV, Taksali SE, Yeckel CW, et al. Obesity and the metabolic syndrome in children and adolescents. N Engl J Med. 2004;350(23):2362-74.
27. Giannini C, Santoro N, Caprio S, Kim G, Lartaud D, Shaw M, et al. The triglyceride-to-HDL cholesterol ratio: association with insulin resistance in obese youths of different ethnic backgrounds. Diabetes Care. 2011;34(8):1869-74.
28. Quijada Z, Paoli M, Zerpa Y, Camacho N, Cichetti R, Villarroel V, et al. The triglyceride/HDL-cholesterol ratio as a marker of cardiovascular risk in obese children; association with traditional and emergent risk factors. Pediatr Diabetes. 2008;9(5):464-71.
29. Weiss R, Otvos JD, Sinnreich R, Miserez AR, Kark JD. The triglyceride to high-density lipoprotein–cholesterol ratio in adolescence and subsequent weight gain predict nuclear magnetic resonance–measured lipoprotein subclasses in adulthood. J Pediatr. 2011;158(1):44-50.
30. Urbina EM, Khoury PR, McCoy CE, Dolan LM, Daniels SR, Kimball TR. Triglyceride to HDL-C ratio and increased arterial stiffness in children, adolescents, and young adults. Pediatrics. 2013;131(4):e1082-90.
31. Rosner W. The functions of corticosteroid-binding globulin and sex hormone-binding globulin: recent advances. Endocr Rev. 1990;11(1):80-91.
32. Peter A, Kantartzis K, Machann J, Schick F, Staiger H, Machicao F, et al. Relationships of circulating sex hormone–binding globulin with metabolic traits in humans. Diabetes. 2010;59(12):3167-73.
33. Gascon F, Valle M, Martos R, Ruz FJ, Rios R, Montilla P, et al. Sex hormone-binding globulin as a marker for hyperinsulinemia and/or insulin resistance in obese children. Eur J Endocrinol. 2000;143(1):85-9.
34. De Oya I, Schoppen S, Lasunción MA, Lopez-Simon L, Riestra P, De Oya M, et al. Sex hormone-binding globulin levels and metabolic syndrome and its features in adolescents. Pediatr Diabetes. 2010;11(3):188-94.
35. Appleton SL, Seaborn CJ, Visvanathan R, Hill CL, Gill TK, Taylor AW, et al. Diabetes and cardiovascular disease outcomes in the metabolically healthy obese phenotype: a cohort study. Diabetes Care. 2013;36(8):2388-94.

Chapter 5

NMR-based metabolomics: development of a robust protocol to accurately assign metabolites in the ^{1}H-NMR spectrum of plasma and urine

The metabolite spiking part is related to the following study:

Evelyne Louis[1*], Liene Bervoets[1*], Gunter Reekmans[2], Eric De Jonge[3], Liesbet Mesotten[1,4], Michiel Thomeer[1,5], Peter Adriaensens[2] (2015) **Phenotyping human blood plasma by ^{1}H-NMR: a robust protocol based on metabolite spiking and its evaluation in breast cancer.** *Metabolomics* 11(1): 225-236

*These authors contributed equally to this work

[1]Faculty of Medicine and Life Sciences, Hasselt University, Hasselt, Belgium; [2]Institute for Materials Research, Hasselt University, Hasselt, Belgium; [3]Department of Gynecology, Ziekenhuis Oost-Limburg, Genk, Belgium; [4]Department of Nuclear Medicine, Ziekenhuis Oost-Limburg, Genk, Belgium; [5]Department of Respiratory Medicine, Ziekenhuis Oost-Limburg, Genk, Belgium; [6]University Biobank Limburg and Laboratory of Experimental Hematology, Jessa Hospital, 3500 Hasselt, Belgium

A part of this study was presented as a poster by Liene Bervoets at the 9th Annual Conference of the Metabolomics Society, 1th – 4th July 2013, Glasgow, United Kingdom

Abstract

This study reports an accurate assignment of the resonance signals present in ^{1}H-NMR spectra of human plasma and urine. Hereto, plasma and urine were spiked with respectively 32 and 27 different metabolites in relevant concentrations since reported chemical shift values show quite some variability depending on the biofluid under study and the applied experimental measuring conditions. The resulting information was used to rationally divide the plasma and urine ^{1}H-NMR spectrum in respectively 110 and 134 well-defined integration regions for application in metabolomics. For plasma, a case-control dataset of 43 obese children and 25 normal-weight children was investigated in order to demonstrate the proof of principle. For urine, a case-control dataset of 32 obese children and 24 normal-weight children was investigated. After removal of noisy variables, i.e. variables exceeding a premised threshold for the coefficient of variation, the groups could be discriminated by OPLS-DA multivariate statistics with a sensitivity and specificity of respectively 100% and 96% for plasma and 97% and 83% for urine. In addition, the classification was validated in small but independent cohorts consisting of 22 obese and 12 normal-weight children for the plasma study, and 16 obese and 13 normal-weight children for the urine study. The proposed methodology might pave the way towards a better understanding of disturbances in disease-related biochemical pathways and so, to the clinical relevance of study findings.

5.1 Introduction

The widespread use of the ^{1}H-NMR technique along with its exceptional capacity to handle complex mixtures made it the preferred technology for launching the field of metabolomics [1, 2]. While other techniques such as gas chromatography (GC)- and liquid chromatography (LC)-MS are also increasingly being used in metabolomics, ^{1}H-NMR spectroscopy has still a number of unique advantages. In particular, it is non-invasive, non-biased and easily quantifiable, needs no chemical derivatization, requires little or no sample preparation and permits the identification of novel compounds [3]. However, there is still room for scientific improvement as the accurate interpretation of ^{1}H-NMR spectra in terms of metabolite identities and abundances can be challenging, in particular in crowded regions with severe signal overlap [4, 5].

In current practice, signal assignment often relies on chemical shift values reported for different matrices or even non-human specimens [6-8]. Additionally, most chemical shifts are dependent of the applied experimental measuring conditions such as temperature, ion content, pH and concentration [9-11]. Further room for improvement can also be found in the assignment of noisy variables, which can be defined as signals showing unpredictable variation in intensity from moment to moment and under identical experimental conditions [11]. The identification and removal of these noisy variables should be optimized in order not to complicate the multivariate data analysis [12].

In this study, the identification of the resonance signals observed in ^{1}H-NMR spectra of human blood plasma and urine on the basis of spiking the plasma and urine with respectively 32 and 27 different metabolites is described. The proposed methodology offers a guidance to divide the plasma and urine ^{1}H-NMR spectrum rationally in well-defined integration regions, being the variables for the multivariate data analysis, and will contribute to a better understanding of the (disturbed) biochemical pathways involved in the disease under study. In order to evaluate the proposed analysis platform, it was applied to classify a case-control dataset consisting of obese and normal-weight children and it was validated in small but independent cohorts. In addition, noisy variables were identified and their influence on group differentiation is reported.

5.2 Material and methods

5.2.1 Ethical statement

The study was conducted in accordance with the ethical rules of the Helsinki Declaration and of Good Clinical Practice. The study protocol was approved by the Medical Ethics Committees of Jessa Hospital (Virga Jesse Campus, Hasselt, Belgium), Ziekenhuis Oost-Limburg (Campus Sint-Jan, Genk, Belgium) and Hasselt University (Campus Diepenbeek, Hasselt, Belgium). Informed consent was obtained from all participants prior to their inclusion in the study.

5.2.2 Sample collection, preparation and storage

Plasma

Fasting venous blood was collected (BD Vacutainer® LH 17 I.U. 10 ml tube) and stored at 4°C within 5 to 10 min. Within 30 min after blood collection, blood samples were transported on crushed ice and centrifuged at 1600 g for 15 min at room temperature (RT) (swinging bucket centrifuge, Jouan GR 422). Subsequently, plasma aliquots of 500 µl were transferred into sterile cryovials and immediately stored at -80°C until NMR analysis within six months. Prior to NMR analysis, plasma aliquots were thawed at room temperature, immediately followed by centrifugation at 13000 g for 4 min at 4°C (fixed rotor Eppendorf centrifuge 5415 R, Hamburg, Germany). Next, 200 µl plasma was added to 600 µl deuterium oxide (D_2O, 99.9%, Cambridge Isotope Laboratories Inc., Andover, USA) containing 0.3 µg/µl trimethylsilyl-2,2,3,3-tetradeuteropropionic acid (TSP, 98%, Cambridge Isotope Laboratories Inc., Andover, USA) as a chemical shift reference [13].

For spiking experiments, fasting venous blood from a healthy 44-year-old female was collected and prepared as described above, and further referred to as 'reference plasma'. NMR stock solutions for spiking were prepared by dissolving relevant amounts (~1 mg) of a known metabolite in 100 µl reference plasma. In a next step, 10 µl stock solution was added to 200 µl reference plasma and 600 µl D_2O containing TSP. This procedure was repeated for all 32 plasma metabolites. For the case-control and validation study, fasting venous blood from 65 overweight or obese (OB) and 37 normal-weight (NW) children were collected and prepared as described above in the first paragraph.

Urine

Fasting midstream urine was collected (120 mL BD Vacutainer® plastic urine collection cup) and stored immediately at 4°C. Within 1 h after urine collection, urine was transferred into sterile falcon tubes of 35 ml and immediately stored at -80°C until NMR analysis within six months. Prior to NMR analysis, urine was thawed at room temperature, immediately followed by centrifugation at 200 g for 5 min at RT. The pH of urine was adjusted to 7.40 ± 0.05 with NaOH or HCl, and aliquots of 1200 µl were centrifuged at 13000 g for 4 min at 4°C (fixed rotor Eppendorf centrifuge 5415 R, Hamburg, Germany). Next, 200 µl urine was added to 600 µl deuterium oxide (D_2O, 99.9%, Cambridge Isotope Laboratories Inc., Andover, USA) containing 0.3 µg/µl trimethylsilyl-2,2,3,3-tetradeuteropropionic acid (TSP, 98%, Cambridge Isotope Laboratories Inc., Andover, USA) as a chemical shift reference [13].

For spiking experiments, fasting midstream urine from a healthy 27-year-old female was collected and prepared as described above, and further referred to as 'reference' urine. NMR stock solutions for spiking were prepared by dissolving relevant amounts (~1 mg) of a known metabolite in 1000 µl reference urine. Next, 200 µl of the stock solution was added to 600 µl D_2O containing TSP. This procedure was repeated for the 27 metabolites.

For the case-control and validation study, fasting midstream urine from 48 OB and 37 NW children were collected and prepared as described above in the first paragraph.

5.2.3 ^{1}H-NMR analysis

Plasma and urine samples were placed on ice until ^{1}H-NMR analysis. Before ^{1}H-NMR analysis, plasma and urine samples were mixed and transferred into a 5 mm NMR tube (Wilmad-LabGlass, New Jersey, USA) and acclimatized at RT for 7 min. To account for experimental variability, samples were measured in a random order. The ^{1}H-NMR spectra were recorded with 96 scans (acquisition time of 7'44") at 21.2°C on a 400 MHz Varian Inova NMR spectrometer (Agilent Technologies Inc., Santa Clara, CA, USA) having a magnetic field strength of 9.4 Tesla. Slightly T_2-weighted spectra were acquired using the CPMG pulse sequence to attenuate signals of macromolecules such as proteins and polysaccharides (total length of CPMG used: 32 ms; interpulse delay: 0.1 ms), preceded by an initial delay of 0.5

s, followed by 3 s presaturation for water suppression in order to allow optimal detection and quantification of the signals close to the water resonance (total relaxation delay of 3.5 s), 6000 Hz spectral width, an acquisition time of 1.1 s and 13 K complex data points. Each FID was zero-filled to 65 K points and multiplied by a 0.7 Hz exponential line-broadening function prior to Fourier transformation.

5.2.4 Spectral processing

Spectra were phased manually, baseline corrected and referenced to the trimethylsilyl resonance of TSP at 0.015 ppm. Plasma and urine spectra were divided into respectively 110 and 134 fixed variable-sized integration regions defined on the basis of the metabolite spiking results. Thereafter, the signals of water (5.2 to 4.7 ppm for plasma and 5.1 to 4.6 ppm for urine) and TSP (0.3 to -0.3 ppm) were removed. Two sections of the ^{1}H-NMR spectrum (4.6 to 4.8 ppm and 3.7 to 3.85 ppm for plasma, and 7.0 to 8.0 ppm and 2.7 to 2.9 ppm for urine) were double checked in order to see whether the peaks located in these sections of the ^{1}H-NMR spectrum are situated under the defined integrals. For plasma, the integration values (area under the peaks) of the 110 spectral regions were normalized relatively to the sum of all integration values. For urine, the integration values of the 134 spectral regions were normalized relatively to the sum of all integration values, except for those that contain high-intensity resonances, i.e. the following variables (VAR_{UR}): 35, 43, 54, 56, 59, 60, 88, 116, 134 (see Table 5.3 for information on metabolite assignments). This resulted in 110 plasma variables (VAR_{PL}) and 134 urine variables (VAR_{UR}) for statistics.

5.2.5 Identification of noisy variables

In order to identify noisy variables, the following three series of ^{1}H-NMR experiments were performed by using three aliquots of the reference plasma and urine as well as three plasma and urine aliquots originating from an obese child: (1) series A: five consecutive measurements on a sample prepared from a first aliquot (after initial spectrometer conditioning, i.e. locking, shimming and optimization of water suppression); (2) series B: five similar measurements at another time point using a second aliquot and (3) series C: five measurements using a third aliquot but with full spectrometer conditioning before each acquisition, i.e. sample insertion, locking, shimming and optimization of water

suppression. For each series of acquisitions, the data analysis was accomplished by three independent researchers familiar with ^{1}H-NMR metabolomics. This results, for each of the series, in 15 normalized integration values for all variables for which the mean, SD and percentage error (%error = (SD/mean)*100) were calculated. For each of the three series, all variables were subsequently divided into three groups on the basis of their mean normalized integration value. Next, the % error values of each variable were plotted per group for each of the three series. Based on these plots, visually supported thresholds could be defined for the coefficients of variation (CVs in %). If a variable exceeded the predefined threshold in at least two of the three series it was assigned as 'noisy'. A variable for which the CV was higher than the threshold in only one of the series was classified as noisy only if the variation was not the result of a single outlier. Remark that these threshold settings might be dependent on the NMR set-up, and consequently can be even lower for higher magnetic field strengths or when cryo-probes are used.

Application of the analysis procedure in a case–control training study

In order to evaluate the analysis procedure, a multivariate statistical analysis was performed on a case–control dataset consisting of OB and NW children. All study participants were measured wearing underwear only. Standing height was measured to the nearest 0.1 cm using a Harpenden wall stadiometer, and weight was measured to the nearest 0.1 kg using an electronic balance scale. BMI was calculated by dividing weight in kilograms by height in meters squared (BMI = kg/m^2). Children were classified as being overweight or obese (OB) if their BMI exceeded the age- and gender-specific cut off values of BMI 25 at age 18 according to the International Obesity Task Force (IOTF) criteria developed by Cole et al. [22]. Children with a BMI between the age- and gender-specific IOTF cut off values of BMI 18.5 and 25 at age 18 were classified as normal-weight (NW).

The case-control training set for the plasma study existed out of 43 OB and 25 NW children (see Table 5.4 for descriptives of the study population), and the training set for the urine study existed out of 32 OB and 24 NW children (see Table 5.5 for descriptives of the study population).

The influence of noisy variables on the classification of both plasma and urine training cohorts was evaluated by constructing OPLS-DA classifiers with the remaining "non-noisy" variables (see below). The model performance was evaluated for all OPLS-DA classifiers built. The threshold for the CV, and consequently the definition of noisy variables, was determined on the basis of the OPLS-DA classifier with the best model performance.

Application of the analysis procedure in a validation study

The predictive accuracy of both plasma and urine training studies was evaluated by classifying an independent validation cohort. The validation cohort of the plasma study was composed of 22 OB and 12 NW children (see Table 5.4 for descriptives of the study population), and the validation cohort of the urine study existed out of 16 OB and 13 NW children (see Table 5.5 for descriptives of the study population).

5.2.6 Multivariate statistical analysis

All multivariate statistical analyses were performed using SIMCA-P^{+} (Version 13.0, Umetrics, Umea, Sweden). All plasma and urine variables were mean-centered and scaled. Plasma variables were Pareto scaled (weighted by 1/√SD of the mean-centered value), i.e. less weight is assigned to high-intensity signals (e.g. those of glucose or lipids) compared to low-intensity signals, so that the high-intensity signals are less dominant [12]. Urine variables were scaled unit variance (UV) (weighted by 1/SD of the mean-centered value), i.e. equal weight is assigned to all variables as the contribution of high-intensity signals is already minimized by the normalization procedure (see previously) [12]. Unsupervised principal component analyses (PCA) were performed to identify intrinsic clusters, confounding variables and statistical outliers within the case-control dataset. The variance structure of the data in the PCA score plot is explained through linear combinations of the VARs, i.e. PCs. The first PC explains the largest variance within the dataset, followed by the second and third PCs. Outliers that were detected in the PCA score plot (i.e. observations that lie outside the 95% CI), Hotelling's T2 range plot (i.e. observations with a T^2 value larger than the 95% CI) and DModX (i.e. observations with a DModX twice as large as the critical value of DModX), were rejected from the model and a new PCA model was built.

Orthogonal partial least squares discriminant analysis (OPLS-DA) was used to build models (statistical classifiers) to discriminate between patients and controls using a) all plasma or urine variables and b) without the noisy variables for plasma or urine. The OPLS-DA model performance was evaluated on the basis of the explained variation denoted as R^2 ranges from 0 (no explanation) to 1 (complete explanation), and reveals how variables are explained by the model (i.e. goodness-of-fit). $R^2X(cum)$ describes the predictive and orthogonal variation in X that is explained by the model. $R^2Y(cum)$ describes the cumulative variation in Y explained by the model. $Q^2(cum)$ reflects the goodness of prediction calculated by full cross-validation. A $Q^2(cum)$ of 50% or higher describes a strong model. The levels of sensitivity (the percentage of patients that are actually classified as patients) and specificity (the percentage of controls that are actually classified as controls) were also calculated (For more information on multivariate projection methods see Annex Chapter 1, p.53).

5.3 Results and discussion

5.3.1 ^{1}H-NMR chemical shift assignment of plasma and urine metabolites via spiking experiments

Reported chemical shift values of metabolites show quite some variability depending on the biofluid under study and the experimental measuring conditions employed (e.g. temperature, pH, ion strength and concentration) [9-11]. To minimize these uncertainties in order to define a rational setting of the integration regions in NMR spectra, the metabolite chemical shifts have to be critically determined by spiking the biofluid with known metabolites in relevant concentrations (see Figure 5.1 as an example).

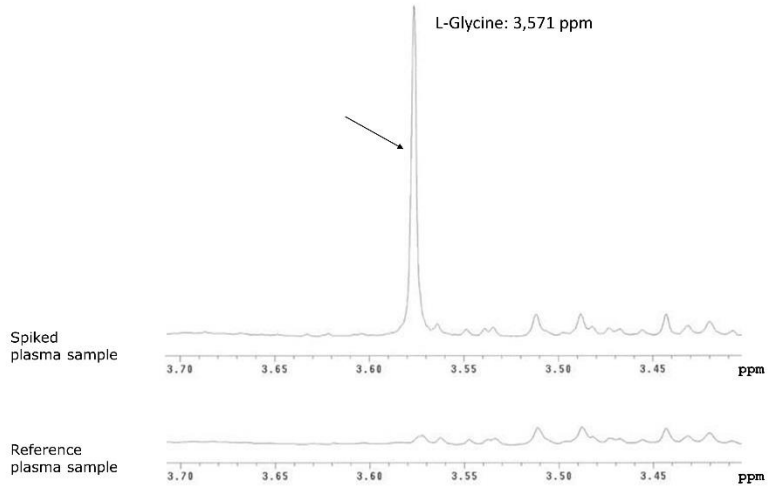

Figure 5.1 An example of spiking human blood plasma with L-glycine.

Although spiking is a commonly used analytical method to accurately identify chemical shifts in a ^{1}H-NMR spectrum [4, 14], the assignment of metabolite signals is often still based on existing literature and databases [6, 7, 15, 16].

Table 5.1 presents the ^{1}H-NMR chemical shift values and J-coupling patterns of plasma and urine metabolites as determined via spiking the respective biofluid with known metabolites. The atom numbering of the metabolites follows the International Union of Pure and Applied Chemistry – International Union of Biochemistry (IUPAC-IUB) nomenclature, unless otherwise indicated in the structures included in Table 5.1. For the determination of the chemical shift values

and J-coupling patterns, 32 aliquots of a reference plasma pool and 27 aliquots of a reference urine pool, all derived from healthy volunteers, were spiked with respectively 32 and 27 known metabolites.

Table 5.1 ^{1}H-NMR chemical shifts (δ in ppm) of low molecular weight plasma and urine metabolites and their J-coupling constants (in Hz).

Metabolite	Proton	δ (ppm)	Multiplicity	J (Hz)	Connectivity
Amino acids					
L-Alanine (Ala)[b]	$^{\alpha}CH$	3.790	q	7.2	α-β
(CHEBI:57972)	$^{\beta}CH_3$	1.509	d	7.2	β-α
L-Arginine (Arg)[b]	$^{\alpha}CH$	3.690	t	6.1	α-β; α-β′
(CHEBI:32682)	$^{\beta}CH_2$	1.700	m	-	-
	$^{\gamma}CH_2$	1.902	m	-	-
	$^{\delta}CH_2$	3.266	t	6.9	δ-γ
L-Asparagine (Asn)[b]	$^{\alpha}CH$	3.999	dd	7.8; 4.3	α-β; α-β'
(CHEBI:58048)	$^{\beta}CH_2$	2.845	dd	16.7; 4.3	β-β'; β-α
	-	2.962	dd	16.7; 7.8	β'-β; β'-α
L-Aspartate (Asp)[b]	$^{\alpha}CH$	3.930	dd	8.9; 3.7	α-β; α-β'
(CHEBI:29991)	$^{\beta}CH_2$	2.702	dd	17.5; 3.7	β-β'; β-α
	-	2.850	dd	17.5; 8.9	β'-β; β'-α
L-Cysteine (Cys)[a]	$^{\alpha}CH$	3.973	dd	5.7; 4.3	α-β; α-β'
(CHEBI:35235)	$^{\beta}CH_2$	3.052	dd	14.7; 4.3	β-β'; β-α
		3.112	dd	14.7; 5.7	β'-β; β'-α
L-Glutamine (Gln)[b]	$^{\alpha}CH$	3.786	t	6.2	α-β; α-β′
(CHEBI:58359)	$^{\beta}CH_2$	2.160	m	-	-
	$^{\gamma}CH_2$	2.480	m	-	-
L-Glutamate (Glu)[a]	$^{\alpha}CH$	3.788	dd	7.1; 4.9	α-β; α-β'
(CHEBI:29985)	$^{\beta}CH_2$	2.120	m	-	-
	$^{\gamma}CH_2$	2.388	m	-	-
L-Glycine (Gly)[b]	$^{\alpha}CH_2$	3.586	s	-	-
(CHEBI:57305)					
L-Histidine (His)[b]	$^{\alpha}CH$	4.012	dd	8.0; 4.9	α-β; α-β'
(CHEBI:57595)	$^{\beta}CH_2$	3.150	dd	15.5; 8.0	β-β'; β-α
	-	3.260	dd	15.5; 4.9	β'-β; β′-α
	$^{\gamma}CH$	7.802	s	-	-
	$^{\delta}CH$	7.086	s	-	-
L-Isoleucine (Ile)[b]	$^{\alpha}CH$	3.673	d	4.0	α-β
(CHEBI:58045)	$^{\beta}CH$	1.990	m	-	-
	$^{\gamma}CH_3$	1.015	d	7.0	γ-β
	$^{\delta}CH_2$	1.476	m	-	-
	$^{\epsilon}CH_3$	0.945	t	7.4	ε-δ
L-Leucine (Leu)[b]	$^{\alpha}CH$	3.769	dd	7.0; 1.3	α-β; α-β′
(CHEBI:57427)	$^{\beta}CH_2$	1.742	m	-	-
	$^{\gamma}CH$	1.742	m	-	-
	$^{\delta}CH_3$	0.987	d	4.7	δ-γ
	-	1.003	d	4.7	δ'-γ
L-Lysine (Lys)[b]	$^{\alpha}CH$	3.772	t	6.0	α-β; α-β′
(CHEBI:32551)	$^{\beta}CH_2$	1.928	m	-	-
	$^{\gamma}CH_2$	1.502	m	-	-
	$^{\delta}CH_2$	1.751	p	7.5	γ-δ; δ-ε
	$^{\epsilon}CH_2$	3.060	t	7.5	ε-δ
L-Methionine (Met)[b]	$^{\alpha}CH$	3.875	dd	7.0; 5.4	α-β; α-β'
(CHEBI:57844)	$^{\beta}CH_2$	2.195	m	-	-
	$^{\gamma}CH_2$	2.673	t	7.6	γ-β; γ-β'
	$^{\delta}CH_3$	2.167	s	-	-
L-Phenylalanine (Phe)[b]	$^{\alpha}CH$	3.998	dd	7.7; 5.2	α-β; α-β'
(CHEBI:58095)	$^{\beta}CH_2$	3.140	dd	14.4; 5.2	β-β'; β-α
	-	3.310	dd	14.4; 7.7	β'-β; β′-α
	$^{\gamma}CH$	7.353	d	7.2	γ-δ
	$^{\delta}CH$	7.454	t	7.2	δ-γ; δ-ε
	$^{\epsilon}CH$	7.414	t	7.2	ε-δ

Table 5.1 continued.

Metabolite	Proton	δ (ppm)	Multiplicity	J (Hz)	Connectivity
Amino acids					
L-Proline (Pro)[a]	$^{\alpha}CH$	4.162	dd	8.9; 6.3	α-β; α-β'
(CHEBI:60039)	$^{\beta}CH_2$	2.382	m	-	-
	$^{\gamma}CH_2$	2.060	m	-	-
	$^{\delta}CH_2$	3.365	t	7.0	δ-γ
	-	3.441	t	7.0	δ'-γ
L-Serine (Ser)[b]	$^{\alpha}CH$	3.845	dd	5.6; 4.0	α-β; α-β'
(CHEBI:33384)	$^{\beta}CH_2$	3.953	dd	12.2; 5.6	β-β'; β-α
	-	4.012	dd	12.2; 4.0	β'-β; β'-α
L-Threonine (Thr)[b]	$^{\alpha}CH$	3.596	d	4.9	α-β
(CHEBI:57926)	$^{\beta}CH$	4.276	dq	6.6; 4.9	β-α; β-γ
	$^{\gamma}CH_3$	1.358	d	6.6	γ-β
L-Tryptophan (Trp)[b]	$^{\alpha}CH$	4.086	dd	8.1; 5.2	α-β; α-β'
(CHEBI:57912)	$^{\beta}CH_2$	3.338	dd	15.3; 8.1	β-β'; β-α
	-	3.224	dd	15.3; 5.2	β'-β; β'-α
	$^{\gamma}CH$	7.351	s	-	-
	$^{\delta}CH$	7.770	d	7.8	δ-ε
	$^{\epsilon}CH$	7.229	t	7.8	ε-δ; ε-ζ
	$^{\zeta}CH$	7.310	t	7.8	ζ-ε; ζ-η
	$^{\eta}CH$	7.570	d	7.8	η-ζ
L-Tyrosine (Tyr)[a]	$^{\alpha}CH$	3.957	dd	7.8; 5.0	α-β; α-β'
(CHEBI:58315)	$^{\beta}CH_2$	3.076	dd	14.2; 7.8	β-β'; β-α
	-	3.227	dd	14.2; 5.0	β'-β; β'-α
	$^{\gamma}CH$	6.924	d	8.4	γ-δ
	$^{\delta}CH$	7.222	d	8.4	δ-γ
L-Valine (Val)[b]	$^{\alpha}CH$	3.635	d	4.3	α-β
(CHEBI:57762)	$^{\beta}CH$	2.305	m	-	-
	$^{\gamma}CH_3$	1.021	d	7.1	γ-β
	-	1.074	d	7.1	γ'-β
Carbohydrates					
D-glucose[a]					
α-anomer	C1H	5.264	d	3.8	-
(CHEBI:17925)	C2H	3.563	dd	9.8; 3.8	-
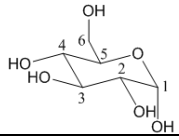	C3H	3.744	t	9.4	-
	C4H	3.439	t	9.4	-
	C5H	3.888	m	-	-
	C6H	3.858	dd	10; 2.2	-
	C6'H	3.792	dd	13.1; 6.3	-
β-anomer	C1H	4.678	d	7.8	-
(CHEBI:15903)	C2H	3.272	t	8.3	-
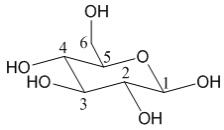	C3H	3.518	t	9.2	-
	C4H	3.428	t	9.4	-
	C5H	3.492	m	-	-
	C6H	3.933	dd	12.2; 2.0	-
	C6'H	3.752	dd	12.2; 5.7	-
Myo-Inositol[a]	C5H	4.090	t	2.9	-
(CHEBI:17268)	C4H+C6H	3.562	dd	9.8; 2.9	-
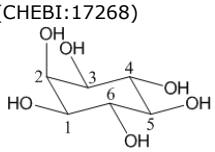	C1H+C3H	3.654	t	9.8	-
	C2H	3.306	t	9.3	-
Organic acids					
Acetate[b]	CH_3	1.948	s	-	-
(CHEBI:30089)					
Acetoacetate[b]	CH_2	2.319	s	-	-
(CHEBI:13705)	CH_3	3.480	s	-	-
α-ketoglutarate[a]	CH_2-CO	3.040	t	6.9	-
(CHEBI:16810)	CH_2-COO^-	2.470	t	6.9	-

Table 5.1 continued.

Metabolite	Proton	δ (ppm)	Multiplicity	J (Hz)	Connectivity
Organic acids					
D-β-hydroxybutyrate[b] (CHEBI:10983) 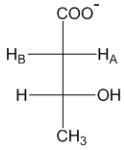	CH_A	2.400	dd	14.5; 7.3	-
	CH_B	2.300	dd	14.5; 7.3	-
	CH	4.184	m	-	-
	CH_3	1.231	d	6.3	-
Citrate[b] (CHEBI:16947) 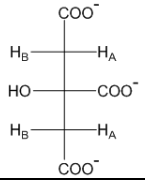	CH_A	2.717	d	15.8	-
	CH_B	2.566	d	15.8	-
L-lactate[a] (CHEBI:16651)	CH	4.138	q	6.9	-
	CH_3	1.354	d	6.9	-
Malonate[c] (CHEBI:15792)	CH_2	3.144	s	-	-
Pyruvate[b] (CHEBI:15361)	CH_3	2.402	s	-	-
Succinate[b] (CHEBI:30031)	CH_2	2.439	s	-	-
Others					
Creatine[b] (CHEBI:57947)	CH_3	3.068	s	-	-
	CH_2	3.962	s	-	-
Creatinine[b] (CHEBI:16737)	CH_3	3.075	s	-	-
	CH_2	4.087	s	-	-
Hypoxanthine[c] (CHEBI:17368)	CH	8.223	s	-	-
	CH	8.201	s	-	-
Betaine[c] (CHEBI:17750)	CH_2	3.926	s	-	-
	CH_3	3.286	s	-	-
	CH_3				
	CH_3				

[a]metabolites spiked in plasma; [b]metabolites spiked in plasma as well as in urine; [c]metabolites spiked in urine. Chemical shifts are expressed relatively to the singlet resonance of the trimethyl protons of TSP at 0.015 ppm and J-coupling patterns are described as: s, singlet; d, doublet; dd, double doublet; dq, double quadriplet; t, triplet; q, quadriplet; p, pentaplet; m, multiplet. Metabolite identifiers from the database of Chemical Entities of Biological Interest (ChEBI) are indicated. The atom numbering of the metabolites follows the IUPAC-IUB nomenclature, unless otherwise indicated in the structures included in Table 5.1.

Plasma

The resulting information allowed us to rationally define 96 fixed, variable-sized, integration regions in the plasma spectrum representing an identified metabolite composition. Including 14 additional integration regions emanating from broad lipid signals and non-identified substances, the plasma ^{1}H-NMR spectrum has been divided into 110 well-defined integration regions, being the variables for the statistical OPLS-DA multivariate analysis.

Table 5.2 presents an overview (start and end values in ppm) of the 110 fixed ^{1}H-NMR integration regions for plasma (VAR_{PL}) as well as their contributing metabolites, defined on the basis of our metabolite spiking experiments.

Table 5.2 Start and end values (in ppm) of the 110 fixed integration regions for plasma (plasma variables: VAR_{PL}) as well as their contributing metabolites, defined on the basis of metabolite spiking experiments.

Variable	Start ppm	End ppm	Metabolite
$VAR_{PL}1$	7,9500	7,8200	NI
$VAR_{PL}2$	7,8200	7,7890	L-Histidine
$VAR_{PL}3$	7,7890	7,7780	L-Tryptophan = §L-Histidine
$VAR_{PL}4$	7,7780	7,7480	L-Tryptophan = §L-Histidine
$VAR_{PL}5$	7,7480	7,7200	NI
$VAR_{PL}6$	7,6800	7,5920	NI
$VAR_{PL}7$	7,5920	7,5480	L-Tryptophan
$VAR_{PL}8$	7,4840	7,3620	L-Phenylalanine
$VAR_{PL}9$	7,3620	7,3300	L-Tryptophan + L-Phenylalanine
$VAR_{PL}10$	7,3300	7,2820	L-Tryptophan
$VAR_{PL}11$	7,2820	7,2550	L-Tryptophan
$VAR_{PL}12$	7,2550	7,2390	L-Tryptophan + L-Tyrosine
$VAR_{PL}13$	7,2390	7,2000	L-Tryptophan + L-Tyrosine
$VAR_{PL}14$	7,1070	7,0656	L-Histidine
$VAR_{PL}15$	6,9430	6,9050	L-Tyrosine
$VAR_{PL}16$	6,9050	6,8810	NI
$VAR_{PL}17$	6,7445	6,7020	NI
$VAR_{PL}18$	5,4300	5,2752	*Lipids: -**H**C=C**H**- in fatty acid chain
$VAR_{PL}19$	5,2752	5,2526	D-Glucose
$VAR_{PL}20$	5,2526	5,2030	*Lipids: C_2**H** in glycerol backbone of PL/TG
$VAR_{PL}21$	4,6940	4,6620	D-Glucose
$VAR_{PL}22$	4,5560	4,5380	NI
$VAR_{PL}23$	4,5380	4,4100	*Lipids: C_1**H** in glycerol backbone of PL
$VAR_{PL}24$	4,4100	4,3159	*Lipids: C_1**H** and C_3**H** in glycerol backbone of TG + OC**H₂** of choline in SM/PC
$VAR_{PL}25$	4,3159	4,2332	L-Threonine + *OC**H₂** of choline in SM/PC
$VAR_{PL}26$	4,2000	4,1885	L-Proline + D-β-hydroxybutyrate
$VAR_{PL}27$	4,1885	4,1750	L-Proline + D-β-hydroxybutyrate + L-Lactate
$VAR_{PL}28$	4,1750	4,1260	L-Proline + D-β-hydroxybutyrate + L-Lactate
$VAR_{PL}29$	4,1260	4,1110	D-β-hydroxybutyrate + L-Lactate
$VAR_{PL}30$	4,1110	4,1032	D-β-hydroxybutyrate + L-Tryptophan
$VAR_{PL}31$	4,1032	4,0700	L-Tryptophan + myo-Inositol + Creatinine § = L-Tryptophan + Creatinine
$VAR_{PL}32$	4,0700	4,0570	L-Tryptophan
$VAR_{PL}33$	4,0570	4,0310	L-Histidine + L-Serine
$VAR_{PL}34$	4,0310	4,0136	L-Asparagine + L-Histidine + L-Phenylalanine + L-Serine
$VAR_{PL}35$	4,0136	4,0010	L-Asparagine + L-Histidine + L-Phenylalanine + L-Serine
$VAR_{PL}36$	4,0010	3,9810	L-Asparagine + L-Cysteine + L-Histidine + L-Phenylalanine + L-Serine
$VAR_{PL}37$	3,9810	3,9590	L-Asparagine + L-Cysteine + L-Histidine + L-Serine + L-Tyrosine + Creatine
$VAR_{PL}38$	3,9590	3,8330	L-Aspartate + L-Cysteine + L-Methionine + L-Serine + L-Tyrosine + D-Glucose
$VAR_{PL}39$	3,8330	3,8100	L-Alanine + L-Serine + D-Glucose
$VAR_{PL}40$	3,8100	3,7956	L-Alanine + L-Glutamate + L-Glutamine + D-Glucose
$VAR_{PL}41$	3,7956	3,7820	L-Alanine + L-Glutamate + L-Glutamine + L-Leucine + L-Lysine + D-Glucose
$VAR_{PL}42$	3,7820	3,7550	L-Alanine + L-Glutamate + L-Glutamine + L-Leucine + L-Lysine + D-Glucose
$VAR_{PL}43$	3,7550	3,7390	L-Alanine + L-Leucine + D-Glucose
$VAR_{PL}44$	3,7390	3,7141	D-Glucose
$VAR_{PL}45$	3,7141	3,6680	L-Arginine + L-Isoleucine + myo-Inositol = §Glycerol
$VAR_{PL}46$	3,6680	3,6500	myo-Inositol = §Glycerol
$VAR_{PL}47$	3,6500	3,6376	L-Valine + myo-Inositol = §Glycerol
$VAR_{PL}48$	3,6376	3,6240	L-Valine + myo-Inositol = §L-Valine
$VAR_{PL}49$	3,6240	3,6097	L-Threonine + myo-Inositol = §L-Threonine
$VAR_{PL}50$	3,6097	3,5914	L-Threonine = §L-Threonine
$VAR_{PL}51$	3,5914	3,5649	L-Glycine + L-Threonine + D-Glucose + myo-Inositol = §Glycine + Glycerol
$VAR_{PL}52$	3,5649	3,5510	D-Glucose + myo-Inositol = §D-Glucose
$VAR_{PL}53$	3,5510	3,5360	D-Glucose + myo-Inositol = §D-Glucose
$VAR_{PL}54$	3,5360	3,3980	L-Proline + D-Glucose + Acetoacetate

Table 5.2 continued.

Variable	Start ppm	End ppm	Metabolite
VAR$_{PL}$55	3,3980	3,3765	L-Proline + L-Tryptophan = = §Methanol + NI
VAR$_{PL}$56	3,3765	3,3430	L-Proline + L-Tryptophan
VAR$_{PL}$57	3,3430	3,3230	L-Phenylalanine + L-Proline + L-Tryptophan + myo-Inositol § =L-Phenylalanine + L-Proline + L-Tryptophan
VAR$_{PL}$58	3,3230	3,2186	L-Arginine + L-Histidine + L-Phenylalanine + L-Tyrosine + D-Glucose + myo-Inositol + *-N^+(CH_3)$_3$ of choline head group in SM/PC § =L-Arginine + L-Histidine + L-Phenylalanine + L-Tyrosine + D-Glucose + *-N^+(CH_3)$_3$ of choline head group in SM/PC
VAR$_{PL}$59	3,2186	3,1930	L-Tyrosine
VAR$_{PL}$60	3,1930	3,1760	L-Phenylalanine + L-Histidine = §NI
VAR$_{PL}$61	3,1760	3,1462	L-Cysteine + L-Histidine + L-Phenylalanine = §NI
VAR$_{PL}$62	3,1462	3,1090	L-Cysteine + L-Histidine + L-Phenylalanine
VAR$_{PL}$63	3,1090	3,0860	L-Cysteine + L-Lysine + L-Tyrosine
VAR$_{PL}$64	3,0860	3,0716	L-Cysteine + L-Lysine + L-Tyrosine + Creatinine
VAR$_{PL}$65	3,0716	3,0640	L-Cysteine + L-Lysine + L-Tyrosine + Creatinine + Creatine
VAR$_{PL}$66	3,0640	2,9950	L-Cysteine + L-Lysine + L-Tyrosine + α-ketoglutarate
VAR$_{PL}$67	2,9950	2,8860	*Lipids: =CH-C**H**$_2$-CH= in fatty acid chain + L-Asparagine + α-ketoglutarate
VAR$_{PL}$68	2,8860	2,8550	*Lipids: =CH-C**H**$_2$-CH= in fatty acid chain + L-Asparagine + L-Aspartate
VAR$_{PL}$69	2,8550	2,7500	*Lipids: =CH-C**H**$_2$-CH= in fatty acid chain + L-Asparagine + L-Aspartate
VAR$_{PL}$70	2,7500	2,7360	L-Aspartate + Citrate
VAR$_{PL}$71	2,7360	2,6600	L-Aspartate + L-Methionine + Citrate
VAR$_{PL}$72	2,6600	2,6300	L-Methionine
VAR$_{PL}$73	2,5960	2,5340	Citrate
VAR$_{PL}$74	2,5340	2,5150	NI
VAR$_{PL}$75	2,5150	2,4920	L-Glutamine
VAR$_{PL}$76	2,4920	2,4500	L-Glutamine + α-ketoglutarate + D-β-hydroxybutyrate
VAR$_{PL}$77	2,4500	2,4324	α-ketoglutarate + D-β-hydroxybutyrate + Succinate
VAR$_{PL}$78	2,4324	2,4148	D-β-hydroxybutyrate + L-Proline
VAR$_{PL}$79	2,4148	2,4050	D-β-hydroxybutyrate + L-Proline + L-Glutamate
VAR$_{PL}$80	2,4050	2,3990	L-Glutamate + L-Proline + Pyruvate
VAR$_{PL}$81	2,3990	2,3640	L-Glutamate + L-Proline + D-β-hydroxybutyrate
VAR$_{PL}$82	2,3640	2,3500	L-Glutamate + L-Proline + D-β-hydroxybutyrate
VAR$_{PL}$83	2,3500	2,3380	L-Proline + L-Valine + D-β-hydroxybutyrate
VAR$_{PL}$84	2,3380	2,3170	L-Proline + L-Valine + D-β-hydroxybutyrate + Acetoacetate
VAR$_{PL}$85	2,3170	2,3040	L-Valine + D-β-hydroxybutyrate + Acetoacetate
VAR$_{PL}$86	2,3040	2,2915	*Lipids: -C**H**$_2$-C=O and -C**H**$_2$-CH=CH- in fatty acid chain + L-Valine + D-β-hydroxybutyrate
VAR$_{PL}$87	2,2915	2,2690	*Lipids: -C**H**$_2$-C=O and -C**H**$_2$-CH=CH- in fatty acid chain + L-Valine + L-Methionine
VAR$_{PL}$88	2,2690	2,2300	*Lipids: -C**H**$_2$-C=O and -C**H**$_2$-CH=CH- in fatty acid chain + L-Valine + L-Methionine + §Acetone
VAR$_{PL}$89	2,2180	2,1970	L-Glutamate + L-Methionine
VAR$_{PL}$90	2,1970	2,1230	L-Glutamate + L-Glutamine + L-Methionine + L-Proline
VAR$_{PL}$91	2,1230	1,9720	*Lipids: -C**H**$_2$-CH=CH- in fatty acid chain + L-Glutamate + L-Methionine + L-Proline + L-Isoleucine + *N-acetyl signal of glycoproteins
VAR$_{PL}$92	1,9720	1,9240	L-Isoleucine + L-Lysine + Acetate
VAR$_{PL}$93	1,9240	1,8800	L-Arginine + L-Isoleucine + L-Lysine
VAR$_{PL}$94	1,8060	1,6860	L-Arginine + L-Lysine + L-Leucine
VAR$_{PL}$95	1,6860	1,5600	*Lipids: -C**H**$_2$-CH$_2$-C=O and -C**H**$_2$-CH$_2$-CH=CH in fatty acid chain + L-Arginine + L-Lysine
VAR$_{PL}$96	1,5400	1,4900	L-Alanine + L-Isoleucine + L-Lysine
VAR$_{PL}$97	1,4900	1,4200	L-Isoleucine + L-Lysine = §L-Lysine
VAR$_{PL}$98	1,4200	1,3740	L-Lactate
VAR$_{PL}$99	1,3740	1,3450	L-Lactate + L-Threonine
VAR$_{PL}$100	1,3450	1,2458	*Lipids: CH_3-(C**H**$_2$)n- in fatty acid chain + L-Isoleucine + L-Threonine
VAR$_{PL}$101	1,2458	1,2180	L-Isoleucine + D-β-hydroxybutyrate
VAR$_{PL}$102	1,2180	1,1300	NI
VAR$_{PL}$103	1,0930	1,0610	L-Valine
VAR$_{PL}$104	1,0610	1,0400	L-Isoleucine
VAR$_{PL}$105	1,0400	1,0220	L-Valine + L-Isoleucine
VAR$_{PL}$106	1,0220	1,0020	L-Valine + L-Isoleucine + L-Leucine
VAR$_{PL}$107	1,0020	0,9860	L-Isoleucine + L-Leucine
VAR$_{PL}$108	0,9860	0,9760	L-Isoleucine + L-Leucine
VAR$_{PL}$109	0,9760	0,9660	L-Isoleucine
VAR$_{PL}$110	0,9660	0,8000	*Lipids: C**H**$_3$-(CH$_2$)n- in fatty acid chain

*metabolites identified with certainty on the basis of a comprehensive and quantitative experimental assessment/validation as described by Wishart et al. [16] and Kriat et al. [17]. §metabolites identified with certainty on the basis of spiking experiments on a 900MHz NMR spectrometer (Lille, France). NI: non-identified; PC: phosphatidylcholine; PL: phospholipids; SM: sphingomyelin; TG: triglycerides. VAR$_{PL}$ colored in grey are defined as noisy variables with 15% threshold for the CV (see below).

To allow a better interpretation of metabolic alterations, further spiking experiments with all 32 metabolites along with glycerol, methanol and acetone were performed for plasma on a 900 MHz ^{1}H-NMR spectrometer (Lille, France). Compared to a 400 MHz ^{1}H-NMR spectrometer, a 900 MHz spectrometer has a higher signal-to-noise ratio and resolution. However, even in spectra recorded with a 900 MHz spectrometer, no signals of myo-inositol were observed. Myo-inositol was therefore no longer considered as a contributing metabolite for the interpretation of metabolic alterations in plasma.

Urine

In the urine spectrum, we were able to rationally define 83 fixed, variable-sized, integration regions representing an identified metabolite composition. Including 51 additional integration regions emanating from dimethylamine (DMA), hippurate, taurine, trimethylamine N-oxide (TMAO) and urea – as determined with certainty from Bouatra et al. [18] – and non-identified substances, the urine ^{1}H-NMR spectrum was divided into 134 well-defined integration regions, being the variables for the statistical OPLS-DA multivariate analysis.

Table 5.3 presents an overview (start and end values in ppm) of the 134 fixed ^{1}H-NMR integration regions for urine (VAR_{UR}) as well as their contributing metabolites, defined on the basis of our metabolite spiking experiments.

Table 5.3 Start and end values (in ppm) of the 134 fixed integration regions for urine (urine variables: VAR_{UR}) as well as their contributing metabolites, defined on the basis of metabolite spiking experiments.

Variable	Start ppm	End ppm	Metabolite
$VAR_{UR}1$	9,3374	9,2874	NI
$VAR_{UR}2$	9,1874	9,1274	NI
$VAR_{UR}3$	9,1074	9,0274	NI
$VAR_{UR}4$	9,0274	8,8074	NI
$VAR_{UR}5$	8,7074	8,4967	NI
$VAR_{UR}6$	8,4967	8,4648	NI
$VAR_{UR}7$	8,4648	8,3796	NI
$VAR_{UR}8$	8,3796	8,3432	NI
$VAR_{UR}9$	8,3432	8,2561	NI
$VAR_{UR}10$	8,2561	8,1958	Hypoxanthine
$VAR_{UR}11$	8,1958	8,1574	NI
$VAR_{UR}12$	8,1474	8,0774	NI
$VAR_{UR}13$	8,0774	8,0403	NI
$VAR_{UR}14$	8,0403	7,9700	NI
$VAR_{UR}15$	7,9700	7,9385	NI
$VAR_{UR}16$	7,9385	7,8859	NI
$VAR_{UR}17$	7,8859	7,8332	*Hippurate
$VAR_{UR}18$	7,8332	7,8071	NI
$VAR_{UR}19$	7,8071	7,7556	L-Tryptophan

Table 5.3 continued.

Variable	Start ppm	End ppm	Metabolite
VAR$_{UR}$20	7,7556	7,7108	L-Tryptophan
VAR$_{UR}$21	7,7108	7,6915	NI
VAR$_{UR}$22	7,6915	7,6176	*Hippurate
VAR$_{UR}$23	7,6155	7,5420	*Hippurate + L-Tryptophan
VAR$_{UR}$24	7,5420	7,5243	NI
VAR$_{UR}$25	7,5243	7,4574	L-Phenylalanine
VAR$_{UR}$26	7,4574	7,4134	L-Phenylalanine
VAR$_{UR}$27	7,4134	7,3278	L-Phenylalanine + L-Tryptophan
VAR$_{UR}$28	7,3278	7,2601	L-Tryptophan + L-Histidine
VAR$_{UR}$29	7,2601	7,1859	L-Tryptophan
VAR$_{UR}$30	7,1859	7,1320	NI
VAR$_{UR}$31	7,1320	7,0515	NI
VAR$_{UR}$32	7,0515	6,9744	NI
VAR$_{UR}$33	6,9744	6,8478	NI
VAR$_{UR}$34	6,8478	6,6527	NI
VAR$_{UR}$35	6,2118	5,5092	*Urea
VAR$_{UR}$36	5,3985	5,3276	NI
VAR$_{UR}$37	5,3276	5,2092	NI
VAR$_{UR}$38	5,2092	5,1007	D-glucose
VAR$_{UR}$39	4,5263	4,3974	D-glucose
VAR$_{UR}$40	4,3974	4,2489	L-Threonine
VAR$_{UR}$41	4,2489	4,1526	D-β-hydroxybutyrate
VAR$_{UR}$42	4,1526	4,1180	NI
VAR$_{UR}$43	4,1180	4,0636	Creatinine
VAR$_{UR}$44	4,0636	4,0440	L-Asparagine + L-Histidine + L-Tryptophan
VAR$_{UR}$45	4,0440	4,0254	L-Asparagine + L-Histidine + L-Phenylalanine + L-Serine
VAR$_{UR}$46	4,0254	4,0117	L-Asparagine + L-Phenylalanine + L-Serine
VAR$_{UR}$47	4,0117	3,9955	*Hippurate + L-Phenylalanine + L-Serine
VAR$_{UR}$48	3,9955	3,9741	L-Serine
VAR$_{UR}$49	3,9741	3,9625	Creatine + L-Serine
VAR$_{UR}$50	3,9625	3,9264	L-Serine + Betaine
VAR$_{UR}$51	3,9264	3,9016	L-Aspartate + L-Methionine + Betaine
VAR$_{UR}$52	3,9016	3,8961	NI
VAR$_{UR}$53	3,8961	3,8767	L-Aspartate + L-Methionine + L-Serine
VAR$_{UR}$54	3,8767	3,8351	L-Methionine + L-Serine
VAR$_{UR}$55	3,8351	3,8149	L-Alanine
VAR$_{UR}$56	3,8149	3,7569	L-Alanine + L-Glutamine + L-Leucine + L-Lysine
VAR$_{UR}$57	3,7569	3,7381	L-Leucine
VAR$_{UR}$58	3,7381	3,7269	NI
VAR$_{UR}$59	3,7269	3,7000	NI + L-Isoleucine
VAR$_{UR}$60	3,7000	3,6748	L-Isoleucine
VAR$_{UR}$61	3,6748	3,6591	NI
VAR$_{UR}$62	3,6591	3,6356	NI
VAR$_{UR}$63	3,6356	3,6025	L-Valine + L-Threonine
VAR$_{UR}$64	3,6025	3,5784	L-Glycine
VAR$_{UR}$65	3,5784	3,5487	NI
VAR$_{UR}$66	3,5487	3,5346	L-Tryptophan
VAR$_{UR}$67	3,5346	3,5143	L-Tryptophan + Acetoacetate
VAR$_{UR}$68	3,5143	3,4884	L-Tryptophan + Acetoacetate
VAR$_{UR}$69	3,4884	3,4578	Acetoacetate
VAR$_{UR}$70	3,4578	3,4397	L-Arginine + Acetoacetate
VAR$_{UR}$71	3,4397	3,4194	L-Arginine + Acetoacetate + *Taurine
VAR$_{UR}$72	3,4194	3,3934	L-Arginine + Acetoacetate
VAR$_{UR}$73	3,3934	3,3714	NI
VAR$_{UR}$74	3,3714	3,3476	L-Tryptophan
VAR$_{UR}$75	3,3476	3,3324	L-Tryptophan + L-Phenylalanine
VAR$_{UR}$76	3,3324	3,3149	L-Tryptophan + L-Phenylalanine + L-Histidine
VAR$_{UR}$77	3,3149	3,3064	L-Phenylalanine + L-Histidine
VAR$_{UR}$78	3,3064	3,2821	Betaine + *TMAO
VAR$_{UR}$79	3,2821	3,2731	*Taurine

Table 5.3 continued.

Variable	Start ppm	End ppm	Metabolite
VAR$_{UR}$80	3,2731	3,2623	L-Arginine
VAR$_{UR}$81	3,2623	3,2369	Betaine + L-Arginine
VAR$_{UR}$82	3,2369	3,2092	L-Arginine
VAR$_{UR}$83	3,2092	3,1951	NI
VAR$_{UR}$84	3,1951	3,1522	L-Phenylalanine + L-Cysteine
VAR$_{UR}$85	3,1522	3,1392	L-Phenylalanine + Malonate
VAR$_{UR}$86	3,1392	3,1166	L-Phenylalanine
VAR$_{UR}$87	3,1166	3,0996	NI
VAR$_{UR}$88	3,0996	3,0471	Creatinine + Creatine
VAR$_{UR}$89	3,0471	3,0296	L-Lysine
VAR$_{UR}$90	3,0296	2,9715	L-Asparagine
VAR$_{UR}$91	2,9715	2,9337	L-Asparagine
VAR$_{UR}$92	2,9337	2,9141	NI
VAR$_{UR}$93	2,9141	2,8736	L-Asparagine + L-Aspartate
VAR$_{UR}$94	2,8736	2,8390	L-Asparagine + L-Aspartate
VAR$_{UR}$95	2,8390	2,8148	L-Aspartate
VAR$_{UR}$96	2,8148	2,7907	NI
VAR$_{UR}$97	2,7907	2,7606	L-Aspartate
VAR$_{UR}$98	2,7606	2,7365	Citrate + *DMA + L-Aspartate
VAR$_{UR}$99	2,7365	2,7136	Citrate + *DMA + L-Aspartate
VAR$_{UR}$100	2,7136	2,6712	Citrate + L-Aspartate + L-Methionine
VAR$_{UR}$101	2,6712	2,6013	L-Aspartate + L-Methionine + Succinate
VAR$_{UR}$102	2,6000	2,5569	Citrate
VAR$_{UR}$103	2,5569	2,5151	Citrate
VAR$_{UR}$104	2,5151	2,3825	L-Glutamine + D-β-hydroxybutyrate + Pyruvate
VAR$_{UR}$105	2,3825	2,3453	D-β-hydroxybutyrate
VAR$_{UR}$106	2,3453	2,3075	L-Valine + Acetoacetate + D-β-hydroxybutyrate
VAR$_{UR}$107	2,3075	2,2859	L-Valine
VAR$_{UR}$108	2,2859	2,2546	L-Valine + L-Methionine
VAR$_{UR}$109	2,2546	2,1658	L-Glutamine + L-Methionine
VAR$_{UR}$110	2,1658	2,1240	L-Glutamine + L-Methionine
VAR$_{UR}$111	2,1240	2,0756	L-Methionine
VAR$_{UR}$112	2,0756	2,0397	NI + L-Isoleucine
VAR$_{UR}$113	2,0397	1,9875	L-Isoleucine
VAR$_{UR}$114	1,9875	1,8874	L-Lysine + Acetate
VAR$_{UR}$115	1,8874	1,8220	NI
VAR$_{UR}$116	1,8220	1,5564	L-Arginine + L-Leucine + L-Lysine
VAR$_{UR}$117	1,5564	1,5243	L-Isoleucine + L-Lysine
VAR$_{UR}$118	1,5243	1,4921	L-Alanine
VAR$_{UR}$119	1,4921	1,4641	L-Isoleucine + L-Lysine
VAR$_{UR}$120	1,4641	1,4392	NI
VAR$_{UR}$121	1,4392	1,4216	NI
VAR$_{UR}$122	1,4216	1,3956	NI
VAR$_{UR}$123	1,3956	1,3728	L-Threonine
VAR$_{UR}$124	1,3728	1,3246	L-Threonine + L-Isoleucine + D-Lactate
VAR$_{UR}$125	1,3246	1,3046	L-Isoleucine
VAR$_{UR}$126	1,3046	1,2877	L-Isoleucine
VAR$_{UR}$127	1,2877	1,2379	L-Isoleucine + D-β-hydroxybutyrate
VAR$_{UR}$128	1,2379	1,2160	D-β-hydroxybutyrate
VAR$_{UR}$129	1,2160	1,1834	NI
VAR$_{UR}$130	1,1834	1,1484	NI
VAR$_{UR}$131	1,1484	1,1085	NI
VAR$_{UR}$132	1,1085	1,0797	NI + L-Valine
VAR$_{UR}$133	1,0797	1,0474	NI + L-Isoleucine + L-Valine
VAR$_{UR}$134	1,0474	0,7004	L-Isoleucine + L-Leucine + L-Valine

*metabolites identified with certainty on the basis of a comprehensive and quantitative experimental assessment/validation as described by Bouatra et al. [18]. DMA: dimethylamine; NI: non-identified; TMAO: trimethylamine N-oxide. VAR$_{UR}$ colored in grey are defined as noisy variables with 15% threshold for the CV (see below).

5.3.2 Application of the analysis procedure in a case-control training and validation study

Plasma

Subject characteristics of the case-control training and validation cohorts used to evaluate the analysis procedure for plasma as described above, are presented in Table 5.4.

Table 5.4 Subject characteristics of the case-control training and validation cohorts used to evaluate the analysis procedure for plasma.

	Training cohort		Validation cohort	
	OB	NW	OB	NW
Number of subjects, n	43	25	22	12
Gender: male/female, n	25/18	8/17	14/8	10/2
Age, years	13.1 ± 2.0	13.2 ± 2.9	13.1 ± 2.7	12.7 ± 2.4
BMI, kg/m²	31.8 ± 4.7	18.9 ± 2.3	30.9 ± 6.1	17.1 ± 1.8

Data are presented as mean ± SD. BMI: body mass index.

Applying PCA analysis, 3 outliers (2 OB and 1 NW) were identified and excluded from the training cohort. By means of OPLS-DA, a statistical classifier was built by using all variables (the normalized integration values of the fixed 110 integration regions). The model was able to discriminate between obese children and normal-weight controls with a sensitivity and specificity of 100% and 96%, respectively. This model explains 84.1% of the predictive and orthogonal variation in X ($R^2X(cum)$) and 82.0% of the cumulative variation in Y ($R^2Y(cum)$) (Figure 5.4A and Table 5.7).

In addition, the predictive accuracy of this model was evaluated by classifying an independent cohort consisting of 22 obese children and 12 normal-weight children, resulting in a correct classification of 100 % obese and 67% of the normal-weight children.

The BMI of subjects that were wrongly classified in both the training and validation set of plasma was not higher for NW or lower for OB subjects and therefore BMI was not a confounding factor for the misclassification.

Urine

Subject characteristics of the case-control training and validation cohorts used to evaluate the analysis procedure for urine as described above, are presented in Table 5.5.

Table 5.5 Subject characteristics of the case-control training and validation cohorts used to evaluate the analysis procedure for urine.

	Training cohort		Validation cohort	
	OB	NW	OB	NW
Number of subjects, n	32	24	16	13
Gender: male/female, n	18/14	12/12	11/5	6/7
Age, years	13.4 ± 2.4	13.0 ± 2.9	12.1 ± 1.5	13.0 ± 2.5
BMI, kg/m²	31.1 ± 5.9	18.1 ± 2.3	30.3 ± 4.4	18.7 ± 2.4

Data are presented as mean ± SD. BMI: body mass index.

Applying PCA analysis, 2 outliers (1 OB and 1 NW) were identified and excluded from the training cohort. By means of OPLS-DA, a statistical classifier was built by using all variables (the normalized integration values of the fixed 134 integration regions). The model was able to discriminate between obese children and normal-weight controls with a sensitivity and specificity of 97% and 83%, respectively. This model explains 23.4% of the predictive and orthogonal variation observed in X ($R^2X(cum)$) and 63.8% of the cumulative variation in Y ($R^2Y(cum)$) (Figure 5.7A and Table 5.9).

In addition, the predictive accuracy of this model was evaluated by classifying an independent cohort consisting of 16 OB children and 13 NW children, resulting in a correct classification of 75% obese and 62% of the normal-weight children.

The BMI of subjects that were wrongly classified in both the training and validation set of urine was not higher for NW or lower for OB subjects and therefore BMI was not a confounding factor for the misclassification.

5.3.3 Identification and influence of noisy variables

Although the discriminative power of the model built by using all variables is already fairly good, we have to keep in mind that experimental data are always subjected to a certain degree of noise. In a fixed NMR set-up (with a defined magnetic field strength and probe-head), the signal-to-noise ratio (S/N) mainly depends on the chosen plasma or urine concentration and the number of accumulations (number of excitations by the radiofrequency (RF)-pulse) to acquire the spectrum. Although a higher plasma or urine concentration will result in a higher S/N, starting from a certain level it will unfortunately also reduce the spectral resolution (an increase of line-broadening due to a decrease of the T_2-relaxation decay times with increasing concentration). So, once the plasma or urine concentration is chosen in the analysis protocol (in our study 200 µl plasma/urine diluted with 600 µl D_2O) the S/N will be determined by the number

of accumulations. However, also a reasonable time frame per sample has to be taken into account, especially if a high sample throughput is desirable as for metabolomics. In our analysis protocol, we have chosen to acquire 96 accumulations per sample, resulting in an acquisition time of 7'44''. The fact that some degree of noise can never be excluded from experimental data and that noisy variables can complicate the multivariate data analysis, explains our effort to implement a protocol that allows to identify and classify noisy variables and subsequently to study the impact of their removal from the dataset on group differentiation.

Plasma

For reference plasma (Figure 5.2) and plasma of an obese child (Figure 5.3), plots were generated for each series of ^{1}H-NMR experiments (A-C; as described in paragraph 5.2.5), of the resulting coefficients of variation for all variables which are, for clarity, divided into three groups on the basis of their mean normalized integration value, i.e. 0.1-5, 5-10, 10-200. Based on these plots, four visual thresholds could be defined, i.e. coefficients of variation below 5, 10, 15 and 20%. If a variable exceeded the predefined threshold in at least two of the three series it was assigned as 'noisy'. A variable for which the CV was higher than the threshold in only one of the series was classified as noisy only if the variation was not the result of a single outlier. Remark that these threshold settings might be dependent on the NMR set-up, and consequently can be even lower for higher magnetic field strengths or when cryo-probes are used.

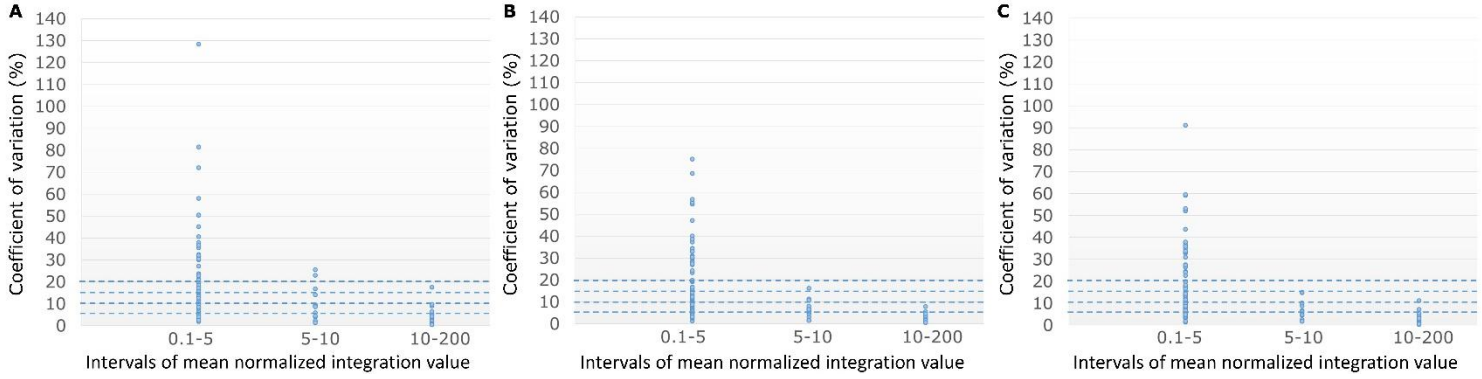

Figure 5.2 CV (%) for the 110 variables of the <u>reference</u> plasma which are divided into three groups on the basis of their mean normalized integration values, i.e. those with a mean normalized integration value between 0.1-5 (80 variables), 5-10 (12 variables) and 10–200 (18 variables). Based on these plots, visual thresholds were subsequently defined as the coefficients of variation, i.e. 5%, 10%, 15% and 20%. A, B and C refer to series A, B and C as described in section 5.2.5.

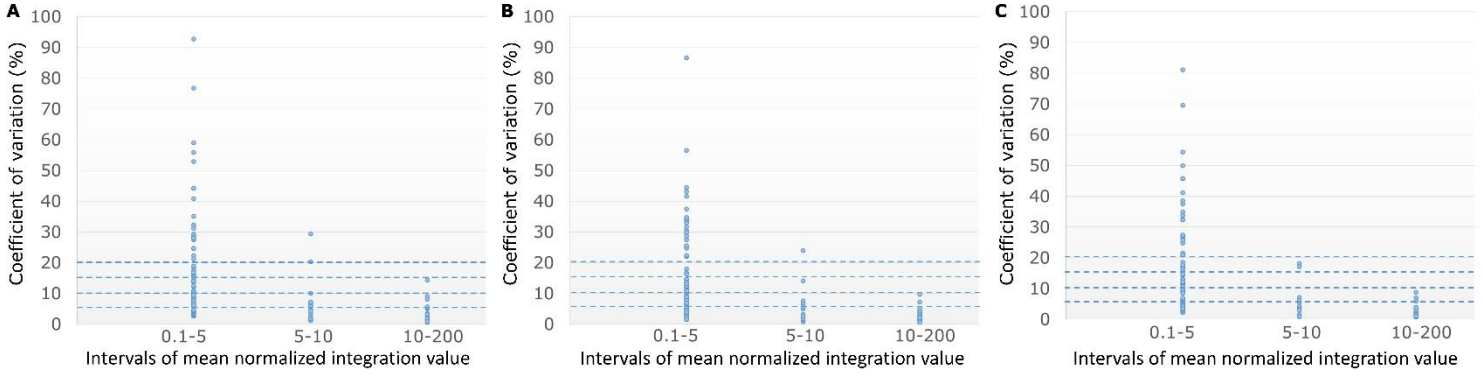

Figure 5.3 CV (%) for the 110 plasma variables of an <u>obese</u> subject which are divided into three groups on the basis of their mean normalized integration values, i.e. those with a mean normalized integration value between 0.1-5 (74 variables), 5-10 (17 variables) and 10–200 (19 variables). Based on these plots, visual thresholds were subsequently defined as the coefficients of variation, i.e. 5%, 10%, 15% and 20%. A, B and C refer to series A, B and C as described in section 5.2.5.

Table 5.6 presents the number of noisy variables for each defined CV derived from the reference and obese plasma sample. The final set of noisy variables are those detected both in the reference and obese plasma ^{1}H-NMR spectra, i.e. the mutual noisy variables.

Table 5.6 Overview of the number of noisy variables obtained for each defined CV for the reference and obese plasma sample.

	CV	Number of noisy variables detected for plasma
Reference sample	20%	26
	15%	35
	10%	51
	5%	76
Obese sample	20%	23
	15%	31
	10%	41
	5%	67
Mutual noisy variables	20%	19
	15%	27
	10%	41
	5%	67

CV: coefficient of variation

By means of this information, the influence of noisy variables on the classification of the case-control training cohort was investigated. Hereto, OPLS-DA classifiers were built and compared after removal of the noisy variables according to the above defined criteria. An overview of the results is presented for plasma (Table 5.7 and Figure 5.4).

The complete model containing all 110 NMR variables shows that 84.1% of variation in X ($R^2X(cum)$), and 82.0% of the variation in Y ($R^2Y(cum)$) can be explained by the model. Also, the model shows 68.6% ($Q^2(cum)$) predictive ability. The model has a sensitivity of 100% (i.e. a correct classification of all obese subjects) and a specificity of 96% (i.e. 96% of all normal-weight children were correctly classified). In order to evaluate if the complete model is not influenced too much by analytic noise, it is important to identify noisy variables. Hence, the identification of noisy variables could improve (i) model classification provided that the noisy variables do not significantly contribute to the model; (ii) insight into misclassification of noisy variables in studies based on small sample sizes, i.e. noisy variables could by accident be classified as being important (i.e. high variable importance on projection (VIP) value); (iii) explanation of the metabolic pathways involved.

Table 5.7 The number of LV, the total explained variation in X and Y (R^2X(cum) and R^2Y(cum)), predictive ability (Q^2(cum)), and sensitivity and specificity for OPLS-DA models constructed for the training and validation cohort of the plasma study with a decreasing number of variables.

	Threshold for CV				
	None	**20%**	**15%**	**10%**	**5%**
Training cohort					
Remaining variables	110	91	83	69	43
LV	4	4	4	4	4
R^2X(cum)	0.841	0.858	0.874	0.888	0.923
R^2Y(cum)	0.820	0.819	0.814	0.794	0.783
Q^2(cum)	0.686	0.692	0.693	0.681	0.691
Sensitivity, %	100	100	100	100	100
Specificity, %	96	96	96	96	96
Validation cohort					
Predicted sensitivity, %	100	100	100	100	100
Predicted specificity, %	67	67	67	67	67

A decreasing threshold limit for the CV, from 20% to 5%, was used as an exclusion criterion to define noisy variables. CV: coefficient of variation; LV: latent variable.

As presented in Table 5.7, R^2X is highest in the 5% CV model, R^2Y is highest in the 20% CV model, Q^2 is highest in the 15% CV model, and sensitivity and specificity remained unchanged for all CV models. In more detail, R^2X improves in going from a threshold setting of 20% to 5%. Besides, R^2Y and Q^2 slightly decline upon lowering the threshold from 15% to 10%, indicating a slight loss of discriminative power. This loss can be explained by the fact that only about half of the NMR variables (69 out of 110) still contribute to the model and might indicate that the 14 variables, which were additionally removed in going from a threshold of 15% to 10%, have some importance in group differentiation. Taking all these criteria into account, the model built with a threshold of 15% for the CV seems to be a good compromise, showing the best cross-validation (highest Q^2). It can be stated that the discriminating power of the remaining 83 variables, and so constituting metabolites, is still very strong. In addition, also in a larger study of our group consisting of 53 breast cancer patients and 52 controls, the removal of variables with a CV above 15% appeared to be most beneficial for group classification [19].

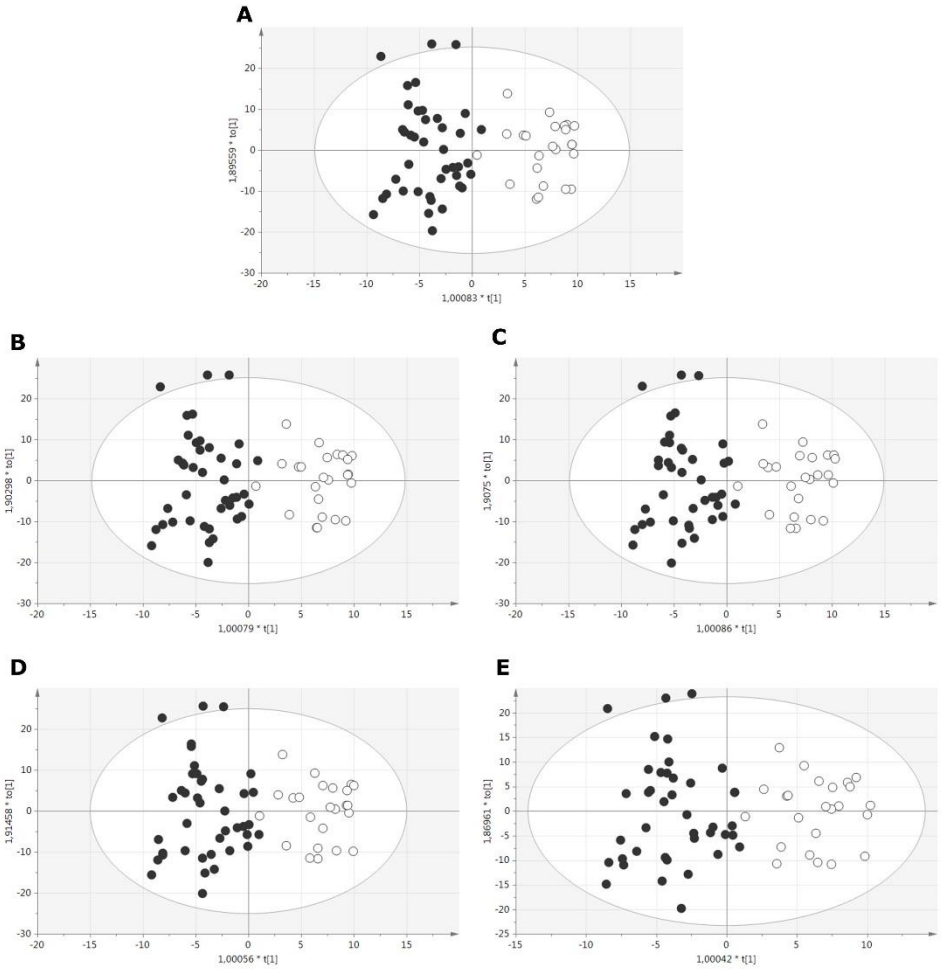

Figure 5.4 Plasma OPLS-DA score plots of the models build with all 110 variables (A), with 91 variables (B), with 83 variables (C), with 69 variables (D) and with 43 variables (E). Variables exceeding a predefined threshold for the CV, i.e. 20 % (B), 15 % (C), 10 % (D) and 5 % (E) were assigned as 'noisy' and excluded for the building of the classifier. Obese patients are marked as ● and healthy controls as ○. The first predictive component t[1] explains the variation between both study groups and the first orthogonal component to[1] explains the variation within both study groups.

To double check that none of the 27 excluded variables is highly important for group differentiation, they were also excluded one by one, i.e. 27 OPLS-DA classifiers were built with the remaining 109 variables, and evaluated. The resulting classifiers performed evenly than the one constructed with all 110 variables. In addition, all noisy variables had a VIP value lower than 0.53 indicating they are not important for group differentiation (variables with a VIP value greater than 1 are considered as being highly important in the plasma study,

see also Chapter 7). Altogether, this confirms that the 27 variables with a CV above 15% might be noisy and are not important for group differentiation. Indeed, these noisy variables, marked in grey in Table 5.2, all represent very low intensity signals. Among them, 9 are not identified, 9 are specific for a single metabolite, and 9 are specific for two or more metabolites. Despite of this reduction in a number of variables, all metabolites are still represented, either via a unique signal or via a composite signal.

In a next step, the influence of removing these noisy variables on the predictive accuracy of the classification was examined in the independent validation cohort. Although the size of the cohort is still limited, removal of the noisy variables has no clear influence on the discriminative power, indicating that all models built by means of the training cohort are rather strong.

Urine

For urine, the same procedure to identify and determine the influence of noisy variables was applied as for plasma. For reference urine (Figure 5.5) and urine of an obese child (Figure 5.6), plots were generated for each series of experiments (A-C), of the CV of all variables which are divided into three groups on the basis of their mean normalized integration value, i.e. 0.01-5, 5-10, 10-200.

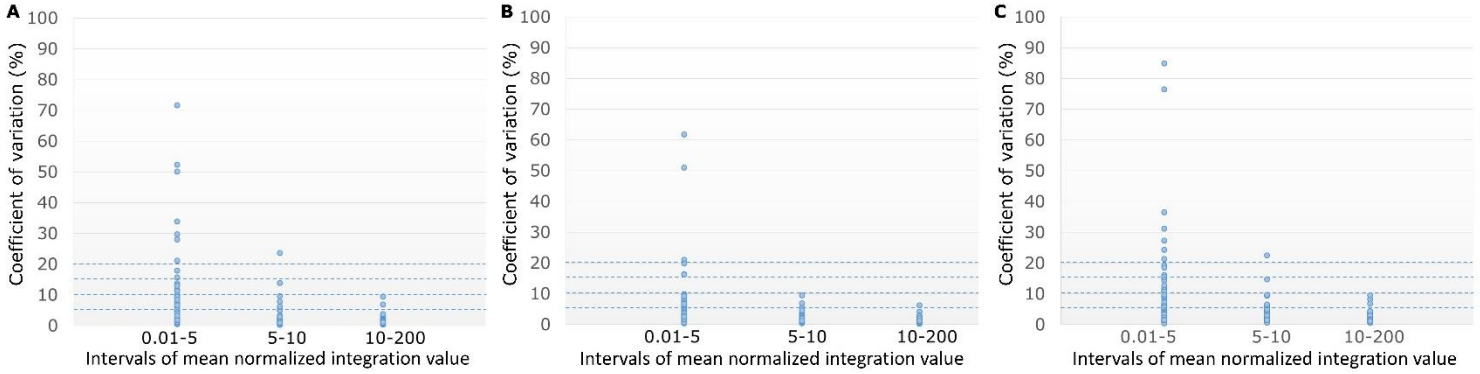

Figure 5.5 CV (%) for the 134 variables of the reference urine which are divided into three groups on the basis of their mean normalized integration values, i.e. those with a mean normalized integration value between 0.01-5 (53 variables), 5-10 (34 variables) and 10–200 (47 variables). Based on these plots, visual thresholds were subsequently defined as the coefficients of variation, i.e. 5%, 10%, 15% and 20%. A, B and C refer to series A, B and C as described in section 5.2.5.

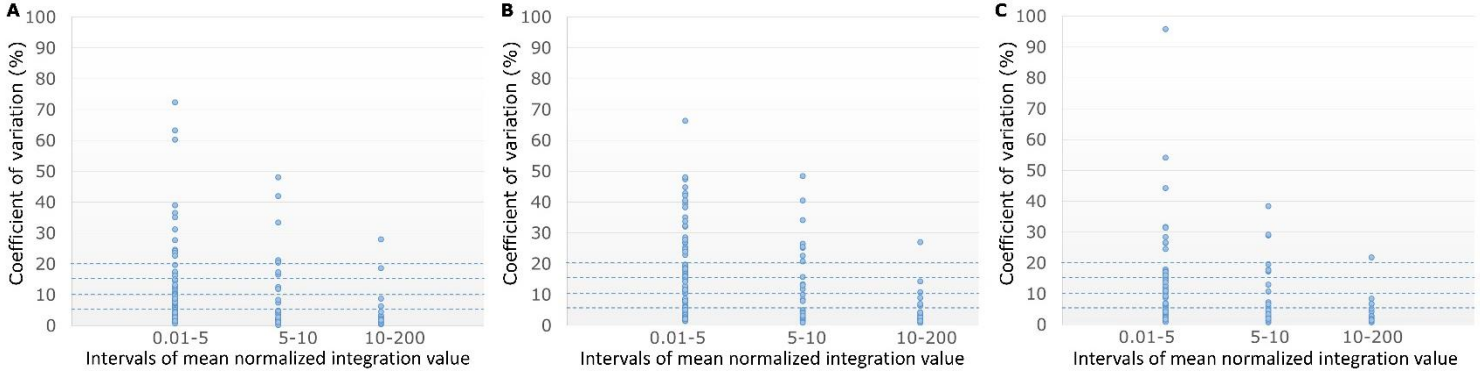

Figure 5.6 CV (%) for the 134 urine variables of an obese subject which are divided into three groups on the basis of their mean normalized integration values, i.e. those with a mean normalized integration value between 0.01-5 (78 variables), 5-10 (33 variables) and 10–200 (23 variables). Based on these plots, visual thresholds were subsequently defined as the coefficients of variation, i.e. 5%, 10%, 15% and 20%. A, B and C refer to series A, B and C as described in section 5.2.5.

Based on these plots, four visual thresholds could be defined, i.e. coefficients of variation below 5, 10, 15 and 20%. Table 5.8 presents the number of noisy variables for each defined CV derived from the reference and obese urine sample. The final set of noisy variables are those detected both in the ^{1}H-NMR spectra of the reference as well as obese urine sample, i.e. the mutual noisy variables.

Table 5.8 Overview of the number of noisy variables obtained for each defined CV for the reference and obese urine sample.

	CV	Number of noisy variables detected for urine
Reference sample	20%	8
	15%	11
	10%	16
	5%	38
Obese sample	20%	22
	15%	32
	10%	45
	5%	71
Mutual noisy variables	20%	4
	15%	7
	10%	10
	5%	28

CV: coefficient of variation

By means of this information, the influence of noisy variables on the classification of the training set was investigated (Table 5.9). Hereto, OPLS-DA classifiers were built and compared after removal of the noisy variables according the above defined criteria. An overview of the results is presented in (Table 5.9 and Figure 5.7).

Table 5.9 The number of latent variables (LV), the total explained variation in X and Y (R^2X(cum) and R^2Y(cum)), predictive ability (Q^2(cum)), and sensitivity and specificity for OPLS-DA models constructed for the training and validation cohort of the urine study with a decreasing number of variables.

	Threshold for CV				
	None	**20%**	**15%**	**10%**	**5%**
Training cohort					
Remaining variables	134	130	127	124	106
LV	2	2	2	2	2
R^2X(cum)	0.234	0.237	0.239	0.237	0.258
R^2Y(cum)	0.638	0.640	0.641	0.642	0.631
Q^2(cum)	0.342	0.352	0.358	0.357	0.356
Sensitivity, %	97	97	97	97	97
Specificity, %	83	83	83	78	83
Validation cohort					
Predicted sensitivity, %	75	75	75	75	69
Predicted specificity, %	62	62	69	69	62

A decreasing threshold limit for the CV, from 20% to 5%, was used as an exclusion criterion to define noisy variables. CV: coefficient of variation; LV: latent variable.

The complete model containing all 134 variables shows that 23.4% of the variation in X (R^2X), and 63.8% of the variation in Y (R^2Y) can be explained by the model. Also, the model shows a moderate predictive ability of 34.2% (Q^2). It should be noted that the discriminative power of the urine model is lower than this observed for plasma, probably due to the combination of a smaller amount of samples and higher number of variables. The model has a sensitivity of 97% (i.e. a correct classification of all obese subjects) and a specificity of 83% (i.e. 83% of all normal-weight children were correctly classified).

In order to evaluate if the complete model is not influenced too much by analytic noise, it is important to identify noisy variables. Hence, the identification of noisy variables could improve (i) model classification provided that the noisy variables do not significantly contribute to the model; (ii) insight into misclassification of noisy variables in studies based on small sample sizes, i.e. noisy variables could by accident be classified as being important (i.e. high VIP value); (iii) explanation of the metabolic pathways involved.

Overall, R^2X, R^2Y and Q^2 show only slight variation in going from a CV threshold of 20% to 5% (Table 5.9). This is because only a limited number of variables is excluded as noisy when going from the highest to the lowest threshold value. This suggests that the S/N ratio in the ^{1}H-NMR spectra of urine is higher than in these of plasma. Indeed, with respect to the signal intensity of TSP, the signal intensities of urine peaks are generally higher than that of plasma peaks. For example, in the aromatic region between 8 and 7 ppm, the urine ^{1}H-NMR spectrum contains

a lot of high intensity signals (such as those of hippurate), whereas in the plasma ^{1}H-NMR spectrum low intensity signals are observed (e.g. those of aromatic amino acids).

In more detail, R^2X is highest in the 5% CV model, while R^2Y is highest in the 10% CV model. The classifier with the 15% threshold for CV shows, on the other hand, the highest Q^2 indicating the strongest discriminating power and the best cross-validation, with average values for R^2X and R^2Y. Based on this it can be concluded that removing variables with a CV above 15% has a small beneficial effect on group differentiation. Deleting 3 variables with a CV above 10% results in a drop of specificity with 5% (to 78%) as compared to the classifier constructed with 127 variables. Hence, a threshold of 15% for the CV is considered as the best compromise for the identification and exclusion of noisy variables.

To double check that none of the 7 excluded variables is highly important for group differentiation, they were also excluded one by one, i.e. 7 OPLS-DA classifiers were built with the remaining 133 variables, and evaluated. The resulting classifiers performed evenly or even slightly better than the one constructed with all 134 variables. In addition, all noisy variables had a VIP value lower than 1.35 indicating they are not important for group differentiation (only variables with a VIP value greater than 1.8 are considered as being highly important in the urine study because the sample size is small, see also Chapter 7). Altogether, this confirms that the 7 variables with a CV above 15% can be defined as noisy and are not important for group differentiation. Important to note is that these noisy variables, marked in grey in Table 5.3, all represent very low intensity signals. Among them, 5 are not identified, 1 is specific for a single metabolite, and 1 specific for two or more metabolites. Despite of this reduction in variables, all metabolites are still represented, either via a unique signal or via a composite signal.

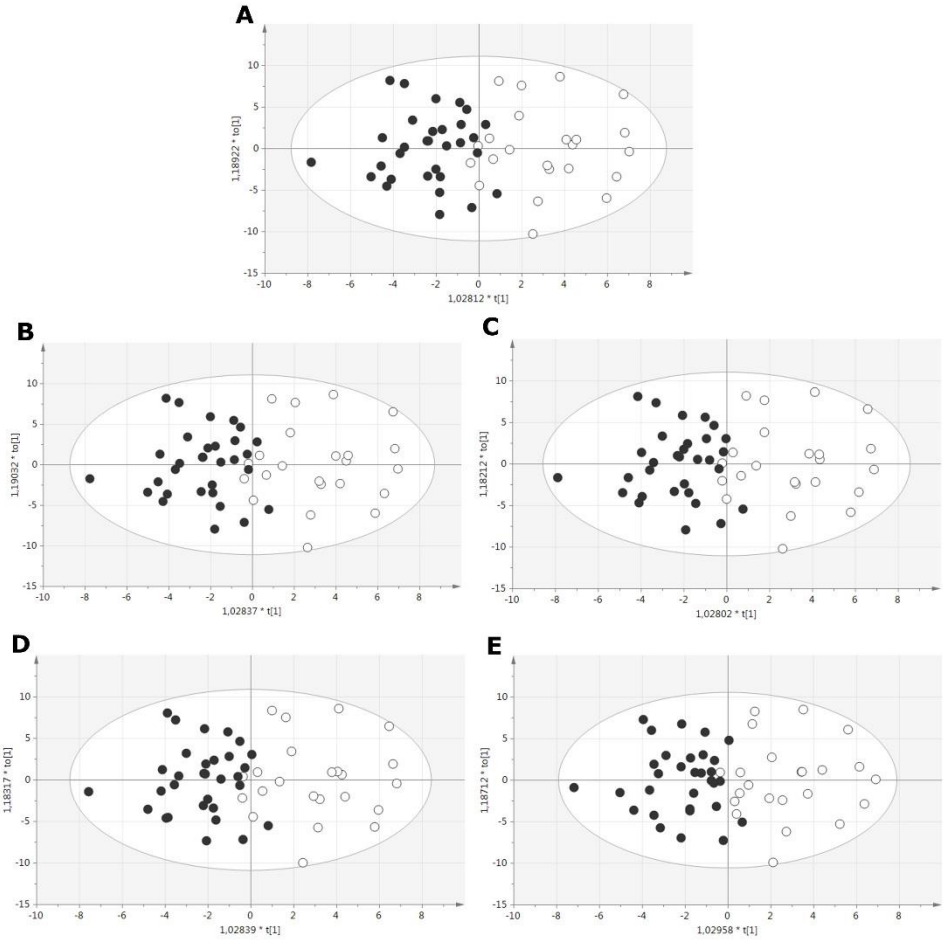

Figure 5.7 Urine OPLS-DA score plots of the models build with all 134 variables (A), with 130 variables (B), with 127 variables (C), with 124 variables (D) and with 106 variables (E). Variables exceeding a predefined threshold for the CV, i.e. 20 % (B), 15 % (C), 10 % (D) and 5 % (E) were assigned as 'noisy' and excluded for the building of the classifier. Obese patients are marked as ● and healthy controls as ○. The first predictive component t[1] explains the variation between both study groups and the first orthogonal component to[1] explains the variation within both study groups.

In a next step, the influence of removing these noisy variables on the predictive accuracy of the classification was examined in the independent validation cohort (Table 5.9). Removal of the noisy variables leads to an increase in predicted specificity from 62% to 69%.

5.4 Conclusion

By spiking 32 and 27 aliquots of respectively a reference human plasma and urine pool with known metabolites, the chemical shift values of these metabolites were determined with high accuracy in the biofluid under study. Hereby, the ^{1}H-NMR spectrum of human blood plasma and urine could be rationally divided into respectively 110 and 134 well-defined integration regions, paving the way towards a better understanding of disturbances in the underlying biochemical pathways. For both plasma and urine, the influence of noisy variables – defined as variables exceeding a premised threshold for the coefficient of variation of 15% for both plasma and urine – on model classification was investigated. Applying the proposed methodology on plasma allowed to discriminate a case-control training dataset of 43 obese and 25 normal-weight children with a sensitivity and specificity of respectively 100% and 96% using OPLS-DA multivariate statistics. For urine, the proposed methodology allowed to discriminate a case-control training dataset of 32 obese and 24 normal-weight children with a sensitivity and specificity of respectively 97% and 83% using OPLS-DA multivariate statistics. A general observation was that the number of noisy variables appearing in the ^{1}H-NMR spectra of plasma is higher as compared to urine. This can be explained by the higher intensity of signals observed in the urine ^{1}H-NMR spectra compared to these of plasma. In addition to an evaluation of the influence of noisy variables on the discrimination power of the training set, we also applied the constructed classifiers (models) to a small but independent validation cohort. In the plasma validation study consisting of 22 obese and 12 normal-weight subjects, the model with a 15% threshold level for the coefficient of variation resulted in a predicted sensitivity of 100% and specificity of 67%. In the urine validation study consisting of 16 obese and 13 normal-weight subjects, the model with a 15% threshold level for the coefficient of variation resulted in a predicted sensitivity of 75% and specificity of 69%. Although the training and validation cohorts are rather small, the proposed methodology seems promising and might offer new possibilities for future research, e.g. to discriminate between metabolically "healthy" and unhealthy obese subjects or between subjects with and without antipsychotica-induced weight gain. However, as the performance of the model for urine was still too low due to the limited number of subjects in the study, we decided to focus further research only on plasma.

References

1. Nicholson JK, Wilson ID. Understanding 'global' systems biology: metabonomics and the continuum of metabolism. Nat Rev Drug Discov. 2003;2(8):668-76.
2. German JB, Hammock BD, Watkins SM. Metabolomics: building on a century of biochemistry to guide human health. Metabolomics. 2005;1(1):3-9.
3. Wishart DS. Quantitative metabolomics using NMR. Trends Analyt Chem. 2008;27(3):228-37.
4. Zheng C, Zhang S, Ragg S, Raftery D, Vitek O. Identification and quantification of metabolites in 1H NMR spectra by Bayesian model selection. Bioinformatics. 2011;27(12):1637-44.
5. O'Connell TM. Recent advances in metabolomics in oncology. Bioanalysis. 2012;4(4):431-51.
6. Salek RM, Maguire ML, Bentley E, Rubtsov DV, Hough T, Cheeseman M, et al. A metabolomic comparison of urinary changes in type 2 diabetes in mouse, rat, and human. Physiol Genomics. 2007;29(2):99-108.
7. Garcia E, Andrews C, Hua J, Kim HL, Sukumaran DK, Szyperski T, et al. Diagnosis of early stage ovarian cancer by 1H NMR metabonomics of serum explored by use of a microflow NMR probe. J Proteome Res. 2011;10(4):1765-71.
8. Wang L, Chen J, Chen L, Deng P, Bu Q, Xiang P, et al. 1H-NMR based metabonomic profiling of human esophageal cancer tissue. Mol Cancer. 2013;12:25.
9. Chang D, Weljie A, Newton J. Leveraging latent information in NMR spectra for robust predictive models. Pac Symp Biocomput. 2007;12:115-26.
10. Staab JM, O'Connell TM, Gomez SM. Enhancing metabolomic data analysis with Progressive Consensus Alignment of NMR Spectra (PCANS). BMC Bioinformatics. 2010;11(1):123.
11. Kohl SM, Klein MS, Hochrein J, Oefner PJ, Spang R, Gronwald W. State-of-the art data normalization methods improve NMR-based metabolomic analysis. Metabolomics. 2012;8(1):146-60.
12. van den Berg RA, Hoefsloot HC, Westerhuis JA, Smilde AK, van der Werf MJ. Centering, scaling, and transformations: improving the biological information content of metabolomics data. BMC Genomics. 2006;7(1):142.
13. Beckonert O, Keun HC, Ebbels TM, Bundy J, Holmes E, Lindon JC, et al. Metabolic profiling, metabolomic and metabonomic procedures for NMR spectroscopy of urine, plasma, serum and tissue extracts. Nat Protoc. 2007;2(11):2692-703.
14. Yang W, Wang Y, Zhou Q, Tang H. Analysis of human urine metabolites using SPE and NMR spectroscopy. Science in China Series B: Chemistry. 2008;51(3):218-25.
15. Markley JL, Ulrich EL, Berman HM, Henrick K, Nakamura H, Akutsu H. BioMagResBank (BMRB) as a partner in the Worldwide Protein Data Bank (wwPDB): new policies affecting biomolecular NMR depositions. J Biomol NMR. 2008;40(3):153-5.
16. Wishart DS, Jewison T, Guo AC, Wilson M, Knox C, Liu Y, et al. HMDB 3.0-The Human Metabolome Database in 2013. Nucleic Acids Res. 2012;41:D801-7.
17. Kriat M, Vion-Dury J, Confort-Gouny S, Favre R, Viout P, Sciaky M, et al. Analysis of plasma lipids by NMR spectroscopy: application to modifications induced by malignant tumors. J Lipid Res. 1993;34(6):1009-19.
18. Bouatra S, Aziat F, Mandal R, Guo AC, Wilson MR, Knox C, et al. The human urine metabolome. PLoS One. 2013;8(9):e73076.
19. Louis E, Bervoets L, Reekmans G, De Jonge E, Mesotten L, Thomeer M, et al. Phenotyping human blood plasma by ^{1}H-NMR: a robust protocol based on metabolite spiking and its evaluation in breast cancer. Metabolomics. 2015;11(1):225-36.

Chapter 6

Influence of preanalytical sampling conditions on the ^{1}H-NMR metabolic profile of human blood plasma and introduction of the Standard PREanalytical Code used in biobanking

Based on:

Liene Bervoets[1*], Evelyne Louis[1*], Gunter Reekmans[2], Liesbet Mesotten[1,3], Michiel Thomeer[1,4], Peter Adriaensens[2], Loes Linsen[5] (2015) **Influence of preanalytical sampling conditions on the ^{1}H-NMR metabolic profile of human blood plasma and introduction of the Standard PREanalytical Code used in biobanking.** *Metabolomics* DOI: 10.1007/s11306-015-0774-y

[*]These authors contributed equally to this work

[1]Faculty of Medicine and Life Sciences, Hasselt University, Hasselt, Belgium; [2]Institute for Materials Research, Hasselt University, Hasselt, Belgium; [3]Department of Nuclear Medicine, Ziekenhuis Oost-Limburg, Genk, Belgium; [4]Department of Respiratory Medicine, Ziekenhuis Oost-Limburg, Genk, Belgium; [5]University Biobank Limburg and Laboratory of Experimental Hematology, Jessa Hospital, 3500 Hasselt, Belgium

Abstract

Variations in sample collection, processing and storage within the field of clinical metabolomics might hamper its effective implementation. In this study, the impact of relevant preanalytical conditions on the ^{1}H-NMR metabolic profile of blood plasma was examined. The biobanking community recently developed a method for coding preanalytical conditions called the Standard PREanalytical Code (SPREC). It is envisaged that SPREC will ultimately identify which samples are fit for a particular analysis, based on prior validation by a panel of experts in the respective field. In an effort to validate SPREC for ^{1}H-NMR-based plasma metabolomics, we have coded the conditions used here, when possible, according to SPREC and evaluated its power to identify preanalytical conditions that affect the ^{1}H-NMR metabolic profile of plasma. ^{1}H-NMR metabolic profiles of blood subjected to a double lithium-heparin concentration at collection, a short-term exposure to an oxidative atmosphere, hemolysis, different processing delays (time between collection and centrifugation) and storage procedures were investigated in 20 healthy volunteers. The studied preanalytical conditions were annotated and evaluated with SPREC version 2. From all preanalytical conditions studied, only prolonged processing delays (3 h and 8 h) have a significant impact on the plasma ^{1}H-NMR metabolic profile as compared to the reference condition (30 min). Principal component analysis shows a clear systematic shift as a function of increasing processing delay. Nevertheless, the inter-individual variation is clearly much larger than this preanalytical variation, indicating that the impact on multivariate group classification will be minimal. Nonetheless, we recommend to keep the time gap between blood collection and centrifugation similar for all samples within a study. The implementation of SPREC within clinical metabolomics allows for an appropriate sample encoding and exclusion of samples that were subjected to unwanted, interfering preanalytical conditions. Without doubt, it will contribute to the validation of ^{1}H-NMR metabolomics in clinical, biobank and multicenter research settings.

6.1 Introduction

Metabolomics is a powerful tool to detect metabolites in biological samples. It has great promise for the discovery of novel clinical biomarkers and the elucidation of disease-specific pathways to improve prognosis, diagnosis and therapy [1-5]. Metabolomics research is mainly based on MS and/or NMR spectroscopy combined with multivariate statistics in order to understand and interpret the resulting data [6-8]. NMR-based metabolomics has several advantages which make it highly suitable for clinical implementation. First, it can be used to study biofluids (e.g. plasma or serum and urine) and second, requires only limited sample preparation and processing [9]. Plasma gives a direct read-out of the systemic metabolism at the time of sampling [10] and is preferred over serum in laboratory medicine, because it is more time-saving, has a higher yield and prevents coagulation-induced interferences [11]. For ^{1}H-NMR analysis, lithium-heparin (LiHe) is described as the most suitable anticoagulant for the collection of plasma samples because it shows no interfering signals in the ^{1}H-NMR spectrum in contrast to EDTA or citrate [12, 13].

Nevertheless, due to the nature of the clinical setting, samples can be subjected to preanalytical variations in collection, processing and storage procedures. Additionally, the high number of samples needed for discovery and validation metabolomics is often gathered from multiple research centers, clinics or biobanks, increasing the likelihood of discrepancies between sample handling [9]. It has been described for LC-MS-based metabolomics in particular that preanalytical changes can have a major impact on the quality of samples, impeding interpretation of analytical results and decreasing the credibility of research outcomes [14-18]. As this can potentially affect clinical implementation of metabolomics, it is clear that the impact of clinical sources of preanalytical bias on the plasma ^{1}H-NMR metabolome needs to be elucidated.

Although efforts are currently made within the field of metabolomics to move towards defining standard operation procedures (SOPs) for preanalytical handling [19], complete standardization of the preanalytical processing is not yet feasible between and within clinical settings. Alternatively, application of a preanalytical sample code that traces and manages these variations would allow sample harmonization. Hereto, the Standard Preanalytical Code (SPREC) was developed within the field of biobanking [20, 21]. This is an easy to implement and

comprehensive tool, consisting of seven elements that document the critical preanalytical details of biospecimens. However, its value within clinical metabolomics remains to be evaluated.

To investigate the potential of metabolomics for implementation in the clinic, we examined the impact of relevant preanalytical conditions on the plasma ^{1}H-NMR metabolic profile. The preanalytical protocols used in this study were encoded according to SPREC in order to evaluate their power with respect to the identification of preanalytical conditions that affect the plasma ^{1}H-NMR metabolic profile. This was done in order to contribute to the validation of SPREC in clinical metabolomics.

6.2 Material and methods

6.2.1 Subjects

Twenty volunteers (8 males and 12 females) aged between 21 and 72 (median age: 32 years) were included in the study. The study participants consisted of university staff and controls, who were recruited in 2013 as participants in another metabolomics study conducted at Ziekenhuis Oost-Limburg (Genk, Belgium). All subjects had fasted at least 12 h before blood collection. The study was conducted in accordance with the ethical rules of the Helsinki Declaration and Good Clinical Practice, and was approved by the ethical committees of Jessa Hospital and Hasselt University. All participants gave written informed consent prior to inclusion in the study.

6.2.2 Sample collection, preparation and storage

Blood samples were collected into 10 ml LiHe tubes (BD Vacutainer® LH 17 I.U.) at 9 am according to the World Health Organization guidelines on drawing blood [22]. An overview of the entire study protocol is presented in Figure 6.1. The reference processing protocol consisted of keeping the freshly drawn blood for 5 min at RT, followed by a 30 min incubation on ice, 15 min centrifugation at 1600 g at 4°C and subsequent storage at -80°C in 1 ml cryovials as 350 µl aliquots (Figure 6.1).

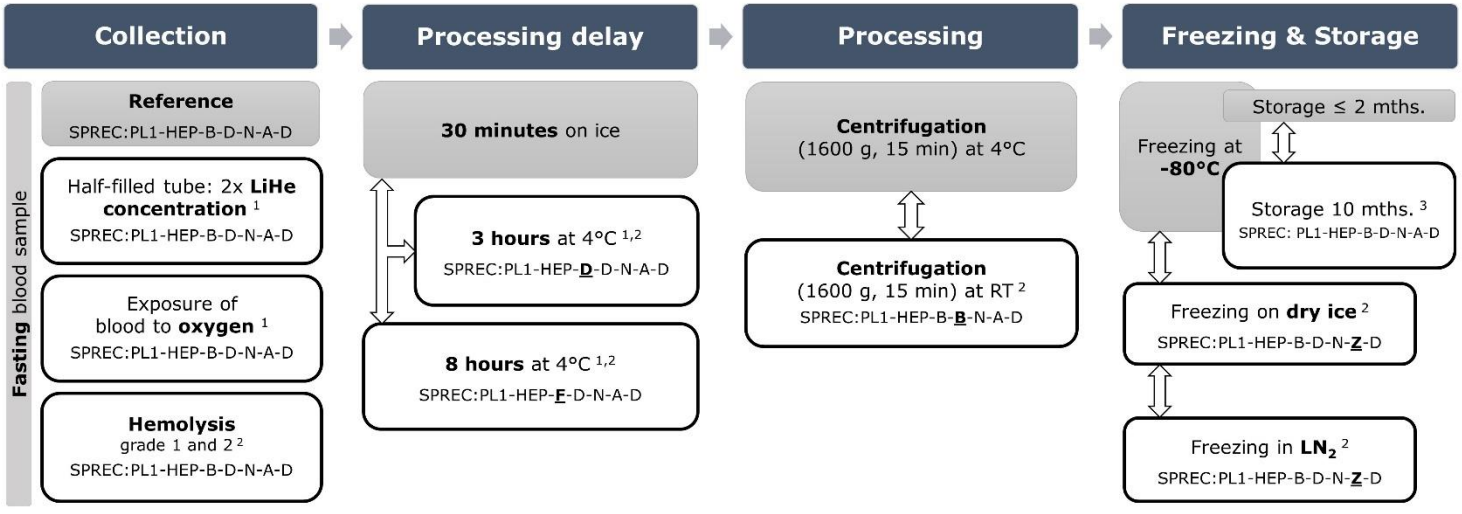

Figure 6.1 Overview of the study protocol for plasma. Fasting blood samples were obtained and handled according to the reference protocol (grey boxes) or subjected to several preanalytical conditions: (1) a double LiHe concentration or an oxidative atmosphere, in combination with a processing delay of 3 h or 8 h at 4°C was investigated in study group 1 (n=6); (2) hemolysis grade 1 and 2, a processing delay of 3 h and 8 h at 4°C, centrifugation at RT, and 8 h freezing on dry ice or in LN_2 was examined in study group 2 (n=6); (3) storage of plasma aliquots during 10 months at -80°C was studied in study group 3 (n=10). SPREC annotations that are different from the reference are indicated in bold and are underlined. LiHe: lithium-heparin; LN_2: liquid nitrogen; mths: months; SPREC: Standard PREanalytical Code.

In *study group 1* (n=6), a double concentration of LiHe was obtained by drawing only 5 ml blood in the 10 ml tube. Short-term exposure to an oxidative atmosphere was acquired by transferring blood from the primary tube to another. Blood samples subjected to both preanalytical conditions were also subjected to a subsequent 3 h and 8 h processing delay at 4°C to determine potential cumulative effects. In *study group 2* (n=6), hemolysis grade 1 (moderate) and 2 (strong) was induced by putting the blood samples directly on dry ice for three and six minutes, respectively [23]. The free hemoglobin concentration was determined on a Roche/Hitachi MODULAR P analyzer (D-BIL Cobas, Roche Diagnostics, Mannheim, Germany). Hemolysis grade 1 corresponds to a free hemoglobin concentration ≥ 10 mg/dl and hemolysis grade 2 to a concentration ≥ 100 mg/dl (H index, manual MODULAR P analyzer). The effect of a variable processing delay was examined as described for study group 1. To examine the effect of centrifugation temperature, blood samples were centrifuged at 4°C or RT after a standard processing delay of 30 min on ice. To examine freezing procedure effects, plasma was aliquoted into 1 ml cryovials and immediately stored at -80°C or kept for 8 h on dry ice before storage at -80°C or kept in liquid nitrogen (LN_2) for 8 h before storage at -80°C. The effect of plasma storage duration at -80°C in *study group 3* (n=10) was determined by storing the samples at -80°C for 2 and 10 months.

6.2.3 ^{1}H-NMR sample preparation

Plasma aliquots were thawed at room temperature immediately followed by centrifugation at 13000 g for 4 min at 4°C. Next, 200 µl plasma supernatant was added to 600 µl deuterium oxide (D_2O, 99.9%, Cambridge Isotope Laboratories Inc., Andover, USA) containing 0.3 µg/µl trimethylsilyl-2,2,3,3-tetradeuteropropionic acid (TSP, 98%, Cambridge Isotope Laboratories Inc., Andover, USA) as a chemical shift reference. Samples were placed on ice until ^{1}H-NMR analysis.

6.2.4 ^{1}H-NMR analysis

^{1}H-NMR analysis was performed as described in Chapter 5: 5.2.3 ^{1}H-NMR analysis. To account for experimental variability, samples were measured in a random order and in duplicate. To exclude inter-operator variability, samples were prepared,

measured and post-processed by the same operator. All samples were measured within one month.

6.2.5 Spectral processing

See Chapter 5: 5.2.4 Spectral processing.

6.2.6 Statistical and spectral analysis

Statistical analyses were performed on the basis of the 110 spectral integration regions which were defined and consequently numbered as previously described (see Chapter 5) [24]. To study influences of preanalytical conditions on the plasma ^{1}H-NMR profile, multivariate statistics was performed (SIMCA-P^{+}, Version 13.0.3, Umetrics, Umeå, Sweden). Plasma samples were measured in duplicate, and the averaged value for each variable was used in the multivariate statistics. After mean-centering and Pareto scaling (weighted by 1/√SD of the mean-centered value, i.e. less weight is assigned to high-intensity signals) of all plasma variables, unsupervised PCA was performed to identify patterns or clusters. The variance structure of the data is explained through linear combinations of the VARs, i.e. PCs. The first PC explains the largest variance within the dataset, followed by the second and third PCs. This multivariate analysis was performed by means of the 110 VAR_{PL} which were defined and numbered as previously described (see Chapter 5). Additionally, as 27 of the 110 plasma variables were assigned as 'noisy', i.e. having a threshold of 15% for the coefficient of variation, the multivariate analysis was also performed by using only the remaining 83 VAR_{PL} (see Chapter 5). However, no significant differences were detected as can be seen for the processing delay of blood (Figure 6.2) as an example.

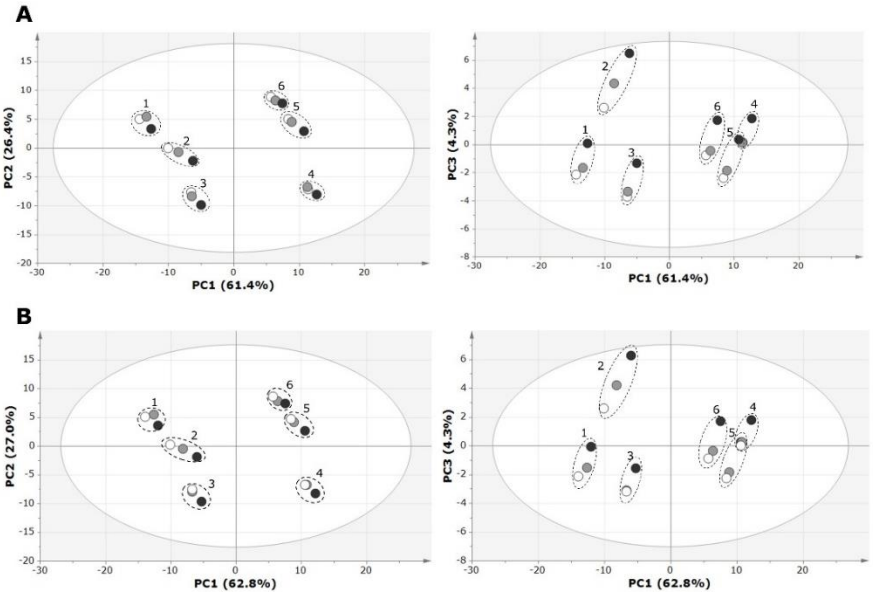

Figure 6.2 PCA score plots showing the influence of processing delay (time between blood collection and centrifugation) and made by using (A) all 110 integration values and (B) only the 83 'non-noisy' integration values of the plasma ^{1}H-NMR spectra. Plasma samples originating from blood processed after a delay of 30 min (○, reference), 3 h (◍) and 8 h (●). No significant differences are observed between the two plots.

Therefore, multivariate analyses were performed by using all 110 VAR_{PL}. To explore the discriminating variables more in detail, univariate statistics was performed on data obtained from all measurements (e.g. for a double LiHe concentration, measurements of the six samples and their duplicates, n=12) (IBM SPSS Statistic; Version 22, IBM Corp., Armonk, NY, USA). Since univariate statistics is more prone to noise compared to multivariate statistics, the 27 plasma noisy variables were excluded. Univariate statistical analyses were accomplished by non-parametric testing (Kruskal-Wallis test for more than two groups or Mann-Whitney U test for two groups). P values smaller than 0.05 are considered significant.

6.3 Results and discussion

Nowadays, the powerful combination of analytical techniques and multivariate statistics is increasingly used to study differences between healthy and diseased subjects and to discover disease-related biomarkers in clinical metabolomics [25]. Because clinical metabolomics seems to shed new light on i) biochemical pathways involved in the etiology of diseases, ii) disease diagnosis and iii) new markers to judge therapy response [26], it is crucial to ensure its robustness, i.e. its reproducibility and accuracy. In other words, the variability should be under tight control in a clinical setting, ensuring that differences in the metabolic profile are resulting from the physiological status and not from differences in preanalytical sampling conditions such as collection, preparation and storage procedures [17, 27, 28]. Preanalytical conditions which induce variation surpassing the inter-individual variation should be avoided (or samples collected under such conditions removed from the study).

6.3.1 Impact of a double LiHe concentration on the plasma metabolome

Due to time constraints or incorrect blood drawing in routine clinical practice, blood collection tubes can be under-filled leading to an increased concentration of the anticoagulant in the blood. To our knowledge, a possible influence on the plasma metabolome has not been investigated before. To this end, ^{1}H-NMR spectra of plasma obtained from half-filled blood tubes (double LiHe concentration) were compared with those from plasma obtained via a reference protocol (reference plasma) as described in Figure 6.1. Furthermore, we investigated a possible confounding time-dependent effect by subjecting both the reference and conditioned sample to a processing delay of 3 h and 8 h at 4°C. As shown in the PCA score plots of Figure 6.3A, the plasma metabolome of blood subjected to a double LiHe concentration (△) could not be discriminated from that of reference plasma (○), also not after a processing delay of 8 h. As the inter-individual variation is clearly exceeding this preanalytical variation, it can be concluded that plasma samples originating from blood collected in LiHe tubes which are only half-filled are still reliable for ^{1}H-NMR metabolomics. On the other hand, a clear and systematic change is observed as a function of increasing

processing delay which can be attributed to alterations in the concentration of pyruvate and lactate (see below).

6.3.2 Impact of short-term exposure of blood to an oxidative atmosphere on the plasma metabolome

While blood collection using a vacuum collection tube holder is standard practice, it sometimes cannot be applied (e.g. in pediatric setting). Consequently, blood will be exposed to an oxidative atmosphere during transfer from syringe to tube, which might initiate specific enzymatic/chemical reactions [19]. Here, we examined whether a short-term exposure of blood to an oxidative atmosphere induces changes in the plasma metabolome as compared to reference plasma (Figure 6.1). Furthermore, we investigated a possible confounding time-dependent effect by subjecting both the reference and conditioned sample to a processing delay of 3 h and 8 h at 4°C. As shown in the PCA score plots of Figure 6.3B, the plasma metabolome of blood subjected to an oxidative atmosphere (∆) could not be discriminated from that of reference plasma (○), also not after a processing delay of 8 h. As the inter-individual variation is clearly exceeding this preanalytical variation, it can be concluded that a short exposure of blood to an oxidative atmosphere does not affect the plasma ^{1}H-NMR metabolic profile. On the other hand, again a clear and systematic change is observed as a function of increasing processing delay which can be attributed to alterations in the concentration of pyruvate and lactate (see below).

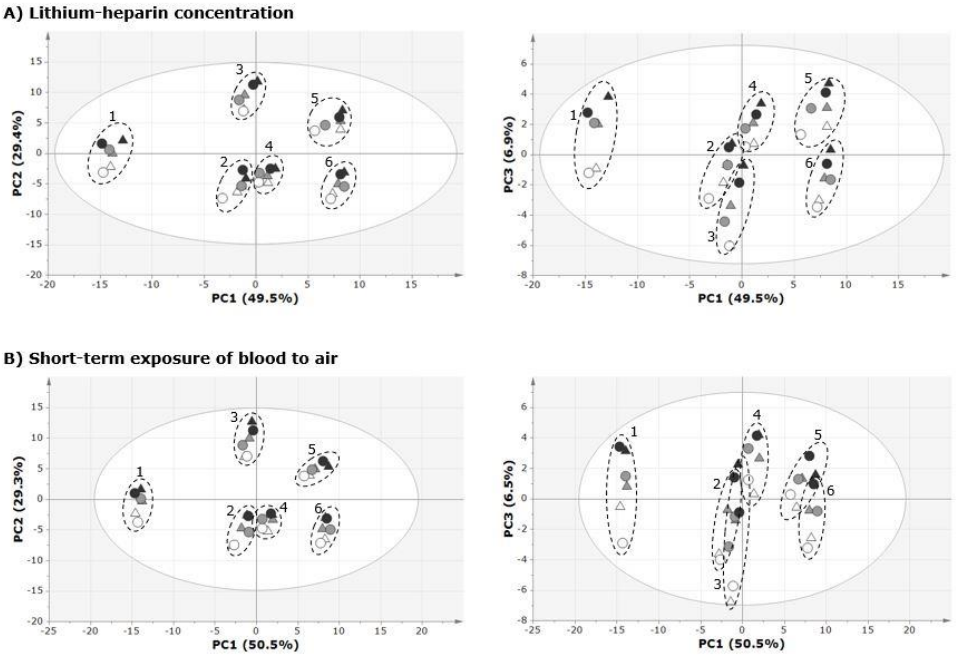

Figure 6.3 PCA score plots showing the influence of a double lithium-heparin (LiHe) concentration (A) and oxidative atmosphere (B), made by the 110 integration regions of the plasma ^{1}H-NMR spectra of study group 1 (n=6). Plasma samples originating from blood exposed to a double concentration of LiHe or oxidative atmosphere (Δ) as compared to reference plasma (○). Blood samples processed after a processing delay of 30 min (white; reference), 3 h (grey) and 8 h (black).

6.3.3 Effect of hemolysis on the plasma metabolome

Hemolysis frequently occurs in clinical routine because of incorrect blood drawing techniques, e.g. improper choice of venipuncture site, prolonged tourniquet time, blood collection through a peripheral IV catheter or exposure to excessive heat or cold [23, 29, 30]. The release of hemoglobin and intracellular species in the plasma due to red blood cell lysis affects several biochemical laboratory tests [31-33]. Nevertheless, the effect on the human plasma ^{1}H-NMR metabolome has to our knowledge not yet been investigated. Hereto, moderate hemolysis (grade 1) and severe hemolysis (grade 2) were induced by exposing blood to excessive cold and the degree of hemolysis was defined on the basis of the concentration of free hemoglobin. No significant differences were observed between the reference and hemolytic plasma metabolomes (Figure 6.4A). This in contrast to Yin et al. who found 69 species to be significantly altered in moderate and severe hemolytic plasma by non-targeted LC-MS [17]. However, as LC-MS requires a more extensive sample preparation (e.g. extractions) and has increased sensitivity

compared to NMR [17, 34, 35], it is consequently also more prone to preanalytical variation. In summary, we can conclude that hemolysis does not affect the plasma ^{1}H-NMR metabolic profile.

6.3.4 Impact of processing delay on the plasma metabolome

Because of clinical sample flow, it is often not possible to process blood immediately after collection. Moreover, samples have to be transferred to on- or offsite laboratories for analysis, which can take up to several hours. Therefore, the effect of an increasing processing delay between blood collection and centrifugation was examined, i.e. delays of 3 h and 8 h at 4°C were compared to the reference protocol (i.e. 30 min on ice). The PCA score plot shows a clear and systematic change as a function of increasing processing delay (Figure 6.4B), as was already observed previously (see Figure 6.2).

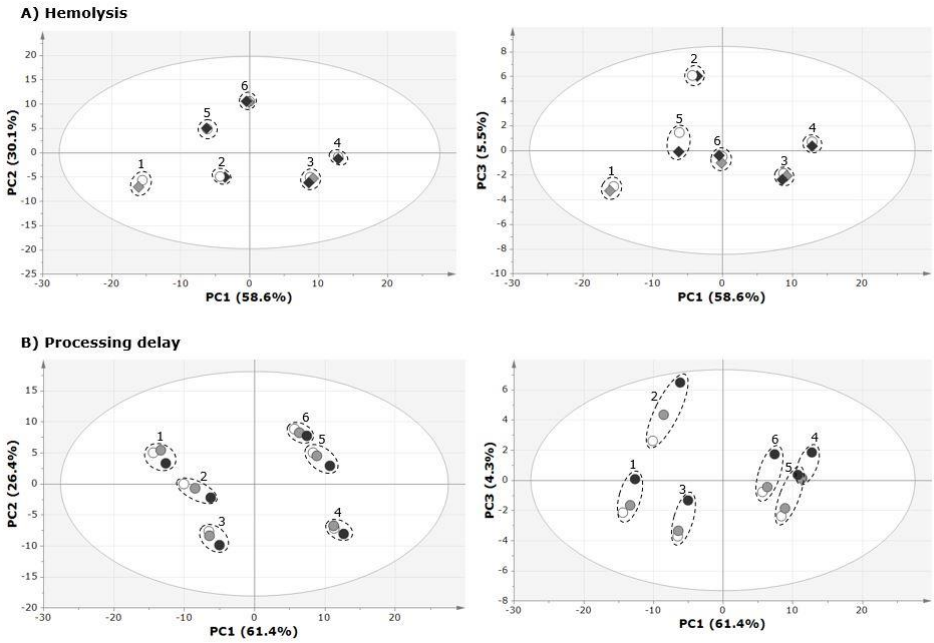

Figure 6.4 PCA score plots showing the influence of hemolysis (A) and processing delay (B), made by the 110 integration regions of the plasma ^{1}H-NMR spectra from study group 2 (n=6). Plasma samples without hemolysis (A; ○, reference), with hemolysis grade 1 (A; ♦) and hemolysis grade 2 (A; ♦). Plasma samples originating from blood processed after a delay of 30 min (B; ○, reference), 3 h (B; ●) and 8 h (B; ●).

In order to find out which metabolites are responsible, univariate statistics was performed of which the outcome demonstrates that processing after 3 h instead of 30 min results in a significant decrease of the pyruvate signal between 2.405-2.399 ppm (VAR80: p = 0.023) (Figure 6.5). Processing after 8 h induces an additional rise of lactate signals between 4.175-4.111 ppm (VAR28: p = 0.019 and VAR29: p = 0.028) and between 1.374-1.345 ppm (VAR99: p = 0.016) next to a downward trend in the glucose signal between 3.536-3.398 ppm (VAR54: p = 0.049).

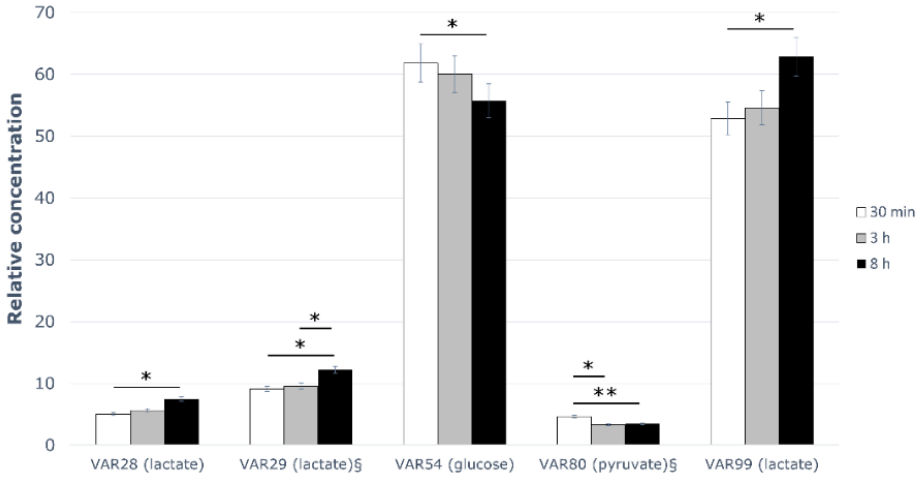

Figure 6.5 Relative concentrations of lactate, pyruvate and glucose in plasma originating from a cooled blood sample which is processed after 30 min (white), 3 h (grey) and 8 h (black). The mean value, obtained from all measurements per condition, are presented with an error bar 95% CI. §Relative concentrations of lactate (VAR29) and pyruvate (VAR80) were multiplied by 10 for a better representation. VAR: variable. * P < 0.05; ** P = 0.005.

Presumably, these changes are attributable to a continued anaerobic cell metabolism due to the contact with erythrocytes, i.e. in the erythrocytes, pyruvate is reduced to lactate by lactate dehydrogenase by which NAD^+ is regenerated so that additional glycolysis occurs [36]. For serum, Fliniaux et al. report no impact when blood is kept at 4°C during a processing delay from 4 h to 24 h but report changes in lactate and glucose concentrations upon storage at RT [27]. In agreement with our findings, Bernini et al. report a decreased plasma concentration of pyruvate when blood is kept at 4°C and further confirm that preservation at 4°C causes less profound changes as compared to RT [19]. Nevertheless our results show that increasing the processing delay affects lactate, pyruvate and glucose concentrations, the inter-individual variation is clearly much

larger than this preanalytical variation, indicating that the impact of a processing delay at 4°C of up to 8 h on a multivariate cluster analysis will be minimal (for a variable to contribute significantly to the differentiating power of a statistical classifier which differentiates between groups of healthy and diseased subjects, its variation between the groups has to be larger than within the groups). Nonetheless, we recommend to keep the time gap between blood collection and centrifugation similar for all samples within a study.

6.3.5 Effect of centrifugation temperature on the plasma metabolome

To slow down enzymatic activity, it is standard practice in metabolomics to cool samples around 4°C during processing [19]. However, since a refrigerated centrifuge is not always accessible, the impact of centrifugation at RT was examined. No significant difference was found between centrifugation at RT or 4°C (Figure 6.6A), indicating that 15 min centrifugation time is too short to induce changes in pre-cooled samples and therefore has no significant impact on the plasma ^{1}H-NMR metabolic profile.

6.3.6 Impact of freezing procedure on the plasma metabolome

In metabolomics, it is common practice to store plasma aliquots immediately at -80°C to ensure a quench of the metabolism and to allow ^{1}H-NMR measurements in larger sample series. However, since not all laboratories have a -80°C freezer, samples are often transported to another laboratory for processing and storage. Hereto, plasma samples are kept temporarily on dry ice (-78.5°C) or in liquid nitrogen (LN_2; -196°C). Alternatively, it is common practice in biobanks to snap-freeze plasma samples in LN_2 to quickly attenuate biochemical activity and to preserve structural integrity [21]. Nevertheless, and to our knowledge, the effect of different freezing conditions on the plasma ^{1}H-NMR metabolic profile has not been examined before. As shown in Figure 6.6B, our experimental data show no significant differences between plasma samples immediately stored at -80°C (reference plasma) and samples kept for 8 h on dry ice or in LN_2 before storage at -80°C.

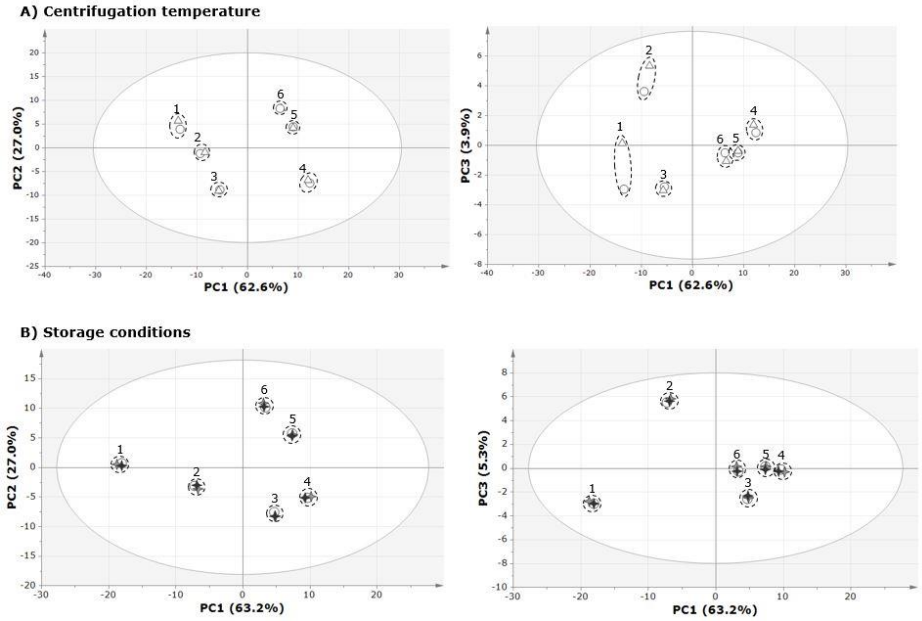

Figure 6.6 PCA score plots showing the influence of centrifugation temperature (A) and initial plasma freezing on dry ice or in LN_2 (B), made by the 110 integration regions of the plasma ^{1}H-NMR spectra from study group 2 (n=6). Plasma samples originating from blood centrifuged at 4°C (A; ○ , reference) or at RT (A; ∆). Plasma samples stored directly at -80°C (B; ○ , reference), and after a delay of 8 h on dry ice (B; ✦) or 8 h in LN_2 (B; ✦).

6.3.7 Effect of storage duration at -80°C on the plasma metabolome

Often, the delay between sample storage and effective measurement can exceed several months, especially when samples are stored in biobanks. However, long-term storage might modify interactions between macromolecules and small molecules such as amino acids and consequently affect their plasma ^{1}H-NMR signals, introducing non-disease related artefacts [37]. Additionally, long-term storage might induce a shift of some of the metabolite signals due to a change in pH [37]. To investigate whether the duration of plasma storage at -80°C has an impact on ^{1}H-NMR results, we compared plasma of 10 controls stored at -80°C for two and ten months, respectively. No significant differences were detected as shown in Figure 6.7, indicating that plasma is stable at -80°C for at least 10 months, being in line with the findings of Deprez et al. [37] who demonstrated that rat plasma is stable for up to 6 months at -80°C. Furthermore, Pinto et al. showed that human plasma is stable for up to 30 months when stored at -80°C [28].

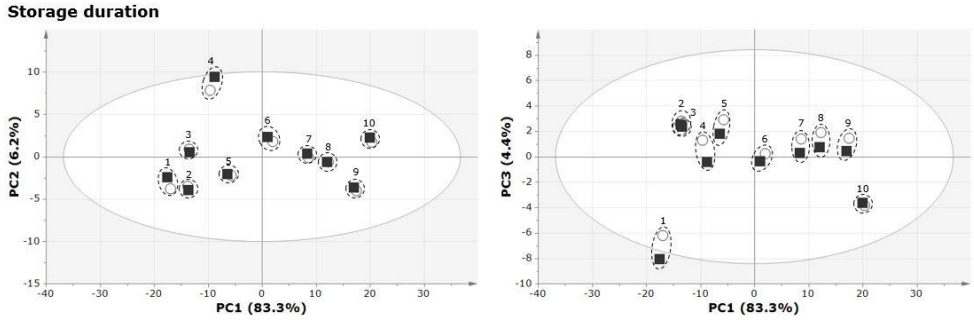

Figure 6.7 PCA score plots showing the influence of storage duration at -80°C, made by the 110 integration regions of the plasma ^{1}H-NMR spectra from study group 3 (n=10). Plasma samples stored for maximum 2 months (○, reference) and for 10 months (■) at -80°C.

6.3.8 Evaluation of SPREC to document preanalytical variation in clinical ^{1}H-NMR-based metabolomics

SPREC was developed within the biobank environment to facilitate documentation and communication of the most important preanalytical quality parameters for different types of research biospecimens [20, 21]. It allows to exclusively select samples that are fit for the purpose aimed for, while excluding samples that were subjected to unwanted, interfering preanalytical conditions. While it has become a standard within the biobank field, it is relatively unknown in other clinical settings and its usefulness therein remains to be determined. However, its implementation in clinical laboratories is rather straightforward as the 7 elements of SPREC can easily be extracted from the Laboratory Information Management System. We annotated the samples of our study with SPREC version 2 and evaluated if this is in agreement with our experimental findings and of practical value in clinical metabolomics [21]. As shown below, this study clearly illustrate the value of SPREC to encode relevant preanalytical conditions and fully support its implementation in clinical metabolomics.

As shown in Figure 6.1 and Table 6.1, the reference condition is translated as single spun plasma samples – primary container with LiHe (without gel) – pre-centrifugation delay 2-10°C < 2 h – centrifugation at 2-10°C 10-15 min < 3000 g (with braking) – no second centrifugation – post-centrifugation delay < 1 h 2-10°C – long-term storage in cryovial 1 to 2 ml at -85°C to -65°C, which is encoded as PL1-HEP-B-D-N-A-D. Hemolysis, exposure to oxygen and insufficient tube filling (i.e. increased LiHe concentration) are not contained within the current version of SPREC, resulting in an identical code as the reference condition. This is

not disadvantageous, however, as these variations did not introduce significant differences in the plasma ^{1}H-NMR metabolic profile. Differences in centrifugation temperature and freezing method are encoded within SPREC version 2, but also did not induce differences in the ^{1}H-NMR metabolome. Interestingly, the processing delays of 3 h and 8 h, which induce a systematic variation in the plasma metabolome, are discriminated by the SPREC codes, i.e. PL1-HEP-**D**-D-N-A-D and PL1-HEP-**F**-D-N-A-D, respectively. This means that SPREC allows to select plasma samples with a known time gap between blood collection and centrifugation for metabolomics applications. To further test the potential of SPREC, we expanded this evaluation to plasma samples which were subjected to other preanalytical conditions as described by Pinto et al. [28]. Again, SPREC identifies the conditions that affect the plasma ^{1}H-NMR metabolic profile (Table 6.1). In addition to plasma, Fliniaux et al. previously introduced SPREC into the field of serum ^{1}H-NMR analysis for biobanks [27]. These combined plasma and serum studies clearly illustrate the value of SPREC to encode relevant preanalytical conditions and fully support its implementation in clinical metabolomics.

Table 6.1 SPREC annotation for preanalytical conditions tested in plasma samples by ^{1}H-NMR spectroscopy.

Condition	SPREC	Impact on ^{1}H-NMR profile?
Reference sample	PL1-HEP-B-D-N-A-D	No
Double LiHe concentration	PL1-HEP-B-D-N-A-D	No
Oxygen exposure	PL1-HEP-B-D-N-A-D	No
Hemolysis	PL1-HEP-B-D-N-A-D	No
Processing delay 3 h at 4°C	PL1-HEP-**D**-D-N-A-D	Yes
Processing delay 8 h at 4°C	PL1-HEP-**F**-D-N-A-D	Yes
Centrifugation at RT	PL1-HEP-B-**B**-N-A-D	No
Freezing on dry ice	PL1-HEP-B-D-N-Z-D	No
Freezing in LN_2	PL1-HEP-B-D-N-Z-D	No
Storage at -80°C (for 10 mths)	PL1-HEP-B-D-N-A-D	No (storage time$^{\$}$)
Reference sample Pinto et al.*	PL1-HEP-A^{1}-D-N-X-A^{2}	No
EDTA additive	PL1-**SED**-A^{1}-D-N-X-A^{2}	Yes
Processing delay 2,5-21 h at RT*	PL1-HEP-**C/E/G/I**-D-N-X- A^{2}	Yes
Storage at -20°C (for 1 mth)*	PL1-HEP-A^{1}-D-N-X-**B**^{2}	Yes (storage time$^{\$}$)
Freeze/thaw cycles*	PL1-HEP-A^{1}-D-N-X-A^{2}	Yes$^{\$}$
Non-fasting donor*	PL1-HEP-A^{1}-D-N-X-A^{2}	No$^{\$}$

*: conditions obtained from Pinto et al. [28]; ^{1}: assumption preprocessing delay at RT; ^{2}: assumption storage in standard polypropylene tube; $^{\$}$: beyond scope of SPREC as no true preanalytical condition; impacting elements of SPREC are indicated in bold. SPREC: Standard PREanalytical Code; LiHe: lithium-heparin; RT: room temperature; LN: liquid nitrogen; EDTA: ethylenediaminetetraacetic acid.

6.4 Conclusion

Since metabolomics is gaining increasing interest for clinical biomarker research, knowledge of its sensitivity to variations in sample collection, processing and storage becomes essential in the discussions regarding its clinical implementation. Our results show no significant impact of a double LiHe concentration, a short-term exposure to an oxidative atmosphere, hemolysis, centrifugation temperature, freezing procedure and storage duration at -80°C on the ^{1}H-NMR plasma metabolic profile. Only increasing the processing delay from 30 min to 3 h and 8 h has a significant impact on the plasma concentration of pyruvate, lactate and glucose. Presumably, these changes are attributable to a continued anaerobic cell metabolism due to the contact with erythrocytes, i.e. in the erythrocytes, pyruvate is reduced to lactate by lactate dehydrogenase by which NAD^{+} is regenerated so that additional glycolysis occurs [36]. Nevertheless, as the inter-individual variation is still much larger than the preanalytical variation, the impact on multivariate group classification will be minimal. Nonetheless, we recommend to keep the time gap between blood collection and centrifugation similar for all samples within a study. Hereto, the implementation of SPREC within clinical metabolomics can be of great value as it allows for an appropriate sample encoding and exclusion of samples that were subjected to unwanted, interfering preanalytical conditions. Without doubt, SPREC will contribute to the validation of ^{1}H-NMR metabolomics in clinical, biobank and multicenter research settings.

References

1. Brindle JT, Antti H, Holmes E, Tranter G, Nicholson JK, Bethell HW, et al. Rapid and noninvasive diagnosis of the presence and severity of coronary heart disease using 1H-NMR-based metabonomics. Nat Med. 2002;8(12):1439-45.
2. Fiehn O. Metabolomics–the link between genotypes and phenotypes. Plant Mol Biol. 2002;48(1-2):155-71.
3. Madsen RK, Lundstedt T, Gabrielsson J, Sennbro C-J, Alenius G-M, Moritz T, et al. Diagnostic properties of metabolic perturbations in rheumatoid arthritis. Arthritis Res Ther. 2011;13(1):R19.
4. Zhang A, Sun H, Wang X. Power of metabolomics in biomarker discovery and mining mechanisms of obesity. Obes Rev. 2013;14(4):344-9.
5. Shen J, Yan L, Liu S, Ambrosone CB, Zhao H. Plasma metabolomic profiles in breast cancer patients and healthy controls: by race and tumor receptor subtypes. Transl Oncol. 2013;6(6):757.
6. Van der Greef J, Tas A, Bouwman J, Ten Noever de Brauw M, Schreurs W. Evaluation of field-desorption and fast atom-bombardment mass spectrometric profiles by pattern recognition techniques. Anal Chim Acta. 1983;150:45-52.
7. Nicholson JK, Lindon JC, Holmes E. 'Metabonomics': understanding the metabolic responses of living systems to pathophysiological stimuli via multivariate statistical analysis of biological NMR spectroscopic data. Xenobiotica. 1999;29(11):1181-9.
8. Lindon JC, Nicholson JK. Spectroscopic and statistical techniques for information recovery in metabonomics and metabolomics. Annu Rev Anal Chem. 2008;1:45-69.
9. Teahan O, Gamble S, Holmes E, Waxman J, Nicholson JK, Bevan C, et al. Impact of analytical bias in metabonomic studies of human blood serum and plasma. Anal Chem. 2006;78(13):4307-18.
10. Nicholson JK, Holmes E, Kinross JM, Darzi AW, Takats Z, Lindon JC. Metabolic phenotyping in clinical and surgical environments. Nature. 2012;491(7424):384-92.
11. World Health Organization. Use of anticoagulants in diagnostic laboratory investigations. Geneva: 2002.
12. Nicholson JK, Buckingham MJ, Sadler PJ. High resolution 1H-NMR studies of vertebrate blood and plasma. Biochem J. 1983;211:605-15.
13. Nicholson JK, Foxall PJ, Spraul M, Farrant RD, Lindon JC. 750 MHz 1H and 1H-13C NMR spectroscopy of human blood plasma. Anal Chem. 1995;67(5):793-811.
14. Dunn WB, Broadhurst D, Ellis DI, Brown M, Halsall A, O'Hagan S, et al. A GC-TOF-MS study of the stability of serum and urine metabolomes during the UK Biobank sample collection and preparation protocols. Int J Epidemiol. 2008;37(Suppl 1):i23-i30.
15. Wood JT, Williams JS, Pandarinathan L, Courville A, Keplinger MR, Janero DR, et al. Comprehensive profiling of the human circulating endocannabinoid metabolome: clinical sampling and sample storage parameters. Clin Chem Lab Med. 2008;46(9):1289-95.
16. Yang W, Chen Y, Xi C, Zhang R, Song Y, Zhan Q, et al. Liquid chromatography–tandem mass spectrometry-based plasma metabonomics delineate the effect of metabolites' stability on reliability of potential biomarkers. Anal Chem. 2013;85(5):2606-10.
17. Yin P, Peter A, Franken H, Zhao X, Neukamm SS, Rosenbaum L, et al. Preanalytical aspects and sample quality assessment in metabolomics studies of human blood. Clin Chem. 2013;59(5):833-45.
18. Kamlage B, Maldonado SG, Bethan B, Peter E, Schmitz O, Liebenberg V, et al. Quality markers addressing preanalytical variations of blood and plasma processing identified by broad and targeted metabolite profiling. Clin Chem. 2014;60(2):399-412.
19. Bernini P, Bertini I, Luchinat C, Nincheri P, Staderini S, Turano P. Standard operating procedures for pre-analytical handling of blood and urine for metabolomic studies and biobanks. J Biomol NMR. 2011;49(3-4):231-43.
20. Betsou F, Lehmann S, Ashton G, Barnes M, Benson EE, Coppola D, et al. Standard preanalytical coding for biospecimens: defining the sample PREanalytical code. Cancer Epidem Biomar. 2010;19(4):1004-11.

21. Lehmann S, Guadagni F, Moore H, Ashton G, Barnes M, Benson E, et al. Standard preanalytical coding for biospecimens: review and implementation of the Sample PREanalytical Code (SPREC). Biopreserv Biobank. 2012;10(4):366-74.
22. World Health Organization. WHO guidelines on drawing blood: best practices in phlebotomy. Geneva: 2010.
23. Kroll MH, Elin RJ. Interference with clinical laboratory analyses. Clin Chem. 1994;40(11):1996-2005.
24. Louis E, Bervoets L, Reekmans G, De Jonge E, Mesotten L, Thomeer M, et al. Phenotyping human blood plasma by ^{1}H-NMR: a robust protocol based on metabolite spiking and its evaluation in breast cancer. Metabolomics. 2015;11(1):225-36.
25. Issaq HJ, Van QN, Waybright TJ, Muschik GM, Veenstra TD. Analytical and statistical approaches to metabolomics research. J Sep Sci. 2009;32(13):2183-99.
26. Collino S, Martin FP, Rezzi S. Clinical metabolomics paves the way towards future healthcare strategies. Br J Clin Pharmacol. 2013;75(3):619-29.
27. Fliniaux O, Gaillard G, Lion A, Cailleu D, Mesnard F, Betsou F. Influence of common preanalytical variations on the metabolic profile of serum samples in biobanks. J Biomol NMR. 2011;51(4):457-65.
28. Pinto J, Domingues MRM, Galhano E, Pita C, do Céu Almeida M, Carreira IM, et al. Human plasma stability during handling and storage: impact on NMR metabolomics. Analyst. 2014:1168-77.
29. Kennedy C, Angermuller S, King R, Noviello S, Walker J, Warden J, et al. A comparison of hemolysis rates using intravenous catheters versus venipuncture tubes for obtaining blood samples. J Emerg Nurs. 1996;22(6):566-9.
30. Burns ER, Yoshikawa N. Hemolysis in serum samples drawn by emergency department personnel versus laboratory phlebotomists. Lab Med. 2002;33(5):378-80.
31. Yucel D, Dalva K. Effect of in vitro hemolysis on 25 common biochemical tests. Clin Chem. 1992;38(4):575-7.
32. Lippi G, Salvagno GL, Montagnana M, Brocco G, Guidi GC. Influence of hemolysis on routine clinical chemistry testing. Clin Chem Lab Med. 2006;44(3):311-6.
33. Koseoglu M, Hur A, Atay A, Cuhadar S. Effects of hemolysis interferences on routine biochemistry parameters. Biochem Med (Zagreb). 2011;21(1):79-85.
34. Kentgens A, Bart J, Van Bentum P, Brinkmann A, Van Eck E, Gardeniers J, et al. High-resolution liquid-and solid-state nuclear magnetic resonance of nanoliter sample volumes using microcoil detectors. J Chem Phys. 2008;128(5):052202.
35. Felli IC, Brutscher B. Recent advances in solution NMR: fast methods and heteronuclear direct detection. Chem Phys Chem. 2009;10(9-10):1356-68.
36. Baynes JW, Dominiczak MH. Medical Biochemistry. Amsterdam: Elsevier; 2010. 712 p.
37. Deprez S, Sweatman BC, Connor SC, Haselden JN, Waterfield CJ. Optimisation of collection, storage and preparation of rat plasma for 1H NMR spectroscopic analysis in toxicology studies to determine inherent variation in biochemical profiles. J Pharm Biomed Anal. 2002;30(4):1297-310.

Chapter 7

Search for biomarkers of obesity-related metabolic alterations in children and adolescents using ^{1}H-NMR-based metabolic profiling

In preparation for submission:

Liene Bervoets[1], Guy Massa[1,2], Wanda Guedens[3], Gunter Reekmans[3], Jean-Paul Noben[4], Peter Adriaensens[3] (2015) **Search for biomarkers of obesity-related metabolic alterations in children and adolescents using ^{1}H-NMR-based metabolic profiling.**

[1] Faculty of Medicine and Life Sciences, Hasselt University, Hasselt, Belgium; [2] Department of Pediatrics, Jessa Hospital, Hasselt, Belgium; [3] Institute for Materials Research, Hasselt University, Hasselt, Belgium; [4] Biomedical Research Institute, Hasselt University, Hasselt, Belgium.

A part of this study was presented by Liene Bervoets at:

- First Belgian-Netherlands Joint symposium on Metabolomics. 13th and 14th May, 2013, Spa, Belgium (oral and poster presentation)
- Young Belgium Magnetic Resonance Scientist (YBMRS), 2nd – 3rd December 2013, Blankenberge, Belgium (poster presentation)
- Knowledge for Growth, 8th May 2014, Ghent, Belgium (poster presentation)

Abstract

Metabolomics is increasingly used as a tool to study metabolic pathways that play a role in obesity, however, its implementation in pediatric studies is limited. The main objective of this study was to compare blood plasma metabolic profiles of obese and normal-weight children and adolescents using an untargeted ^{1}H-NMR-based metabolomics approach. In addition, plasma metabolic profiles of obese children classified as metabolically "healthy" (MHO) or unhealthy obese (MUO) – i.e. absence or presence, respectively, of the metabolic syndrome defined according to the International Diabetes Federation criteria – were compared and associations with conventional biochemical parameters were explored. Fasting plasma samples of 65 obese (mean BMI: 31.5 ± 5.2 kg/m²) and 37 normal-weight (mean BMI: 18.3 ± 2.3 kg/m²) children and adolescents aged between 8 and 18 (mean age: 13.1 ± 2.4 years) were analyzed by means of ^{1}H-NMR spectroscopy in combination with multivariate statistical analyses. The constructed multivariate statistical model allowed to correctly classify 95% of obese patients and 92% of normal-weight controls with an AUROC of 0.965. It was found that obese children have increased plasma levels of lipids, lactate and N-acetyl glycoproteins, and decreased levels of choline-containing phospholipids, glucose and α-ketoglutarate compared to the normal-weight metabolome. The obese study group was further divided into MHO (n=18), MUO (n=17) and intermediate 'at risk' obese (n=30, left out for statistical analysis) children and adolescents. Although this sample size was small, the plasma metabolic profiles of MHO and MUO phenotypes could be clearly discriminated. It was found that plasma triglyceride concentrations correlated strongly with metabolites that were different between MHO and MUO phenotypes. In conclusion, the present study provides a basis for a better understanding of biochemical mechanisms behind childhood obesity and its metabolic phenotypes. However, future longitudinal research in larger populations is required to substantiate, validate and complement the current findings.

7.1 Introduction

Although the prevalence of childhood obesity is stabilizing [1], numbers are high in developed countries and are still rising in developing countries [2, 3]. Besides, a trend is emerging towards more extreme childhood obesity [4, 5]. It is generally accepted that obesity is caused by a combination of a sedentary lifestyle, the consumption of high-caloric dense food or drinks (often consumed in too large proportion sizes), genetic predisposition, psychosocial factors, toxic substances in the environment and gut microbiota [6]. Obese children and adolescents are at high risk to develop metabolic disorders such as insulin resistance, the metabolic syndrome, type 2 diabetes mellitus, coronary artery diseases and non-alcoholic fatty liver disease [7]. Additionally, the majority of obese children will become also obese as an adult [8]. Although progress is being made to combat childhood obesity, it is of utmost importance to develop effective and targeted prevention and treatment strategies [9]. Hereto, the concept of metabolically "healthy" or protected obesity (MHO) was recently introduced [10, 11]. MHO children are obese, but do not show any metabolic complications [10, 11]. Early screening for metabolically healthy or unhealthy obesity (MUO) might help to refocus current prevention and treatment strategies, and may eventually result in a reduction of health-care costs. However, a good understanding of obesity-related biochemical mechanisms is inevitable for the development of appropriate screening strategies.

In recent years, human-based metabolomics has emerged into a powerful high-throughput tool to accurately identify and quantify metabolites in biofluids such as plasma or urine [12]. The so-called metabolome provides a direct read-out of an organism's clinical phenotype, an indicator of both genetic and environmental (e.g. diet, drug, lifestyle) perturbations [13]. Consequently, the interest in metabolomics as a platform to study the underlying biochemical mechanisms of obesity and related metabolic disorders is increasing [14]. However, metabolomics studies focusing on childhood obesity are still scarce and concern only MS as analytical characterization tool [15, 16]. High resolution ^{1}H-NMR spectroscopy has previously proven to be a robust and reproducible technique to investigate disease mechanisms and might subsequently offer new insights into biochemical pathways associated with childhood obesity [12, 14, 17].

The main objective of this study was to investigate in-depth plasma metabolic profiles of obese and normal-weight children using an untargeted ^{1}H-NMR-based

metabolomics approach. In addition, plasma metabolic profiles of obese children classified as MHO or MUO were examined and associations with conventional biochemical parameters were explored, something that has – to our knowledge – not been considered before.

7.2 Material and methods

7.2.1 Study participants

The study participants included in this study are those of the combined training and validation cohorts of the plasma study of Chapter 5. Overweight or obese (OB) children who underwent an oral glucose tolerance test as part of a multidisciplinary obesity evaluation were recruited at the outpatient pediatric obesity clinic of the Jessa Hospital (Hasselt, Belgium) between February 2012 and December 2013. Normal-weight (NW) children were recruited among the offspring of personnel working at the Jessa Hospital or Hasselt University (Hasselt, Belgium). Inclusion criteria were as follows: (1) aged 8 to 18; (2) normal-weight, overweight or obese according to the IOTF BMI criteria [18]; (3) fasted for at least 8 hours. Subjects taking any medication or having serious chronic or acute illness within two weeks preceding the clinical examination, were excluded from the study. Patients of foreign origin (e.g. Turkish or Moroccan) were classified as non-native. The study was conducted in accordance with the ethical rules of the Helsinki Declaration and Good Clinical Practice. The study protocol was approved by the medical-ethical committees of the Jessa Hospital and Hasselt University (Hasselt, Belgium). Informed and written consent was obtained from all study participants and their parents or legal guardian.

7.2.2 Anthropometric measurements

The pubertal developmental stage was determined according to Tanner by clinical examination or self-assessment using realistic color images [19, 20]. Tanner stage was determined on the basis of breast development and genital size and was categorized into three groups: pre-pubertal (Tanner stage I), pubertal (Tanner stage II-IV) and post-pubertal (Tanner stage V). All study participants were measured wearing underwear only. Standing height was measured to the nearest 0.1 cm using a Harpenden wall stadiometer, and weight was measured to the nearest 0.1 kg using an electronic balance scale. BMI was calculated by dividing weight in kilograms by height in meters squared (BMI = kg/m^2). BMI SDS was calculated by the LMS method based on the IOTF criteria recently proposed by Cole et al. [18]. Seated blood pressure was measured twice with an electronic

sphygmomanometer (Omron®, Omron Healthcare, IL, USA) according to a validated protocol and the two measurements were averaged [21].

7.2.3 Conventional biochemical analyses

Biochemical laboratory parameters were only assessed in the obese study group. After an overnight fast, venous blood samples were taken for the analysis of the following biochemical parameters: glucose, insulin, HbA1c, HDL-C, triglycerides, LDL-C, AST, ALT, g-GT, uric acid, WBC and SHBG. Plasma glucose was measured by the glucose oxidase method using a Synchron LX20 analyzer (Beckman Coulter, Brea, CA, USA). Serum insulin was determined by immuno-reactive insulin (IRI) assay (ADVIA Centaur Insulin IRI; Siemens Medical Solutions Diagnostics, Tarrytown, NY, USA). Plasma HbA1c was measured using ion exchange chromatography (Menarini HA-8160 HbA1c auto-analyser, Menarini Diagnostics, Belgium). Plasma HDL-C and triglycerides were measured on a Beckman Coulter AU 2700 automatic analyzer (Brea, CA, USA). LDL-C was calculated according to the Friedewald equation [22]. Plasma AST, ALT, g-GT and uric acid were measured on a Beckman Coulter AU 2700 automatic analyzer (Brea, CA, USA). WBC was automatically assessed using Siemens Advia 2120 (Siemens Healthcare Diagnostics, Deerfield, IL, USA). Serum SHBG concentration was measured by immunoassay on an Architect i2000SR (Abbott Diagnostics, Ill., USA).

7.2.4 Definition of metabolically "healthy" obesity

We applied the first classification strategy described in Chapter 4 to determine metabolic risk status. This strategy (MR_{IDF}) is based on the absence or presence of the metabolic syndrome defined according to the criteria of the International Diabetes Federation (IDF) consensus for children older than 10 years [23] and was previously also applied by other researchers [10, 24]. Metabolically "healthy" obese (MHO) were classified as being obese (defined according to the IOTF criteria) but having none of the components of the metabolic syndrome, and metabolically unhealthy obese (MUO) children were classified as being obese and having two or more components. Apart from obesity, the metabolic syndrome is defined as having two or more of the following abnormalities: (1) HDL-C < 40 mg/dl (females 16 years or older: HDL-C < 50 mg/dl) (2) triglycerides ≥ 150

mg/dl; (3) SBP ≥ 130 mm Hg or DBP ≥ 85 mm Hg; (4) FPG ≥ 100 mg/dl. A group that fell in-between the classification of MHO and MUO was termed metabolically "at-risk" obese, however, this group was not included for statistical analyses.

7.2.5 ^{1}H-NMR analysis

Fasting venous blood samples were collected (BD Vacutainer® LH 17 I.U. 6 ml tube) and consequently processed as described in Chapter 5: 5.2.2 Sample collection, preparation and storage. Plasma ^{1}H-NMR analysis was performed as described in Chapter 5: 5.2.3 ^{1}H-NMR analysis. Spectra were processed as described in Chapter 5: 5.2.4 Spectral processing.

7.2.6 Statistical analyses

Univariate statistical analyses

Differences in descriptive characteristics between patients and controls were examined using univariate statistical analyses (IBM SPSS version 20.0, SPSS Inc., Chicago, IL, USA). Distribution of the data was tested with the Kolmogorov-Smirnov test. To compare normally distributed continuous variables between patient and control groups, the independent samples *t* test was used and results are presented as mean ± SD. Non-normally distributed variables were tested with non-parametric Mann-Whitney *U* test and are presented as median (interquartile range (IQR)). Post-hoc Benjamini-Hochberg method was used to correct for multiple testing. Chi square test of association ($n \geq 10$) or Fisher exact probability test ($n < 10$) was applied to test nominal or ordinal variables between two or more groups. For 3 x 2 contingency tables with $n < 10$, the Freeman-Halton extension of the Fisher exact probability test was used. Nominal or ordinal scale variables are presented as a number with percentage (%). Spearman's correlation analysis was performed to test for associations between conventional biochemical parameters and plasma variables most strongly discriminating between MHO and MUO (as determined by multivariate statistics, see below). All p-values smaller than 0.05 are considered significant. To reduce the chances of obtaining false-positive results (type I errors), Bonferroni corrected p-values were applied.

Multivariate statistical analyses

Multivariate statistical analyses were performed as described in Chapter 5. The most important discriminating plasma variables (VAR_{PL}) between patient and control groups were defined on the basis of their variable influence on projection (VIP) value that had to be greater than 1. Some of these VAR_{PL} (integration regions) result from a single metabolite. In case a VAR_{PL} contains signals of more metabolites, the following procedure was used to define the most contributing metabolite: (i) visual inspection of characteristic metabolite J-patterns and their intensities in ^{1}H-NMR spectra for the respective VAR_{PL}, and (ii) confirmation of the observed concentration increase/decrease by means of evaluating the concentration of other integration regions in which the same metabolite appears.

If the model was strong, the area under the receiver operating characteristic (AUROC) curve was determined to quantify the overall ability of the test to discriminate between the plasma metabolic profile of patient and controls. AUROC was calculated on the basis of sample class prediction during 100 cross validations and was performed using receiver operating characteristic curve explorer and tester (ROCCET) [25]. A permutation plot for PLS-DA was developed to assess the risk that the PLS-DA model is spurious, i.e. if the model fits the training set well but does not predict Y well for new observations (see Chapter 1: Annex p.62).

7.3 Results

7.3.1 Plasma ^{1}H-NMR metabolic profile of obese and normal-weight children and adolescents

Descriptive characteristics of the study population consisting of 65 overweight or obese (OB) and 37 normal-weight (NW) children and adolescents aged between 8 and 18 (mean age: 13.1 ± 2.4 years) are presented in Table 7.1.

Table 7.1 Descriptive characteristics of the study population.

	Overweight or obese (OB)	Normal-weight (NW)	p value
Number, n	65	37	
Age, years	13.1 ± 2.2	13.0 ± 2.7	0.798
Gender, n (%)			0.304
Male	39 (60.0)	18 (48.6)	
Female	26 (40.0)	19 (51.4)	
Ethnicity, n (%)			<0.001
Native	39 (60.0)	36 (97.3)	
Non-native	26 (40.0)	1 (2.7)	
Pubertal stage*, n (%)			0.531
I (pre-pubertal)	14 (21.5)	11 (29.7)	
II-IV (pubertal)	26 (40.0)	13 (35.1)	
V (post-pubertal)	21 (32.3)	9 (24.3)	
BMI, kg/m²	32.0 (6.3)	18.0 (3.4)	<0.001
BMI SDS	2.8 (0.5)	-0.1 (1.1)	<0.001

Values are presented as mean ± SD, median (IQR) or number (percentage). The p-values shown are the result of independent samples t test or Mann Whitney U test between OB and NW study groups. BMI: body mass index, BMI SDS: body mass index standard deviation score. *8 subjects refused clinical examination to determine pubertal stage.

OB and NW subjects do not differ significantly in terms of age, gender and pubertal stage. Ethnicity is significantly different between OB and NW study groups. However, ethnicity is no confounding factor in the discrimination between OB and NW based on the metabolic phenotype (see below). BMI and BMI SDS are significantly higher in OB as compared to NW children and adolescents.

Multivariate statistical analysis was performed on blood plasma obtained from 65 OB and 37 NW study subjects. By means of the PCA score plot, hotelling's T^2 range plot and distance to model (DModX) plot, five statistical outliers (4 OB and 1 NW) were detected and subsequently excluded from the dataset. This resulted in a dataset of 61 OB and 36 NW subjects. With the use of PCA, this dataset was tested for unwanted confounding effects of age, gender, ethnicity and pubertal stage (Figure 7.1).

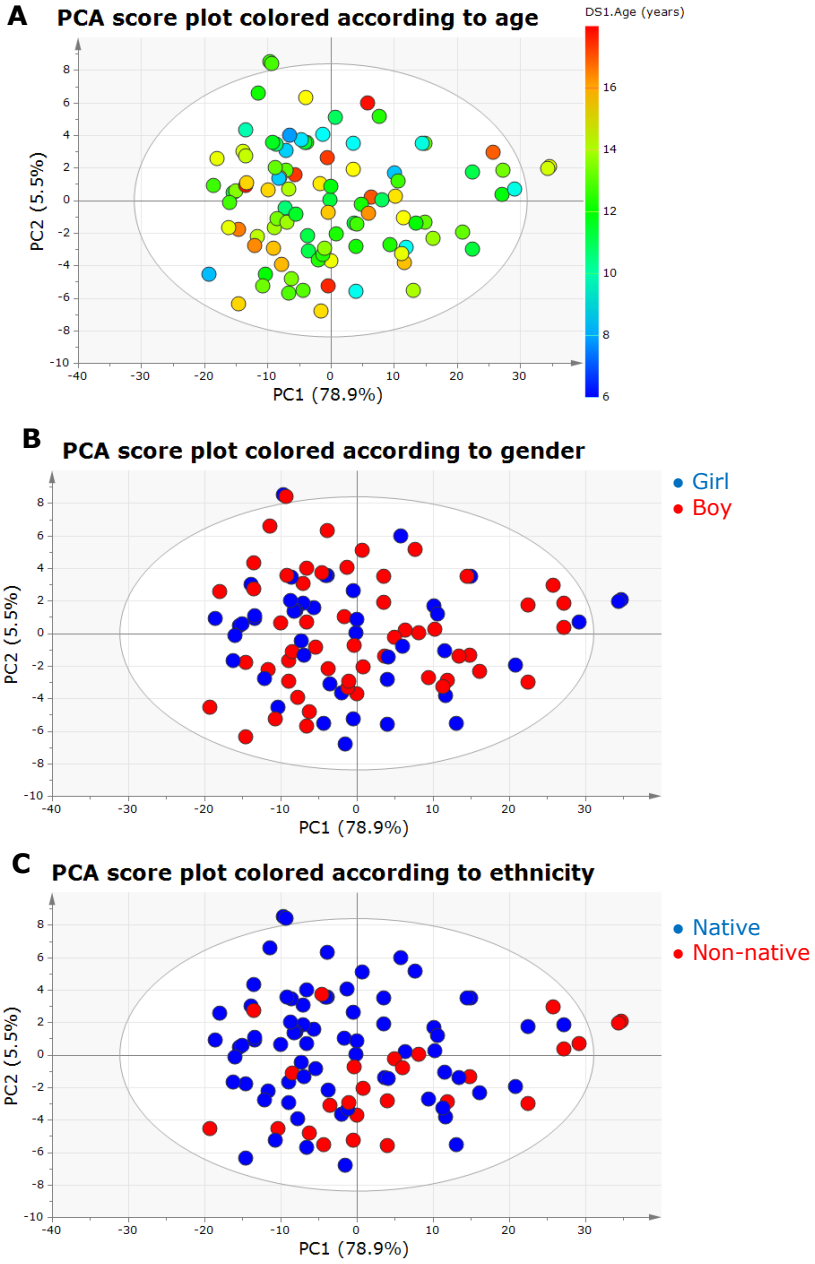

Figure 7.1 (partial). For figure legend see next page.

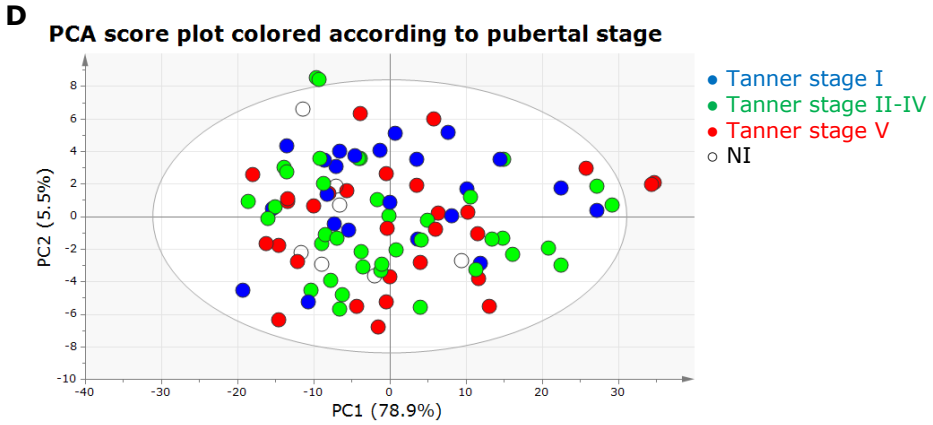

Figure 7.1 PCA score plots colored according to age (A), gender (B), ethnicity (C), and pubertal stage (D). Age (A) is continuously colored according to an age between 8 and 18 yrs; Gender (B) is colored according to girls (blue) and boys (red); Ethnicity (C) is colored according to native (blue) and non-native (red); Pubertal stage (D) is colored according to Tanner stage I (blue), II-IV (green), and V (red) or not identified (white).

For age, gender and pubertal stage, no clustering or patterns were observed in the PCA score plots and consequently these variables are no confounding factors. On the basis of PCA, it is somewhat more difficult to determine whether ethnicity is a confounding factor. Therefore, an OPLS-DA model was constructed in addition to discriminate between native (n=71) and non-native (n=26) subjects (Figure 7.2). The sensitivity and predictive accuracy of this model are poor (sensitivity = 27%, specificity = 93%, Q^2(cum) = 9%). Hence, we can conclude that ethnicity is not a confounding factor.

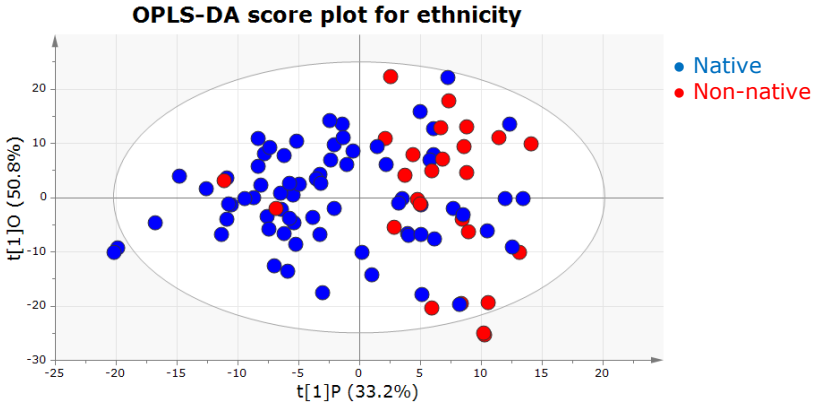

Figure 7.2 Supervised OPLS-DA score plot based on all 110 variables derived from plasma ^{1}H-NMR CPMG spectra of native (blue) and non-native (red) subjects.

The unsupervised PCA model – built with all 110 plasma variables – showed pattern clustering of OB and NW plasma metabolic profiles (Figure 7.3A). The supervised OPLS-DA model – built with all 110 plasma variables – was performed on the case-control dataset to construct a robust model to discriminate between OB and NW (Figure 7.3B). The predictive and orthogonal explained variation in X was 86% (R^2X (cum)) and in Y was 73% (R^2Y (cum)). The model showed a strong predictive ability of 62% (Q^2 (cum)) and allowed to classify 95% (58/61) OB subjects and 92% (33/36) of NW subjects correctly with an AUROC of 0.961 (Table 7.2).

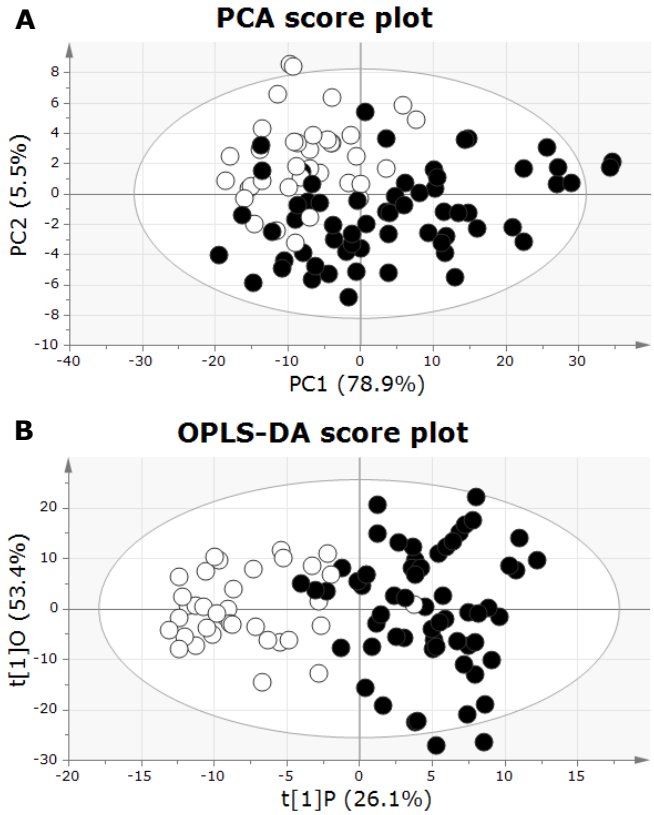

Figure 7.3 Unsupervised PCA score plot (A) and supervised OPLS-DA score plot (B) based on all 110 variables derived from plasma ^{1}H-NMR CPMG spectra of OB (●) and NW (○) subjects. The ^{1}H-NMR metabolic profile of a given subject is plotted as a single point. PC1 (78.9%) and PC2 (5.5%) of the PCA score plot explain the largest and second largest variation within the data, respectively. In the OPLS-DA score plot, the first predictive component (t[1]P: 26.1%) explains the cumulative predictive and orthogonal variation in X, and the first orthogonal component (t[1]O: 53.4%) explains the variation in Y.

To investigate the impact of noisy variables on the model performance, OPLS-DA models were constructed and compared as previously described in Chapter 5 (Table 7.2). ROC-curves were also constructed to determine the AUROC, a quantification of the overall ability of each model to discriminate between OB and NW subjects.

Table 7.2 Multivariate model characteristics (OPLS-DA and ROC analyses) of the plasma ^{1}H-NMR dataset consisting of 61 OB and 36 NW subjects presented according to a decreasing threshold limit for coefficient of variation.

	Threshold limits for coefficient of variation*				
	None	**20%**	**15%**	**10%**	**5%**
Number of remaining VAR_{PL}	110	91	83	69	43
LV	3	3	3	3	3
R^2X (cum)	0.863	0.878	0.893	0.904	0.932
R^2Y (cum)	0.725	0.718	0.721	0.702	0.686
Q^2 (cum)	0.624	0.628	0.636	0.622	0.623
Sensitivity (%)	95.1	95.1	95.1	95.1	95.1
Specificity (%)	91.7	91.7	91.7	91.7	91.7
AUROC (95% CI)	0.961 (0.912 – 0.997)	0.963 (0.914 – 0.998)	0.965 (0.920 – 0.999)	0.961 (0.910 – 0.998)	0.962 (0.912 – 0.997)

*Threshold limits for coefficient of variation from 20 to 5% were used as an exclusion criteria for noisy variables. VAR_{PL}: plasma variables; LV: latent variables; R^2X (cum): cumulative variation within study groups; R^2Y (cum): cumulative variation between study groups; Q^2 (cum): predictive ability (cross-validation); AUROC: area under the ROC-curve.

The model built on the basis of the 15% threshold for the coefficient of variation including 83 variables (27 noisy variables were removed from the entire model), showed the best predictive ability (Q^2(cum) = 64% and AUROC = 0.965) compared to all other models, which is in accordance with results of Chapter 5. Therefore, and because the PLS-DA permutation test confirms the validity of this model, it was selected as the most optimal model and was subsequently used for further analysis (Figure 7.4).

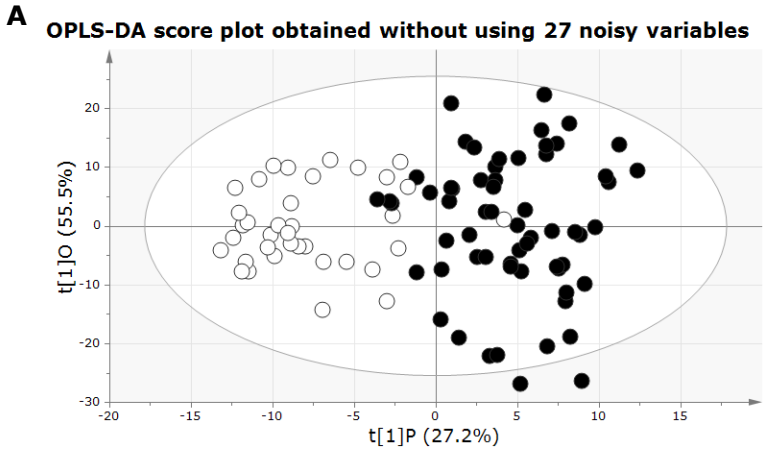

Figure 7.4 (partial). For figure legend see next page.

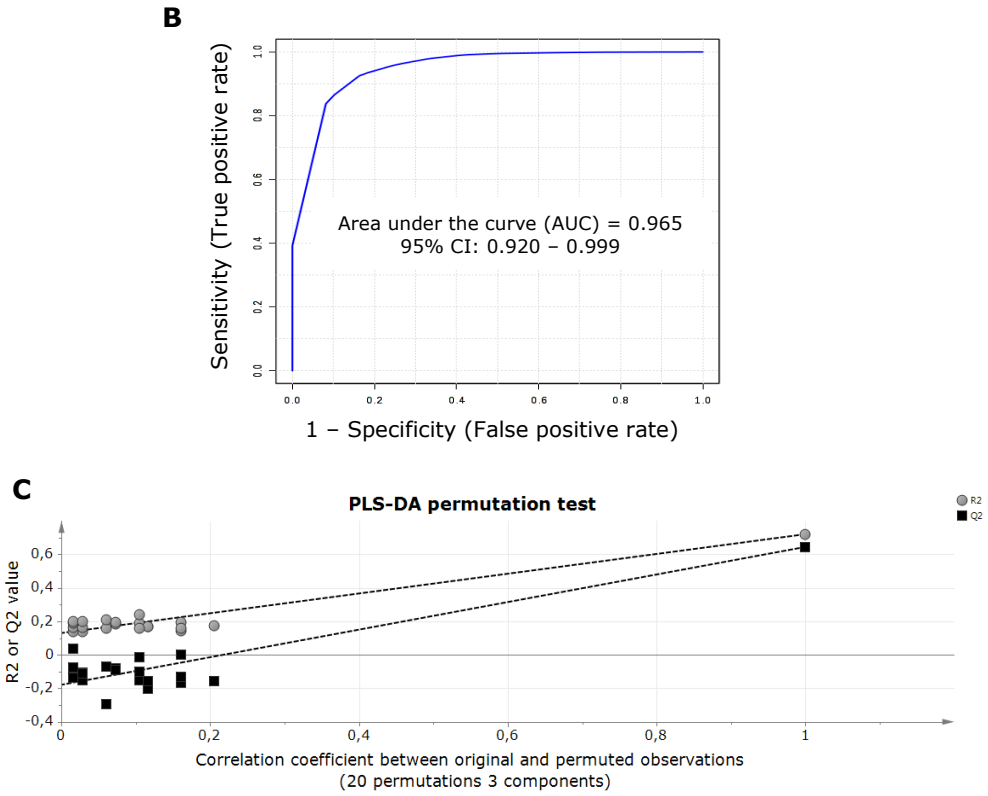

Figure 7.4 Supervised OPLS-DA score plot (A), ROC-curve (B) and PLS-DA permutation test based on 83 variables derived from plasma ^{1}H-NMR CPMG spectra of 61 OB (•) and 36 NW (○) subjects. The ^{1}H-NMR metabolic profile of a given subject is plotted as a single point. In the OPLS-DA score plot (A), the first predictive component (t[1]P: 27.2%) explains the variation between both study groups and the first orthogonal component (t[1]O: 55.5%) explains the variation within both study groups. The overall predictive ability of the reduced model is given by AUC of the ROC-curve (B). The PLS-DA permutation test illustrates the validity of the model (C): For a model to be valid, R^2 (grey dots) and Q^2 (black boxes) values for each permuted observation have to be lower than 0.3 and 0.05, respectively.

To further determine the influence of each plasma variable on the model, a VIP plot was constructed. Only plasma variables having a VIP value exceeding 1 were selected as strong discriminating variables (Table 7.3). $VAR_{PL}100$ represents CH_3-($C\mathbf{H}_2$)$_n$- signals of fatty acid chains. Because in plasma the sum of the average concentration of low-density lipoprotein (LDL) and very low-density lipoprotein (VLDL) is higher than for high-density lipoprotein (HDL), and because LDL and VLDL contain longer fatty acid chains, $VAR_{PL}100$ is mainly reflecting LDL and VLDL concentrations.

Table 7.3 Plasma variables that contributed most to the discrimination between OB and NW subjects with a VIP higher than 1, ranked from strongest to least strong discriminatory power.

VAR_{PL}	Start and end ppm	VIP ± cvSE	Metabolites assigned by spiking experiments	Metabolite most contributing to VAR_{PL}
100	1.3450 – 1.2458	4.07 ± 0.40	Lipids: CH_3-(CH_2)$_n$- in fatty acid chain + L-Isoleucine + L-Threonine	Lipids (mainly VLDL-C and LDL-C): CH_3-(CH_2)$_n$- in fatty acid chain
58	3.3230 – 3.2186	3.74 ± 0.46	L-Arginine + L-Histidine + L-Phenylalanine + L-Tyrosine + D-Glucose + -N^+(CH_3)$_3$ of choline head group in SM/PC	-N^+(CH_3)$_3$ of choline head group in SM/PC
99	1.3740 – 1.3450	2.78 ± 0.22	L-Lactate + L-Threonine	L-Lactate
54	3.5360 – 3.3980	2.46 ± 0.15	L-Proline + D-Glucose + Acetoacetate	D-Glucose
91	2.1230 – 1.9720	2.11 ± 0.32	Lipids: -CH_2-CH=CH- in fatty acid chain + L-Glutamate + L-Methionine + L-Proline + L-Isoleucine + N-acetyl signal of glycoproteins	Lipids: -CH_2-CH=CH- in fatty acid chain + N-acetyl signal of glycoproteins
98	1.4200 – 1.3740	2.06 ± 0.23	L-Lactate	L-Lactate
95	1.6860 – 1.5600	1.74 ± 0.18	Lipids: -CH_2-CH_2-C=O and -CH_2-CH_2-CH=CH in fatty acid chain + L-Arginine + L-Lysine	Lipids: -CH_2-CH_2-C=O and -CH_2-CH_2-CH=CH in fatty acid chain
38	3.9590 – 3.8330	1.64 ± 0.35	L-Aspartate + L-Cysteine + L-Methionine + L-Serine + L-Tyrosine + D-Glucose	D-Glucose
18	5.4300 – 5.2752	1.43 ± 0.20	Lipids: -HC=CH- in fatty acid chain	Lipids: -HC=CH- in fatty acid chain
66	3.0640 – 2.9950	1.32 ± 0.12	L-Cysteine + L-Lysine + L-Tyrosine + α-ketoglutarate	α-ketoglutarate
87	2.2915 – 2.2690	1.26 ± 0.07	Lipids: -CH_2-C=O and -CH_2-CH=CH- in fatty acid chain + L-Valine + L-Methionine	Lipids: -CH_2-C=O and -CH_2-CH=CH- in fatty acid chain
67	2.9950 – 2.8860	1.23 ± 0.22	Lipids: =CH-CH_2-CH= in fatty acid chain + L-Asparagine + α-ketoglutarate	α-ketoglutarate
42	3.7820 – 3.7550	1.17 ± 0.10	L-Alanine + L-Glutamate + L-Glutamine + L-Leucine + L-Lysine + D-Glucose	D-Glucose
21	4.6940 – 4.6620	1.13 ± 0.13	D-Glucose	D-Glucose

VAR_{PL}: plasma variable; VIP: variable influence on projection; cvSE: standard error of cross-validation. LDL-C: low-density lipoprotein cholesterol; NI: non-identified; PC: phosphatidylcholine; SM: sphingomyelin; VLDL-C: very-low density lipoprotein cholesterol.

To explore the model contribution and statistical reliability of these discriminating variables, an S-plot – corresponding to the OPLS-DA score plot – was constructed (Figure 7.5). Plasma variables that correlate positively with the OB phenotype are located in the upper right part, and variables that correlate positively with the NW phenotype are located in the bottom left part of the S-plot. $VAR_{PL}100$ representing lipids (mainly VLDL-C and LDL-C) is most important (VIP value: 4.07 ± 0.40) in the discrimination between OB and NW subjects and is positively correlated with the OB phenotype. $VAR_{PL}100$ has a strong model contribution (p[1]=0.449) and high statistical reliability as discriminating variable (p(corr)[1]=0.512). Also $VAR_{PL}58$ representing choline-containing phospholipids is highly important (VIP value: 3.74 ± 0.46) in the discrimination between OB and NW subjects and is negatively correlated with the OB phenotype. $VAR_{PL}58$ has a strong model contribution (p[1]=-0.411) and high statistical reliability as discriminating variable (p(corr)[1]=-0.746).

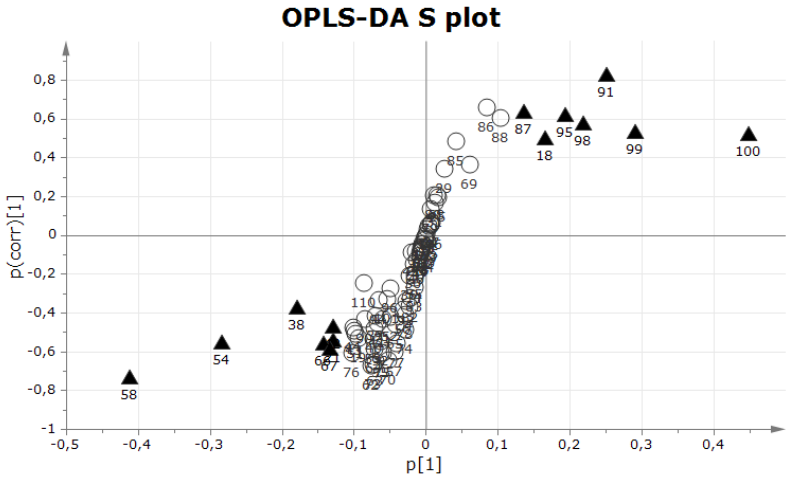

Figure 7.5 Supervised OPLS-DA S-plot based on 83 variables derived from plasma [1]H-NMR CPMG spectra of 61 OB and 36 NW subjects. The S-plot corresponds to the OPLS-DA score plot shown in Figure 7.4. The S-plot is composed of p(corr)[1] and p[1] vectors of the predictive component; p[1] reflects the model contribution of each variable and p(corr)[1] reflects the statistical reliability as discriminating variable. All plasma variables are presented by their unique number. Variables with a VIP > 1 are illustrated as black triangles, and variables with a VIP < 1 are illustrated as white dots.

From multivariate OPLS-DA analysis, it can be derived that OB patients show higher plasma levels of lipids, lactate, and N-acetyl glycoproteins, and lower levels of choline-containing phospholipids, glucose and α-ketoglutarate compared to NW controls. Significant differences between relative concentrations of VAR_{PL} most

strongly discriminating between OB and NW were confirmed by univariate analysis (Table 7.4).

Table 7.4 Relative concentrations of VAR_{PL} differing between OB and NW children.

VAR_{PL}	Metabolite most contributing to VAR_{PL}	OB (n=61)	NW (n=36)	p-value
100	Lipids (mainly VLDL-C and LDL-C): CH_3-(CH_2)$_n$- in fatty acid chain	175.8 ± 41.5	141.1 ± 21.1	$4.06x10^{-7}$
58	-N^+(CH_3)$_3$ of choline head group in SM/PC	61.2 ± 14.2	81.3 ± 7.1	$7.52x10^{-15}$
99	L-Lactate	62.2 ± 16.1	47.1 ± 9.9	$1.25x10^{-7}$
54	D-Glucose	62.9 ± 13.1	74.9 ± 8.1	$2.08x10^{-7}$
91	Lipids: -C**H**$_2$-CH=CH- in fatty acid chain + N-acetyl signal of glycoproteins	69.7 ± 3.8	63.4 ± 3.5	$1.42x10^{-12}$
98	L-Lactate	20.7 ± 7.9	12.9 ± 3.5	$2.14x10^{-9}$
95	Lipids: -C**H**$_2$-CH_2-C=O and -C**H**$_2$-CH_2-CH=CH in fatty acid chain	16.0 ± 5.2	10.6 ± 2.4	$6.31x10^{-10}$
38	D-Glucose	61.3 ± 12.5	68.7 ± 5.9	$1.00x10^{-4}$
18	Lipids: -**H**C=C**H**- in fatty acid chain	31.0 ± 6.3	26.3 ± 3.6	$8.08\ x10^{-6}$
66	α-ketoglutarate	14.1 ± 3.1	17.3 ± 1.9	$1.10x10^{-8}$
87	Lipids: -C**H**$_2$-C=O and -C**H**$_2$-CH=CH- in fatty acid chain	6.3 ± 2.5	3.6 ± 1.1	$6.70x10^{-11}$
67	α-ketoglutarate	10.1 ± 2.5	12.8 ± 1.7	$7.72x10^{-9}$
42	D-Glucose	19.1 ± 3.8	22.1 ± 2.0	$1.85x10^{-6}$
21	D-Glucose	12.8 ± 2.7	15.4 ± 1.9	$5.35x10^{-7}$

Relative concentrations are presented as mean ± SD. All VAR_{PL} were significantly different between OB and NW using the independent samples *t* test with Benjamini-Hochberg correction. LDL-C: low-density lipoprotein cholesterol; NW: normal-weight; OB: overweight or obese; PC: phosphatidylcholine; SM: sphingomyelin; VAR_{PL}: plasma variables; VLDL-C: very-low density lipoprotein cholesterol.

The relative concentrations of VAR_{PL}54, VAR_{PL}38, VAR_{PL}42 and VAR_{PL}21 (VIP value higher than 1) representing glucose are lower for OB compared to NW subjects. To further explore the reliability of this finding, the relative concentrations of all other VAR_{PL} representing glucose in the plasma ^{1}H-NMR spectrum (i.e. VAR_{PL}19, VAR_{PL}39-44 and VAR_{PL}52-53; see Table 5.2 in Chapter 5) were evaluated. It was found that these are all pointing in the same direction – i.e. lower for OB compared to NW subjects – and have a VIP higher than 0.4, indicating reliable findings. The relative concentrations of VAR_{PL}66-67 (VIP value higher than 1) representing α-ketoglutarate are lower for OB compared to NW subjects. The relative concentrations of VAR_{PL}76-77 (VIP value higher than 0.4) representing both α-ketoglutarate (see Table 5.2 in Chapter 5) are also lower for OB compared to NW subjects. VAR_{PL}98-99 representing lactate had a VIP higher than 2.0 and were both higher in OB as compared to NW. Although lactate appears also in VAR_{PL}28-29, the VIP of these variables already becomes lower than 0.3. Except for VAR_{PL}58, signals of lipids (VIP values higher than 0.3) are all pointing in the same direction, i.e. higher in concentration for OB compared to NW subjects. Relative plasma concentrations of choline-containing phospholipids (VAR_{PL}58) are lower for OB compared to NW.

7.3.2 Plasma [1]H-NMR metabolic profile of metabolically "healthy" and unhealthy obese children and adolescents

Descriptive characteristics of the obese study group classified as MHO or MUO according to the absence or presence, respectively, of the metabolic syndrome as defined by the pediatric IDF criteria, are presented in Table 7.5.

Table 7.5 Descriptive characteristics of MHO and MUO children and adolescents.

	MHO	MUO	p-value
Number, n	18	17	
Age, years	13.4 ± 2.0	13.2 ± 2.0	0.552
Gender, n (%)			1.000
Male	10 (55.6)	10 (58.8)	
Female	8 (44.4)	7 (41.2)	
Ethnicity, n (%)			0.041
Native	14 (77.8)	7 (41.2)	
Non-native	4 (22.2)	10 (58.8)	
Pubertal stage, n (%)			0.494
I (pre-pubertal)	4 (22.2)	2 (11.8)	
II-IV (pubertal)	9 (50.0)	7 (41.2)	
V (post-pubertal)	5 (27.8)	8 (47.0)	
BMI, kg/m²	30.8 ± 3.5	33.7 ± 5.0	0.099
BMI SDS	2.7 (0.5)	2.9 (0.5)	0.075

Results of continuous variables are presented as mean ± SD or median (IQR) and nominal or ordinal scale variables are presented as a number with percentage (%). The p-values shown are the result of independent samples t test or Mann Whitney U test between MHO and MUO study groups. BMI: body mass index; BMI SDS: body mass index standard deviation score; MHO: metabolically healthy obese; MUO: metabolically unhealthy obese.

No univariate statistical significant differences were found for age, gender, pubertal stage, BMI and BMI SDS between MHO and MUO subjects. Ethnicity is significantly different between MHO and MUO study groups. However, ethnicity is no confounding factor in the discrimination between MHO and MUO based on the metabolic phenotype (see below).

Multivariate statistical analyses were performed on plasma obtained from 35 OB study subjects classified as MHO or MUO. By means of the PCA score plot, hotelling's T^2 range plot and distance to model (DModX) plot, no statistical outliers were detected. With the use of PCA, the dataset was tested for unwanted confounding effects of age, gender, ethnicity, pubertal stage and BMI SDS (Figure 7.6).

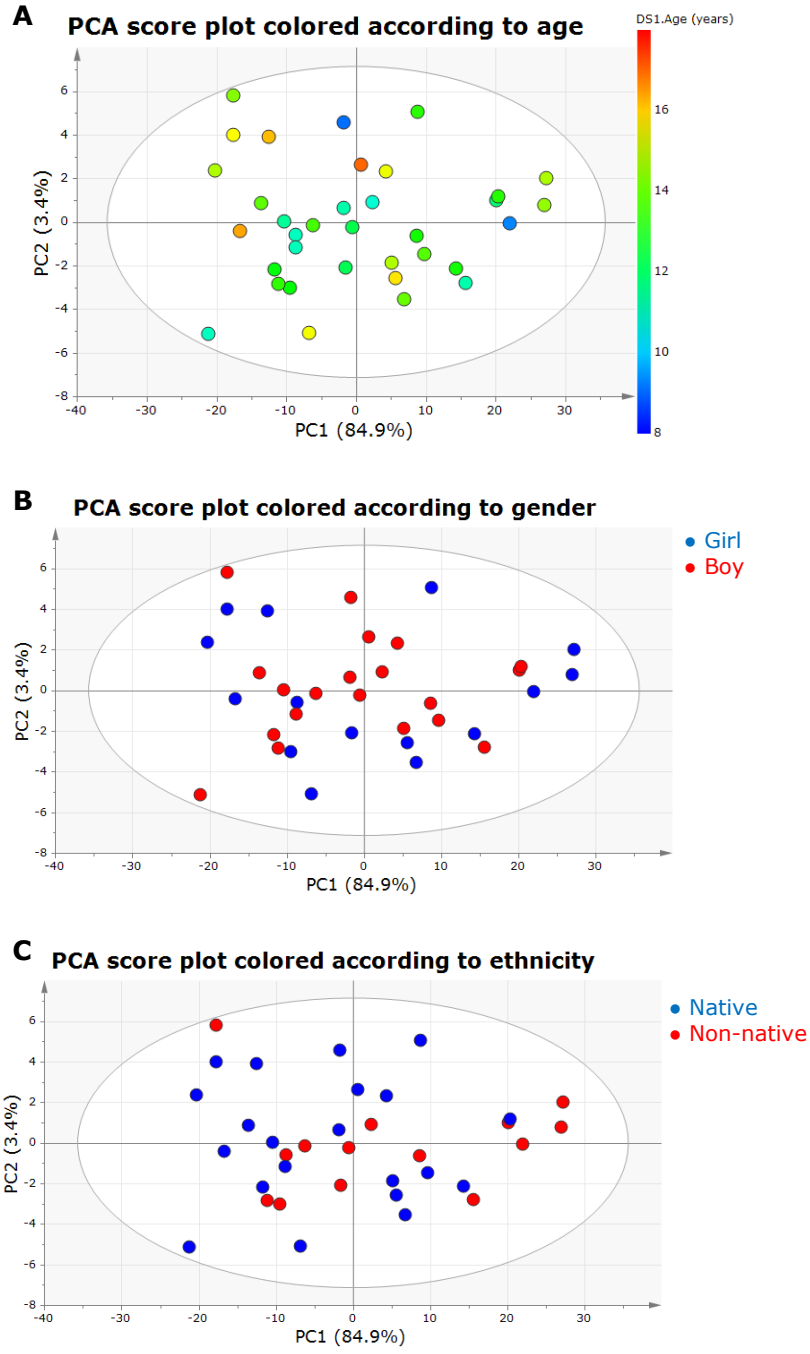

Figure 7.6 (partial). For figure legend see next page.

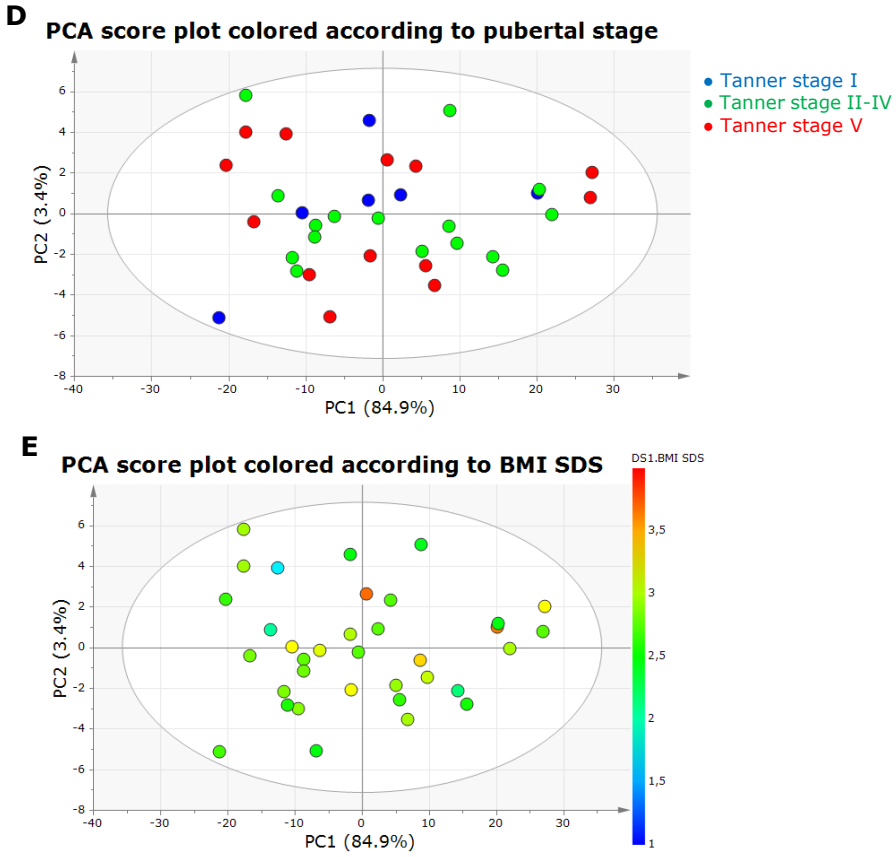

Figure 7.6 PCA score plots of 35 OB subjects colored according to age (A), gender (B), ethnicity (C), pubertal stage (D) and BMI SDS (E). Age (A) is continuously colored according to an age between 8 and 18 yrs; Gender (B) is colored according to girls (blue) and boys (red); Ethnicity (C) is colored according to native (blue) and non-native (red); Pubertal stage (D) is colored according to Tanner stage I (blue), II-IV (green) and V (red); BMI SDS (E) is continuously colored according to a BMI SDS between 1 and 4.

No clustering patterns were observed in the PCA plots, and consequently these variables were not considered as confounding factors. An unsupervised PCA and supervised OPLS-DA score plot – built with 110 plasma variables – was constructed for OB subjects classified as MHO or MUO (Figure 7.7).

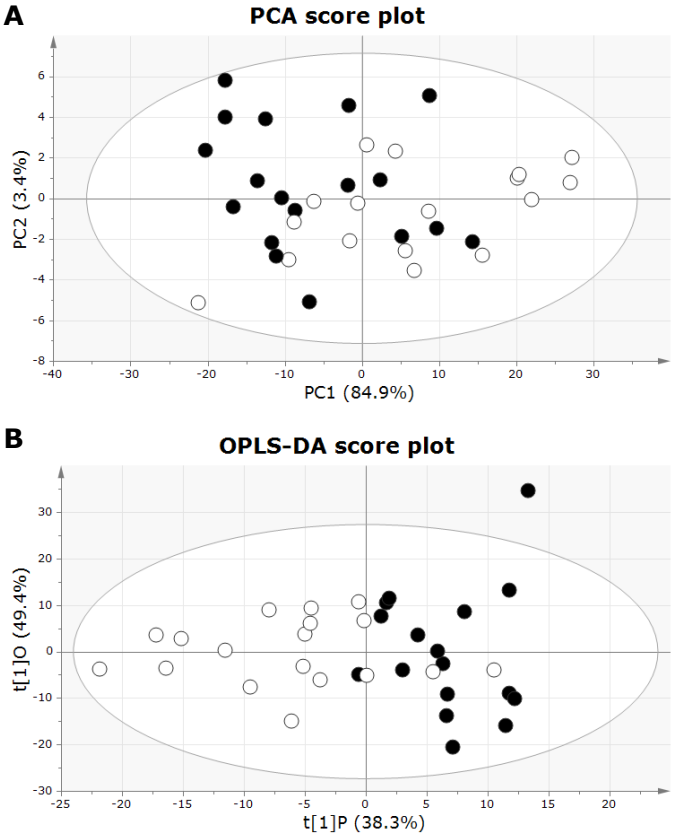

Figure 7.7 PCA (A) and OPLS-DA (B) score plots based on 110 plasma ^{1}H-NMR variables of 18 MHO (○) and 17 MUO (•) subjects. The ^{1}H-NMR metabolic profile of a given subject is plotted as a single point. PC1 (84.9%) and PC2 (3.4%) of the PCA score plot explain the largest and second largest variation within the data, respectively. In the OPLS-DA score plot (LV=2), the first predictive component (t[1]P=38.3%) explains the cumulative predictive and orthogonal variation in X and the first orthogonal component (t[1]O=49.4%) explains the variation in Y.

The OPLS-DA model built has a predictive and orthogonal explained variation in X of 87.7% (R_2X(cum)), and explained variation in Y is 50.5% (R_2Y(cum)). This model showed a moderate predictive ability of 24.9% (Q_2 (cum)) and allowed to classify 94% (16/17) MUO subjects and 89% (16/18) MHO subjects correctly.

To exclude the effect of noisy variables, the model was re-built on the basis of the 15% threshold for the coefficient of variation including 83 variables (27 noisy variables were removed from the entire model) (Figure 7.8). The model showed a R_2X(cum) of 90.4%, a slightly lower R_2Y(cum) of 48.3%, a predictive ability of 28.3%, and allowed to classify 94% (16/17) MUO subjects and 78% (14/18) MHO subjects correctly.

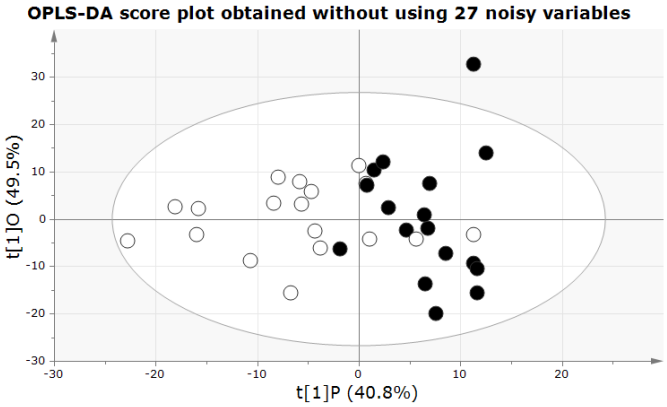

Figure 7.8 Supervised OPLS-DA score plot based on 83 variables derived from plasma ^{1}H-NMR CPMG spectra of 18 MHO (○) and 17 MUO (●) subjects. The ^{1}H-NMR metabolic profile of a given subject is plotted as a single point. The first predictive component (t[1]P: 40.8%) explains the cumulative predictive and orthogonal variation in X and the first orthogonal component (t[1]O: 49.5%) explains the variation in Y (LV=2).

To determine which plasma variables discriminated best between MHO and MUO subjects, a VIP plot was constructed. Plasma variables with a VIP value exceeding 1 were selected as those with the strongest discriminating power (Table 7.6).

Table 7.6 Plasma variables that contributed most to the discrimination between MHO and MUO subjects with a VIP higher than 1, ranked from strongest to least strong discriminatory power.

VAR_{PL}	Start and end ppm	VIP ± cvSE	Metabolites assigned by spiking experiments	Metabolite(s) most contributing to VAR_{PL}
100	1.3450 – 1.2458	4.45 ± 0.24	Lipids: CH_3-(CH_2)$_n$- in fatty acid chain + L-Isoleucine + L-Threonine	Lipids (mainly VLDL-C and LDL-C): CH_3-(CH_2)$_n$- in fatty acid chain
58	3.3230 – 3.2186	3.35 ± 0.89	L-Arginine + L-Histidine + L-Phenylalanine + L-Tyrosine + D-Glucose + -N^+(CH_3)$_3$ of choline head group in SM/PC	-N^+(CH_3)$_3$ of choline head group in SM/PC
99	1.3740 – 1.3450	2.85 ± 0.46	L-Lactate + L-Threonine	L-Lactate
38	3.9590 – 3.8330	2.22 ± 0.30	L-Aspartate + L-Cysteine + L-Methionine + L-Serine + L-Tyrosine + D-Glucose	D-Glucose
98	1.4200 – 1.3740	1.98 ± 0.33	L-Lactate	L-Lactate
54	3.5360 – 3.3980	1.95 ± 0.59	L-Proline + D-Glucose + Acetoacetate	D-Glucose
95	1.6860 – 1.5600	1.66 ± 0.26	Lipids: -C**H**$_2$-CH_2-C=O and -C**H**$_2$-CH_2-CH=CH in fatty acid chain + L-Arginine + L-Lysine	Lipids: -C**H**$_2$-CH_2-C=O and -C**H**$_2$-CH_2-CH=CH in fatty acid chain
18	5.4300 – 5.2752	1.65 ± 0.35	Lipids: -**H**C=C**H**- in fatty acid chain	Lipids: -**H**C=C**H**- in fatty acid chain
91	2.1230 – 1.9720	1.33 ± 0.44	Lipids: -C**H**$_2$-CH=CH- in fatty acid chain + L-Glutamate + L-Methionine + L-Proline + L-Isoleucine + N-acetyl signal of glycoproteins	Lipids: -C**H**$_2$-CH=CH- in fatty acid chain + N-acetyl signal of glycoproteins
45	3.7141 – 3.6680	1.24 ± 0.53	Glycerol	Glycerol
42	3.7820 – 3.7550	1.19 ± 0.12	L-Alanine + L-Glutamate + L-Glutamine + L-Leucine + L-Lysine + D-Glucose	D-Glucose + L-Lysine + L-Alanine
87	2.2915 – 2.2690	1.16 ± 0.16	Lipids: -C**H**$_2$-C=O and -C**H**$_2$-CH=CH- in fatty acid chain + L-Valine + L-Methionine	Lipids: -C**H**$_2$-C=O and -C**H**$_2$-CH=CH- in fatty acid chain
94	1.8060 – 1.6860	1.06 ± 0.27	L-Arginine + L-Lysine + L-Leucine	L-Lysine
96	1.5400 – 1.4900	1.06 ± 0.26	L-Alanine + L-Isoleucine + L-Lysine	L-Lysine + L-Alanine
44	3.7390 – 3.7141	1.03 ± 0.11	D-Glucose	D-Glucose
66	3.0640 – 2.9950	1.00 ± 0.34	L-Cysteine + L-Lysine + L-Tyrosine + α-ketoglutarate	α-ketoglutarate + L-lysine

LDL-C: low-density lipoprotein cholesterol; PC: phosphatidylcholine; SM: sphingomyelin; VAR_{PL}: plasma variable; VLDL-C: very-low density lipoprotein cholesterol; VIP: variable influence on projection; cvSE: standard error of cross-validation.

To explore the model contribution and statistical reliability of these discriminating variables, an S-plot – corresponding to the OPLS-DA score plot – was constructed (Figure 7.9). Plasma variables that correlate positively with the MHO phenotype are located in the bottom left part, and variables that correlate positively with the MUO phenotype are located in the upper right part of the S-plot.

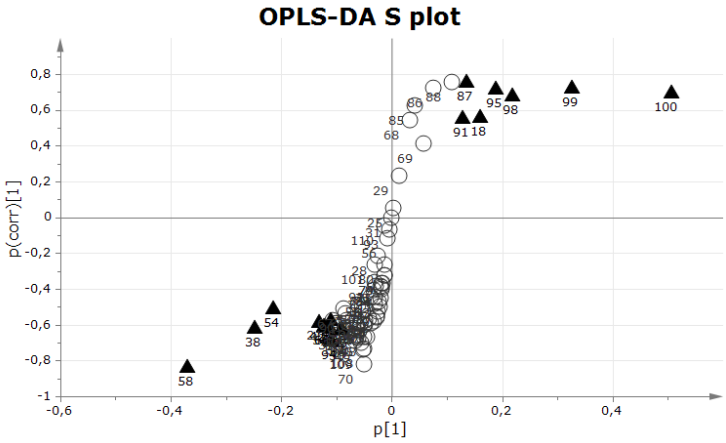

Figure 7.9 Supervised OPLS-DA S-plot based on 83 variables derived from plasma [1]H-NMR CPMG spectra of 18 MHO and 17 MUO subjects. The S-plot corresponds to the OPLS-DA score plot shown in Figure 7.8. The S-plot is composed of p(corr)[1] and p[1] vectors of the predictive component; p[1] reflects the model contribution of each variable and p(corr)[1] reflects the statistical reliability as discriminating variable. All plasma variables are presented by their unique number and variables with a VIP > 1 are illustrated as black triangles.

$VAR_{PL}100$ representing lipids (mainly of VLDL-C and LDL-C) is most important (VIP value: 4.45 ± 0.24) in the discrimination between MHO and MUO subjects and is positively correlated with the MUO phenotype. $VAR_{PL}100$ has a strong model contribution (p[1]=0.506) and high statistical reliability as discriminating variable (p(corr)[1]=0.692). $VAR_{PL}58$ representing choline-containing phospholipids is also a strongly discriminating variable (VIP value: 3.35 ± 0.89) and is negatively correlated to the MUO phenotype. $VAR_{PL}58$ has a strong model contribution (p[1]=-0.371) and high statistical reliability as discriminating variable (p(corr)[1]=-0.841).

As already described above, most plasma metabolites are represented by more than one signal in the [1]H-NMR spectrum and are therefore characterized by more than one VAR_{PL}, except for the N-acetyl signal of glycoproteins ($VAR_{PL}91$). Consequently, it was investigated whether all VAR_{PL} representing a certain metabolite were all correlated in the same direction with the MHO phenotype.

Relative concentrations of VAR_{PL}98-99 (VIP values higher than 1.9) both representing lactate were pointing in the same direction, i.e. lower in MHO as compared to MUO. Although lactate appears also in VAR_{PL}28-29, the VIP of these variables already becomes lower than 0.3. Except for choline-containing phospholipids (VAR_{PL}58), relative concentrations of other lipids (VIP values higher than 0.3) were lower in MHO as compared to MUO. All of the VAR_{PL} representing glucose (VAR_{PL}19, VAR_{PL}21, VAR_{PL}38-44, and VAR_{PL}52-54; VIP values greater than 0.5) showed relative concentrations higher for MHO as compared to MUO. Relative concentrations of VAR_{PL}45 (VIP higher than 1), VAR_{PL}47 and VAR_{PL}51 (VIP values higher than 0.4) representing glycerol were higher for MHO as compared to MUO. Relative concentrations of VAR_{PL}41-42, VAR_{PL}63-66, VAR_{PL}92-94 and VAR_{PL}96 (VIP values greater than 0.3) representing lysine were all higher in MHO as compared to MUO. Relative concentrations of VAR_{PL}39-43 and VAR_{PL}96 (VIP values greater than 0.7) representing alanine were all higher in MHO as compared to MUO. Relative concentrations of VAR_{PL}66 (VIP value higher than 1), VAR_{PL}67 and VAR_{PL}76-77 (VIP values greater than 0.1) representing α-ketoglutarate were higher in MHO as compared to MUO.

From OPLS-DA multivariate statistical analysis, it can be derived that MHO subjects have lower levels of lipids, lactate and N-acetyl glycoproteins, and higher levels of choline-containing phospholipids, glucose, glycerol, lysine, alanine and α-ketoglutarate compared to MUO. These findings were confirmed with univariate statistical analysis (Table 7.7).

Table 7.7 Relative concentrations of VAR_{PL} differing between MHO and MUO children.

VAR_{PL}	Metabolite(s) most contributing to VAR_{PL}	MHO (n=18)	MUO (n=17)	p-value
100	Lipids (mainly VLDL-C and LDL-C): CH_3-$(CH_2)_n$- in fatty acid chain	158.9 ± 37.6	201.2 ± 45.2	0.005
58	$-N^+(CH_3)_3$ of choline head group in SM/PC	69.2 ± 14.6	50.1 ± 13.0	$2.63x10^{-4}$
99	L-Lactate	56.1 ± 13.5	72.9 ± 18.0	0.004
38	D-Glucose	65.8 ± 10.5	54.4 ± 14.1	0.010
98	L-Lactate	17.3 ± 6.0	25.7 ± 9.7	0.006
54	D-Glucose	67.2 ± 11.2	56.7 ± 16.8	0.035
95	Lipids: -C**H**$_2$-CH_2-C=O and -C**H**$_2$-CH_2-CH=CH in fatty acid chain	13.5 ± 4.7	19.2 ± 6.0	0.004
18	Lipids: -**H**C=C**H**- in fatty acid chain	28.5 ± 5.8	34.6 ± 7.3	0.009
91	Lipids: -C**H**$_2$-CH=CH- in fatty acid chain + N-acetyl signal of glycoproteins	67.9 ± 3.8	71.9 ± 4.8	0.010
45	Glycerol	13.9 ± 3.0	10.8 ± 2.5	0.002
42	D-Glucose + L-Lysine + L-Alanine	20.4 ± 3.3	16.9 ± 4.5	0.014
87	Lipids: -C**H**$_2$-C=O and -C**H**$_2$-CH=CH- in fatty acid chain	5.2 ± 2.3	7.9 ± 2.7	0.003
94	L-Lysine	10.2 ± 1.7	7.9 ± 2.1	0.002
96	L-Lysine + L-Alanine	8.5 ± 1.4	6.5 ± 1.7	$4.98x10^{-4}$
44	D-Glucose	13.1 ± 2.2	10.7 ± 2.9	0.008
66	α-ketoglutarate + L-Lysine	14.9 ± 2.8	12.3 ± 3.6	0.023

Relative concentrations are presented as mean ± SD. All results are significantly different between MHO and MUO using the independent samples t test with Benjamini-Hochberg correction. LDL-C: low-density lipoprotein cholesterol; NW: normal-weight; OB: overweight or obese; PC: phosphatidylcholine; SM: sphingomyelin; VAR_{PL}: plasma variables; VLDL-C: very-low density lipoprotein cholesterol.

7.3.3 Correlations between conventional biochemical parameters and plasma ^{1}H-NMR metabolic profile of obese children and adolescents classified as MHO or MUO

Clinical and biochemical parameters measured in 18 MHO and 17 MUO children and adolescents are presented in Table 7.8.

Table 7.8 Clinical and biochemical characteristics of MHO and MUO children and adolescents.

	MHO	MUO	p-value
Number, n	18	17	
SBP, mm Hg	114 ± 9	128 ± 9	<0.001
DBP, mm Hg	69 ± 8	79 ± 6	<0.001
Fasting glucose, mg/dl	92 ± 4	98 ± 7	0.009
Fasting insulin, µU/ml	16.0 (10.6)	24.5 (19.1)	0.019
HbA1c, %	5.4 (0.3)	5.6 (0.2)	0.013
HDL-C, mg/dl	47 (15)	39 (7)	<0.001
Triglycerides, mg/dl	78 (69)	134 (166)	0.003
LDL-C, mg/dl	75 (32)	92 (42)	0.082
AST, U/l	25 (7)	24 (16)	0.704
ALT, U/l	19 (15)	19 (29)	0.448
g-GT, U/l	16 (9)	17 (13)	0.333
Uric acid, mg/dl	5.4 ± 1.1	6.7 ± 1.2	0.005
WBC count, 10^9/l	7.0 ± 1.3	7.0 ± 1.7	0.947
SHBG, nmol/l	29 (25)	19 (5)	0.006

Results of continuous variables are presented as mean ± SD or median (IQR). The p-values shown are the result of independent samples t test or Mann Whitney U test between MHO and MUO study groups. Bonferroni adjusted p-values < 0.003 are considered statistical significant between MHO and MUO. ALT: alanine transaminase; AST: aspartate transaminase; DBP: diastolic blood pressure; g-GT: gamma glutamyl transpeptidase; HbA1c: hemoglobin A1C; HDL-C: high-density lipoprotein cholesterol; HOMA-IR: homeostatic model assessment for insulin resistance; IDF: International Diabetes Federation; LDL-C: low-density lipoprotein cholesterol; MHO: metabolically healthy obese; MR: metabolic risk; MUO: metabolically unhealthy obese; SBP: systolic blood pressure; SHBG: sex-hormone binding globulin; WBC: white blood cell.

Blood pressure, and levels of HDL-C and triglycerides are significantly different (Bonferroni adjusted p-values <0.003) between MHO and MUO using univariate statistical analysis. To explore correlations between conventionally measured biochemical parameters and VAR_{PL} most strongly discriminating between MHO and MUO, a PCA score plot of plasma ^{1}H-NMR spectra of MHO and MUO subjects was constructed based on 83 plasma variables. The PCA plot was colored according to each biochemical parameter: i.e. fasting plasma glucose, fasting serum insulin, HbA1c, HDL-C, triglycerides, LDL-C, AST, ALT, g-GT, uric acid, WBC count and SHBG, measured in fasting blood of obese children and adolescents. A gradual increase was observed only for triglycerides towards a more obese (Figure 7.10A) and MUO (Figure 7.10B) phenotype.

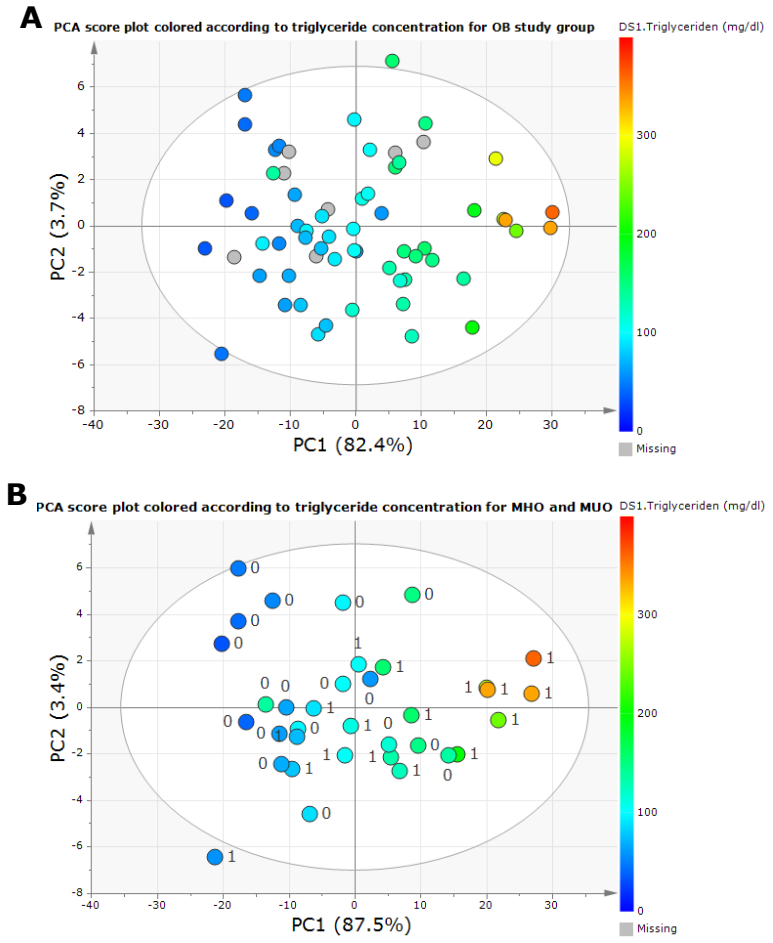

Figure 7.10 PCA score plot colored according to fasting plasma triglyceride concentration of the OB study group (A), and MHO and MUO subjects (B). The [1]H-NMR metabolic profile of a given subject (MHO=0; MUO=1) is plotted as a single point. Triglyceride levels ranged from 33 mg/dl (blue) to 361 mg/dl (red). PC1 and PC2 of the PCA score plot explain the largest and second largest variation within the data, respectively.

In Figure 7.10A and B, a similar trend can be observed. The low triglyceride concentrations situated at the left of the PCA plot, are mostly corresponding to the MHO phenotype whereas high triglyceride concentrations situated at the right of the PCA plot are mostly corresponding to MUO phenotype. This observation was confirmed with univariate Spearman correlation analysis (Table 7.9). Triglyceride levels were highly associated ($p<0.001$) with VAR_{PL} discriminating most between 18 MHO and 17 MUO.

Table 7.9 Spearman correlations between triglyceride levels and VAR_{PL} discriminating most between MHO and MUO.

		Triglyceride concentration	
VAR_{PL}	**Metabolite(s) most contributing to VAR_{PL}**	**r_s**	**p-value**
100	Lipids (mainly VLDL-C and LDL-C): CH_3-(CH_2)$_n$- in fatty acid chain	0.892	5.41×10^{-21}
58	-N^+(CH_3)$_3$ of choline head group in SM/PC	-0.881	7.05×10^{-20}
99	L-Lactate	0.875	2.72×10^{-19}
38	D-Glucose	-0.888	1.46×10^{-20}
98	L-Lactate	0.834	4.48×10^{-16}
54	D-Glucose	-0.876	2.06×10^{-19}
95	Lipids: -C**H**$_2$-CH_2-C=O and -C**H**$_2$-CH_2-CH=CH in fatty acid chain	0.824	1.91×10^{-15}
18	Lipids: -**H**C=C**H**- in fatty acid chain	0.828	1.06×10^{-15}
91	Lipids: -C**H**$_2$-CH=CH- in fatty acid chain + N-acetyl signal of glycoproteins	0.752	1.06×10^{-11}
45	Glycerol	-0.808	1.88×10^{-14}
42	D-Glucose + L-Lysine + L-Alanine	-0.884	4.20×10^{-20}
87	Lipids: -C**H**$_2$-C=O and -C**H**$_2$-CH=CH- in fatty acid chain	0.884	3.97×10^{-20}
94	L-Lysine	-0.854	1.64×10^{-17}
96	L-Lysine + L-Alanine	-0.767	2.14×10^{-12}
44	D-Glucose	-0.892	5.88×10^{-21}
66	α-ketoglutarate + L-Lysine	-0.793	1.24×10^{-13}

Spearman's correlation coefficient r_s measures the degree and direction of correlation between triglycerides and VAR_{PL}. LDL-C: low-density lipoprotein cholesterol; PC: phosphatidylcholine; SM: sphingomyelin; VAR_{PL}: plasma variable; VLDL-C: very-low density lipoprotein cholesterol.

7.4 Discussion

In this study, we applied untargeted plasma ^{1}H-NMR-based metabolomics to investigate obesity in children and adolescents. Our results show metabolic differences in plasma of obese and normal-weight children and adolescents. Obese children had significantly higher concentrations of lipids, lactate and N-acetyl glycoproteins, and lower concentrations of choline-containing phospholipids, glucose and α-ketoglutarate compared to normal-weight children and adolescents. In addition, the plasma metabolic profile of metabolically "healthy" obese (MHO) and metabolically unhealthy obese (MUO) children and adolescents could be clearly discriminated. In addition, the – conventionally measured – triglyceride concentration is highly correlated with the plasma metabolites which discriminate most strongly between MHO and MUO phenotypes.

Dyslipidemia is a typical symptom of childhood obesity and is traditionally characterized by increased plasma levels of triglycerides, slightly elevated LDL-C and decreased HDL-C [26]. Using ^{1}H-NMR spectroscopy of plasma, the obese children in this study showed elevated levels of lipid signals originating from VLDL-C and LDL-C compared to normal-weight children. In line with our findings, a ^{1}H-NMR-based study in adults showed that obesity is related to a 50-100% increase in plasma concentrations of pro-atherogenic lipoproteins VLDL and LDL, as well as a small – biologically probably insignificant – 10% increase of HDL particle concentration [27]. Among a small group of obese adolescents with normal glucose tolerance, it was shown that the presence of hepatic steatosis is associated with an increase in VLDL particle size and number, an increase in small dense LDL concentrations and a decrease in the number of large HDL particles [28]. These findings suggest that not only the concentration of lipoproteins in plasma is important, but also their particle size. Within the obese study group, we observed a gradual increase in conventionally measured triglyceride concentrations towards higher levels of VLDL-C and LDL-C as measured with ^{1}H-NMR spectroscopy. This finding was also observed by Cali et al. [28], and points most likely to an increased hepatic production of triglycerides with a consequent increased secretion of triglyceride containing VLDL particles in the blood that are subsequently converted to LDL-C [29]. Evidence is rising that the concentration of fasting triglycerides is probably the most important component of the metabolic syndrome to best characterize metabolic heterogeneity and changes in metabolic

risk in obese children and adolescents [30]. Triglyceride levels in late adolescence and its change within 5 years of follow-up can predict the development of diabetes [31] and of coronary heart disease [32] even when measurements are within the seemingly 'normal' range. However, future studies are needed to reveal whether triglyceride levels in childhood have consequences that last into adulthood [33].

In addition to increased lipid concentrations, choline-containing phospholipid signal intensity in the ^{1}H-NMR spectrum was decreased in plasma of obese children. The ^{1}H-NMR signal of these specific phospholipids represents signals originating both from sphingomyelins and phosphatidylcholines. Choline-containing phospholipids, largely consisting of phosphatidylcholine, are components of cell membranes and a decreased concentration was previously linked to obesity-related metabolic complications [34]. Previous MS-based studies revealed increased levels of phosphatidylcholines in plasma of obese children and adolescents after weight loss intervention [16, 35]. Thus, it is suggested that the decrease in choline-containing phospholipids found in plasma of obese children is mainly due to decreased levels of phosphatidylcholines. However, further in-depth characterization of choline-containing phospholipids – e.g. using a MS-based metabolomics approach – is needed to confirm this. In addition, a recent ^{1}H-NMR-based metabolomics study in overweight adolescents showed that plasma levels of phosphatidylcholine were elevated in girls compared to boys [36]. In our study, however, no gender differences were detected.

Obese children and adolescents showed a significant increase in lactate accompanied by a decrease in glucose compared to normal-weight individuals. This finding might suggest an altered glucose-derived carbon metabolism with an increased glycolytic activity in obese children and adolescents. Glycolysis occurs in all tissues for the oxidation of glucose to provide energy – in the form of adenosine triphosphate (ATP) – and intermediates for other metabolic pathways [29]. Anaerobic glycolysis takes place in tissues or cells deprived of sufficient oxygen. There is growing evidence that hypoxia occurs in adipocytes that become distant from the vasculature as adipose tissue mass expands [37, 38], resulting in the utilization of glucose and production of lactate in obese individuals [39, 40]. However, the exact mechanisms behind increased levels of lactate and decreased levels of glucose in obese children and adolescents need to be explored further.

It is generally assumed that obese children and adolescents are at increased risk for insulin resistance leading to high fasting and postprandial glucose levels, and an increased risk for future T2DM [41, 42]. However, the majority of obese children show fasting blood glucose values within the normal range [43, 44]. The observation of lower fasting plasma glucose levels in obese compared to normal-weight children is most likely a reflection of the short duration of obesity compared to adults and the presence of metabolic adaptive mechanisms in childhood that may gradually fail when becoming obese as an adult [45, 46]. Further longitudinal investigations are needed to confirm this hypothesis.

Interestingly, [1]H-NMR spectra of obese subjects showed a significantly increased signal intensity of the N-acetyl group from glycoproteins, mainly from acute phase α-1 acid glycoproteins as indicated by Bell et al. [47]. The synthesis of N-acetyl glycoproteins involves the utilization of glucose, which could also be a rationale for the low glucose levels observed in obese children. Acute phase α-1 acid glycoprotein, which is produced by the liver in response to pro-inflammatory cytokines, has been found to be increased in inflammation [48]. It was previously suggested that inflammatory mechanisms linking obesity to its metabolic and cardiovascular complications are already activated in childhood [49]. In addition, chronic inflammatory disease initiated in adipose tissue is proposed to play a crucial role in obesity-related insulin resistance [50]. It is increasingly recognized that chronic low-grade inflammation is involved in the pathogenesis of obesity-related insulin resistance, T2DM and CVD [51, 52].

In the present study, α-ketoglutarate was found to be lower in plasma of obese compared to normal-weight children and adolescents. As α-ketoglutarate is a component of the tricarboxylic acid cycle (TCA cycle), a decline in its concentration might be linked to an impaired TCA cycle, i.e. disturbed energy metabolism [29]. Low levels of α-ketoglutarate have previously also been linked to an increased cardiovascular risk in healthy individuals [53]. It was speculated that an alteration of the mitochondrial redox potential might play a role [53]. In contrast to these findings, an increased concentration of α-ketoglutarate was found in obese compared to lean adults and it was suggested to be a surrogate biomarker of non-alcohol fatty liver disease [54]. Our study group consisted out of obese children and adolescents whose underlying metabolic mechanisms may be different from those observed in adults.

Within the obese group, the plasma metabolic profiles of MHO and MUO phenotypes are clearly different. MHO children and adolescents showed a more 'healthier' obese plasma metabolic profile compared to MUO. In addition, MUO had lower levels of lysine and alanine compared to MHO. Previous studies in obese mice models suggest that decreased levels of lysine are linked to increased insulin resistance [55, 56]. It was previously also found that obese adolescents with T2DM had lower alanine levels compared to obese and normal-weight individuals without T2DM [15]. Our findings confirm that obese children and adolescents can be characterized with different metabolic phenotypes representing their metabolic health status. However, it remains to be determined if the proposed classification into MHO and MUO has a good ability to predict future T2DM and/or CVD. We suggest to perform large-scale longitudinal follow-up studies to provide a more comprehensive overview of the MHO phenotype and to monitor the development of the MHO state. In future, the implementation of the concept of MHO in clinical practice might offer new perspectives for targeted prevention and individual treatment strategies of childhood obesity and associated cardiometabolic complications.

A limitation of this study is the lack of an independent cohort to validate our findings. Nonetheless, research was conducted according to a very accurate and well-controlled experimental protocol, which guarantees the quality and reliability of our study findings. Important to note is also that, in complex biofluids such as plasma, ^{1}H-NMR spectroscopy cannot differentiate between the lengths of acyl chains of lipids [57]. The same holds for the differentiation between choline-containing phospholipids, i.e. phosphatidylcholine and sphingomyelin.

In summary, our findings provide evidence for obesity-related alterations in the plasma metabolic profile of children and adolescents. Lipids, lactate, glucose, α-ketoglutarate, choline-containing phospholipids and N-acetyl glycoproteins are suggested to play a major role in the altered metabolism detected in obese children and adolescents. An increase in conventionally measured fasting triglycerides is highly linked to a more obese and MUO phenotype. Triglycerides should possibly get more attention in the management of childhood obesity. In the near future, the plasma ^{1}H-NMR metabolic profile could be useful in detecting different phenotypes of obesity and in identifying those at greatest risk for developing metabolic diseases later in life. Further studies with larger cohorts and

with a longitudinal design are needed to confirm our findings and assure validity. Eventually, this might provide new insights for the prevention and treatment strategies of childhood obesity and related metabolic complications, resulting in a better life expectancy for the growing child.

References

1. Olds T, Maher C, Zumin S, Péneau S, Lioret S, Castetbon K, et al. Evidence that the prevalence of childhood overweight is plateauing: data from nine countries. Int J Pediatr Obes. 2011;6(5-6):342-60.
2. Gupta N, Goel K, Shah P, Misra A. Childhood obesity in developing countries: epidemiology, determinants, and prevention. Endocr Rev. 2012;33(1):48-70.
3. Ng M, Fleming T, Robinson M, Thomson B, Graetz N, Margono C, et al. Global, regional, and national prevalence of overweight and obesity in children and adults during 1980-2013: a systematic analysis for the Global Burden of Disease Study 2013. Lancet. 2014;384(9945):766-81.
4. Farrant B, Utter J, Ameratunga S, Clark T, Fleming T, Denny S. Prevalence of severe obesity among New Zealand adolescents and associations with health risk behaviors and emotional well-being. J Pediatr. 2013;163(1):143-9.
5. Skinner AC, Skelton JA. Prevalence and trends in obesity and severe obesity among children in the United States, 1999-2012. JAMA Pediatr. 2014;168(6):561-6.
6. Skelton JA, Irby MB, Grzywacz JG, Miller G. Etiologies of obesity in children: nature and nurture. Pediatr Clin North Am. 2011;58(6):1333-54.
7. Lakshman R, Elks CE, Ong KK. Childhood obesity. Circulation. 2012;126(14):1770-9.
8. Biro FM, Wien M. Childhood obesity and adult morbidities. Am J Clin Nutr. 2010;91(5):S1499-505.
9. Spruijt-Metz D. Etiology, treatment and prevention of obesity in childhood and adolescence: a decade in review. J Res Adolesc. 2011;21(1):129-52.
10. Mangge H, Zelzer S, Puerstner P, Schnedl WJ, Reeves G, Postolache TT, et al. Uric acid best predicts metabolically unhealthy obesity with increased cardiovascular risk in youth and adults. Obesity. 2013;21(1):E71-7.
11. Prince RL, Kuk JL, Ambler KA, Dhaliwal J, Ball GD. Predictors of metabolically healthy obesity in children. Diabetes Care. 2014;37(5):1462-8.
12. Dona AC, Jimenez B, Schafer H, Humpfer E, Spraul M, Lewis MR, et al. Precision high-throughput proton NMR spectroscopy of human urine, serum, and plasma for large-scale metabolic phenotyping. Anal Chem. 2014;86(19):9887-94.
13. Holmes E, Wilson ID, Nicholson JK. Metabolic phenotyping in health and disease. Cell. 2008;134(5):714-7.
14. Zhang A, Sun H, Wang X. Power of metabolomics in biomarker discovery and mining mechanisms of obesity. Obes Rev. 2013;14(4):344-9.
15. Mihalik SJ, Michaliszyn SF, de las Heras J, Bacha F, Lee S, Chace DH, et al. Metabolomic profiling of fatty acid and amino acid metabolism in youth with obesity and type 2 diabetes: evidence for enhanced mitochondrial oxidation. Diabetes Care. 2012;35(3):605-11.
16. Wahl S, Holzapfel C, Yu Z, Breier M, Kondofersky I, Fuchs C, et al. Metabolomics reveals determinants of weight loss during lifestyle intervention in obese children. Metabolomics. 2013;9(6):1157-67.
17. Emwas AH, Salek RM, Griffin JL, Merzaban J. NMR-based metabolomics in human disease diagnosis: applications, limitations, and recommendations. Metabolomics. 2013;9:1048-72.
18. Cole T, Lobstein T. Extended international (IOTF) body mass index cut-offs for thinness, overweight and obesity. Pediatr Obes. 2012;7(4):284-94.
19. Marshall WA, Tanner JM. Variations in pattern of pubertal changes in girls. Arch Dis Child. 1969;44(235):291-303.
20. Marshall WA, Tanner JM. Variations in the pattern of pubertal changes in boys. Arch Dis Child. 1970;45(239):13-23.
21. Falkner B, Daniels SR. Summary of the fourth report on the diagnosis, evaluation, and treatment of high blood pressure in children and adolescents. Hypertension. 2004;44(4):387-8.

22. Friedewald WT, Levy RI, Fredrickson DS. Estimation of the concentration of low-density lipoprotein cholesterol in plasma, without use of the preparative ultracentrifuge. Clin Chem. 1972;18(6):499-502.
23. Zimmet P, Alberti K, George MM, Kaufman F, Tajima N, Silink M, et al. The metabolic sydrome in children and adolescents - an IDF consensus report. Pediatr Diabetes. 2007;8:299-306.
24. Weghuber D, Zelzer S, Stelzer I, Paulmichl K, Kammerhofer D, Schnedl W, et al. High risk vs. "metabolically healthy" phenotype in juvenile obesity-neck subcutaneous adipose tissue and serum uric acid are clinically relevant. Exp Clin Endocrinol Diabetes. 2013;121(7):384-90.
25. Xia J, Broadhurst DI, Wilson M, Wishart DS. Translational biomarker discovery in clinical metabolomics: an introductory tutorial. Metabolomics. 2013;9(2):280-99.
26. Daniels SR. Lipid concentrations in children and adolescents: it is not all about obesity. Am J Clin Nutr. 2011;94(3):699-700.
27. Magkos F, Mohammed BS, Mittendorfer B. Effect of obesity on the plasma lipoprotein subclass profile in normoglycemic and normolipidemic men and women. Int J Obes (Lond). 2008;32(11):1655-64.
28. Cali AM, Zern TL, Taksali SE, de Oliveira AM, Dufour S, Otvos JD, et al. Intrahepatic fat accumulation and alterations in lipoprotein composition in obese adolescents: a perfect proatherogenic state. Diabetes Care. 2007;30(12):3093-8.
29. Ferrier DR. Biochemistry. 6th Edition ed. Harvey RA, editor. North America: Wolters Kluwer, Lippincott Williams & Wilkins; 2014. 552 p.
30. Hobkirk JP, King RF, Gately P, Pemberton P, Smith A, Barth JH, et al. The predictive ability of triglycerides and waist (hypertriglyceridemic waist) in assessing metabolic triad change in obese children and adolescents. Metab Syndr Relat Disord. 2013;11(5):336-42.
31. Tirosh A, Shai I, Bitzur R, Kochba I, Tekes-Manova D, Israeli E, et al. Changes in triglyceride levels over time and risk of type 2 diabetes in young men. Diabetes Care. 2008;31(10):2032-7.
32. Tirosh A, Rudich A, Shochat T, Tekes-Manova D, Israeli E, Henkin Y, et al. Changes in triglyceride levels and risk for coronary heart disease in young men. Ann Intern Med. 2007;147(6):377-85.
33. de Ferranti SD, Crean S, Cotter J, Boyd D, Osganian SK. Hypertriglyceridemia in a pediatric referral practice: experience with 300 patients. Clin Pediatr (Phila). 2011;50(4):297-307.
34. Pietilainen KH, Rog T, Seppanen-Laakso T, Virtue S, Gopalacharyulu P, Tang J, et al. Association of lipidome remodeling in the adipocyte membrane with acquired obesity in humans. PLoS Biol. 2011;9(6):e1000623.
35. Reinehr T, Wolters B, Knop C, Lass N, Hellmuth C, Harder U, et al. Changes in the serum metabolite profile in obese children with weight loss. Eur J Nutr. 2015;54(2):173-81.
36. Zheng H, Yde CC, Arnberg K, Molgaard C, Michaelsen KF, Larnkjaer A, et al. NMR-based metabolomic profiling of overweight adolescents: an elucidation of the effects of inter-/intraindividual differences, gender, and pubertal development. Biomed Res Int. 2014;2014:537157.
37. Hosogai N, Fukuhara A, Oshima K, Miyata Y, Tanaka S, Segawa K, et al. Adipose tissue hypoxia in obesity and its impact on adipocytokine dysregulation. Diabetes. 2007;56(4):901-11.
38. Trayhurn P. Hypoxia and adipose tissue function and dysfunction in obesity. Physiol Rev. 2013;93(1):1-21.
39. Pasarica M, Sereda OR, Redman LM, Albarado DC, Hymel DT, Roan LE, et al. Reduced adipose tissue oxygenation in human obesity: evidence for rarefaction, macrophage chemotaxis, and inflammation without an angiogenic response. Diabetes. 2009;58(3):718-25.
40. Trayhurn P, Alomar SY. Oxygen deprivation and the cellular response to hypoxia in adipocytes - perspectives on white and brown adipose tissues in obesity. Front Endocrinol (Lausanne). 2015;6:19.

41. Goran MI, Ball GDC, Cruz ML. Obesity and risk of type 2 diabetes and cardiovascular disease in children and adolescents. J Clin Endocr Metab. 2003;88(4):1417-27.
42. Rosenbloom AL, Silverstein JH, Amemiya S, Zeitler P, Klingensmith GJ. Type 2 diabetes in children and adolescents. Pediatr Diabetes. 2009;10 Suppl 12:17-32.
43. Weiss R, Dziura J, Burgert TS, Tamborlane WV, Taksali SE, Yeckel CW, et al. Obesity and the metabolic syndrome in children and adolescents. N Engl J Med. 2004;350(23):2362-74.
44. Pedrosa C, Oliveira BM, Albuquerque I, Simoes-Pereira C, Vaz-de-Almeida MD, Correia F. Markers of metabolic syndrome in obese children before and after 1-year lifestyle intervention program. Eur J Nutr. 2011;50(6):391-400.
45. Csabi G, Torok K, Jeges S, Molnar D. Presence of metabolic cardiovascular syndrome in obese children. Eur J Pediatr. 2000;159(1-2):91-4.
46. Aucouturier J, Duche P, Timmons BW. Metabolic flexibility and obesity in children and youth. Obes Rev. 2011;12(5):e44-53.
47. Bell JD, Brown JC, Nicholson JK, Sadler PJ. Assignment of resonances for 'acute-phase' glycoproteins in high resolution proton NMR spectra of human blood plasma. FEBS Lett. 1987;215(2):311-5.
48. Gabay C, Kushner I. Acute-phase proteins and other systemic responses to inflammation. N Engl J Med. 1999;340(6):448-54.
49. Schipper HS, Nuboer R, Prop S, van den Ham HJ, de Boer FK, Kesmir C, et al. Systemic inflammation in childhood obesity: circulating inflammatory mediators and activated CD14++ monocytes. Diabetologia. 2012;55(10):2800-10.
50. Xu H, Barnes GT, Yang Q, Tan G, Yang D, Chou CJ, et al. Chronic inflammation in fat plays a crucial role in the development of obesity-related insulin resistance. J Clin Invest. 2003;112(12):1821-30.
51. Dregan A, Charlton J, Chowienczyk P, Gulliford MC. Chronic inflammatory disorders and risk of type 2 diabetes mellitus, coronary heart disease, and stroke: a population-based cohort study. Circulation. 2014;130(10):837-44.
52. Esser N, Legrand-Poels S, Piette J, Scheen AJ, Paquot N. Inflammation as a link between obesity, metabolic syndrome and type 2 diabetes. Diabetes Res Clin Pract. 2014;105(2):141-50.
53. Bernini P, Bertini I, Luchinat C, Tenori L, Tognaccini A. The cardiovascular risk of healthy individuals studied by NMR metabonomics of plasma samples. J Proteome Res. 2011;10(11):4983-92.
54. Rodriguez-Gallego E, Guirro M, Riera-Borrull M, Hernandez-Aguilera A, Marine-Casado R, Fernandez-Arroyo S, et al. Mapping of the circulating metabolome reveals alpha-ketoglutarate as a predictor of morbid obesity-associated non-alcoholic fatty liver disease. Int J Obes (Lond). 2015;39(2):279-87.
55. Shearer J, Duggan G, Weljie A, Hittel DS, Wasserman DH, Vogel HJ. Metabolomic profiling of dietary-induced insulin resistance in the high fat-fed C57BL/6J mouse. Diabetes Obes Metab. 2008;10(10):950-8.
56. Won EY, Yoon MK, Kim SW, Jung Y, Bae HW, Lee D, et al. Gender-specific metabolomic profiling of obesity in leptin-deficient ob/ob mice by 1H NMR spectroscopy. PLoS One. 2013;8(10):e75998.
57. Griffin JL, Nicholls AW. Metabolomics as a functional genomic tool for understanding lipid dysfunction in diabetes, obesity and related disorders. Pharmacogenomics. 2006;7(7):1095-107.

Chapter 8

General discussion and main conclusions

In the past decades, the worldwide prevalence of obesity has dramatically risen to epidemic levels [1]. As a consequence, healthcare costs resulting from the treatment of chronic diseases that are etiologically linked to obesity, particularly type 2 diabetes (T2DM) and cardiovascular diseases (CVD) have increased tremendously [2]. It is of great concern that obesity with all its consequences is already observed in children, and even in infants and preschoolers [3]. Compared to adults, children are more prone to and will more rapidly develop obesity-related metabolic health consequences [4]. In addition, obese children and adolescents are at increased risk of both premature mortality and adult morbidity, particularly cardiometabolic morbidity [5]. Therefore, it has become highly important to study the metabolic health of obese children and adolescents using non-invasive, easily applicable and highly accessible methods. Early detection of obese children and adolescents at low or high risk for the development of metabolic complications can support the establishment of effective prevention and treatment strategies. This can eventually result in a reduction of healthcare costs, and a better quality of life and life expectancy for the growing child. In this thesis, the metabolic health of obese children and adolescents was studied by clinical and metabolomics research.

Are morbidly obese children and adolescents at higher risk for metabolic complications than severely obese?

The number of children and adolescents with more extreme forms of obesity is on the rise [6, 7]. This trend was also noticed at the multidisciplinary pediatric obesity clinic of the Jessa Hospital (Hasselt, Belgium). To date, however, it is unclear which anthropometric cut-off point should be used to accurately define morbid obesity in children and adolescents. The body mass index (BMI) has proven to be a fairly accurate screening tool for overweight and obesity in the pediatric population regardless of the fact that the BMI is an indirect measure of adiposity and is based on weight and height – both of which change greatly during growth in childhood [8]. The BMI is easy to use, non-invasive, and inexpensive which favors its clinical implementation. Nowadays, the BMI is widely used to identify obese children and adolescents. However, the plethora of BMI references and cut-offs that are currently available and its varying use, leads to inconsistency of study results and prevalence data. A majority of studies have established cut-off values based on BMI-for-age at the 95th or the 99th percentile [9, 10]. However, these

BMI cut-off points depend on the reference population and are therefore not internationally applicable or accepted. The recently developed International Obesity Task Force (IOTF) BMI references established for 2 to 18 years old children are usually preferred to use as they are internationally based, less arbitrary than other cut-offs, and less geographically and temporally dependent than others [11]. Unfortunately, the present IOTF criteria do not include BMI reference values for children between 2 and 18 years which reaches BMI 40 at age 18, to define morbid obesity. To this end, age- and sex-specific pediatric IOTF BMI criteria for morbid obesity were calculated corresponding to BMI 40 at age 18 (99.95^{th} percentile) using the LMS method proposed by Cole and Lobstein [11] (**Chapter 2**). The application of these cut-off values on large study populations will allow to calculate prevalence rates of morbid childhood obesity within and between different countries, and to compare these with adult prevalence rates. The application of these cut-off values on a cohort of 217 obese children and adolescents aged between 2 and 18 who visited the multidisciplinary pediatric obesity clinic of the Jessa Hospital (Hasselt, Belgium), showed that 33.6% and 25.8% were classified as being severely and morbidly obese, respectively. This confirms that a substantial number of obese children consulting the multidisciplinary pediatric obesity clinic are extremely obese, which is of great concern. Due to the fact that this study group was selected from patients referred to our clinic, we were not able to calculate regional prevalence data of severe or morbid obesity. However, in line with current evidence from the US [7] and the Netherlands [6], we expect that numbers of more extremely obese children have also increased in Belgium. Further studies in which the obesity prevalence rates are reanalyzed on the basis of the pediatric IOTF BMI criteria allowing the international and uniform comparison of prevalence rates of severe and morbid childhood obesity, are needed to confirm this.

In addition to the worldwide use of various definitions for morbid childhood obesity, its terminology is inconsistent. In order to ensure consistency, Rolland-Cachera [12] proposed to simplify the terminology of obesity in children according to the adult WHO 1995 definition [13]. However, the suggestion to use 'grade 1' and 'grade 2' overweight instead of overweight and obesity in children obscures the heterogeneity of this group. In an attempt to standardize the terminology use for obesity in children, we defined BMI 25, 30, 35 and 40 at age 18 as overweight,

'class I obesity' or obese, 'class II obesity' or severely obese, and 'class III obesity' or morbidly obese, respectively, according to the WHO 2000 definition [14].

To explore the clinical importance of the newly constructed IOTF BMI 40 cut-offs, we compared metabolic parameters between different classes or degrees of obesity in 90 out of 217 children and adolescents aged between 7 and 18 (**Chapter 2**). Morbidly obese children had a significantly increased waist circumference and systolic blood pressure than severely and class I obese children. A recent study showed that severely obese children are at nearly three-fold greater risk of hypertension than moderately obese children [15]. It is believed that a combination of hyperactivity of the sympathetic nervous system, insulin resistance, and abnormalities in vascular structure and function could contribute to obesity-related hypertension in children [16]. Obesity and hypertension are strongly associated with increased rates of premature death [17]. In addition, both severely and morbidly obese children had significantly higher concentrations of fasting insulin compared to class I obese children. Hyperinsulinemia has been identified as an independent precursor for impaired glucose tolerance and T2DM [18]. A study in 463 obese children aged 6 to 19 demonstrated that severely obese children and adolescents had higher levels of blood pressure, insulin, HDL-C, triglycerides, leptin, resistin, interleukin 6 and high-sensitive C-reactive protein, lower concentrations of adiponectin, and a higher prevalence of the metabolic syndrome compared to class I obese children as classified by the pediatric IOTF criteria [19]. Although almost half of morbidly obese children had the metabolic syndrome in our study, no significant differences were detected with severely obese children, neither for HDL-C nor for triglyceride levels. In contrast to our findings, a study including 225 children and adolescents with a mean age of 13 years, showed significantly higher levels of triglycerides, total cholesterol and LDL-C and lower levels of HDL-C in extremely obese children (BMI ≥ 120% of 95th percentile) [20]. For fasting glucose, we found no significant differences between severely and class I obese children and adolescents, which is in line with findings from other studies [19, 20]. According to recent literature, fasting plasma glucose largely underestimates the number of patients with impaired glucose tolerance and is therefore no good screening test for prediabetes or T2DM in obese children [21].

Although the sample population of this study was relatively small and data on adipokines and inflammatory markers were lacking, morbidly obese children showed a significantly increased waist circumference, systolic blood pressure and fasting insulin level compared to less severely obese children. Therefore, morbidly obese children are highly prone to develop future T2DM, CVD and premature death [9, 17, 22]. It has previously also been shown that severely obese children and adolescents are more likely to become obese adults than are moderately obese children [9]. Although early prevention of childhood obesity is very important, effective and more targeted treatment approaches are urgently needed for the existing generation, especially among severely and morbidly obese children and adolescents in whom current treatment options are limited by availability, effectiveness and costs [2, 23].

In conclusion, a substantial number of obese children and adolescents referred to our clinic were classified as morbidly obese according to the newly constructed pediatric IOTF BMI 40 cut off criteria. We recommend to reanalyze obesity prevalence studies, especially in countries with a high prevalence of childhood obesity, in order to define the prevalence of morbid obesity defined according to the IOTF BMI 40 criteria. Morbidly obese children show an increased waist circumference, systolic blood pressure and hyperinsulinemia compared to less severely obese children, which may ultimately result in the future development of T2DM, CVD and premature death. Although early prevention is of utmost importance, more effective and targeted treatment approaches are urgently needed to reduce weight and metabolic risk in this subgroup of obese children and adolescents.

This explains why we searched for clinical useful tools, other than the BMI, to identify metabolic health in the pediatric obese population.

Can the shape of the OGTT curve be used to identify early abnormalities in β-cell function and insulin sensitivity in end-pubertal obese girls?

The inability of the pancreatic β-cell to secrete an adequate amount of insulin in the presence of insulin resistance, is the primary defect observed in T2DM which is a metabolic disorder characterized by chronic hyperglycemia [24]. Several methods can be applied to investigate the level of insulin sensitivity, secretion and

glucose regulation. The hyperinsulinemic euglycemic clamp is often referred to as being the gold standard technique to assess insulin sensitivity [25]. However, clamp tests are invasive, time-consuming and expensive to use for screening and large studies. Another technique more frequently used to assess the level of glucose tolerance, is the oral glucose tolerance test (OGTT). The OGTT is less invasive, less time-consuming and less expensive than the gold standard and is therefore the preferred technique for pediatric investigations [26]. Measurements of fasting plasma glucose or 2-hour glucose obtained during an OGTT can be used for the diagnosis of prediabetes or diabetes [27]. The progression from normal glucose tolerance to clinical diabetes involves an intermediate stage of hyperglycemia, characterized by impaired fasting glucose (IFG) and/or impaired glucose tolerance (IGT), known as prediabetes [27]. T2DM and the two prediabetic conditions, IFG and IGT, are becoming increasingly more common in obese children and adolescents [28], but also girls, adolescents in puberty and individuals with a family history of diabetes suffer more frequently from T2DM [29]. Nonetheless, the majority of obese children and adolescents with T2DM often remains undiagnosed [30]. In addition, relying only on fasting glucose levels greatly underestimates the number of subjects at risk for T2DM [31]. Hence, an OGTT to determine post-glucose challenge values is considered necessary [31]. It has previously been shown that even obese adolescents with normal glucose tolerance show early signs of a reduced β-cell function occurring in the background of insulin resistance, which increases their risk to develop IGT [32]. Therefore, focusing attention on the earliest stages of T2DM before the onset of any alterations in glucose tolerance has become increasingly important in obese children and adolescents [33]. Besides measuring glucose tolerance, the OGTT can also be used to calculate surrogate indices that estimate the degree of insulin secretion, insulin sensitivity or the combination of both [26]. Unfortunately, there is still no consensus on which parameter and cut-offs to use for the detection of poor insulin secretion and/or insulin resistance in obese children and adolescents.

Previous reports in adults [34] and children [35, 36] have demonstrated that the shape of the OGTT curve could be used to assess the future risk of T2DM. In **Chapter 3**, we described different shape types of the OGTT curve and evaluated its relationship with glucose and insulin metabolism, and components of the metabolic syndrome. Taking into account the fact that obese adolescent girls are

at high risk for T2DM and onset of T2DM is peaking around puberty, we focused our study on a homogeneous group of end-pubertal obese girls. In this way, we also excluded the confounding effect of transient insulin resistance taking place during puberty. Another reason to focus on this specific study group is the fact that these subjects are also at increased risk for metabolic and endocrine aberrations including the polycystic ovary syndrome, a leading cause of metabolic and reproductive health complications in young women [37]. In our study, three major OGTT shape patterns were observed, i.e. monophasic, biphasic and triphasic pattern, in addition to a pattern that could not be classified. The biphasic shape was most prevalent. In contrast, Nolfe et al. [36] found that the monophasic curve was more prevalent in a large cohort of obese children and adolescents. In addition, they detected a monotonous pattern that was not observed in our study [36]. Kim et al. [35] have not found a triphasic shape pattern in Latino adolescents, a pattern that was clearly present in our study and that of Nolfe et al. [36]. Differences in these findings may be explained by differences in age, genetic background, geographical location and/or environmental exposure between the study groups.

Our study indicates that end-pubertal obese girls with a monophasic OGTT shape had increased area under the curve (AUC) for glucose, reduced early-phase insulin secretion, reduced β-cell function relative to insulin sensitivity, increased triglycerides and increased triglyceride-to-HDL-C ratio as compared to the biphasic shape pattern. Our findings are in line with those of Nolfe et al. [36] who also observed increased AUC for glucose, reduced early-phase insulin secretion and reduced β-cell function relative to insulin sensitivity in obese children and adolescents with a monophasic pattern. It can be speculated that, compared to those with a bi- or triphasic shape pattern, obese adolescents with a monophasic shape can less efficiently clear the administered glucose load due to a reduced β-cell insulin secretion combined with the presence of insulin resistance. An impaired pancreatic β-cell response relative to the degree of insulin sensitivity has been demonstrated to be a good predictor for IGT development in obese adolescents [32], and to be a major defect leading to T2DM in both children and adults [38, 39]. Unfortunately, the different shape types could not be discriminated on the basis of the prevalence of parental diabetes, prediabetes or the metabolic syndrome, which might be due to the small cohort studied here. The finding of

higher triglycerides and triglyceride-to-HDL-C ratio in the monophasic compared to the biphasic shape group further points towards a role of the OGTT shape as an early indicator of insulin resistance [40] and possibly cardiovascular risk [41, 42] in end-pubertal obese girls. Although a trend was observed towards higher HOMA-IR and lower WBISI (estimates of insulin resistance) in the monophasic shape group, no significant differences were observed between the shape types. The shape of the OGTT curve may differentiate in the risk for T2DM and CVD even before a dysregulation of glucose or insulin metabolism is observed by these parameters. However, further research to investigate the predictive properties of the OGTT shape is recommended. When undertaking future research, we suggest to perform a duplicate OGTT for each individual to investigate the reproducibility of the OGTT. In addition, a recent study showed that plasma glucose values obtained during a 3-hour OGTT could be of added value to detect abnormal glucose tolerance in obese children [43].

In summary, end-pubertal obese girls with a monophasic OGTT shape pattern showed a reduced β-cell function relatively to the degree of insulin sensitivity which is believed to be a good predictor for IGT development in obese adolescents and a major defect leading to T2DM. In addition, subjects with a monophasic OGTT shape were characterized by higher levels of triglyceride and the triglyceride-to-HDL-C ratio compared to those with a biphasic shape. Although our investigation was performed on a relatively small population, early metabolic disturbances were already observed in obese girls with the monophasic shape type. Further longitudinal research in larger cohorts is needed to confirm, validate and complement our findings. In this way, the predictive properties of the OGTT shape could be examined with regard to the development of T2DM and CVD in obese children and adolescents.

Can metabolically "healthy" or unhealthy obese children and adolescents be differentiated?

Although the majority of obese children and adolescents are at increased risk for metabolic complications [4], a certain portion of these individuals are free from – most frequently investigated – obesity-related metabolic consequences. A concept previously introduced to describe obese individuals without any metabolic complications is called the metabolically "healthy" obese (MHO) phenotype [44-

46]. The common underlying principle to identify MHO individuals is the absence of any metabolic complication (i.e. hypertension, dyslipidemia and inflammation) and/or preserved insulin sensitivity [46]. Although the existence of this subtype of obesity is now well recognized, studies in children and adolescents are limited. This is mainly due to the lack of a universally accepted definition for the metabolic syndrome and insulin resistance in children and adolescents. We defined the MHO phenotype in obese children and adolescents on the basis of the pediatric consensus-based International Diabetes Federation (IDF) criteria for the metabolic syndrome [47] and/or the homeostatic model assessment for insulin resistance (HOMA-IR) [48] (**Chapter 4**). Both criteria are most frequently used to define in MHO in obese children and adolescents [49-51], and are based on fasting values that makes them ideal for screening purposes. According to the definition used (MR_{IDF}, $MR_{HOMA\text{-}IR}$ or the combined $MR_{IDF/HOMA\text{-}IR}$), 6 to 19% of obese children and adolescents in our study population were classified as MHO. This is lower compared to previous studies in obese youth where the prevalence is estimated around 16 to 30% [49-51], and in obese adults were it is estimated around 10 to 30% [52]. The main reason for varying MHO prevalence rates can be found in the application of different MHO classifications used. Until the MHO definition is not standardized for both children and adults, there will remain a difficulty to adequately identify MHO individuals. There is a need to standardize the MHO definition in order to enable the comparison of prevalence rates and study outcomes. This will be a great challenge for pediatric investigations as age, gender and pubertal status influence insulin levels and components of the metabolic syndrome [53, 54]. Moreover, the lack of standardized insulin assays will further complicate the establishment of a uniform definition.

In the current study, MHO children and adolescents generally showed lower fasting insulin values, lower triglycerides and lower triglyceride-to-HDL-C ratio. These findings are in line with those of previous research [50, 51]. It is known that hyperinsulinemia (i.e. greater pancreatic β-cell insulin secretory response relative to insulin sensitivity and/or reduced insulin clearance) occurs even before the glucose metabolism becomes dysregulated (i.e. prediabetes and T2DM) [55]. Prediabetes was already detected in our study population and it was more prevalent in metabolically unhealthy obese (MUO) children compared to MHO. It has recently been demonstrated that the triglyceride-to-HDL-C ratio may help to

identify children and adolescents at greater risk for structural vascular changes and metabolic derangement [56]. In addition, triglycerides and HDL-C may be useful for predicting the type of metabolic state that is likely to develop with weight gain [57]. Altogether, these findings suggest that early identification of MHO children and adolescents could detect those at low risk for future metabolic complications. It has previously been shown that MHO children were more likely to retain the MHO status in adulthood compared to metabolically unhealthy obese children [58]. Furthermore, longitudinal follow-up studies in adults have shown that MHO individuals are at lower risk for all-cause, cancer and CVD mortality than metabolically unhealthy obese [59, 60].

Studies in obese children and adults have shown that uric acid is a significant predictor of unhealthy obesity [50, 61]. The MHO definition in these studies was based on IDF criteria [62]. In our study, uric acid levels were also significantly different between MHO and MUO subjects but only for the MR_{IDF} definition when not correcting for BMI SDS. Hence, study outcomes highly depend on which MHO classification is used. No differences were found for hemoglobin A1c, liver enzymes, white blood cell count and sex-hormone binding globulin between the two metabolic states. Future studies with large sample sizes are needed to confirm our findings. In addition, we suggest to include other relevant biomarkers of MetS such as adiponectin, intercellular adhesion molecules or microalbuminuria in the definition of MHO. In this way, the MHO phenotype is defined more comprehensively and the risk for future T2DM and CVD might be better predicted.

This study has been able to discriminate between MHO and MUO subjects, however, some important remarks must be made. The application of our classification system resulted in a metabolically 'intermediate'/'at risk' phenotype that fell in-between the MHO and MUO phenotypes defined according to MR_{IDF} and $MR_{IDF/HOMA\text{-}IR}$ definition. It still remains unclear whether and how fast a MHO child can develop into 'at risk' and consequently MUO, or vice versa [57, 63]. It has previously been shown that individuals who maintain MHO show a significantly lower risk to develop T2DM and CVD [64]. So if the metabolic status is reversible, a targeted and intensive intervention (e.g. multidisciplinary obesity management or bariatric surgery) could be useful to reverse metabolically 'at risk' or MUO children to MHO [65]. In order to confirm this, it is required to perform longitudinal follow-up studies in future. Also important to note is that screening for MHO or

MUO could target obese individuals for effective prevention and treatment approaches and thus lead to a reduction of health care costs.

To conclude, 6 to 19% of obese children and adolescents were classified as MHO depending on the definition used. MHO children and adolescents showed lower fasting insulin values, lower triglycerides, a lower triglyceride-to-HDL-C ratio, and a lower prevalence of prediabetes compared to MUO children. Important to note, however, prevalence rates and study results highly depend of which MHO classification is used. Therefore, the development of standardized criteria to define MHO is highly advisable. Screening for fasting metabolic status in children and adolescents may target those at greatest need for more aggressive and specialized therapy and could assist in refocusing current prevention strategies. Nonetheless, future longitudinal research in larger cohorts is needed to further investigate the value of discriminating between MHO and MUO children and adolescents.

Can ^{1}H-NMR-based metabolomics be used to study the metabolic health of obese children and adolescents?

In order to shed new light on our clinical findings, to better understand the underlying pathophysiological processes and to search for putative biomarkers for childhood obesity and associated metabolic complications, we performed ^{1}H-NMR-based metabolomics. ^{1}H-NMR-based metabolomics is a powerful tool to detect metabolites in biological samples, it is non-invasive, non-biased, easy quantifiable, requires little or no sample preparation, needs no chemical derivatization and permits the identification of novel compounds [66]. For an accurate implementation in this doctoral project, however, this technique needed to be scientifically improved both on the level of sample handling in a clinical environment and ^{1}H-NMR experimental analysis.

The accurate interpretation of 1D ^{1}H-NMR spectra can be challenging in terms of metabolite identities and abundances, in particular in crowded regions with severe signal overlap, leading to uncertainty in NMR signal assignments [67, 68]. The assignment of metabolite signals in NMR spectra is generally performed on the basis of chemical shift values and signal multiplicities, and is frequently accomplished with reference to the literature and confirmatory spectral editing

techniques [69, 70]. However, these techniques are not accurate enough to allow a reliable identification of metabolites in complex biofluids such as plasma or urine [71]. Additionally, several chemical shift values can vary under different experimental measuring conditions such as temperature or pH [72]. In this thesis, we accurately assigned 32 plasma and 27 urine metabolites in the 400 MHz ^{1}H-NMR spectrum by means of spiking experiments, i.e. by adding a known compound in a relevant amount, to plasma and urine reference samples (**Chapter 5**). Hereby, we were able to rationally define 110 plasma and 134 urine integration regions in the ^{1}H-NMR spectrum, being the variables for multivariate statistics. The main advantages of using this approach compared to fixed bucketing methods are the reduction of the influence of small chemical shift changes on the study results and the avoidance of splitting signals randomly, resulting in more accurate study results and data interpretation. However, in spectral regions where weakly concentrated metabolites are present, instrumental noise will be apparent. This problem can be alleviated by excluding noisy integration regions, defined according to a specified threshold, from the dataset [73]. Therefore, and in addition to the accurate assignment of plasma and urine metabolites and the introduction of variable-sized fixed integration regions in the ^{1}H-NMR spectrum, we identified noisy variables (i.e. with unpredictable variation in signal intensity) in plasma and urine ^{1}H-NMR spectra and evaluated their influence on group differentiation. For our experimental setting, a 15% threshold for the coefficient of variation was obtained as the best for both plasma and urine ^{1}H-NMR data. It was demonstrated that removal of these noisy variables had no significant influence on the predictive sensitivity and specificity, indicating that the proposed methodology seems promising and could contribute to a better understanding and interpretation of the study findings.

To further improve the complete analysis procedure towards a possible application in clinic, we evaluated the impact of preanalytical variation on the plasma ^{1}H-NMR metabolome that can occur at the level of collection, processing and storage (**Chapter 6**). Plasma levels of lactate, pyruvate and glucose changed in cooled fasting blood samples processed with a delay of 3 h to 8 h. These changes could be attributed to a continued anaerobic cell metabolism in the collected blood during the prolonged contact with erythrocytes. Hereby, pyruvate is reduced to lactate by lactate dehydrogenase resulting in additional glycolysis

[74]. In line with our findings, it has previously been shown that plasma pyruvate and glucose levels decreased, and lactate levels increased upon storage of blood during 3 h at 4°C [75]. In contrast to our findings, it has previously been demonstrated that serum lactate and glucose levels changed during a 4 h to 24 h storage at room temperature but not during storage at 4°C [76]. This might be due to different blood collection tubes used, i.e. a lithium heparin tube was used in our study and in the study of Fliniaux et al. [76] a sodium fluoride tube was used. Fluoride is known to inhibit in vitro anaerobic glycolysis (mainly by inhibiting enolase in a later part of the glycolytic pathway) that takes place in blood resulting in maintained concentrations of glucose and lactate [77]. Nonetheless, lithium heparin is usually the preferred anticoagulant for ^{1}H-NMR spectroscopic analysis as it produces negligible interference with the signals in the ^{1}H-NMR spectrum [78]. Besides, it has been previously demonstrated that accurate and similar glucose and lactate results can be obtained with either lithium heparin or fluoride-containing tubes, provided that the sample is cooled and centrifugated within 30 minutes [77, 79]. In order to avoid an impact of processing delay on our study results described in Chapter 7, blood samples were immediately cooled on ice and centrifugated within 30 minutes. It should be noted, however, that the inter-individual variation observed was much larger than the preanalytical variation, i.e. than a processing delay of 3 h to 8 h. Consequently, the impact of preanalytical variation on multivariate group classification will be minimal. However, caution should be taken with the interpretation of individual concentrations of lactate, glucose and pyruvate when a processing delay of 30 minutes is exceeded.

Although efforts are currently made within the field of metabolomics to move towards defining standard operation procedures (SOPs) for preanalytical handling [75], complete standardization of the preanalytical processing is not yet feasible between and within clinical settings. Alternatively, application of preanalytical sample codes that traces and manages these variations would allow sample harmonization. To this end, the biobanking community recently developed the Standard PREanalytical Code (SPREC) which allows for coding preanalytical conditions [80, 81]. It is suggested that SPREC will identify samples that are fit for a particular analysis and exclude those that were subjected to unwanted, interfering preanalytical conditions. In an effort to validate SPREC for ^{1}H-NMR plasma metabolomics, we have coded the conditions used here, when possible,

according to SPREC. Our results show that SPREC is easily implementable and could contribute to the validation of ^{1}H-NMR metabolomics in clinical, biobank and multicenter research settings.

The experimental analysis procedure of ^{1}H-NMR spectroscopy for plasma and urine was optimized to allow an accurate assignment of metabolites in 400 MHz ^{1}H-NMR spectra. In addition, preanalytical influences introduced by differences in sample handling were evaluated to further improve the complete ^{1}H-NMR measurement procedure towards a possible application in clinic. Although the inter-individual variation was much larger than the preanalytical variation, the processing delay of a cooled blood sample should be limited to prevent individual variations in levels of lactate, pyruvate and glucose. SPREC is easily implementable and could contribute to the validation of ^{1}H-NMR metabolomics in clinical, biobank and multicenter research settings.

In **Chapter 7**, we implemented the described experimental analysis protocol for ^{1}H-NMR spectroscopy of plasma in a prospective study including obese and normal-weight children and adolescents. The plasma metabolome of obese children and adolescents was characterized by higher levels of lipids, lactate and N-acetyl glycoproteins, and lower levels of choline-containing phospholipids, glucose and α-ketoglutarate compared to the normal-weight plasma metabolome. Hence, it is suggested that the (interrelated) metabolism of obese children is altered for lipids and choline-containing phospholipids, and is characterized by an increased glycolytic activity, inflammation and a disturbed energy metabolism. A MS-based metabolomics study previously showed that levels of two acylcarnitines were elevated in serum of obese children, whereas glutamine, methionine, proline, and phosphatidylcholines were found to be decreased [82]. In our study, no relevant differences were detected for amino acids but the level of choline-containing phospholipids (i.e. phosphatidylcholine and sphingomyelin) was significantly lower in obese compared to normal-weight children. In line with our findings, increased levels of phosphatidylcholines were detected by MS in plasma of obese children and adolescents after weight loss intervention [83, 84]. Compared to adults, obese children and adolescents generally show early metabolic alterations which may be a reflection of the short duration of obesity

and the presence of metabolic adaptive mechanisms in childhood that may gradually fail when becoming obese as an adult [85, 86].

Within the obese study group, a further subdivision was made into MHO and MUO children and adolescents. These metabolic phenotypes could be clearly distinguished and MHO showed a 'healthier' plasma metabolic profile. This is, to our knowledge, the first ^{1}H-NMR-based metabolomics study in which the plasma metabolic profile of the MHO phenotype is studied in children and adolescents. Nonetheless, further longitudinal research is needed to monitor the development and state (i.e. transient or stable) of MHO and MUO phenotypes, before the ability of this subdivision to predict T2DM or CVD can be determined. In our study, it was also demonstrated that levels of conventionally measured fasting plasma triglycerides gradually increased towards a more obese and MUO metabolic profile. It is therefore suggested that plasma triglycerides and choline-containing phospholipids best characterizes the metabolic heterogeneity and changes in metabolic health risk in obese children and adolescents. However, future studies are needed to reveal whether triglyceride and choline-containing phospholipid levels in childhood have consequences that last into adulthood [87].

A drawback of the current study was the lack of conventional biochemical data for normal-weight children and adolescents which limited the implementation of our study results. Consequently, this study has been unable to define the metabolic risk state in normal-weight children and to compare this profile with that of obese subjects. Another limitation of this study is the lack of an independent cohort to validate our findings. Nonetheless, research was conducted according to a very accurate and well-controlled experimental protocol, increasing the quality and reliability of our study findings.

In the near future, the plasma ^{1}H-NMR metabolic profile might become useful in detecting differential phenotypes of obesity and in identifying those at greatest risk for developing metabolic diseases later in life. Further studies with larger cohorts and with a longitudinal design are needed to confirm our findings and assure validity. Eventually, this might open new perspectives for the prevention and treatment strategies of childhood obesity and related metabolic complications, resulting in a better life expectancy and quality of life for the current and next generation of children and adolescents.

The implementation of a robust and accurate analysis protocol for ^{1}H-NMR spectroscopy, allowed to clearly differentiate between the plasma metabolome of obese and normal-weight children and adolescents. The metabolism of obese children is characterized by an altered metabolism of lipids and phospholipids, an increased glycolytic activity, inflammation and a disturbed energy metabolism. A subdivision of metabolic phenotypes could be made within the obese population, and MHO showed to have a 'healthier' plasma metabolic profile than MUO. Triglycerides should possibly get more attention in the management of obesity-related metabolic complications in children and adolescents. However, future research is needed to continue the search for biomarkers that are important in obesity-related metabolic complications in children and adolescents.

Clinical implications

The rapid increase in the prevalence and severity of childhood obesity will undoubtedly have a significant impact on our health care system. At the moment, it remains a great challenge to offer an appropriate treatment for morbidly obese children as conventional approaches are often ineffective. Hence, early detection of children at risk for or with extreme obesity is of utmost importance. To this end, we recommend to implement the newly developed international IOTF BMI 40 cut-off values in clinical research and daily practice. As such, prevalence rates of morbid childhood obesity can be calculated and be implemented in policy decisions and future research. Eventually, targeted and more aggressive approaches for prevention and treatment of severe childhood obesity can be developed in order to combat the current obesity epidemic.

Although obesity is the most important trigger of cardiometabolic complications in the general population, within obese cohorts, the degree of weight excess might not be so important in determining the metabolic risk. In this context, we studied the abilities of the OGTT curve shape, the classification of obese individuals in MHO or MUO, and ^{1}H-NMR-based plasma metabolomics as clinically useful tools to early identify metabolic alterations in obese children and adolescents. Children and adolescents are an important target population, because they are likely to develop obesity-related metabolic complications over a shorter time frame than adults. The difficulty of studying this specific population is the influence of transient insulin resistance associated with puberty. To correct for this confounding, we studied the shape of the OGTT only in end-pubertal obese girls. Differences in the OGTT shape pattern were mainly explained by differences in the insulin secretory capacity of the pancreatic β-cell which appears to be an early defect of T2DM in obese adolescents [88, 89]. Of note, the evaluation of the shape of the OGTT curve is less practical, more expensive and time-consuming than the classification of obese children into MHO or MUO according to fasting measurements. We showed that MHO children and adolescents were primarily characterized by lower fasting insulin, lower triglyceride levels and TG/HDL-C ratio compared to MUO. Additional ^{1}H-NMR-based plasma metabolomics showed that the MHO phenotype showed a clearly different metabolic profile compared to the MUO phenotype, and that the triglyceride level characterizes the metabolic heterogeneity of obese children and adolescents very well.

However, a lot of questions still remain concerning the clinical utility of the presented tools: (1) How to include insulin resistance in the definition of metabolic health risk when normal pediatric ranges or when uniform assays to determine insulin concentration are still missing? (2) Is it tolerable to use fixed cut-off values instead of normalized values for a specific pediatric population in the definition of metabolic health risk, and is it possible to generalize normalized values across obese pediatric populations? (3) Is it possible to identify obesity-related metabolic complications using fasting indices alone or is an OGTT necessary to perform? (4) Can the OGTT shape, metabolic health risk definition or ^{1}H-NMR plasma metabolic profile be used to predict the occurrence of future CVD and T2DM? To clarify these questions, efforts are required by medical and research communities in order to reach a consensus and longitudinal research in large study populations are needed.

Screening of obese children and adolescents at low or high risk for metabolic complications can be of clinical importance in the development of targeted and individual prevention and treatment strategies. Although our results indicate that the presented tools could be of added value in clinical practice, their implementation in clinic remains incomplete. Future research should be aimed at determining the ability of these tools to predict the development of T2DM and CVD in the pediatric obesity population.

Future directions

The results obtained during this doctoral project provide fundamentals for further clinical and metabolomics research into childhood obesity and associated metabolic complications. The presented tools enabled us to classify obese children and adolescents according to their weight status and metabolic health state.

The implementation of the IOTF BMI 40 cut-off values in clinical research enables to calculate international prevalence rates of morbid childhood obesity. Eventually, this might open new perspectives to future research, policy decisions, and the clinical management of morbid childhood obesity.

Investigating the shape of the OGTT curve demonstrated that end-pubertal obese girls with a monophasic shape type already show early metabolic disturbances in insulin secretion. However, future studies of the OGTT shape including a larger and heterogeneous sample population are needed to confirm and validate our study results. In addition, they should address whether the OGTT shape is able to predict the development of T2DM and/or CVD. When undertaking future research, we also suggest to perform a duplicate or confirmatory OGTT for each individual to investigate the reproducibility of the OGTT. Although a 3-hour OGTT is more time-consuming and expensive than a 2-hour OGTT, it could be of added value to detect abnormal glucose tolerance in obese children [43]. Future studies should include pubertal status as a confounding factor as the presence of transient insulin resistance could influence the study results. Although there is still no consensus regarding normal pediatric ranges or assays for insulin, the shape of insulin response curves could also be evaluated as it has proven to predict the development of T2DM in adults [90].

By classifying obese children and adolescents based on their metabolic health risk (i.e. MHO or MUO), those at lower health risk can be guided to less intensive therapy (e.g. self-management or outpatient therapy), whereas those at higher health risk can be directed to more intensive treatment approaches (e.g. family-based multidisciplinary obesity management, pharmacotherapy or bariatric surgery), resulting in a reduction of health care costs. However, a consensus should first be reached regarding the classification of MHO or MHO in pediatrics. Eventually, future longitudinal research may focus on the time frame and reversibility of the progression into the MUO phenotype, and assessment of future risk for T2DM and/or CVD. In the meanwhile, general prevention of childhood

obesity is still of utmost importance as obese individuals are always at greater risk for adverse long-term outcomes compared to their normal-weight counterparts [91].

In the near future, the plasma ^{1}H-NMR metabolic profile could be useful in detecting differential phenotypes of obesity and in identifying those at greatest risk for developing metabolic diseases later in life. In future, longitudinal research in large cohorts using higher-field ^{1}H-NMR spectroscopy in combination with MS, new statistical models and an integrative approach to analyze gene-transcriptome-proteome-metabolite data can be used to find relevant biomarkers for the assessment of obesity-related metabolic diseases. The inclusion of other biofluids such as urine, salivary or feces which are less invasive than obtaining plasma from children and adolescents, could be of added value for pediatric research. Also the inclusion of factors such as nutrition, level of physical activity or gut microbiota composition will add great value to this research.

The preliminary results of this thesis are very promising for future research of the metabolic health of obese children and adolescents and can be the beginning of further interesting research. Future longitudinal prospective research in larger study cohorts is needed to further examine the feasibility and validity of the presented tools to early identify metabolic alterations in obese children and adolescents. Eventually, this might open new perspectives to develop more targeted and personalized clinical management of childhood obesity, reduce health care costs and result in a better life expectancy and quality of life for the current and next generation of children and adolescents.

References

1. Ng M, Fleming T, Robinson M, Thomson B, Graetz N, Margono C, et al. Global, regional, and national prevalence of overweight and obesity in children and adults during 1980-2013: a systematic analysis for the Global Burden of Disease Study 2013. Lancet. 2014;384(9945):766-81.
2. Wang YC, McPherson K, Marsh T, Gortmaker SL, Brown M. Health and economic burden of the projected obesity trends in the USA and the UK. Lancet. 2011;378(9793):815-25.
3. Cattaneo A, Monasta L, Stamatakis E, Lioret S, Castetbon K, Frenken F, et al. Overweight and obesity in infants and pre-school children in the European Union: a review of existing data. Obes Rev. 2010;11(5):389-98.
4. Goran MI, Ball GDC, Cruz ML. Obesity and risk of type 2 diabetes and cardiovascular disease in children and adolescents. J Clin Endocr Metab. 2003;88(4):1417-27.
5. Reilly JJ, Kelly J. Long-term impact of overweight and obesity in childhood and adolescence on morbidity and premature mortality in adulthood: systematic review. Int J Obes. 2011;35(7):891-8.
6. van Dommelen P, Schonbeck Y, van Buuren S, HiraSing RA. Trends in a life threatening condition: morbid obesity in Dutch, Turkish and Moroccan children in The Netherlands. PLoS One. 2014;9(4):e94299.
7. Skinner AC, Skelton JA. Prevalence and trends in obesity and severe obesity among children in the United States, 1999-2012. JAMA Pediatr. 2014;168(6):561-6.
8. Freedman DS, Ogden CL, Blanck HM, Borrud LG, Dietz WH. The abilities of body mass index and skinfold thicknesses to identify children with low or elevated levels of dual-energy X-ray absorptiometry-determined body fatness. J Pediatr. 2013;163(1):160-6.
9. Freedman DS, Mei Z, Srinivasan SR, Berenson GS, Dietz WH. Cardiovascular risk factors and excess adiposity among overweight children and adolescents: the Bogalusa Heart Study. J Pediatr. 2007;150(1):12-7.
10. de Onis M, Onyango AW, Borghi E, Siyam A, Nishida C, Siekmann J. Development of a WHO growth reference for school-aged children and adolescents. Bull World Health Organ. 2007;85(9):660-7.
11. Cole T, Lobstein T. Extended international (IOTF) body mass index cut-offs for thinness, overweight and obesity. Pediatr Obes. 2012;7(4):284-94.
12. Rolland-Cachera MF. Towards a simplified definition of childhood obesity? A focus on the extended IOTF references. Pediatr Obes. 2012;7(4):259-60.
13. World Health Organisation. Physical status: the use and interpretation of anthropometry. Report of a WHO Expert Committee, WHO Technical Report Series N°854. Geneva: WHO, 1995.
14. World Health Organisation. Obesity: preventing and managing the global epidemic. Report of a WHO Expert Committee, WHO Technical Report Series, N°894. Geneva: WHO, 2000.
15. Lo JC, Chandra M, Sinaiko A, Daniels SR, Prineas RJ, Maring B, et al. Severe obesity in children: prevalence, persistence and relation to hypertension. Int J Pediatr Endocrinol. 2014;2014(1):3.
16. Sorof J, Daniels S. Obesity hypertension in children: a problem of epidemic proportions. Hypertension. 2002;40(4):441-7.
17. Franks PW, Hanson RL, Knowler WC, Sievers ML, Bennett PH, Looker HC. Childhood obesity, other cardiovascular risk factors, and premature death. N Engl J Med. 2010;362(6):485-93.
18. Morrison JA, Glueck CJ, Horn PS, Wang P. Childhood predictors of adult type 2 diabetes at 9-and 26-year follow-ups. Arch Pediatr Adolesc Med. 2010;164(1):53-60.
19. Rank M, Siegrist M, Wilks DC, Langhof H, Wolfarth B, Haller B, et al. The cardio-metabolic risk of moderate and severe obesity in children and adolescents. J Pediatr. 2013;163(1):137-42.

20. Norris AL, Steinberger J, Steffen LM, Metzig AM, Schwarzenberg SJ, Kelly AS. Circulating oxidized LDL and inflammation in extreme pediatric obesity. Obesity (Silver Spring). 2011;19(7):1415-9.
21. Brar PC, Mengwall L, Franklin BH, Fierman AH. Screening obese children and adolescents for prediabetes and/or type 2 diabetes in pediatric practices: a validation study. Clin Pediatr (Phila). 2014;53(8):771-6.
22. Yeung EH, Zhang C, Louis GM, Willett WC, Hu FB. Childhood size and life course weight characteristics in association with the risk of incident type 2 diabetes. Diabetes Care. 2010;33(6):1364-9.
23. Johnston CA, Tyler C, Palcic JL, Stansberry SA, Gallagher MR, Foreyt JP. Smaller weight changes in standardized body mass index in response to treatment as weight classification increases. J Pediatr. 2011;158(4):624-7.
24. Nolan CJ, Damm P, Prentki M. Type 2 diabetes across generations: from pathophysiology to prevention and management. Lancet. 2011;378(9786):169-81.
25. DeFronzo RA, Tobin JD, Andres R. Glucose clamp technique: a method for quantifying insulin secretion and resistance. Am J Physiol Endocrinol Metab. 1979;237(3):214-23.
26. Stumvoll M, Mitrakou A, Pimenta W, Jenssen T, Yki-Järvinen H, Van Haeften T, et al. Use of the oral glucose tolerance test to assess insulin release and insulin sensitivity. Diabetes Care. 2000;23(3):295-301.
27. American Diabetes Association. Diagnosis and classification of diabetes mellitus. Diabetes Care. 2014;37:S81-90.
28. Rosenbloom AL, Silverstein JH, Amemiya S, Zeitler P, Klingensmith GJ. Type 2 diabetes in children and adolescents. Pediatr Diabetes. 2009;10 (Suppl 12):17-32.
29. Writing Group for the Search for Diabetes in Youth Study Group, Dabelea D, Bell RA, D'Agostino RB, Jr., Imperatore G, Johansen JM, et al. Incidence of diabetes in youth in the United States. JAMA. 2007;297(24):2716-24.
30. Reinehr T, Kiess W, Kapellen T, Wiegand S, Holl RW, Apv, et al. Children with diabetes mellitus type 2 in Europe: an underserved population. Arch Dis Child. 2010;95(11):954.
31. Bartoli E, Fra GP, Carnevale Schianca GP. The oral glucose tolerance test (OGTT) revisited. Eur J Intern Med. 2011;22(1):8-12.
32. Giannini C, Weiss R, Cali A, Bonadonna R, Santoro N, Pierpont B, et al. Evidence for early defects in insulin sensitivity and secretion before the onset of glucose dysregulation in obese youths: a longitudinal study. Diabetes. 2012;61(3):606-14.
33. Caprio S. Development of type 2 diabetes mellitus in the obese adolescent: a growing challenge. Endocr Pract. 2012;18(5):791-5.
34. Abdul-Ghani MA, Lyssenko V, Tuomi T, Defronzo RA, Groop L. The shape of plasma glucose concentration curve during OGTT predicts future risk of type 2 diabetes. Diabetes Metab Res Rev. 2010;26(4):280-6.
35. Kim JY, Coletta DK, Mandarino LJ, Shaibi GQ. Glucose response curve and type 2 diabetes risk in Latino adolescents. Diabetes Care. 2012;35(9):1925-30.
36. Nolfe G, Spreghini MR, Sforza RW, Morino G, Manco M. Beyond the morphology of the glucose curve following an oral glucose tolerance test in obese youth. Eur J Endocrinol. 2012;166:107-14.
37. Vilmann LS, Thisted E, Baker JL, Holm JC. Development of obesity and polycystic ovary syndrome in adolescents. Horm Res Paediatr. 2012;78(5-6):269-78.
38. Kahn SE. The relative contributions of insulin resistance and beta-cell dysfunction to the pathophysiology of Type 2 diabetes. Diabetologia. 2003;46(1):3-19.
39. Gungor N, Bacha F, Saad R, Janosky J, Arslanian S. Youth type 2 diabetes: insulin resistance, beta-cell failure, or both? Diabetes Care. 2005;28(3):638-44.
40. Giannini C, Santoro N, Caprio S, Kim G, Lartaud D, Shaw M, et al. The triglyceride-to-HDL cholesterol ratio: association with insulin resistance in obese youths of different ethnic backgrounds. Diabetes Care. 2011;34(8):1869-74.
41. Quijada Z, Paoli M, Zerpa Y, Camacho N, Cichetti R, Villarroel V, et al. The triglyceride/HDL-cholesterol ratio as a marker of cardiovascular risk in obese children; association with traditional and emergent risk factors. Pediatr Diabetes. 2008;9(5):464-71.

42. Urbina EM, Khoury PR, McCoy CE, Dolan LM, Daniels SR, Kimball TR. Triglyceride to HDL-C ratio and increased arterial stiffness in children, adolescents, and young adults. Pediatrics. 2013;131(4):e1082-90.
43. Yin C, Zhang H, Xiao Y, Liu W. Shape of glucose curve can be used as a predictor for screening prediabetes in obese children. Acta Paediatr. 2014;103(5):e199-205.
44. Wildman RP, Muntner P, Reynolds K, McGinn AP, Rajpathak S, Wylie-Rosett J, et al. The obese without cardiometabolic risk factor clustering and the normal weight with cardiometabolic risk factor clustering: prevalence and correlates of 2 phenotypes among the US population (NHANES 1999-2004). Arch Intern Med. 2008;168(15):1617-24.
45. Blüher M. The distinction of metabolically 'healthy' from 'unhealthy' obese individuals. Curr Opin Lipidol. 2010;21(1):38-43.
46. Primeau V, Coderre L, Karelis AD, Brochu M, Lavoie ME, Messier V, et al. Characterizing the profile of obese patients who are metabolically healthy. Int J Obes (Lond). 2011;35(7):971-81.
47. Zimmet P, Alberti K, George MM, Kaufman F, Tajima N, Silink M, et al. The metabolic sydrome in children and adolescents - an IDF consensus report. Pediatr Diabetes. 2007;8:299-306.
48. Keskin M, Kurtoglu S, Kendirci M, Atabek ME, Yazici C. Homeostasis model assessment is more reliable than the fasting glucose/insulin ratio and quantitative insulin sensitivity check index for assessing insulin resistance among obese children and adolescents. Pediatrics. 2005;115:500-3.
49. Mangge H, Zelzer S, Puerstner P, Schnedl WJ, Reeves G, Postolache TT, et al. Uric acid best predicts metabolically unhealthy obesity with increased cardiovascular risk in youth and adults. Obesity. 2013;21(1):E71-7.
50. Weghuber D, Zelzer S, Stelzer I, Paulmichl K, Kammerhofer D, Schnedl W, et al. High risk vs. "metabolically healthy" phenotype in juvenile obesity-neck subcutaneous adipose tissue and serum uric acid are clinically relevant. Exp Clin Endocrinol Diabetes. 2013;121(7):384-90.
51. Prince RL, Kuk JL, Ambler KA, Dhaliwal J, Ball GD. Predictors of metabolically healthy obesity in children. Diabetes Care. 2014;37(5):1462-8.
52. van Vliet-Ostaptchouk JV, Nuotio ML, Slagter SN, Doiron D, Fischer K, Foco L, et al. The prevalence of metabolic syndrome and metabolically healthy obesity in Europe: a collaborative analysis of ten large cohort studies. BMC Endocr Disord. 2014;14:9.
53. Solorzano CMB, McCartney CR. Obesity and the pubertal transition in girls and boys. Reproduction. 2010;140(3):399-410.
54. Deboer MD. Ethnicity, obesity and the metabolic syndrome: implications on assessing risk and targeting intervention. Expert Rev Endocrinol Metab. 2011;6(2):279-89.
55. Cali AMG, Dalla Man C, Cobelli C, Dziura J, Seyal A, Shaw M, et al. Primary defects in beta-cell function further exacerbated by worsening of insulin resistance mark the development of impaired glucose tolerance in obese adolescents. Diabetes Care. 2009;32(3):456-61.
56. Pacifico L, Bonci E, Andreoli G, Romaggioli S, Di Miscio R, Lombardo CV, et al. Association of serum triglyceride-to-HDL cholesterol ratio with carotid artery intima-media thickness, insulin resistance and nonalcoholic fatty liver disease in children and adolescents. Nutr Metab Cardiovasc Dis. 2014;24(7):737-43.
57. Achilike I, Hazuda HP, Fowler SP, Aung K, Lorenzo C. Predicting the development of the metabolically healthy obese phenotype. Int J Obes (Lond). 2015;39(2):228-34.
58. Li S, Chen W, Srinivasan SR, Xu J, Berenson GS. Relation of childhood obesity/cardiometabolic phenotypes to adult cardiometabolic profile the Bogalusa Heart study. Am J Epidemiol. 2012;176(Suppl 7):S142-9.
59. Calori G, Lattuada G, Piemonti L, Garancini MP, Ragogna F, Villa M, et al. Prevalence, metabolic features, and prognosis of metabolically healthy obese Italian individuals the Cremona Study. Diabetes Care. 2011;34(1):210-5.
60. Hamer M, Stamatakis E. Metabolically healthy obesity and risk of all-cause and cardiovascular disease mortality. J Clin Endocrinol Metab. 2012;97(7):2482-8.
61. Mangge H, Almer G, Truschnig-Wilders M, Schmidt A, Gasser R, Fuchs D. Inflammation, adiponectin, obesity and cardiovascular risk. Curr Med Chem. 2010;17(36):4511-20.

62. Alberti K, Zimmet P, Shaw J. Metabolic syndrome - a new world-wide definition. A consensus statement from the International Diabetes Federation. Diabetic Med. 2006;23(5):469-80.
63. Goodman E, Li C, Tu YK, Ford E, Sun SS, Huang TT. Stability of the factor structure of the metabolic syndrome across pubertal development: confirmatory factor analyses of three alternative models. J Pediatr. 2009;155(3: S5):e1-8.
64. Appleton SL, Seaborn CJ, Visvanathan R, Hill CL, Gill TK, Taylor AW, et al. Diabetes and cardiovascular disease outcomes in the metabolically healthy obese phenotype: a cohort study. Diabetes Care. 2013;36(8):2388-94.
65. Kantartzis K, Machann J, Schick F, Rittig K, Machicao F, Fritsche A, et al. Effects of a lifestyle intervention in metabolically benign and malign obesity. Diabetologia. 2011;54(4):864-8.
66. Wishart DS. Quantitative metabolomics using NMR. Trends Analyt Chem. 2008;27(3):228-37.
67. Zheng C, Zhang S, Ragg S, Raftery D, Vitek O. Identification and quantification of metabolites in 1H NMR spectra by Bayesian model selection. Bioinformatics. 2011;27(12):1637-44.
68. O'Connell TM. Recent advances in metabolomics in oncology. Bioanalysis. 2012;4(4):431-51.
69. Nicholson JK, Foxall PJ, Spraul M, Farrant RD, Lindon JC. 750 MHz 1H and 1H-13C NMR spectroscopy of human blood plasma. Anal Chem. 1995;67(5):793-811.
70. Salek RM, Maguire ML, Bentley E, Rubtsov DV, Hough T, Cheeseman M, et al. A metabolomic comparison of urinary changes in type 2 diabetes in mouse, rat, and human. Physiol Genomics. 2007;29(2):99-108.
71. Lindon JC, Nicholson JK, Everett JR. NMR spectroscopy of biofluids. Ann R NMR S. 1999;38:1-88.
72. Kohl SM, Klein MS, Hochrein J, Oefner PJ, Spang R, Gronwald W. State-of-the art data normalization methods improve NMR-based metabolomic analysis. Metabolomics. 2012;8(1):146-60.
73. Halouska S, Powers R. Negative impact of noise on the principal component analysis of NMR data. J Magn Reson. 2006;178(1):88-95.
74. Baynes JW, Dominiczak MH. Medical Biochemistry. Amsterdam: Elsevier; 2010. 712 p.
75. Bernini P, Bertini I, Luchinat C, Nincheri P, Staderini S, Turano P. Standard operating procedures for pre-analytical handling of blood and urine for metabolomic studies and biobanks. J Biomol NMR. 2011;49(3-4):231-43.
76. Fliniaux O, Gaillard G, Lion A, Cailleu D, Mesnard F, Betsou F. Influence of common preanalytical variations on the metabolic profile of serum samples in biobanks. J Biomol NMR. 2011;51(4):457-65.
77. Shi RZ, Seeley ES, Bowen R, Faix JD. Rapid blood separation is superior to fluoride for preventing in vitro reductions in measured blood glucose concentration. J Clin Pathol. 2009;62(8):752-3.
78. Nicholson JK, O'Flynn MP, Sadler PJ, Macleod AF, Juul SM, Sonksen PH. Proton-nuclear-magnetic-resonance studies of serum, plasma and urine from fasting normal and diabetic subjects. Biochem J. 1984;217(2):365-75.
79. Mikesh LM, Bruns DE. Stabilization of glucose in blood specimens: mechanism of delay in fluoride inhibition of glycolysis. Clin Chem. 2008;54(5):930-2.
80. Betsou F, Lehmann S, Ashton G, Barnes M, Benson EE, Coppola D, et al. Standard preanalytical coding for biospecimens: defining the sample PREanalytical code. Cancer Epidem Biomar. 2010;19(4):1004-11.
81. Lehmann S, Guadagni F, Moore H, Ashton G, Barnes M, Benson E, et al. Standard preanalytical coding for biospecimens: review and implementation of the Sample PREanalytical Code (SPREC). Biopreserv Biobank. 2012;10(4):366-74.
82. Wahl S, Yu Z, Kleber M, Singmann P, Holzapfel C, He Y, et al. Childhood obesity is associated with changes in the serum metabolite profile. Obes Facts. 2012;5(5):660-70.
83. Wahl S, Holzapfel C, Yu Z, Breier M, Kondofersky I, Fuchs C, et al. Metabolomics reveals determinants of weight loss during lifestyle intervention in obese children. Metabolomics. 2013;9(6):1157-67.

84. Reinehr T, Wolters B, Knop C, Lass N, Hellmuth C, Harder U, et al. Changes in the serum metabolite profile in obese children with weight loss. Eur J Nutr. 2015;54(2):173-81.
85. Csabi G, Torok K, Jeges S, Molnar D. Presence of metabolic cardiovascular syndrome in obese children. Eur J Pediatr. 2000;159(1-2):91-4.
86. Aucouturier J, Duche P, Timmons BW. Metabolic flexibility and obesity in children and youth. Obes Rev. 2011;12(5):e44-53.
87. de Ferranti SD, Crean S, Cotter J, Boyd D, Osganian SK. Hypertriglyceridemia in a pediatric referral practice: experience with 300 patients. Clin Pediatr (Phila). 2011;50(4):297-307.
88. Bacha F, Lee S, Gungor N, Arslanian SA. From pre-diabetes to type 2 diabetes in obese youth: pathophysiological characteristics along the spectrum of glucose dysregulation. Diabetes Care. 2010;33(10):2225-31.
89. Bacha F, Gungor N, Lee S, Arslanian SA. Progressive deterioration of beta-cell function in obese youth with type 2 diabetes. Pediatr Diabetes. 2013;14(2):106-11.
90. Hayashi T, Boyko EJ, Sato KK, McNeely MJ, Leonetti DL, Kahn SE, et al. Patterns of Insulin Concentration During the OGTT Predict the Risk of Type 2 Diabetes in Japanese Americans. Diabetes Care. 2013;36:1229-35.
91. Kramer CK, Zinman B, Retnakaran R. Are metabolically healthy overweight and obesity benign conditions? A systematic review and meta-analysis. Ann Intern Med. 2013;159(11):758-69.

Childhood obesity is a multifactorial complex disorder which is closely associated with the presence of metabolic complications such as insulin resistance, the metabolic syndrome, prediabetes and premature coronary disease. In the past decades, the prevalence of extreme childhood obesity has rapidly increased. To define morbid childhood obesity and to calculate its prevalence, the international (IOTF) BMI cut-off points which correspond to a BMI higher than 40 at the age of 18 years were established. The future application of these BMI cut-off values in clinical research and daily practice will eventually lead to a simple and cost-effective screening of morbid childhood obesity. Additional research showed that morbidly obese children have higher fasting insulin and systolic blood pressure levels compared to less extremely obese children. Apart from the use of the BMI to screen for metabolic complications in obese children, other screening methods were also studied, including the OGTT curve and metabolically "healthy" obesity (MHO). This study revealed that end-pubertal obese girls with a monophasic OGTT shape pattern showed early signs of β-cell insulin secretory failure as opposed to those with a biphasic or triphasic shape pattern. In addition, MHO children and adolescents had significantly lower levels of fasting insulin, triglycerides and TG/HDL-C ratio as compared to MUO children. In addition to clinical research, NMR-based metabolomics was applied to identify biomarkers of metabolic complications of childhood obesity. Hereto, ^{1}H-NMR experimental analysis was first optimized and a robust and practical protocol for sample collection and processing in a clinical setting was developed. Using ^{1}H-NMR-based plasma metabolomics, the metabolic profile of obese and normal-weight children and adolescents was determined and compared. As an extension, the plasma metabolic profile of a metabolically "healthy" but obese (MHO) phenotype was investigated. This showed that the obese and metabolically unhealthy phenotype was characterized by an increased lipid content, decreased levels of choline-containing phospholipids, an increased glycolytic activity, low-grade inflammation, and alterations in energy metabolism. In addition to this, it appeared that triglyceride concentrations were strongly correlated to the obese metabolic unhealthy phenotype. In brief, the fundamental clinical and metabolomics research performed in this doctoral project provides a basis for the future development of clinically useful screening tools for the early detection of obesity and associated metabolic complications in children and adolescents.

Kinderobesitas is een multifactoriële complexe aandoening, die vaak voorkomt in associatie met metabole complicaties zoals insulineresistentie, het metabool syndroom, prediabetes en premature hartfalen. De laatste jaren is de prevalentie van kinderen met extreme obesitas sterk toegenomen. Om morbide kinderobesitas te definiëren en de prevalentie ervan in kader te brengen, werden de internationale (IOTF) BMI afkapwaarden die overeenkomen met een BMI hoger dan 40 op 18-jarige leeftijd ontwikkeld. De toekomstige applicatie van deze BMI afkapwaarden in klinisch onderzoek en dagelijkse praktijk zal een eenvoudige en kosteneffectieve screening van morbide kinderobesitas kunnen realiseren. Verder onderzoek toonde aan dat kinderen met morbide obesitas een verhoogde nuchtere insulineconcentratie en verhoogde systolische bloeddruk hadden vergeleken met kinderen met minder extreme obesitas. Behalve het gebruik van de BMI om te screenen voor metabole complicaties bij obese kinderen, werden ook andere screeningsmethoden onderzocht, waaronder de OGTT curve en metabool "gezonde" obesitas (MHO). Uit dit onderzoek bleek dat post-puberale obese meisjes met een monofasische vorm van de OGTT curve, vroege tekenen van een verstoorde β-cel insuline secretie vertoonden in tegenstelling tot diegenen met een bi- of trifasische curve. Daarnaast vertoonden MHO kinderen en adolescenten significant lagere concentraties van nuchtere insuline, triglyceriden en TG/HDL-C ratio in vergelijking met metabool ongezonde obese kinderen. Naast het uitgevoerde klinisch onderzoek, werd ook NMR-gebaseerde metabolomics toegepast om biomarkers van metabole complicaties bij kinderobesitas te identificeren. Hiervoor werd eerst de ^{1}H-NMR experimentele analyse geoptimaliseerd en een robuust en praktisch protocol voor staalverzameling en verwerking in een klinische setting ontwikkeld. Aan de hand van ^{1}H-NMR-gebaseerde plasma metabolomics, werd het metabool profiel van obese en normaalgewicht kinderen bepaald en vergeleken. Als uitbreiding werd het plasma metabool profiel van het metabool gezond en obese (MHO) fenotype onderzocht. Hieruit bleek dat het obese en metabool ongezonde fenotype werd gekarakteriseerd door een verhoogd lipide gehalte, een verlaagd gehalte van choline-bevattende fosfolipiden, een verhoogde glycolytische activiteit, laaggradige inflammatie, en een verstoord energiemetabolisme. Hiernaast bleken triglyceride concentraties zeer sterk gecorreleerd te zijn aan het obese metabool ongezonde fenotype. Kortom, het fundamenteel klinisch en metabolomics

onderzoek dat werd uitgevoerd tijdens dit doctoraatsproject vormt een basis voor de verdere ontwikkeling van klinisch bruikbare screeningstools voor de vroegtijdige detectie van obesitas en geassocieerde metabole complicaties bij kinderen en adolescenten.

Liene Bervoets was born on May 29th 1986 in Hasselt, Belgium. After completion of secondary school mathematics-sciences in 2004 at the Koninklijk Atheneum Alicebourg in Lanaken, she started her bachelor studies in Bio-Engineering at the Catholic University of Leuven. In 2005, she started her bachelor studies in Biomedical Sciences at Hasselt University. She studied her master in Biomedical Sciences at the University of Antwerp (UA) and performed her master internship at the Laboratory of Medical Microbiology UA in collaboration with the department of Pediatrics at the University Hospital Antwerp (UZA). During this internship, she aimed to determine whether there is a difference in the composition of gut microbiota between obese and lean children. In June 2010, she graduated with great honors as a master in Biomedical Sciences. In the same year she started her PhD-project at the Hasselt University in the context of the 'Limburg Clinical Research Program' (LCRP) which is a collaboration between the Faculty of Medicine and Life Sciences of Hasselt University, Jessa Hospital (Hasselt, Belgium) and Ziekenhuis Oost-Limburg (Genk, Belgium). **She is currently studying the metabolic health of obese children and adolescents by clinical and metabolomics research.** She is mainly interested in biomedical research related to obesity, gut microbiota and nutrition. She is a member of the Belgian Association for the Study of Obesity (BASO).

Publications

Nelissen S, **Bervoets L** and Massa G (2010) Severe weight gain in 2 boys treated with risperidone. *Tijdschrift van de Belgische Kinderarts* 12(4):48-49
No IF

Bervoets L, Van Hoorenbeeck K, Kortleven I, Van Noten C, Hens N, Vael C, Goossens H, Desager KN, Vankerckhoven V (2013) Differences in gut microbiota composition between obese and lean children: a cross-sectional study. *Gut Pathogens* 5(1):10
IF: 2.738

Bervoets L and Massa G (2014) Defining morbid obesity in children based on BMI 40 at age 18 using the extended international (IOTF) cut-offs. *Pediatric Obesity* 9(5):e94-8
IF: 2.276

Bervoets L, Van Noten C, Van Roosbroeck S, Hansen D, Van Hoorenbeeck K, Verheyen E, Van Hal G, Vankerckhoven V (2014). Reliability and Validity of the Dutch Physical Activity Questionnaires for Children (PAQ-C) and Adolescents (PAQ-A). *Archives of Public Health* 72:47
No IF

Louis E*, **Bervoets L***, Reekmans G, De Jonge E, Mesotten L, Thomeer M, Adriaensens P (2015). Phenotyping human blood plasma by ^{1}H-NMR: a robust protocol based on metabolite spiking and its evaluation in breast cancer. *Metabolomics* 11(1): 225-236
*These authors contributed equally to this work.
IF: 3.965

Bervoets L, Mewis A, Massa G (2015). The shape of the plasma glucose curve during an oral glucose tolerance test as an indicator of beta-cell function and insulin sensitivity in end-pubertal obese girls. *Hormone and Metabolic Research, in press*. DOI: 10.1055/s-0034-1395551
IF: 2.038

Massa G, Achten W, **Bervoets L**, Faust K, Raes M (2014). Morbide obesitas bij kinderen en adolescenten. *Tijdschrift voor Geneeskunde* 70(23):1401-1410.
No IF

Bervoets L*, Louis E*, Reekmans G, Mesotten L, Thomeer M, Adriaensens P, Linsen L (2015). Influence of preanalytical sampling conditions on the ^{1}H-NMR metabolic profile of human blood plasma and introduction of the Standard PREanalytical Code used in biobanking. *Metabolomics, in press.* DOI: 10.1007/s11306-015-0774-y
*These authors contributed equally to this work
IF: 3.965

Published abstracts

Bervoets L and Massa G. Prevalence of metabolic syndrome and impaired glucose tolerance in Flemish obese children (2011) *International Journal of Obesity Supplements* 1,S6-S28
IF: 4.691

Vankerckhoven V, **Bervoets L**, Van Hoorenbeeck K, Lammens C, Chapelle S, Vael C, Desager K and Goossens H. Relationship between the gut microbiota and obesity in children and adolescents (2011) *Clinical Microbiology and Infection* 17,S1-S107
IF: 4.540

Oral presentations

Bervoets L and Massa G. Weight gain in children and adolescents during treatment with atypical antipsychotics. Belgian Association for the Study of Obesity Free Communications Meeting, 5th February 2011, Brussels, Belgium.

Bervoets L and Massa G. The shape of the plasma glucose curve during an oral glucose tolerance test harbours information on whole body insulin sensitivity and β-cell function. Belgian Association for the Study of Obesity Free Communications Meeting, 4th February 2012, Leuven, Belgium.

Bervoets L, Van Hoorenbeeck K, Kortleven I, Van Noten C, Hens N, Vael C, Goossens H, Desager KN, Vankerckhoven V. Relationship between the gut microbiota, diet, physical activity and obesity in children. European Congress on Obesity, 9th-12th May 2012, Lyon, France.

Bervoets L, Michiels L, Noben JP, Adriaensens P and Massa G. Antipsychotica bij kinderen en adolescenten: te dik gezaaid? PhD symposium "Patiëntgericht wetenschappelijk onderzoek in de Limburgse ziekenhuizen". 24th November 2012, Genk, Belgium.

Bervoets L and Massa G. The distinction of metabolically 'healthy' from metabolically 'unhealthy' obese children and adolescents. Belgian Association for the Study of Obesity Free Communications Meeting, 23rd February 2013, Brussels, Belgium.

Bervoets L, Massa G, Reekmans G and Adriaensens P. Differentiation of the plasma metabolite profile detected with ^{1}H-NMR spectroscopy of obese and normal-weight children and adolescents. First Belgian-Netherlands Joint symposium on Metabolomics. 13th and 14th May, 2013, Spa, Belgium.

Bervoets L and Massa G. Defining morbid obesity in children based on BMI 40 at age 18 using the extended international (IOTF) cut-offs. Belgian Association for the Study of Obesity Free Communications Meeting, 15th February 2014, Brussels, Belgium.

Poster presentations

Bervoets L and Massa G. Prevalence of metabolic syndrome and impaired glucose tolerance in Flemish obese children. 21st Workshop of European Childhood Obesity Group and 1st European Congress of Childhood Obesity, 8th – 10th September 2011, Pécs, Hungary.

Bervoets L, Michiels L, Deprez K, Baeten K, Adriaensens P and Massa G. Weight gain induced by atypical antipsychotics in children. Annual symposium Limburg Clinical Research Program: Kick-off meeting. 18th October 2012, Diepenbeek, Belgium.

Bervoets L and Massa G. The shape of the plasma glucose curve during an oral glucose tolerance test harbours information on whole body insulin sensitivity and β-cell function. 22nd Workshop of European Childhood Obesity Group. 17th – 19th October 2012, Palma de Mallorca, Spain.

Bervoets L and Massa G. The shape of the plasma glucose curve during an oral glucose tolerance test harbours information on whole body insulin sensitivity and β-cell function. 51th Annual Meeting of the European Society for Paediatric Endocrinology, 20th – 23rd September 2012, Leipzig, Germany.

Bervoets L, Massa G, Reekmans G and Adriaensens P. Differentiation of the plasma metabolite profile detected with ^{1}H-NMR spectroscopy of obese and normal-weight children and adolescents. First Belgian-Netherlands Joint symposium on Metabolomics. 13th and 14th May, 2013, Spa, Belgium.

Bervoets L, Louis E, Mesotten L, Reekmans G, Thomeer M and Adriaensens P. Identification of the chemical shifts of a series of metabolites appearing in the ^{1}H-NMR spectrum of blood plasma by spiking. 9th Annual Conference of the Metabolomics Society, 1th – 4th July 2013, Glasgow, United Kingdom.

Bervoets L, Massa G, Reekmans G and Adriaensens P. Obese and normal-weight children display a different plasma metabolic profile as measured with ^{1}H-NMR spectroscopy. Young Belgium Magnetic Resonance Scientist (YBMRS), 2nd – 3rd December 2013, Blankenberge, Belgium.

Bervoets L, Massa G, Reekmans G and Adriaensens P. The plasma metabolic profile of obese vs lean children as determined by ^{1}H-NMR spectroscopy. Knowledge for Growth, 8th May 2014, Ghent, Belgium.

Courses

General

- Lab book taking, good scientific conduct and lab safety by the Doctoral School for Medicine and Life Sciences
- Venipuncture by Limburg Catholic University College
- Metabolic syndrome and obesity by Nutrimedes
- Workshop Omics Revolution by FTNLS

Statistics

- Parametric and non-parametric statistical methods for the life sciences by the Doctoral School for Medicine and Life Sciences
- FLAMES summer school methodology and statistics by Flames
- Multivariate data analysis by Umetrics

Writing and presentation

- Scientific writing and oral presentations by VIB
- Academic English by Prof. dr. Eric Caers

Teaching

- Research College organized by Prof. dr. Leen De Ryck
- Practicum Metabolism organized by Prof. dr. Jean-Paul Noben
- Practicum Sequence analysis organized by Prof. dr. Veerle Somers
- Practicum Bio-informatics organized by Prof. dr. Luc Michiels
- Practicum DNA damage and genetic susceptibility organized by Prof. dr. Luc Michiels

Student supervision

- Year assignment organized by Prof. Dr. Marjan Vandersteen
- Exploration organized by Prof. Dr. Marjan Vandersteen

Management

- Module Project Management by True Colours
- OPPINO Module 3 by Knowledge for Growth

Organization PhD symposium

Patient-oriented research in Limburg hospitals, on November 24th, 2012

Participation in writing a submitted grant proposal

'The relationship between intestinal microbiota and childhood obesity', submitted to Scientific Research Committee, Faculty of Medicine, University of Antwerp, on July 8th, 2010.

Dankwoord

Graag zou ik iedereen die mij gesteund en geholpen heeft tijdens de periode van dit doctoraat, heel erg willen bedanken!

Allereerst mijn promotor, *Prof. Dr. Guy Massa*. Bedankt om mij te laten starten als doctoraatsstudente binnen de cluster obesitas van het LCRP. Aan het begin van deze onderzoeksperiode hebben we beiden onze weg een beetje moeten zoeken. Uiteindelijk is alles in zijn plooi gevallen, en denk ik dat we fier mogen zijn op onze prestatie. Uw expertise en nauwkeurigheid hebben bijgedragen aan dit mooie werk en de daaruit voortvloeiende presentaties en publicaties. Naast het onderzoek heeft u mij ook de kans gegeven om deel te nemen aan cursussen en congressen. Ik wil u voor dit alles graag bedanken.

Prof. dr. Peter Adriaensens, ik heb veel waardering voor uw gedrevenheid voor de wetenschap. U heeft mij tijdens dit doctoraatsproject veel geholpen. Zelfs tijdens de voor u meest drukke periodes maakte u tijd vrij voor mij, waar ik u heel dankbaar voor ben. Uw expertise, uw precisie en kritische visie zijn voor dit project van grote waarde geweest. Samen met *Evelyne, Kurt, Gunter* en *Koen* stond u steeds paraat om te helpen met "de NMR". Bedankt voor alles.

Prof. dr. Jean-Paul Noben, ik heb veel appreciatie voor uw uitgebreide kennis over het metabolisme. Als ik vragen had over de metabole pathways, stond u meteen voor mij klaar. Bedankt. Jammer genoeg zijn we niet in zee gegaan met de zebravisjes (☺), maar het was toch het proberen waard. Hiernaast wil ik u graag bedanken om mij de kans te geven om het practicum metabolisme te begeleiden, alsook *Monique* en *Kristel*, die dit mee in goede banen hebben geleid.

Prof. dr. Luc Michiels, aan het begin van dit doctoraat heeft u mij geholpen bij het opzetten van de genetische studie betreffende antipsychotica-geïnduceerde gewichtstoename. Ondanks dat dit project niet heeft standgehouden, wil ik u toch graag bedanken voor uw bereidheid mij hierbij te helpen. Ook *Karolien*, bedankt voor alle hulp.

Ik bedank ook graag alle *leden van de jury* voor hun nuttige feedback op mijn proefschrift. *Prof. dr. Dominique Hansen*, u heeft de METAFIT studie helpen opzetten, jammer genoeg heeft ook deze het niet uitgezongen. Toch bedank ik u graag voor onze samenwerking die reeds mooie publicaties heeft opgeleverd. Dank ook aan uw masterstage studenten *Nastasia* en *Matthias* voor hun inzet bij de verwerking van de resultaten.

Evelyne, als naaste collega's hebben we samen heel wat tijd doorgebracht aan onze bureau, maar ook aan "de NMR", tijdens meetings en congressen. Ik blijf hier vele mooie herinneringen aan hebben. Als ik vragen had over SIMCA, validatiestudies of 'waar is Peter'? ☺ schoot je meteen ter hulp. Ook als ik mijn hart (weer eens) moest luchten, was je een luisterend oor. Bedankt voor alles! En veel succes met het afronden van je doctoraat, je gaat dat goed doen! Ook jouw promotoren *Prof. Dr. Michiel Thomeer* en *Prof. Dr. Liesbet Mesotten*, en collega *Dr. Karolien Vanhove* wil ik bedanken voor hun waardevolle feedback tijdens onze meetings.

Bojoura, Laura en Kristel, ik wil jullie ook graag bedanken voor de fijne tijd die we samen hebben doorgebracht. Ik vond onze gezellige middaglunches en babbels superleuk en ik heb er veel aan gehad! Zeker iets om in de toekomst te blijven doen! *Kristel*, jou wil ik in het bijzonder nog bedanken voor je hulp tijdens dit onderzoek!

dr. Helene Piccard, ik herinner mij nog goed dat ik aan het begin van dit doctoraat aan het aftellen was voor de komst van de coördinator van LCRP. We hebben toen samen de onderzoeksvoorstellen voor de ethische commissies opgesteld. Je gaf me ook goede tips & tricks na onze lange (soms urenlange) gesprekken. Bedankt voor alles! *Marleen Missotten*, bedankt voor je hulp bij het verwerken van de stalen voor de studie. *Kathleen Ungricht, Ilse Henckens en Jean Fastré*, bedankt voor jullie hulp bij de administratie. *Veronique Pousset*, heel erg bedankt om altijd voor mij klaar te staan en mij te helpen met de voorbereiding van mijn doctoraatsverdediging.

Prof. dr. Loes Linsen, bedankt voor je waardevolle input en hulp! Jouw gedrevenheid, encyclopedische kennis en geweldige humor hebben op mij hun effect niet gemist ☺. *Severina* en *Karen*, onze slappe lach-momenten waren 'outta control'! Ik heb mij enorm geamuseerd in jullie aanwezigheid, ik zal dit nooit vergeten en we gaan dit blijven doen! *Yati*, bedankt voor je hulp bij de METAFIT studie en de grappige momenten tijdens ons 'apenwerk' ☺. Ook *Yanick, Leen, Annick, Jeroen* en *Remco,* bedankt voor alles. *Prof. dr. Jean-Luc Rummens,* bedankt om mij toegang te verlenen aan het klinisch labo van het Jessa ziekenhuis, *Fien Achten* bedankt voor het bezorgen van de ontbrekende gegevens van de databanken en *dr. Alex Mewis* bedankt voor uw input omtrent biochemische assays.

Ik bedank ook *Prof. dr. Ziv Shkedy* en *Prof. dr. Niel Hens*, voor de statistische input, *Prof. dr. Eric Caers*, voor de verbeteringen van de Engelse taal, en mijn *collega's van BIOMED* voor al hun hulp. *Dorien*, bedankt om mij de ELISA techniek aan te leren! Ook alle *kinderpsychiaters* die initieel betrokken waren bij het doctoraatsproject wil ik bedanken voor hun bereidwilligheid om deel te nemen aan de studies en om patiëntjes door te verwijzen. *Dr. Vanessa Vankerckhoven* en *Prof. dr. Guido van Hal* van de Universiteit Antwerpen, héél erg bedankt voor jullie hulp, motivatie, expertise en enthousiasme wat het mogelijk heeft gemaakt om nog twee mooie papers tijdens deze doctoraatsperiode te publiceren. Ook dank aan alle kinderen die hebben deelgenomen aan de studies, en hun ouders.

Achter de schermen van dit doctoraatsproject waren er ook een heel aantal personen die mij door dik en dun (☺) gesteund hebben en waar ik heel dankbaar voor ben.

Mijn vriendinnen *Mariet, Goele, Sarah* en *Saskia*, jullie luisterden naar mij als ik het eens moeilijk had en pepten mij terug op met leuke gesprekken en grapjes! En 'by the way', vanaf nu heb ik geen excuus meer dat ik aan mijn boekje moet werken ☺ Ook de meisjes en trainer van de *volleybal*, en mannen en vrouwen van de *duikclub*, bedankt voor jullie sportieve steun! De *vrienden en vriendinnen van Tim*, en dat zijn er teveel om op te noemen ☺, jullie hebben mij –

waarschijnlijk onbewust – geholpen om mijn gedachten eens op iets anders te zetten tijdens onze gezellige onderonsjes. Ik kijk al uit naar de rest van de zomer! Ook de familie van Tim, *Patrick en Ulla*, *Davine en David*, bedankt om mij te steunen en er steeds voor mij te zijn.

Mama en papa. Zonder jullie had ik dit nooit bereikt. Jullie hebben mij de kans gegeven om te studeren aan de universiteit, en jullie hebben mij hierin heel erg gesteund. Als ik weer eens begon af te ratelen ☺, waren jullie een luisterend oor. *Mama*, je was laatst zo verwonderd over mijn doorzettingsvermogen. Maar jij hebt eens tegen mij gezegd: 'Dat waar je aan begint, moet je ook afmaken'. Je hebt mij zelf laten beslissen als ik voor moeilijke keuzes stond, en daar ben ik je heel dankbaar voor! *Papa*, je zou het misschien niet zeggen, maar ik ben dr. Bervoets nu ☺ Zo staat het toch op papier... In de werkelijkheid ben ik nog altijd je kleine meisje dat erg opkijkt naar wat je allemaal verwezenlijkt hebt! Mijn allerliefste zusjes, *Katrijn* en *Jana*! Jullie zijn fantastisch. Jullie stonden (en staan) altijd voor mij klaar en begrijpen mij als geen ander. Ook als ik jullie eens niet begrijp ☺ *Katrijn* en *Mathijs,* en *Jana en Yannick,* veel geluk in jullie nieuwe huisje!

Last but definitely not least (!), *Tim*. Het weinige dat ik hier ga neerschrijven kan niet omvatten wat je allemaal voor mij betekend hebt. Ik heb mezelf leren kennen tijdens de moeilijke momenten waar jij mij hebt doorgeholpen. Je stond altijd voor mij klaar en ik moet je bedanken voor je (vele ☺) geduld en begrip! Het was geen gemakkelijke periode, maar toch heb ik een fantastische tijd met jou beleefd! Ik kijk heel erg uit naar onze toekomst… Die begint vanaf… Nu!

Liene, 2 juli 2015

"Learn from yesterday, live for today, hope for tomorrow.
The important thing is not to stop questioning."
Albert Einstein